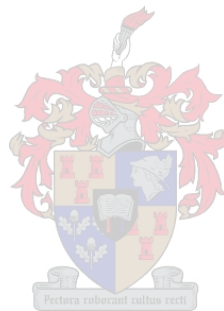# An evaluation of the hepatic proteomic signature in identifying cancer tolerance and resistance mechanisms in a mouse allograft system

by

Gustav van Niekerk

Dissertation presented for the degree of Doctor of Philosophy (Physiology)
in the Faculty of Sciences at Stellenbosch University

Supervisors: Prof Anna-Mart Engelbrecht

Co-supervisors: Dr Benjamin Loos, Dr Theo Nell

March 2017

Declaration

By submitting this dissertation electronically, I declare that the entirety of the work contained therein is my own, original work, that I am the sole author thereof (save to the extent explicitly otherwise stated), that reproduction and publication thereof by Stellenbosch University will not infringe any third party rights and that I have not previously in its entirety or in part submitted it for obtaining any qualification.

This dissertation includes one original paper published in a peer-reviewed journal. The development and writing of the paper were the principal responsibility of myself.

March 2017

Abstract

Background

The unfavourable therapeutic index of most treatment modalities has greatly impeded progress in the development of effective cancer therapy. Therefore a need exists for treatment modalities that are less taxing on a patient's health status (i.e. maintain a patients reserve capacity and thus prolong survival) while additionally not invoking counter evolutionary strategies from tumour cells. Plant biologist have long distinguished between the host's ability to accommodate pathogen burden, as oppose to its ability to antagonise pathogen load. Hence, the disease trajectory is not only dependent on the hosts' ability to *resist* an infection, but also on the capacity to *tolerate* pathogen burden. This distinction have only recently been applied to animals. A number of observations suggest that this distinction may be of great immunological relevance, including the prevalence of asymptomatic carriers and natural variation in the population with regards to disease progression. Thus, the tolerance/resistance (T/R) paradigm represents a novel approach for understanding disease progression. We hypothesise that similar mechanisms might underlie host-tumour dynamics.

Study aims and experimental design

The current study aimed to evaluate the application of the T/R framework within an oncological context. A syngeneic mice model system was used to compare tolerance and resistance between two cancer cell lines. C57BL/6 mice were inoculated with either mammary carcinoma cells (EO771) or melanoma cells (B16). In a clinical setting, health status would not only be influenced by tumour load, but also by therapeutic interventions such as cytotoxic therapies, which must also be tolerated. Thus, a second study was performed using chemotherapeutic

regimes as a variable to explore the effect of high (5 mg/kg) and low (2 mg/kg) dose doxorubicin (DXR) treatment on tolerance and resistance in mice. In addition, attempts were made to identify mechanisms underlying differences between groups with regards to variation in tolerance and resistance. To this end, a combination of immunoblotting and proteomic analyses were performed.

Methodology: quantifying tolerance and resistance

Resistance was quantified as the slope of a regression line, with tumour volume as response variable, and time as independent variable. Tolerance was measured similarly, but with body weight as response variable and tumour load as independent variable. Differences in regression slopes was used to compare tolerance and resistance. To confirm tolerance, differences in gastrocnemius muscle cross-sectional area (MCA) were compared between groups.

Results

Mice inoculated with melanoma (B16) cells showed a significantly lower resistance compared to mice inoculated with breast cancer EO771 cells. With regards to tolerance, B16 cells also exhibited lower tolerance, though tests for homogeneity of regression slopes demonstrated that these differences did not reach significance (p = 0.0856). Similarly, B16 and EO771 groups did not exhibit any difference in MCA. Comparing the effect of high and low dose DXR on mice bearing EO771 revealed that DXR decreases resistance: both low dose and higher dose DXR increased tumour growth as demonstrated by significantly steeper slopes in DXR groups compared to the tumour control group.

In order to explain the increase in EO771 tumour growth in mice receiving DXR, the activation of a panel of signalling proteins associated with cell growth and survival (cRaf, ERK, p38 MAPK, JNK, PTEN, PI3Kp85, PDK1, Akt, mTOR, Bcl-2) as well as apoptotic markers

(Caspase 3, 8 and 9) in tumour samples were evaluated by western blot analyses. However, the only significant finding include elevated ERK activation in mice receiving DXR, suggesting that extracellular signalling molecules might drive tumour growth.

Since the liver plays a critical role in energy homeostasis, as well as in the production and clearance of circulating factors, western blot analyses were performed on liver samples. Markers of autophagy (p62 and LC3B-II) as well as growth signalling proteins (Akt and mTOR) and apoptosis (Caspase 3) were evaluated by western blot analyses. Mice inoculated with B16 demonstrated a marked increase in both p62 and LC3B-II, signifying an increase in autophagosome pool size, most likely due to dysfunctional lysosomal fusion. Surprisingly, other makers in both EO771 and B16 did not significantly differ from control liver samples.

Subsequently, liver proteomics were performed making use of a Gene Ontology approach in order to describe biological, functional, structural and other processes that are uniquely altered between groups. Interestingly, a comparison between livers of mice inoculated with B16 melanoma cells and EO771 breast cancer cells also suggested that autophagic activity was not upregulated compared to the control group. DXR groups also did not exhibit differences in autophagic processes, though proteins involved in the proteasomal pathway were upregulated in mice receiving high doses of DXR. An increase expression of enzymes associated with retinoic acid metabolism was observed in the B16 group, which might explain decrease tolerance and resistance in this group. An increase in steroid metabolism was also observed in mice receiving DXR. Since cholesterol form a key component of cell membranes, it is possible that cholesterol synthesis might enable rapidly growing tumours of mice receiving DXR. Finally, concurrent up- and downregulation of certain proteins involved in radical scavenging in DXR mice might suggest a differential free radical scavenging response, thus explaining why anti-oxidant therapies have not proven successful in clinical settings in response to DXR.

Collectively, these observations highlight alteration in hepatic activities through which tolerance and resistance mechanism might manifest.

In summary, this study have demonstrated the implementation of the T/R framework within an oncological setting. Evidence suggest that defects in hepatic autophagy might contribute to lower tolerance, and possibly also resistance. Autophagy was not significantly upregulated in response to DXR which was associated with lower tolerance. Similar, mice inoculated with B16 tumours exhibited lower tolerance as well as evidence for suppressed lysosomal fusion with autophagosome. These observations suggest that a compromised autophagic apparatus might contribute towards the lower tolerance. Proteomic results are also suggestive of a potential role played by altered liver metabolism, including retinoic acid and steroid metabolism. Future studies evaluating the role of this pathways might identify novel tolerance-promoting pathways.

Opsomming

Agtergrond

Die ongunstige terapeutiese indeks van behandelingsopsies het die ontwikkeling van effektiewe kankerterapie grootliks vertraag. Dit is dus noodsaaklik dat behandelingsopsies gevind moet word wat minder stremmend op 'n pasiënt se gesondheidstatus is (dws terapie wat 'n pasient se reserwekapasiteit en gevolglik oorlewing verleng); terwyl dit ook nie teen-evolusionêre strategieë in kankerselle ontlok nie. Plantbioloë het lankal reeds onderskei tussen die gasheer se vermoë om patogene te akkomodeer teenoor sy vermoë om patogeenlading te onderdruk. Die siekteverloop is dus nie net afhanklik van die gasheer se vermoë om *weerstand* teen 'n infeksie te bied nie, maar ook sy vermoë om die patogeen lading te *tolereer*. Hierdie onderskeiding is eers onlangs op diere toegepas. Uit heelwat navorsing blyk dit dat hierdie onderskeiding van groot immunologiese belang kan wees, insluitend die voorkoms van asimptomatiese draers en natuurlike variasie in die populasie ten opsigte van siekteverloop. Die toleransie/weerstand (T/R) paradigma verteenwoordig dus 'n nuwe verstaan van siekteverloop. Ons hipotese is dus dat 'n soortgelyke meganisme gasheer-tumor dinamika onderlê.

Studie doelwitte en eksperimentele plan

Die doel van hierdie studie is om die toepassing van die T/R raamwerk in 'n onkologiese konteks toe te pas. 'n Singeneïese muismodel is gebruik om toleransie en weerstand tussen twee kankersellyne te ondersoek. C57BL/6 muise is ingespuit met borskankerselle (EO771) of met melanoomselle (B16). In 'n klinese opset word gesondheidstatus nie net beïnvloed deur tumorlading nie, maar ook deur intervensies soos sitotoksiese terapieë wat ook getolereer moet

word. 'n Tweede studie is dus gedoen waar chemoterapie as veranderlike gebruik word om die effek van 'n hoë (5 mg/kg) en 'n lae (2 mg/kg) dosis doxorubicin (DXR) behandeling op toleransie en weerstand in muise te bepaal. Daar is verder ook gepoog om meganismes te identifiseer wat onderliggend is aan die verskille tusssen groepe ten opsigte van variasie in toleransie en weerstand. Vir hierdie doel is immunokladtegnieke asook proteoom analises gebruik.

Metodologie: kwantifisering van toleransie en weerstand

Weerstand is gekwantifiseer as die helling van 'n regressielyn, met tumorvolume as responsveranderlike en tyd as onafhanklike veranderlike. Toleransie is soorgelyk gemeet, maar met liggaamsgewig as responsveranderlike en tumorlading as onafhanklike veranderlike. Verskille in die regressie hellings is gebruik om toleransie en weerstand te vergelyk. Om toleransie te bevestig, is verskille in die gastrocnemius spier dwarssnit oppervlak (SDO) vergelyk tussen groepe.

Resultate

Muise wat ingespuit is met melanoom (B16) selle, het 'n insiggewende laer weerstand getoon teenoor muise wat met EO771 borskankerselle ingespuit is. B16 selle het ook 'n laer toleransie getoon, alhoewel homogenisiteit ten opsigte van regressie hellings getoon het dat insiggewendheid nie bereik is nie ($p = 0.0856$). Soortgelyk het B16 en EO771 groepe ook nie insiggewend verskil in die SDO nie. 'n Vergelyking van die effek van 'n hoë en 'n lae dosis DXR in muise met EO771 tumore het getoon dat DXR weerstand laat afneem: beide lae en hoë dosisse DXR het 'n toename in tumorgroei veroorsaak soos aangetoon is in die insiggewende steiler hellings van die DXR groepe in vergelyking met die tumor kontrole groep.

Om die toename in EO771 tumorgroei in muise wat DXR ontvang het, te verklaar, is die aktivering van 'n paneel seinoordrag proteïene wat geassosieer word met selgroei en oorlewing (cRaf, ERK, p38 MAPK, JNK, PTEN, PI3Kp85, PDK1, Akt, mTOR, Bcl-2) sowel as apoptotiese merkers (Caspase 3, 8 and 9) in tumorweefsel geëvalueer deur middel van westelike kladtegnieke. Die enigste insiggewende verandering wat waargeneem is, is 'n verhoging in ERK aktivering in muise wat DXR ontvang het, wat dus voorstel dat ekstrasellulêre seinoordragmolekules tumorgroei in hierdie muise stimuleer het.

Aangesien die lewer 'n kritiese rol in energie homeostase speel, sowel as in die produksie en verwydering van sirkulerende faktore, is westelike kladanalises ook op lewerweefsel gedoen. Merkers van autofagie (p62 and LC3B-II) sowel as groei seinoordragproteïene (Akt en mTOR) en apoptose merkers (Caspase 3) is geëvalueer deur middel van westelike kladtegnieke. Muise wat ingespuit is met B16 selle het 'n merkbare toename in beide p62 en LC3B-II getoon, wat montlik 'n aanduiding kan wees van 'n toename in die aantal autofagosome, heel waarskynlik as gevolg van disfunksionele lisosomale samesmelting. Dit is interessant dat geen ander merkers in beide E0771 en B16 selle insiggewend verskil het van die lewer kontrole weefsel nie.

Lewerproteoom analises is gevolglik uitgevoer waar daar gebruik gemaak is van 'n Geen Ontologie benadering om biologiese, funksionele, strukturele en ander prosesse wat uniek verander is tussen groepe, te bepaal. Interessant, is dat 'n vergelyking tussen lewers van muise wat met B16 melanoom selle en EO771 borskankerselle ingespuit is, aangedui het dat autofagie aktiwiteit nie opgereguleer is in vergelyking met die kontrolegoep nie. DXR groepe het ook geen verskille in autofagie prosesse getoon nie, alhoewel proteïene in die proteosomale paaie opgereguleer is in muise wat hoë dosisse DXR ontvang het. 'n Toename in die uitdrukking van ensieme wat geassosieer word met retinoïese suur metabolisme is waargeneem in die B16

groep wat 'n afname in toleransie en weerstand in hierdie groep kan verklaar. 'n Toename in steroïedmetabolisme is ook waargeneem in muise wat DXR ontvang het. Aangesien cholesterol 'n sleutelkomponent van selmembrane is, kan verhoogde cholesterolsintese moontlik verantwoordelik wees vir die vinnige groei van tumorselle in die DXR groep. Gelyktydige op- en afregulering van sekere proteïene wat betrek kan word by vry radikaal opname, kan moontlik ook verklaar waarom antioksidant terapie onsuksesvol in 'n kliniese konteks in reaksie op DXR is. Hierdie waarnemings plaas klem op veranderinge in hepatiese aktiwiteite waardeur toleransie en weerstand kan manifesteer.

Om op te som, hierdie studie demonstreer die implementering van die T/R raamwerk in 'n onkologiese konteks. Bewyse stel voor dat afwykings in hepatiese autofagie 'n rol kan speel in laer toleransie, asook moontlik in weerstand. Autofagie is nie insiggewend opgereguleer in reaksie op DXR nie wat moontlik met laer toleransie geassosieer kan word. Soortgelyk, muise met B16 tumore het laer toleransie sowel as onderdrukte lisosomale versmelting met autofagosome getoon. Hierdie bewyse toon dat 'n foutiewe autofagie apparaat aanleiding kan gee tot laer toleransie. Proteomiese resultate dui ook aan dat 'n veranderde lewermetabolisme, insluitende retinoïese suur en steroïedmetabolisme, 'n potensiële rol kan speel. Evaluering van die rol van hierdie paaie kan nuwe toleransie promoverende paaie identifiseer in toekomstige studies.

Table of content

List of figures

List of tables

Abbreviations

AMP   adenosine 5'-monophosphate

CCL   cancer cell line

CSC   Cancer stem cell

Cyt C cytochrome C

DXR   Doxorubicin

ER   endoplasmic reticulum

FAC   Functional Annotation Clustering

GAS   Muscularis Gastrocnemius

GF   growth factors GF

GMP   Guanosine 5'-monophosphate

GO   gene ontology

HBSS   Hanks balanced salt solution

HER2   human epidermal growth factor receptor 2

JNK   Jun amino-terminal kinases

KEGG   Kyoto Encyclopedia of Genes and Genomes

LLG   Log-linear growth

LPS   lipopolysaccharide

MCA   Muscle cross-sectional area

mTORC2   mechanistic target of rapamycin complex 2

PDK1   phosphoinositide dependent protein kinase-1

PH   Pleckstrin homology

PI3K   phosphoinositide 3-kinase

PIP_2 phosphatidylinositol (4,5)-bisphosphate

PIP_3 phosphatidylinositol (3,4,5)-trisphosphate

PTEN Phosphatase and tensin homolog

RTK   receptor tyrosine kinase

s.c.   Subcutaneous

SDS-PAGE   sodium dodecyl sulfate polyacrylamide gel electrophoresis

T/R   Tolerance and resistance

TGF-β transforming growth factor-beta

TNF   tumour necrosis factor

List of publications

van Niekerk G, Hattingh SM, Engelbrecht AM. **Enhanced Therapeutic Efficacy in Cancer Patients by Short-term Fasting: The Autophagy Connection**. Front. Oncol. 2016 Nov 14;6:242. eCollection 2016

PMID: 27896219

DOI: 10.3389/fonc.2016.00242

van Niekerk G, Davids LM, Hattingh SM, Engelbrecht AM. **Cancer stem cells: A product of clonal evolution?** Int. J. Cancer. 2016 Sep 27. (publish ahead of print)

PMID: 27676693

DOI: 10.1002/ijc.30448

van Niekerk G, Isaacs AW1, Nell T, Engelbrecht AM. **Sickness-Associated Anorexia: Mother Nature's Idea of Immunonutrition?** Mediators Inflamm. 2016; 2016:8071539.

PMID: 27445441

DOI: 10.1155/2016/8071539

van Niekerk G, Loos B, Nell T, Engelbrecht AM. **Autophagy-A free meal in sickness-associated anorexia**. Autophagy. 2016;12(4):727-34.

PMID: 27050464

DOI: 10.1080/15548627.2016.1147672

van Niekerk G, Loos B, Nell T, Engelbrecht AM. **Cancer tolerance, resistance, pathogenicity and virulence: Deconstructing the disease state**. Future. Oncol. 2016 Jun;12(11):1369-80.

PMID: 27029525

DOI: 10.2217/fon-2015-0024

van Niekerk G, Hattingh SM, Engelbrecht AM**. Invertebrates: Why No Adaptive Immune System?** Scand. J. Immunol. 2016 Feb;83(2):160-1.

PMID: 26608929

DOI: 10.1111/sji.12400

van Niekerk G, Davis T, Engelbrecht AM. **Bone Marrow Fat: What is it Good for?** Semin Arthritis Rheum. 2016 Apr;45(5):e14.

PMID: 26525110

DOI: 10.1016/j.semarthrit.2015.09.011

van Niekerk G, Davis T, Engelbrecht AM. **Was the evolutionary road towards adaptive immunity paved with endothelium?** Biol. Direct. 2015 Sep 4;10:47.

PMID: 26341882

DOI: 10.1186/s13062-015-0079-0

van Niekerk G, Engelbrecht AM. **Commentary on: "A common origin for immunity and digestion"**. Front. Microbiol. 2015 May 27;6:531. eCollection 2015.

PMID: 26074909

DOI: 10.3389/fmicb.2015.00531

van Niekerk G, Engelbrecht AM. **On the evolutionary origin of the adaptive immune system—The adipocyte hypothesis**. Immunol. Lett. 2015 Apr;164(2):81-7.

PMID: 25698354

DOI: 10.1016/j.imlet.2015.02.002

Chapter 1

This chapter describes the framework that guided the research activities. An outline of the dissertation content is also given.

1.1   Introduction

Despite intense global efforts, in most cases, metastatic cancer remains an incurable disease (Hanahan, 2014). The slow progress made in finding effective therapies is exemplified by the Nobel prizes awarded to scientist working within the field of oncology. The 1966 Nobel Prize in Physiology or Medicine was awarded to Peyton Rous for demonstrating the oncogenic effect of certain viruses (in particular, his work on Rous sarcoma virus) and to Charles Brenton Huggins for establishing the dependency of prostate cancer on trophic factors (i.e. the treatment of prostate cancer with hormones). The only other Nobel Prize awarded for cancer-related discoveries was in 2008 to Harald zur Hausen in recognition for his work in establishing the role of papilloma viruses in the development of cervical cancer. Undoubtedly, vaccines against viruses such as human papilloma virus have saved millions of lives (Malagon et al., 2015). Similarly, the androgen-deprivation therapy limited tumour growth in most cases. However, the effect of hormone-starving cancer is usually short lived and the vast majority of cancers do not arise from a viral infection. The marginal impact of these interventions are also reflected by the unfortunate fact that an estimated 15.5 million Americans are currently (2016) living with cancer (Siegel et al., 2016).

This disappointing statistics also raise the question: "Why is it so difficult to find a cure for cancer?" This question is particular relevant when comparing the efficacy of antibiotics in curing a variety of otherwise lethal bacterial infections. In this regard, the problem posed by cancer could be reduced to two key factors. Firstly, cancer cells are directly derived from the host. Consequently, both the host and the cancer cells make use of the same molecular machinery and cellular physiology, thus explaining the unavoidable on-target toxicity of chemotherapeutic drugs. This is in contrast to bacteria which have diverged from eukaryotes billions of years ago. Secondly, cancer cells are constantly evolving: despite the fact that anti-neoplastic therapies effectively decrease tumour volume during initial cycles of therapy, cancer

cells invariably evolve drug resistance. Thus, the fact that the host shares cancer cell vulnerabilities, while cancer cells remain able to evolve novel strategies for developing drug resistance, remain major clinical obstacles.

As lifestyle intervention and better therapeutic options continue to decrease the mortality rate of cardiovascular diseases, cancer mortality is expected to increase: cancer already represent the leading cause of death in 21 states of the USA [(Siegel et al., 2016). However, progress has been made in managing cancer. Recent statistics indicate that, as a result of better cancer prevention (e.g. decrease in smoking and the development of vaccines against oncoviruses), early detection as well as better therapeutic interventions, cancer's mortality rate has declined by almost a quarter (23%) since the 1991 (Siegel et al., 2016).

However, another factor that contributes to the lower mortality rate in cancer is the fact that the life expectancy of patients with cancers has increased. That is, an increase *incidence* of cancer does not translate to an increase in *mortality*, as more advanced clinical support for cancer patients extend life expectancy (Miller et al., 2016). As an example, although the incidence of prostate cancer has increased in most countries, the mortality rates have not similarly increase (Center et al., 2012). These observations indicate that supportive care can increase life expectancies in cancers patients. In fact, some have raised the opinion that, instead of pursuing a 'cure' for cancer, neoplastic infections might be rendered a chronic, but manageable disease in the near future (Beck and Ng, 2014; Gatenby, 2009; Phillips and Currow, 2010). As example, preclinical evidence suggests that administering frequent, but low dose chemotherapy (referred to as 'metronomic chemotherapy') could decrease adverse effects of chemo-toxicity and avoid the evolution of chemo-resistance, while controlling tumour burden (Pasquier et al., 2010).

There is also a feeling that the current approach in treating cancer is not effective, voicing the need of a paradigm shift (Goldstein et al., 2012). Indeed, a number of research centres are currently employing scientists form fields such as physics, mathematics, ecology and even economy and political science in an attempt to develop more effective strategies in the War on Cancer (Blagoev, 2016; Dolgin, 2014; Drake, 2011; Enriquez-Navas et al., 2015; Wu et al., 2015). These attempts clearly demonstrate the unspoken consensus: the current approach to cancer therapy is unsatisfactory.

1.2   The role of a paradigm

The concept of a paradigm and the fundamental role it plays in science may be introduced by reference to a celebrated 'chicken-or-egg' question within the philosophy of science: do observations precede a hypothesis, or follow it? Popper points out that, in science, there is no such thing as a 'view from nowhere' and in fact, that observations are made from the vantage point of the researcher's experience (Popper, 2009):

> *The problem 'Which comes first, the hypothesis (H) or the observation (O),' is soluble; as is the problem, 'Which comes first, the hen (H) or the egg (O)'. The reply to the latter is, 'An earlier kind of egg'; to the former, 'An earlier kind of hypothesis'. It is quite true that any particular hypothesis we choose will have been preceded by observations — the observations, for example, which it is designed to explain. But these observations, in their turn, presupposed the adoption of a frame of reference: a frame of expectations: a frame of theories. If they were significant, if they created a need for explanation and thus gave rise to the invention of a hypothesis, it was because they could not be explained within the old theoretical framework, the old horizon of expectations.*

Popper thus reasons that observations are ultimately theory-laden, as it is theory that would direct the researcher to perform experiments to test the validity of hypothesis (or as Popper would claim, to attempt to refute a conjecture). Consequently, the theory-dependent nature of an observation also explains why research is not a haphazard activity, but guided by insightful research questions.

Thomas Kuhn, in his influential work *The Structure of Scientific Revolutions* forcefully articulates the role of a paradigm in not only directing research questions, but in fact dictating all research activities within a field. Similar to Popper, Kuhn also maintains that science is not 'algorithmic' (i.e. science is not a purely logical activity whereby knowledge is gained by deducting universal theories from neutral observations). However, Kuhn expands the role of the paradigm in guiding research activities conducted by the scientific community. According

to Kuhn, and unlike Popper, such a 'disciplinary matrix' does far more than suggest the observations necessary for explaining a phenomenon.

Instead of recounting the points of departure between Kuhn and Popper, it may be more instructive to view Kuhn's reason for emphasising the formative role of a paradigm on scientific activates. Firstly, two paradigms may invoke contrasting axiomatic structures, with different assumptions about the same phenomena. Since proponents of different paradigms do not share each other's assumptions, they are likely to formulate different conclusions on the same set of data. That is, in addition to the role of a paradigm in instructing the scientist on the kind of observations that would provide insight into a phenomenon, two rational scientists may agree on the outcome of an observation, but disagree on the *interpretation* of the observation, or its *significance*. Secondly, researchers may find appeal in different paradigms for various personal reasons (i.e. motivated by factors outside of science) (Kuhn, 1977). As an example, one paradigm may explain one phenomenon of interest with a higher degree of accuracy, whereas another paradigm may exhibit a superior descriptive explanation in a different context. Similarly, scientists may differ on the stock they place in a particular assumption, or simply feel that one set of assumptions is more reasonable than another. In short, rational researchers may agree on the facts, but derive different conclusions. To summarise in Kuhn's own words: "Practicing in different worlds, the two groups of scientists see different things when they look from the same point in the same direction."

In summary: the way in which a researcher perceives the world depends on the paradigm followed. In turn, the conceptual commitment of the researcher dictates the interpretation of results, what experimental procedure or methodology is considered adequate, and also when an experimental outcome is deemed a result of empirical error or a legitimate refutation. Consequently, the paradigm from which a researcher approaches a topic is likely to play a key role in gaining true insight into a research field.

1.3   Cancer paradigms

There are numerous ways of viewing cancer. Cancer has been described as a "disease of the genome" (Sager, 1985), thus expressing the manifestation of cancer as a cell-autonomous event, resulting from the step-wise accumulation of aberrations within a single cell. Alternatively, cancer has been described as "wounds that never heal" (Dvorak, 1986), thereby

emphasising cancer as a biological process being misapplied, and implicating the role of stromal cells and the host in general. Similarly, the observation that tumours consist of a heterogeneous population of cells is explained by two different paradigms. The cancer stem cell (CSC) hypothesis describes the existence of a sub-population of cancer cells with the ability to divide asymmetrically (i.e. give rise to more differentiated cancer cell progeny) (Magee et al., 2012). The model does not only explain the origin of tumour heterogeneity (i.e. asymmetric cell division giving rise to different cells) but also explains drug resistance: chemotherapy induces cell death in the progeny of CSC, but leaves the CSC population mostly intact, allowing these cells to repopulate the tumour bed after antineoplastic interventions have ablated the differentiated progeny. In contrast, the clonal evolution model of cancer emphasises cancer as an evolutionary process (Nowell, 1976). Here, both drug resistance and tumour heterogeneity can be understood as arising from cancer cells being subjected to different selective pressures within their respective micro-environment.

There are clearly many ways of viewing cancer, and in suit, numerous ways of expressing the challenges faced in finding a cure. At the very least then, each paradigm provides an opportunity to forward different research questions and arrange observations into arguments supporting diverse interpretations. However, different paradigms also moderate certain aspects of a phenomenon, for example by neglecting or obscuring certain complexities, while possibly over-emphasising other aspects. Consequently, not all paradigms provide the same level of insight into all aspects of a complex disease such as cancer.

1.4 Project outline

In this dissertation, the tolerance and resistance (T/R) framework is developed in two ways. Firstly, the T/R framework represents a paradigm – a conceptual framework from which to *understand* the manifestation of pathology and its relevance on the disease trajectory. Secondly, the T/R framework as an empirical tool to *quantify* the disease state is developed in this dissertation. Since a paradigm plays a formative role in research activities, developing novel ways of describing cancer may illuminate our understanding, and present new research questions. One promising approach consists in transferring principles and concepts developed in other fields of study to oncology. In this regard, much interest has been generated in applying more than a century of insight gained from studying ecological systems to oncological

problems as cancer recapitulates many of the same interactions seen in ecological systems (Aktipis and Nesse, 2013; Gatenby et al., 2009; Gatenby et al., 2011; Merlo et al., 2006; Nowell, 1976; Taylor et al., 2012). Similarly, the implementation of the T/R framework within an oncological setting might open up novel therapeutic avenues.

In Chapter 2, the immunological concept of tolerance and resistance (T/R) is introduced. The adaptation of this immunological concept within an oncological setting is also described in this chapter. In Chapter 3 concepts developed in preceding chapters are applied and the manifestation of pathology is revisited. Differences in tumour growth (resistance) was investigated by immunoblotting of tumour samples in order to elucidate the cell signalling cascades which describe altered tumour growth (Chapter 4). Differences in host tolerance was investigated by western blot analyses of liver samples (Chapter 5) followed by a more comprehensive analyses of liver samples through proteomic analyses (Chapter 6). Finally, a brief overview of main findings and future recommendations are provided in Chapter 7.

1.5   References List

Aktipis, C.A., and Nesse, R.M. (2013). Evolutionary foundations for cancer biology. Evol Appl *6,* 144-159.

Beck, S., and Ng, T. (2014). C2c: turning cancer into chronic disease. Genome Medicine *6,* 1.

Blagoev, K.B. (2016). Theoretical Physics and Cancer Research. Bulletin of the American Physical Society

Center, M.M., Jemal, A., Lortet-Tieulent, J., Ward, E., Ferlay, J., Brawley, O., and Bray, F. (2012). International variation in prostate cancer incidence and mortality rates. Eur. Urol. *61,* 1079-1092.

Dolgin, E. (2014). The mathematician versus the malignancy. Nature *201,* 4.

Drake, N. (2011). Forty years on from Nixon's war, cancer research'evolves'. Nat. Med. *17,* 757-757.

Dvorak, H.F. (1986). Tumors: wounds that do not heal. N. Engl. J. Med. *315,* 1650-1659.

Enriquez-Navas, P.M., Wojtkowiak, J.W., and Gatenby, R.A. (2015). Application of Evolutionary Principles to Cancer Therapy. Cancer Res. *75,* 4675-4680.

Gatenby, R.A., Brown, J., and Vincent, T. (2009). Lessons from applied ecology: cancer control using an evolutionary double bind. Cancer Res. *69,* 7499-7502.

Gatenby, R.A., Gillies, R.J., and Brown, J.S. (2011). Of cancer and cave fish. Nat. Rev. Cancer. *11,* 237-238.

Gatenby, R.A. (2009). A change of strategy in the war on cancer. Nature *459,* 508-509.

Goldstein, I., Madar, S., and Rotter, V. (2012). Cancer research, a field on the verge of a paradigm shift? Trends Mol. Med. *18,* 299-303.

Hanahan, D. (2014). Rethinking the war on cancer. Lancet *383,* 558-563.

Kuhn, T.S. (1977). Objectivity, value judgment, and theory choice. Arguing about Science 74-86.

Magee, J.A., Piskounova, E., and Morrison, S.J. (2012). Cancer stem cells: impact, heterogeneity, and uncertainty. Cancer Cell. *21,* 283-296.

Malagon, T., Drolet, M., Boily, M.C., Laprise, J.F., and Brisson, M. (2015). Changing inequalities in cervical cancer: modeling the impact of vaccine uptake, vaccine herd effects, and cervical cancer screening in the post-vaccination era. Cancer Epidemiol. Biomarkers Prev. *24,* 276-285.

Merlo, L.M., Pepper, J.W., Reid, B.J., and Maley, C.C. (2006). Cancer as an evolutionary and ecological process. Nat. Rev. Cancer *6,* 924-935.

Miller, K.D., Siegel, R.L., Lin, C.C., Mariotto, A.B., Kramer, J.L., Rowland, J.H., Stein, K.D., Alteri, R., and Jemal, A. (2016). Cancer treatment and survivorship statistics, 2016. CA Cancer J. Clin. *66*, 271-289.

Nowell, P.C. (1976). The clonal evolution of tumor cell populations. Science *194,* 23-28.

Pasquier, E., Kavallaris, M., and André, N. (2010). Metronomic chemotherapy: new rationale for new directions. Nat. Rev. Clin. Oncol. *7,* 455-465.

Phillips, J.L., and Currow, D.C. (2010). Cancer as a chronic disease. Collegian *17,* 47-50.

Popper, K. (2009). Science: Conjectures and refutations. The Philosophy of Science: An Historical Anthology *471,*

Sager, R. (1985). Genetic suppression of tumor formation. Adv. Cancer Res. *44,* 43-68.

Siegel, R.L., Miller, K.D., and Jemal, A. (2016). Cancer statistics, 2016. CA: A Cancer Journal for Clinicians *66,* 7-30.

Taylor, T.B., Johnson, L.J., Jackson, R.W., Brockhurst, M.A., and Dash, P.R. (2012). First steps in experimental cancer evolution. Evol. Appl. *6*, 535-548.

Wu, A., Liao, D., and Austin, R. (2015). Evolutionary game theory in cancer: first steps in prediction of metastatic cancer progression? Future Oncol. *11,* 881-883.

Chapter 2

In this chapter, an introduction to the distinction between tolerance and resistance (T/R) is provided. We also discuss the application of this paradigm within an oncological context and point out the utility of distinguishing between pathology driven by tumour load, versus the noxious phenotype of cancer, and discuss potential application of the T/R framework.

2.1   Introduction

Humans play host to a vast array of pathogens ranging in complexity from single-celled prokaryotes to multicellular invertebrates. With the singular exception of viruses and certain neglected tropical diseases (Feasey et al., 2010), most classes of pathogens can be treated effectively with tolerable side effects. Yet, despite the political will driving a concerted global effort, marginal (though perceptible) progress has been made in the War on Cancer (Haber et al., 2011; Siegel et al., 2013). One aspect contributing to the comparatively poor progress in managing cancer relates to the severe collateral damage associated with current treatment modalities (Chen et al., 2007; Lord and Ashworth, 2012; Monsuez et al., 2010; Prasanna et al., 2012). In turn, treatment toxicity reflects the phylogenetic relationship we share with cancer: since vertebrates and invertebrates diverged more than half a billion years ago (Smith et al., 2013), the most related pathogen, being an invertebrate, would have shared a common ancestor no more recently than this demarcated timespan (i.e. 0.5 billion years ago). In contrast, cancer is host-derived, implying an immediate common ancestor. Although genetic drift and diverging selective pressure progressively diversify the molecular machinery of pathogens, cancer shares the vast majority of its vital apparatus with its host. Consequently, what might inflict harm on cancer cells will invariably also injure the host.

An additional challenge posed by neoplastic infections takes form in the almost universal development of drug resistance (Gillet and Gottesman, 2012; Gillies et al., 2012; Knight et al., 2010). This process is well exemplified by targeted therapy. In a handful of cases, cancer arises due to a mutated protein within the receptor tyrosine kinase-signalling pathways (Gschwind et al., 2004; Knight et al., 2010) which can be targeted with superb specificity. However, cancer cells often become resistant to therapeutic intervention by either mutating ligand targets of

therapeutics or via alternative activation of redundant signalling pathways (Wilson et al., 2012). Indeed, it has been pointed out that the "much acclaimed success in the development of targeted therapy often provides just a few months of survival advantage to patients with late-stage cancer" (Wan et al., 2013). In addition, many cancer cells simply do not possess the same (or easily drugable) targets (Garraway and Lander, 2013).

Thus, the evolvability of cancer in conjunction with an unfavourable therapeutic index associated with most treatment modalities has greatly impeded progress in the development of effective cancer therapy. Indeed, some deem the current paradigm to be worn out and have expressed the need for a change in tactics if we are to circumvent the persistent difficulties faced in the clinical setting (Gatenby, 2009; Goldstein et al., 2012). One promising approach consists of transferring principles and concepts developed in other fields of study to oncology. For example, much interest has been generated in applying more than a century of insight gained from studying ecological systems to oncological problems as cancer recapitulates many of the same interactions seen in ecological systems (Aktipis and Nesse, 2013; Gatenby et al., 2009; Gatenby et al., 2011; Merlo et al., 2006; Nowell, 1976; Taylor et al., 2012).

Here, we develop a concept predominantly studied in ecology and implement it within an oncological context. During an infection, a host not only has to counteract the spread and dissemination of a pathogen, but also need to deal with the negative consequences associated with an infection which is referred to as tolerance. Resistance on the other hand, describes the host's ability to antagonise the proliferation of pathogens. Similarly, the antagonistic relationship between host and tumour demonstrates comparable characteristics. In particular, disease is not only dependent on tumour load, but also on the host's capacity to accommodate homeostatic challenges imposed by the tumour. A brief outline of tolerance and resistance is provided, focusing on parameters and methodological adaptation in an oncological context. It is also argued that this approach can be expanded. Indeed, it has been noted that, although tolerance and resistance express host performance in dealing with an infection, "there might be some kind of interaction between host genotype and parasite genotype" (Little et al., 2010; Råberg et al., 2009), thus indicating that tolerance and resistance should have a functional counterpart within the pathogen. Indeed, the terms tolerance and resistance both imply the existence of an exogenous factor which is being tolerated or resisted. We define these pathogen-derived factors as virulence and pathogenicity. Hence, the disease state manifests as

an interaction between these host and cancer factors: tolerance, resistance, pathogenicity and virulence. This approach have implications in marker identification (e.g. cancer cachexia) and the development of novel approaches to cancer therapies (e.g. tolerance-promoting or anti-pathogenicity therapeutics).

2.2 Tolerance and resistance: An immunological paradigm

Resistance refers to the host's ability to reduce or eliminate the infectious agent, whereas tolerance, on the other hand, denotes a host's ability to accommodate a given pathogen load (i.e. to reduce the health penalty incurred 'per unit pathogen'). More precisely, tolerance is defined as the slope of a regression line plotted with pathogen load as the independent variable and health (or some other performance parameter as a proxy) as the dependent variable. The distinction between a host's ability to tolerate a pathogen versus resistance has long been realised by plant breeders and pathologists. This concept has, however only recently been explored in animal models, first by Råberg (Råberg et al., 2007) who demonstrated that different mice strains varied in their ability to tolerate and resist a panel of *Plasmodium* strains.

The demarcation between tolerance and resistance as two parallel immunological strategies also impose interesting consequences. As an example, immunologists have long taken note of the fact that most infections result in vastly different disease states in members of the same population: it is estimated that, for every symptomatic cholera infection, between three and 100 individuals experience asymptomatic infection (King et al., 2008). Similarly, certain individuals exhibit an extraordinary asymptomatic carrying capacity for malaria parasites (Boutlis et al., 2006). Indeed, an empirical relationship has been observed for some infections, which suggests that 80% (or occasionally more) of infections are caused by 20% (or less) of carriers (Lau et al., 2013; Woolhouse et al., 1997). The difference in disease progression may partially be explained by differences in the host's immunological strategies in both tolerance and resistance.

In essence, the T/R framework describes how a host manages an antagonistic relationship with a pathogen. As is argued here, this established framework (see (Ayres and Schneider, 2012; Medzhitov et al., 2012; Råberg et al., 2009; Schneider and Ayres, 2008) for cardinal reviews in the field) could also be applied to host-tumour systems which recapitulate similar antagonistic dynamics.

2.3   Resistance within an oncological context

"[R]esistance is typically measured as the inverse of parasite burden" (Råberg et al., 2007). However, this approach may limit the kind of analysis conducted on the data captured. For instance, it has been pointed out that a trade-off between tolerance and resistance cannot be investigated with this quantification approach as "resistance and tolerance are not independent of one another, given that tolerance has parasite burden as the denominator" (Rohr et al., 2010). Thus, it may be advantageous to make use of other metrics.

Tumour growth is often fitted to a logistic growth function (**Figure 2.1**). Biologically, this growth curve provides three parameters of interest. The *carrying capacity* (maximum tumour volume -K) represent the tumour burden at which tumour growth becomes stunted. An example of a factor that may impact on the carrying capacity include inter-cell competition: as the tumour reaches a certain size, cells start competing for resources (e.g. niche space close to capillaries). Secondly, a *lag phase* describes the latent period before exponential growth. This interval may represent the duration wherein cells undergo molecular 'retooling' as they adapt to *in vivo* conditions. Occasionally, this lag period can be extensive, possibly reflecting a period during which clonal selection may take place: even commercially available cell lines exhibit at least some genetic variation (e.g. differences in karyotypes (Chang and Delany, 2004) which may affect tumorigenicity *in vivo* (Masramon et al., 2006). Finally, the slope of the log-linear growth (LLG) phase represents the maximum growth rate of the tumour *in vivo*. Thus, two tumours with different LLG-slopes have different growth rates. This then also provides a means of comparing the ability of two therapeutic strategies to retard tumour growth.
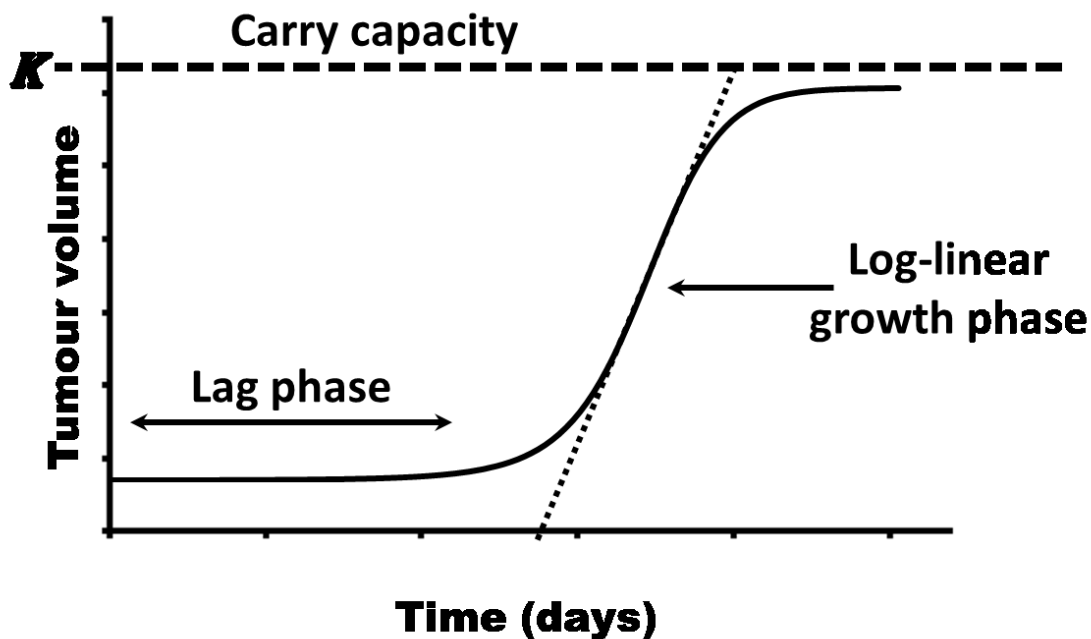
Figure 2.1. Expression of virulence as the maximum growth rate (i.e. the slope of the log-linear growth phase) render it possible to compare differences between different host-tumours systems in a reproducible manner.

Though a logistical growth curve is usually used to model tumour growth within a clinical setting, exponential growth closely approximate tumour growth if tumours are small (i.e. in the log-linear growth phase). This fact allows for a practical adaptation to simplify analysis: if the growth kinetics of the tumour is modelled by an exponential curve, the log of the function will provide a linearized data set. Simple linear regression can subsequently be performed on data from groups and slopes can be compared (**Figure 2.2**). Thus, resistance between hosts infected with a similar cancer can be rated by comparing the LLG-slope of each system, where shallow slopes would imply higher resistance. This approach can be illustrated in a hypothetical example where two groups of tumour-bearing mice each receive two different chemotherapeutic regiments, "Chemo A" and "Chemo B" (**Figure 2.2**). The tumour volume of each mouse is measured, log-transformed and plotted against time. The groups with the lowest slope (in this case, the Chemo B group) represent the intervention that inhibit tumour growth the most.
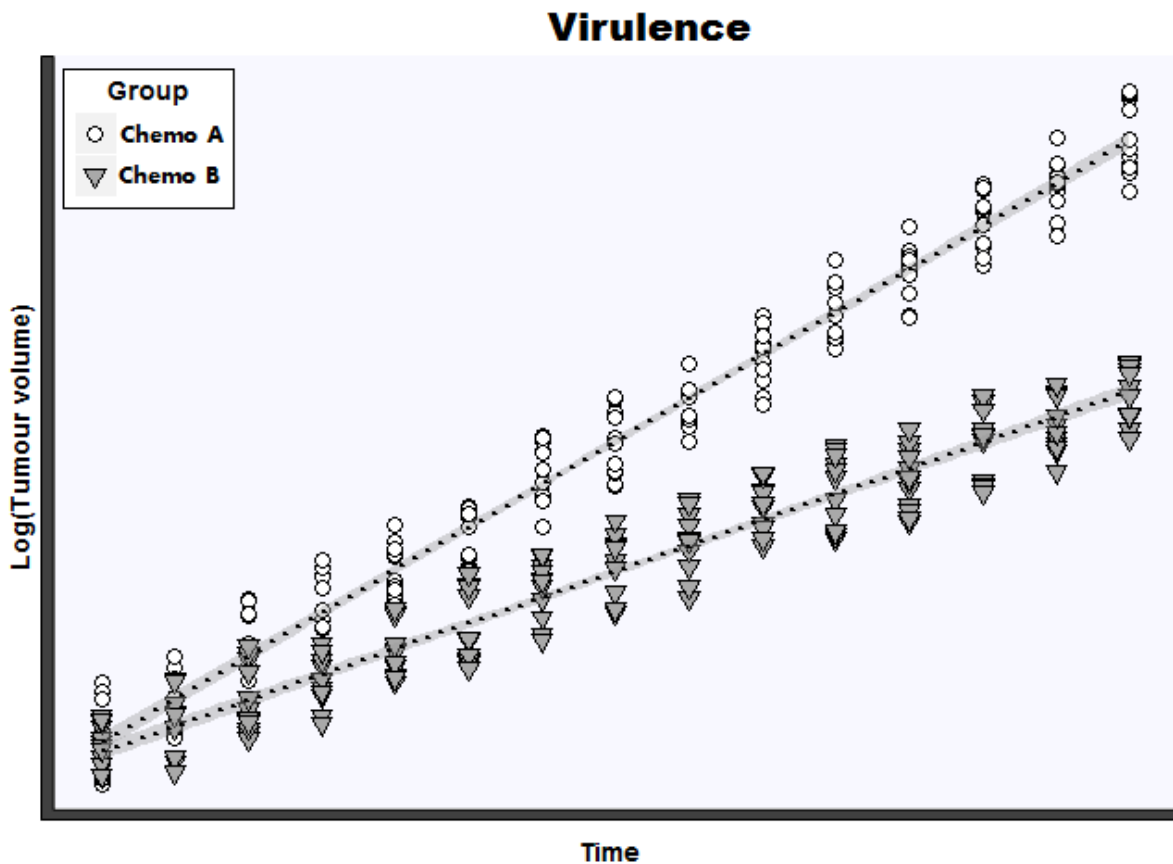
Figure 2.2. Hypothetical effect of chemotherapy on tumour growth in two groups of mice receiving different chemotherapeutic agents. Note, tumour growth is measured during the linear growth phase.

2.4   Tolerance within an oncological context

Similar to resistance, tolerance is expressed by the slope of a regression line. However, tolerance represents 'the unit health cost per unit tumour'. That is, tolerance is the slope of a regression line, with a metric of health as the response variable and tumour load as the predictor variable. As an example, the tolerance to an identical cancer in context of two different chemotherapeutic regimes (Chemo A and Chemo B) can be evaluated by comparing slopes of regressions lines (**Figure 2.3**). In the example, Chemo A exhibit a superior strategy for promoting health status in the face of tumour load.
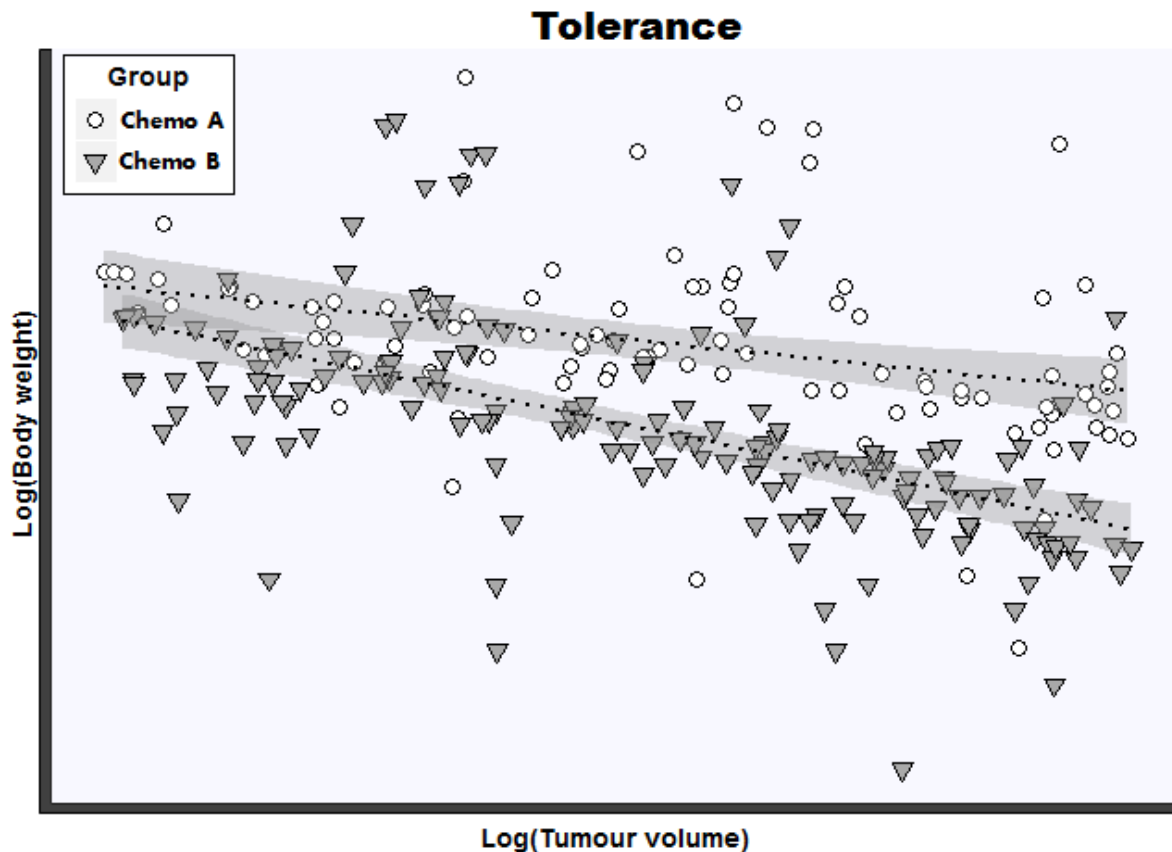
Figure 2.3. Hypothetical effect of a chemotherapy protocol on tolerance. Tolerance is expressed as the slope of a regression line fitted to the log-log plot of body weight (used as metric of health) against tumour volume. Comparative effect of chemotherapeutic efficacy is measured by comparing the slopes of these two groups' regression line.

Therapeutic efficacy of a given intervention can be expressed as a ratio between the tolerance and resistance of a given therapeutic intervention. As an example, Chemo A appears to be less effective in antagonising tumour growth than Chemo B (**Figure 2.2**). However, the tolerance slope of Chemo B is less negative than that of Chemo A (**Figure 2.3**). Thus, a benefit-to-harm ratio may be obtained by comparing regression slopes of resistance (**Figure 2.2**) to tolerance slopes (**Figure 2.3**).

Tolerance is a challenging parameter to quantify, as health is a complex trait. However, various markers of pathology can give an indication of health status. In the interest of rendering results comparable, criteria often associated with cancer cachexia may represent desirable health metrics (Fearon et al., 2011) . As an example, a decrease in body weight, and in particular muscle wasting, are robust indicators of cancer cachexia (Fearon et al., 2011; Martin et al., 2013). Serum markers generally used for prognostic function in cancer patients (Vigano et al.,

2000) are also candidates for quantifying tolerance. Certain acute-phase proteins may also be used, though it should be noted that the half-life of certain molecules is short and thus only presents a snapshot of the disease state (Cray et al., 2009; Epstein et al., 1999; Pang et al., 2010).

Also, applying more than one metric for each parameter can aid in validating results. However, problems may arise when metrics only partially corroborate each other. As an example, in a recent study by Li and co-workers (Li et al., 2013), it was demonstrated that mice may exhibit molecular signs of metabolic deregulation without other overt signs of pathology (e.g. reduction in body weight). In particular, tumour bearing mice demonstrated a healthy body mass, while analysis of serum markers indicated elevated triglycerides and reduced albumin/globulin ratios, indicative of metabolic deregulation and liver dysfunction (Li et al., 2013). Furthermore, elevated serum levels of C-reactive protein and transforming growth factor beta also indicate liver damage (leading to hepatomegaly which possibly inflated body weight, giving the false impression of good health status) (Li et al., 2013). Clearly, metrics of health should be carefully chosen, bearing in mind how the pathology may manifest. As an example, these factors must be taken into account when measuring body weight in diseases associated with oedema or accumulation of fluid.

In a clinical setting, it may be appropriate to measure a critical trait that is unique to each case. In a palliative context, the Edmonton Symptom Assessment System (ESAS) can be used to quantify "symptoms that have a larger subjective component" including depression, pain and general well-being (Richardson and Jones, 2009). However, since cancer cachexia manifests at a late stage of disease and also do not include the early onset pathology elating from chemotherapy, alternative metrics more suited to the initial phase of disease trajectory may be more appropriate. For example, the use of mTOR inhibitors to treat a number of cancers, is often associated with a number of haematological disorders (Xu and Tian, 2014; Zaytseva et al., 2012). In this regard, tolerance may be measured as the decline in blood counts. Similarly, liver function tests could be used as a metric of tolerance during radiation therapy of hepatic cancers. In fact, the T/R framework can also be applied in measuring therapeutic efficacy as the ratio between tumour inhibition versus adverse events or general therapeutic toxicities. Novel therapeutic strategies aimed at abrogating immune-inhibition often lead to various adverse events (Larkin et al., 2015). Here, reduction in tumour load (resistance) can be

compared to alternative metrics of tolerance such as the grade and frequency of adverse effects. Indeed, the T/R model could also be adapted to include well-being and psychological distress as a metric of tolerance when evaluating treatment efficacy.

2.5   Developing the T/R framework

Collectively, the T/R framework presents a reproducible approach with a number of applications (e.g. testing the therapeutic efficacy of an intervention strategy). However, this framework can also be expanded to tackle additional challenges. One application of the T/R framework includes the elucidation of pathogenic circuits that underlie the development of cancer cachexia, an often studied but poorly understood manifestation of cancer pathology, affecting up to 80% of patients with advanced-stage cancer (Ramos et al., 2004) and accounting for about 20% of all cancer-related fatalities (Loberg et al., 2007; Tisdale, 2002). Current failure to identify suitable markers are often ascribed to "population stratification, variable linkage disequilibrium and genotype misclassification" (Tan et al., 2011). In turn, a lack of markers preclude candidate targets to treat cancer cachexia. Consequently none of the current therapies provides a lasting improvement and there is an ongoing search for effective therapeutic targets (Tan et al., 2014). However, we suspect that two additional factors may contribute to the lack of suitable markers.

Firstly, disease may be driven by either tumour load, or the intrinsic noxious phenotype of the cancer. Indeed, mice xenograft models have demonstrated that cancer cells can differ profoundly in their ability to induce cachexia (Mori et al., 1991). This might be a major confounding factor, as a large tumour load may be driving a cachectic phenotype in one patient, whereas the noxious nature of the cancer may be a more prominent factor in another. However, the T/R framework allows for a finer resolution of the disease state and presents a method for identifying cancers that are more prone to inducing pathology.

Second, immunologists have taken note that much of the difficulty in identifying genetic markers for pathogen susceptibility could relate to the fact that pathogen heterogeneity is often taken for granted (Hill, 2012): Host susceptibility towards a pathogen is not only dependent on host genotype, but also that of the pathogen, implying that disease is a bigenomic phenomenon. As an example, innate resistance towards HIV infections observed in certain individuals is dependent on the host genotype as well as the strain of HIV (Saez-Cirion et al., 2009; Stephens,

2005). Similarly, there is a growing appreciation that cancer cachexia manifests as an "interaction between the host and cancer cells" (Gallagher et al., 2016): cancer-associated pathology may depend on the unique nature of stress a given tumour imposes as well as the ability of the host to accommodate such a particular stress. As an example, a highly glycolytic tumour may induce lactic acidosis in an individual with a set of metabolic polymorphisms, resulting in a decreased capacity to metabolise lactate. However, in another individual with normal metabolic capacity, a highly glycolytic tumour would not induce such pathology since adequate reserve capacity in lactate metabolism would buffer against such stress. Thus, the manifestation of pathology is dependent on both cancer (i.e. the nature of stress imposed) and the ability of the host to accommodate the specific stress imposed by cancer.

The T/R framework have been pointed out to be "host centric" (Råberg et al., 2009). In order to emphasise a demarcation between host-derived versus cancer-derived factors that impact on disease, two additional terms will be implemented. Firstly, the host contributes by either resisting the infection or tolerating a tumour. In turn, cancer cells exhibit a level of adaptation to the host environment that allows the spread and dissemination within the host, an ability that will be referred to as *virulence*, while also imposes stress on homeostatic mechanisms, i.e. exhibiting *pathogenicity*. Consequently, the disease progression depends on the resultant interaction between these factors (**Figure 2.4**): host resistance antagonise pathogen virulence, thus impacting on pathogen load. Similarly, the marginal cost of enduring a given pathogen load is dependent on the host ability to tolerate a particular pathogenic phenotype of a cancer.
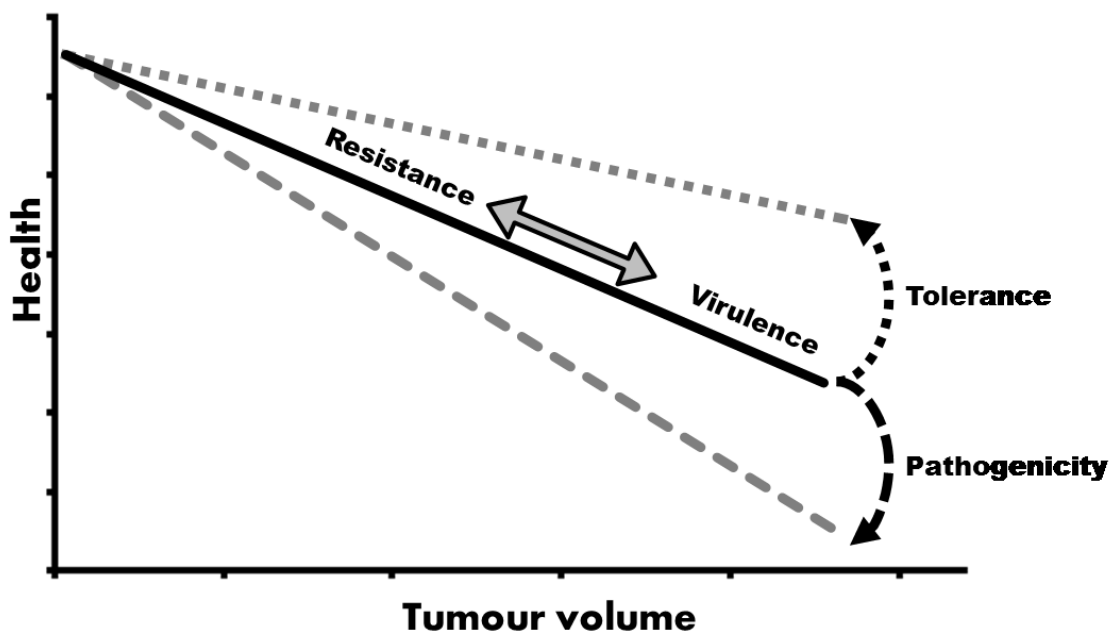
Figure 2.4. Schematic summary of how tolerance, pathogenicity, resistance and virulence affect the disease state.

In summary, the interaction between cancer and host factors dictates the disease trajectory (**Figure 2.5**). An interaction between host- and cancer-derived factors dictate the immediate disease trajectory in terms of directionality (pathogen load and health status providing 'coordinates') as well as magnitude of effect (how swiftly the disease would progress). Considering the disease state as a bigenomic phenotype implies that certain tolerance circuits may only exert a protective effect on health status in the face of a particular challenge and similarly, certain pathogenic factors would only manifest in pathology when placed in the context of a given host. Furthermore, host-derived factors need not be independent –a process that promotes tolerance may also promote resistance or alternatively, act antagonistically. Similarly, pathogen-derived factors may also exhibit pleiotropic effects.
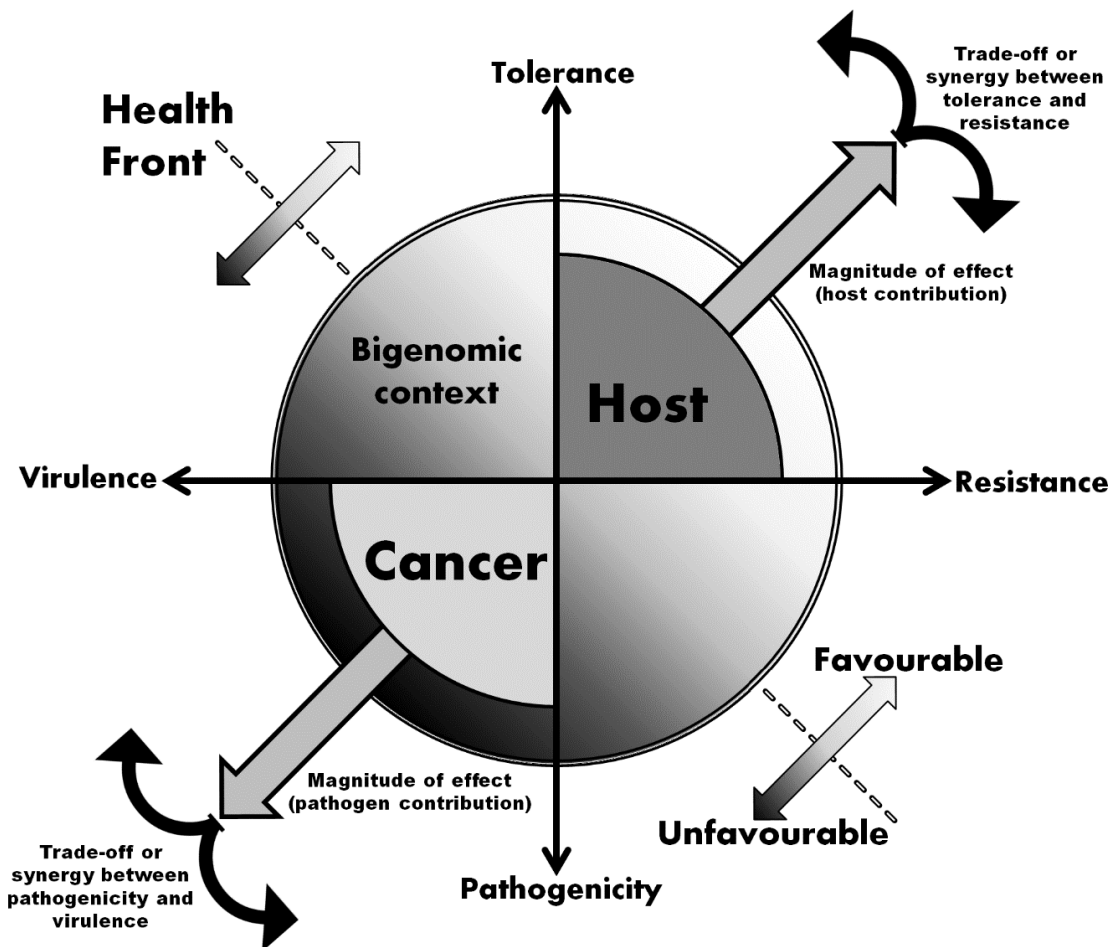
Figure 2.5. The impact on health status by both host and pathogen within the context provided by both interacting genomic landscapes (i.e. genetic and epigenetic modifications present within cancer and host).

2.6 Cancer Tolerance Pathways

It has also been demonstrated that the genetic alteration in cells that develop into cancer often induces an upregulation of the inflammatory response which is associated with aggressive malignancy and metastasis (Borrello et al., 2005). This is of interest since genes involved with immunology are typically highly polymorphic (Abi-Rached et al., 2011; Balkwill and Mantovani, 2001; Maizels, 2009; Robinson et al., 2013; Seruga et al., 2008; Smith and Humphries, 2009). Indeed, polymorphisms in various cytokines have long been known to be associated with the development and prognosis of cancer (Balkwill and Mantovani, 2001; Howell and Rose-Zerilli, 2007; Seruga et al., 2008). It is conceivable that certain individuals would exhibit an 'inflammatome' that would render them more resilient or susceptible to the development of inflammatory-associated pathologies. It is thus likely that numerous genetic

polymorphisms within genes regulating immune aspects can have an impact on the disease trajectory via the dominating effect of immune modulators on other systems. Similarly, metabolic polymorphisms are also likely to play a prominent role in mediating host tolerance to cancer. Polymorphisms in genes encoding glucose metabolism have already been shown to associate with clinical outcome in pancreatic cancer (Dong et al., 2011). Indeed, much of the diversity observed among the numerous metabolic interactions (>8 700) and concentrations of metabolites (~16 000) is brought about by underlying genetic variation (DeBerardinis and Thompson, 2012). However, metabolic anomalies may also manifest from host-cancer metabolic interactions (DeBerardinis and Cheng, 2009; Hensley et al., 2013; Martinez-Outschoorn et al., 2011; Rattigan et al., 2012).

It thus seems likely that metabolism, as affected by immune effectors such as cytokines, presents an excellent candidate system for exploring the complexities of cancer tolerance. Indeed, a metabolic-immunologic crosstalk is exemplified by cancer cachexia (Tsoli and Robertson, 2013). Furthermore, numerous polymorphisms within metabolic and immune structures provide a rich source of variation, potentially explaining much of the heterogeneous disease trajectories observed. Addressing this complexity, "candidate atrogenes", expression signatures of sets of genes involved in muscle wasting during cancer cachexia, have been identified in an omics approach (Gallagher et al., 2016). Carefully designed experiments, capturing necessary data (pathogen load and accurate metrics of health) may identify candidate systems that would point the way towards novel treatment strategies.

2.7   Investigating cancer tolerance and pathogenicity

Considering the disease state as a bigenomic phenotype imply that two distinct hosts (different genotypes) may respond differently to an identical cancer, since pathology does not only manifest from the stress imposed by the cancer, but also as a result of the host response to such a stress. This view is indeed supported in rodent models, where different strains of rodents respond differently to identical tumours. As an example, similar tumours in different animal strains (Walker carcinoma on Sprague-Dawley and Wistar Rats (Jensen and Muntzing, 1970), illustrated variation in resistance to cancer across strains. Conversely, challenging similar strains of mice with different tumours demonstrate variation in cancer pathogenicity. In this regard, Mori and co-workers (Mori et al., 1991) transplanted four different melanoma tumours

into nude mice, observed that certain tumours rapidly induced weight loss with the manifestation of cachexia-like symptoms whereas others did not.

These observations suggest that cancer pathology is dependent on host genotype (i.e. rodent strain) as well as cancer 'genotype'. If the developing pathology associated from cancer is dependent on resilience of the host to the stress imposed by the cancer, markers for the developing pathology should match: a susceptibility marker would only become apparent in a host susceptible to a given stress. Thus, the current approach for identifying "cachexia prone genotypes" based on association of host genotype with cachectic phenotype (Johns et al., 2014) neglect the fact that the particular genotype of the cancer also impact on the development of cancer cachexia. As a hypothetical example, a tumour excreting high levels of TNF will affect two different hosts with different TNF receptor polymorphisms differently. In particular, the effect of TNF on cachexia will only be apparent (and relevant) in hosts that express a receptor with high affinity to TNF. It is thus a necessity to evaluate the role of cancer markers in context of the host genotype.

A more structured approach can be followed to identify host markers that would render a host susceptible to a particular cancer. As an example, the contributing effect of a given cytokine (e.g. TNF) can be investigated by upregulating cytokine expression in cancer cells, and transplanting these cancer cells in hosts either lacking a given receptor (e.g. TNFR $^{-/-}$ mice), or are receptor positive (TNFR$^{+/+}$ mice). This approach is illustrated by a simplified experiment (**Figure 2.6**) consisting of two mice populations, arbitrarily designated as '+/+' and '-/-' to demarcate distinctive genotypes (e.g. *TNFR* polymorphism), as well as two different cancer cell lines (CCL), 'A' and 'B' (e.g. denoting TNF expression). Note that, whether a host or cancer derived attribute is being studied depends on the origin of variation within the system: host derived attributes (tolerance and resistance) are evaluated by comparing different host performances to similar CCL. In contrast, pathogenicity and virulence are cancer-derived traits and are therefore inspected when comparing CCL A and B within a similar host-context. Thus, the relative pathogenicity of a cancer cell in a mouse strain can be expressed as the slope of a regression line obtained from plotting a health metric (e.g. bodyweight) against tumour volume. For example, if CCL A induces greater pathology in +/+ mice than CCL B, CCLA would be considered more pathogenic. IF -/- mice develop less pathology to CCL B than +/+ mice, -/- mice would be considered more tolerant.
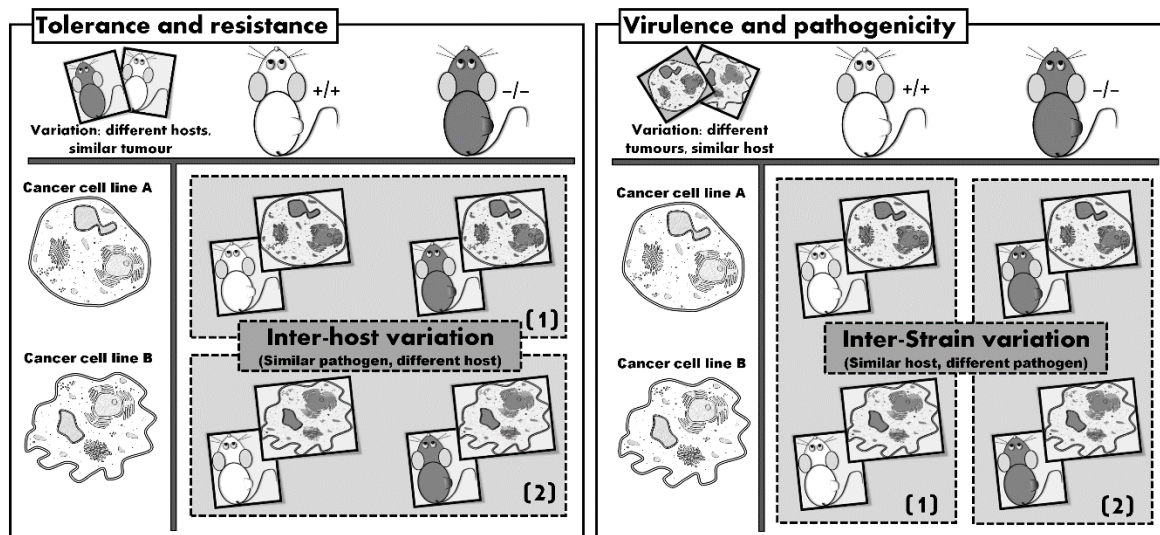
Figure 2.6. Experimental setup: discriminating between host- and pathogen-derived factors.

This approach can be used to investigate the pathogenic effects of a candidate gene (e.g. comparing pathogenicity of cancer cells expressing a candidate gene with an identical cell line in which the gene of interest has been knocked out) or be exploited in a data-driven approach (e.g. by mutagenizing a population of cancer cells, comparing pathogenicity between populations, and correlating genotype with phenotype (Chen et al., 2015). Similarly, instead of evaluating the effect of host genotype on tolerance and resistance, therapeutic interventions could be evaluated (**Figure 2.2**). Two chemotherapeutic agents may be equally effective at eradicating cancer cells, but differ in their toxicity. For example, leukaemia resistance can be measured by the number of circulating blast (a proxy for cancer load), whereas anaemia (or related blood count) provides a metric of tolerance. In this context, efficacy can be expressed as the T/R ratio, i.e. the number of mature blood cells divided by the number of blasts. In particular, similar to the comparison between host and cancer (TNF expression by cancer and host receptor affinity), intervention therapy may exhibit a cancer-specific efficacy (that is, a particular therapy's effectiveness depends on the cancer cell type).

2.8   Implications of T/R framework

The T/R framework argues for a more in-depth approach to cancer pathology. It is likely that the poor performance in identifying good markers for cancer pathologies such as cachexia may result from the way the disease state is viewed. The T/R framework provides the operational resolution to distinguish between pathology manifesting from extensive tumour burden, versus

cancers intrinsically expressing a more pathogenic phenotype. In addition, considering the disease state as a bigenomic phenotype implies that certain tolerance mechanisms may only exert a protective effect on health status in the face of a particular challenge and similarly, certain pathogenic factors may only manifest in pathology when placed in the context of a given host. Taking these factors into consideration, we hypothesise that the T/R framework may provide a novel methodology in studying the nature of cancer pathology. In addition, therapies aimed at enhancing host tolerance would not have a negative impact on cancer fitness and as such do not invoke counter-evolutionary innovation (Roy and Kirchner, 2000). Similarly, therapies decreasing pathogenicity should also avoid evolutionary strategies that undermine therapeutic intervention. As such, tolerogenic and anti-pathogenic therapies would be expected to remain effective for longer.

Furthermore, reducing the adverse effects associated with neoplastic infection would be likely to enhance patients' survivability. Indeed, health status as reflected in weight loss has long been realized to be a powerful prognostic factor (Dewys et al., 1980). Additionally, therapies aimed at increasing tolerance in effect also help to reinforce reserve capacity of the patient and open additional potential therapeutic options, such as second- or third-line therapy. This is of particular relevance in more pathogenic cancers such as pancreatic tumours where patients seldom possess sufficient reserve capacity to endure the toxic side-effects of second-line therapies (Hidalgo, 2010). Similarly, recent development of immunotherapy (Larkin et al., 2015) has again brought attention to the possibility of mobilising the immune system in treating cancer. However, the immune system is often particularly adversely affected by chemotherapy (Zitvogel et al., 2011). This is no surprise as activated immune cells share common metabolic circuits often observed in cancerous cells (Maciver et al., 2008). In this regard, the T/R framework may aid in quantifying the detrimental effect of a given treatment modality by using an immunological metric (e.g. immune cell count) instead of health.

2.9   Conclusion

The fine-scale resolution on the disease state provided by the T/R framework points towards a number of interesting applications. Novel therapeutic interventions promoting tolerance or targeting cancer pathogenicity may enhance the survivability of patients or indeed even aid in redefining therapeutic endpoints. This is not to supplant current efforts on finding a cure for

cancer. Rather, T/R represents an augmented approach to a complex disease. Understanding how host–cancer interactions take shape may also aid in discovering novel biomarkers. Indeed, the T/R framework stresses the need to associate host-derived biomarkers with that of a cancer-specific factor. This undoubtedly implies greater effort with more refined study designs. However, this approach also holds the potential of providing biomarkers of unprecedented accuracy. In this regard, it has become clear that metabolic circuits are profoundly influenced by immunological structures – a crosstalk between systems that are likely to yield many mechanisms by which cancer pathology manifests. Accordingly these systems should enjoy top priority in research on cancer tolerance and pathology.

2.10   Future perspective

The primary goal of antineoplastic intervention is the complete elimination of cancer. However, being able to endure a large tumour load may hold therapeutic advantages where curative endpoints are not realistically perusable. Indeed, some have speculated that a potential future strategy might be in treating cancer "as a chronic manageable disease, such as diabetes and heart disease" (Folkman and Kalluri, 2004) and that "instead of focusing exclusively on a glorious victory, [we] should address the possible benefits of an uneasy stalemate in appropriate situations" (Fillon, 2012). Similarly, others "foresee a future in which the prevention of metastatic cancer will become a mainstream practice by managing MRD [i.e. minimal residual disease], and effective therapeutic agents and strategies will be available to turn fatal metastatic disease into a chronic condition" (Wan et al., 2013). Redefining the therapeutic endpoint as such would necessarily imply that the host must be more tolerant to the neoplastic infection and chemotherapeutic interventions. In addition, the T/R framework provides a mechanism by which therapeutic efficacy can be described by comparing the reduction in tumour load (resistance) versus the health cost (tolerance) of a given intervention. As an example, novel immuno-oncology interventions leading to an upregulation of the immune system often induce a range of adverse effects. Indeed, adverse effect caused discontinuation of therapy in 7.7% of the patients receiving nivolumab, 14.8% on ipilimumab and 36.4% of patients on both (Larkin et al., 2015). In this regard, the T/R framework represents a tool for evaluating therapeutic interventions that do more harm than good. Indeed, since chemotherapy is generally associated with cumulative side-effects, reducing tumour load at an excessive 'cost' in terms of health (or well-being) would be counterproductive.

2.11   Reference List

Abi-Rached, L., Jobin, M.J., Kulkarni, S., McWhinnie, A., Dalva, K., Gragert, L., Babrzadeh, F., Gharizadeh, B., Luo, M., and Plummer, F.A. (2011). The shaping of modern human immune systems by multiregional admixture with archaic humans. Science *334,* 89-94.

Aktipis, C.A., and Nesse, R.M. (2013). Evolutionary foundations for cancer biology. Evol. Appl. *6,* 144-159.

Ayres, J.S., and Schneider, D.S. (2012). Tolerance of infections. Annu. Rev. Immunol. *30,* 271-294.

Balkwill, F., and Mantovani, A. (2001). Inflammation and cancer: back to Virchow? Lancet *357,* 539-545.

Borrello, M.G., Alberti, L., Fischer, A., Degl'Innocenti, D., Ferrario, C., Gariboldi, M., Marchesi, F., Allavena, P., Greco, A., and Collini, P. (2005). Induction of a proinflammatory program in normal human thyrocytes by the RET/PTC1 oncogene. Proc. Natl. Acad. Sci. U. S. A. *102,* 14825-14830.

Boutlis, C.S., Yeo, T.W., and Anstey, N.M. (2006). Malaria tolerance–for whom the cell tolls? Trends Parasitol. *22,* 371-377.

Chang, H., and Delany, M.E. (2004). Karyotype stability of the DT40 chicken B cell line: macrochromosome variation and cytogenetic mosaicism. Chromosome Res. *12,* 299-307.

Chen, S., Sanjana, N.E., Zheng, K., Shalem, O., Lee, K., Shi, X., Scott, D.A., Song, J., Pan, J.Q., and Weissleder, R. (2015). Genome-wide CRISPR screen in a mouse model of tumor growth and metastasis. Cell *160,* 1246-1260.

Chen, Y., Jungsuwadee, P., Vore, M., Butterfield, D.A., and St Clair, D.K. (2007). Collateral damage in cancer chemotherapy: oxidative stress in nontargeted tissues. Mol. Interventions *7,* 147.

Cray, C., Zaias, J., and Altman, N.H. (2009). Acute phase response in animals: a review. Comp. Med. *59,* 517-526.

DeBerardinis, R.J., and Cheng, T. (2009). Q's next: the diverse functions of glutamine in metabolism, cell biology and cancer. Oncogene *29,* 313-324.

DeBerardinis, R.J., and Thompson, C.B. (2012). Cellular metabolism and disease: what do metabolic outliers teach us? Cell *148,* 1132-1144.

Dewys, W.D., Begg, C., Lavin, P.T., Band, P.R., Bennett, J.M., Bertino, J.R., Cohen, M.H., Douglass, H.O.,Jr, Engstrom, P.F., Ezdinli, E.Z*., et al.* (1980). Prognostic effect of weight loss prior to chemotherapy in cancer patients. Eastern Cooperative Oncology Group. Am. J. Med. *69,* 491-497.

Dong, X., Tang, H., Hess, K.R., Abbruzzese, J.L., and Li, D. (2011). Glucose metabolism gene polymorphisms and clinical outcome in pancreatic cancer. Cancer *117,* 480-491.

Epstein, F.H., Gabay, C., and Kushner, I. (1999). Acute-phase proteins and other systemic responses to inflammation. N. Engl. J. Med. *340,* 448-454.

Fearon, K., Strasser, F., Anker, S.D., Bosaeus, I., Bruera, E., Fainsinger, R.L., Jatoi, A., Loprinzi, C., MacDonald, N., and Mantovani, G. (2011). Definition and classification of cancer cachexia: an international consensus. Lancet Oncol. *12,* 489-495.

Feasey, N., Wansbrough-Jones, M., Mabey, D.C., and Solomon, A.W. (2010). Neglected tropical diseases. Br. Med. Bull. *93,* 179-200.

Fillon, M. (2012). Cancer and natural selection. J. Natl. Cancer. Inst. *104*, 1773–1774.

Folkman, J., and Kalluri, R. (2004). Cancer without disease. Nature *427,* 787-787.

Gallagher, I., Jacobi, C., Tardif, N., Rooyackers, O., and Fearon, K. Semin Cell Dev Biol. *54*, 92-103.

Garraway, L.A., and Lander, E.S. (2013). Lessons from the cancer genome. Cell *153,* 17-37.

Gatenby, R.A., Brown, J., and Vincent, T. (2009). Lessons from applied ecology: cancer control using an evolutionary double bind. Cancer Res. *69,* 7499-7502.

Gatenby, R.A., Gillies, R.J., and Brown, J.S. (2011). Of cancer and cave fish. Nat. Rev.Cancer *11,* 237-238.

Gatenby, R.A. (2009). A change of strategy in the war on cancer. Nature *459,* 508-509.

Gillet, J.P., and Gottesman, M.M. (2012). Overcoming multidrug resistance in cancer: 35 years after the discovery of ABCB1. Drug Resist Updat. *15,* 2-4.

Gillies, R.J., Verduzco, D., and Gatenby, R.A. (2012). Evolutionary dynamics of carcinogenesis and why targeted therapy does not work. Nat. Revi.Cancer *12,* 487-493.

Goldstein, I., Madar, S., and Rotter, V. (2012). Cancer research, a field on the verge of a paradigm shift? Trends Mol. Med. *18,* 299-303.

Gschwind, A., Fischer, O.M., and Ullrich, A. (2004). The discovery of receptor tyrosine kinases: targets for cancer therapy. Nat. Rev. Cancer. *4,* 361-370.

Haber, D.A., Gray, N.S., and Baselga, J. (2011). The evolving war on cancer. Cell *145,* 19-24.

Hensley, C.T., Wasti, A.T., and DeBerardinis, R.J. (2013). Glutamine and cancer: cell biology, physiology, and clinical opportunities. J. Clin. Invest. *123,* 3678-3684.

Hidalgo, M. (2010). Pancreatic cancer. N. Engl. J. Med. *362,* 1605-1617.

Hill, A.V. (2012). Evolution, revolution and heresy in the genetics of infectious disease susceptibility. Philos. Trans. R. Soc. Lond. B. Biol. Sci. *367,* 840-849.

Howell, W.M., and Rose-Zerilli, M.J. (2007). Cytokine gene polymorphisms, cancer susceptibility, and prognosis. J. Nutr. *137,* 194S-199S.

Jensen, G., and Muntzing, J. (1970). Differences in the growth of the Walker carcinoma in Sprague-Dawley and Wistar rats. Z. Krebsforsch. *74,* 55-58.

Johns, N., Tan, B., MacMillan, M., Solheim, T., Ross, J., Baracos, V., Damaraju, S., and Fearon, K. (2014). Genetic basis of interindividual susceptibility to cancer cachexia: selection of potential candidate gene polymorphisms for association studies. J. Genet. *93,* 893-916.

King, A.A., Ionides, E.L., Pascual, M., and Bouma, M.J. (2008). Inapparent infections and cholera dynamics. Nature *454,* 877-880.

Knight, Z.A., Lin, H., and Shokat, K.M. (2010). Targeting the cancer kinome through polypharmacology. Nat. Rev.Cancer *10,* 130-137.

Larkin, J., Chiarion-Sileni, V., Gonzalez, R., Grob, J.J., Cowey, C.L., Lao, C.D., Schadendorf, D., Dummer, R., Smylie, M., and Rutkowski, P. (2015). Combined nivolumab and ipilimumab or monotherapy in untreated melanoma. N. Engl. J. Med. *373,* 23-34.

Lau, L.L., Ip, D.K., Nishiura, H., Fang, V.J., Chan, K., Peiris, J.M., Leung, G.M., and Cowling, B.J. (2013). Heterogeneity in Viral Shedding Among Individuals With Medically Attended Influenza A Virus Infection. J. Infect. Dis. *207,* 1281-1285.

Li, F., Patterson, A.D., Krausz, K.W., Jiang, C., Bi, H., Sowers, A.L., Cook, J.A., Mitchell, J.B., and Gonzalez, F.J. (2013). Metabolomics reveals that tumor xenografts induce liver dysfunction. Mol. Cell. Proteomics *12,* 2126-2135.

Little, T.J., Shuker, D.M., Colegrave, N., Day, T., and Graham, A.L. (2010). The coevolution of virulence: tolerance in perspective. PLoS Pathog. *6,* e1001006.

Loberg, R.D., Bradley, D.A., Tomlins, S.A., Chinnaiyan, A.M., and Pienta, K.J. (2007). The lethal phenotype of cancer: the molecular basis of death due to malignancy. CA: A Cancer J. Clin. *57,* 225-241.

Lord, C.J., and Ashworth, A. (2012). The DNA damage response and cancer therapy. Nature *481,* 287-294.

Maciver, N.J., Jacobs, S.R., Wieman, H.L., Wofford, J.A., Coloff, J.L., and Rathmell, J.C. (2008). Glucose metabolism in lymphocytes is a regulated process with significant effects on immune cell function and survival. J. Leukoc. Biol. *84,* 949-957.

Maizels, R.M. (2009). Parasite immunomodulation and polymorphisms of the immune system. J Biol. *8,* 62.

Martin, L., Birdsell, L., Macdonald, N., Reiman, T., Clandinin, M.T., McCargar, L.J., Murphy, R., Ghosh, S., Sawyer, M.B., and Baracos, V.E. (2013). Cancer cachexia in the age of obesity: skeletal muscle depletion is a powerful prognostic factor, independent of body mass index. J. Clin. Oncol. *31,* 1539-1547.

Martinez-Outschoorn, U.E., Pestell, R.G., Howell, A., Tykocinski, M.L., Nagajyothi, F., Machado, F.S., Tanowitz, H.B., Sotgia, F., and Lisanti, M.P. (2011). Energy transfer in "parasitic" cancer metabolism: mitochondria are the powerhouse and Achilles' heel of tumor cells. Cell Cycle *10,* 4208-4216.

Masramon, L., Vendrell, E., Tarafa, G., Capella, G., Miro, R., Ribas, M., and Peinado, M.A. (2006). Genetic instability and divergence of clonal populations in colon cancer cells in vitro. J. Cell. Sci. *119,* 1477-1482.

Medzhitov, R., Schneider, D.S., and Soares, M.P. (2012). Disease tolerance as a defense strategy. Science *335,* 936-941.

Merlo, L.M., Pepper, J.W., Reid, B.J., and Maley, C.C. (2006). Cancer as an evolutionary and ecological process. Nat. Rev. Cancer *6,* 924-935.

Monsuez, J., Charniot, J., Vignat, N., and Artigou, J. (2010). Cardiac side-effects of cancer chemotherapy. Int. J. Cardiol. *144,* 3-15.

Mori, M., Yamaguchi, K., Honda, S., Nagasaki, K., Ueda, M., Abe, O., and Abe, K. (1991). Cancer cachexia syndrome developed in nude mice bearing melanoma cells producing leukemia-inhibitory factor. Cancer Res. *51,* 6656-6659.

Nowell, P.C. (1976). The clonal evolution of tumor cell populations. Science *194,* 23-28.

Pang, W.W., Abdul-Rahman, P.S., Wan-Ibrahim, W.I., and Hashim, O.H. (2010). Can the acute-phase reactant proteins be used as cancer biomarkers? Int. J. Biol. Markers *25,* 1-11.

Prasanna, P.G., Stone, H.B., Wong, R.S., Capala, J., Bernhard, E.J., Vikram, B., and Coleman, C. (2012). Normal tissue protection for improving radiotherapy: where are the gaps? Transl. Cancer Res. *1,* 35.

Råberg, L., Graham, A.L., and Read, A.F. (2009). Decomposing health: tolerance and resistance to parasites in animals. Phil. Trans. R. Soc. B. *364,* 37-49.

Råberg, L., Sim, D., and Read, A.F. (2007). Disentangling genetic variation for resistance and tolerance to infectious diseases in animals. Science *318,* 812-814.

Ramos, E.J., Suzuki, S., Marks, D., Inui, A., Asakawa, A., and Meguid, M.M. (2004). Cancer anorexia-cachexia syndrome: cytokines and neuropeptides. Curr. Opin. Clin. Nutr. Metab. Car. *7,* 427-434.

Rattigan, Y.I., Patel, B.B., Ackerstaff, E., Sukenick, G., Koutcher, J.A., Glod, J.W., and Banerjee, D. (2012). Lactate is a mediator of metabolic cooperation between stromal carcinoma associated fibroblasts and glycolytic tumor cells in the tumor microenvironment. Exp. Cell Res. *318,* 326-335.

Richardson, L.A., and Jones, G.W. (2009). A review of the reliability and validity of the Edmonton Symptom Assessment System. Curr. Oncol. *16,* 53-64.

Robinson, J., Halliwell, J.A., McWilliam, H., Lopez, R., and Marsh, S.G. (2013). IPD—the Immuno Polymorphism Database. Nucleic Acids Res. *41,* D1234-D1240.

Rohr, J.R., Raffel, T.R., and Hall, C.A. (2010). Developmental variation in resistance and tolerance in a multi-host–parasite system. Funct. Ecol. *24,* 1110-1121.

Roy, B., and Kirchner, J. (2000). Evolutionary dynamics of pathogen resistance and tolerance. Evolution *54,* 51-63.

Saez-Cirion, A., Sinet, M., Shin, S.Y., Urrutia, A., Versmisse, P., Lacabaratz, C., Boufassa, F., Avettand-Fenoel, V., Rouzioux, C., Delfraissy, J.F.*, et al.* (2009). Heterogeneity in HIV suppression by CD8 T cells from HIV controllers: association with Gag-specific CD8 T cell responses. J. Immunol. *182,* 7828-7837.

Schneider, D.S., and Ayres, J.S. (2008). Two ways to survive infection: what resistance and tolerance can teach us about treating infectious diseases. Nat. Rev. Immunol. *8,* 889-895.

Seruga, B., Zhang, H., Bernstein, L.J., and Tannock, I.F. (2008). Cytokines and their relationship to the symptoms and outcome of cancer. Nat. Rev. Cancer *8,* 887-899.

Siegel, R., Naishadham, D., and Jemal, A. (2013). Cancer statistics, 2013. CA Cancer. J. Clin. *63,* 11-30.

Smith, A.J., and Humphries, S.E. (2009). Cytokine and cytokine receptor gene polymorphisms and their functionality. Cytokine Growth Factor Rev. *20,* 43-59.

Smith, J.J., Kuraku, S., Holt, C., Sauka-Spengler, T., Jiang, N., Campbell, M.S., Yandell, M.D., Manousaki, T., Meyer, A., Bloom, O.E*., et al.* (2013). Sequencing of the sea lamprey (Petromyzon marinus) genome provides insights into vertebrate evolution. Nat. Genet. *45,* 415-21, 421e1-2.

Stephens, H.A. (2005). HIV-1 diversity versus HLA class I polymorphism. Trends Immunol. *26,* 41-47.

Tan, B.H., Ross, J.A., Kaasa, S., Skorpen, F., and Fearon, K.C. (2011). Identification of possible genetic polymorphisms involved in cancer cachexia: a systematic review. J. Genet. *90,* 165-177.

Tan, C.R., Yaffee, P.M., Jamil, L.H., Lo, S.K., Nissen, N., Pandol, S.J., Tuli, R., and Hendifar, A.E. (2014). Pancreatic cancer cachexia: a review of mechanisms and therapeutics. Front. Physiol. *5,*

Taylor, T.B., Johnson, L.J., Jackson, R.W., Brockhurst, M.A., and Dash, P.R. (2012). First steps in experimental cancer evolution. Evol. Appl. *6*, 535-548

Tisdale, M.J. (2002). Cachexia in cancer patients. Nat. Rev. Cancer *2,* 862-871.

Tsoli, M., and Robertson, G. (2013). Cancer cachexia: malignant inflammation, tumorkines, and metabolic mayhem. Tren. Endo. Metab. *24,* 174-183.

Vigano, A., Bruera, E., Jhangri, G.S., Newman, S.C., Fields, A.L., and Suarez-Almazor, M.E. (2000). Clinical survival predictors in patients with advanced cancer. Arch. Intern. Med. *160,* 861-868.

Wan, L., Pantel, K., and Kang, Y. (2013). Tumor metastasis: moving new biological insights into the clinic. Nat. Med. *19,* 1450-1464.

Wilson, T.R., Fridlyand, J., Yan, Y., Penuel, E., Burton, L., Chan, E., Peng, J., Lin, E., Wang, Y., Sosman, J*., et al.* (2012). Widespread potential for growth-factor-driven resistance to anticancer kinase inhibitors. Nature *487,* 505-509.

Woolhouse, M.E., Dye, C., Etard, J., Smith, T., Charlwood, J., Garnett, G., Hagan, P., Hii, J., Ndhlovu, P., and Quinnell, R. (1997). Heterogeneities in the transmission of infectious agents: implications for the design of control programs. Proc. Natl. Acad. Sci. U. S. A. *94,* 338-342.

Xu, J., and Tian, D. (2014). Hematologic toxicities associated with mTOR inhibitors temsirolimus and everolimus in cancer patients: a systematic review and meta-analysis. Curr. Med. Res. Opin. *30,* 67-74.

Zaytseva, Y.Y., Valentino, J.D., Gulhati, P., and Evers, B.M. (2012). mTOR inhibitors in cancer therapy. Cancer Lett. *319,* 1-7.

Zitvogel, L., Kepp, O., and Kroemer, G. (2011). Immune parameters affecting the efficacy of chemotherapeutic regimens. Nat. Rev. Clin. Oncol. *8,* 151-160.

Chapter 3

This chapter outlines the first study to investigate the role of tolerance and resistance within an oncological setting. By inoculating mice with similar tumours, a comparison between cancers in terms of the tolerance and resistance effect can be assessed directly. Alternatively, the T/R framework can also be applied to investigate the effects of therapeutic intervention. As proof of this concept, both these approaches were implemented in this study.

3.1   Study design

The current study made use of 60 female C57BL/6 mice (five groups with n = 12), the chemotherapeutic agent doxorubicin (DXR) and two syngeneic cancer cell lines: EO771 mammary carcinoma and B16 melanoma (**Figure 3.1**). Two experiments were conducted. First, the effect of DXR on mice tolerance and resistance was investigated. This experiment involved a comparison between tumour (EO771) bearing mice receiving three cycles of high (5 mg/kg), low (2 mg/kg) dose DXR or vehicle control (Hanks balanced salt solution) once tumours were palpable (**Figure 3.2**). The second experiment compared the tolerance and resistance of C57BL/6 mice to EO771 mammary tumours versus B16 melanoma. Note that no chemotherapy was involved in the second experiment.
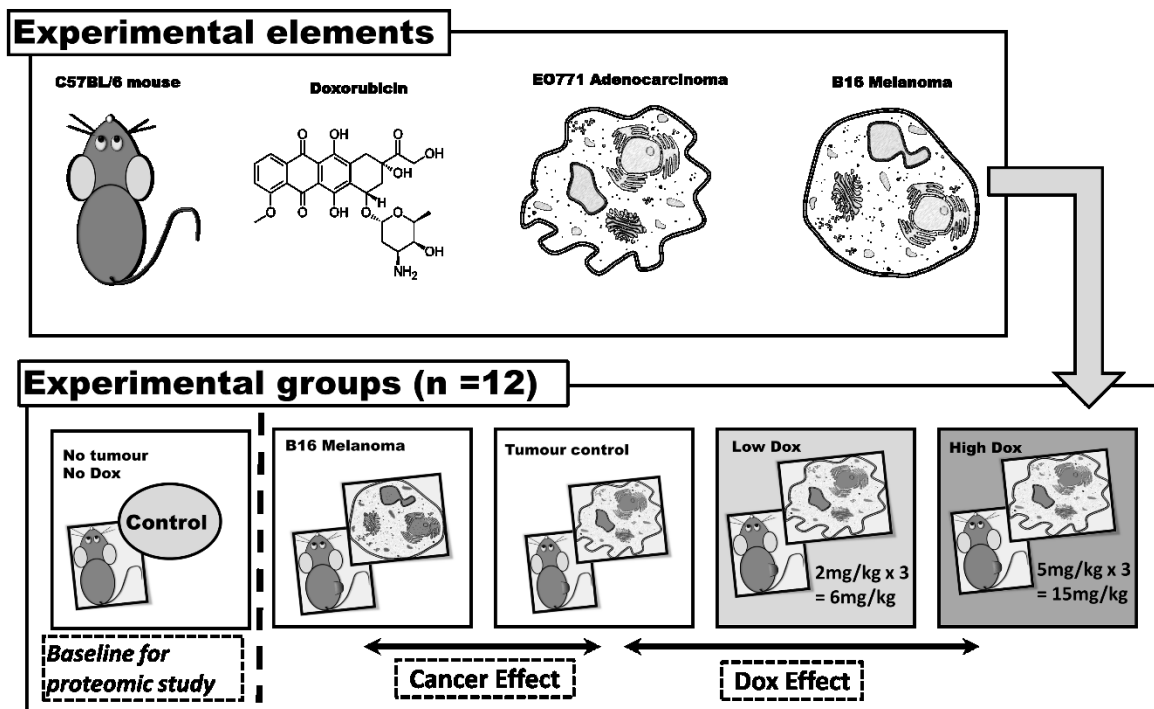
Figure 3.1. Study design and intervention groups.
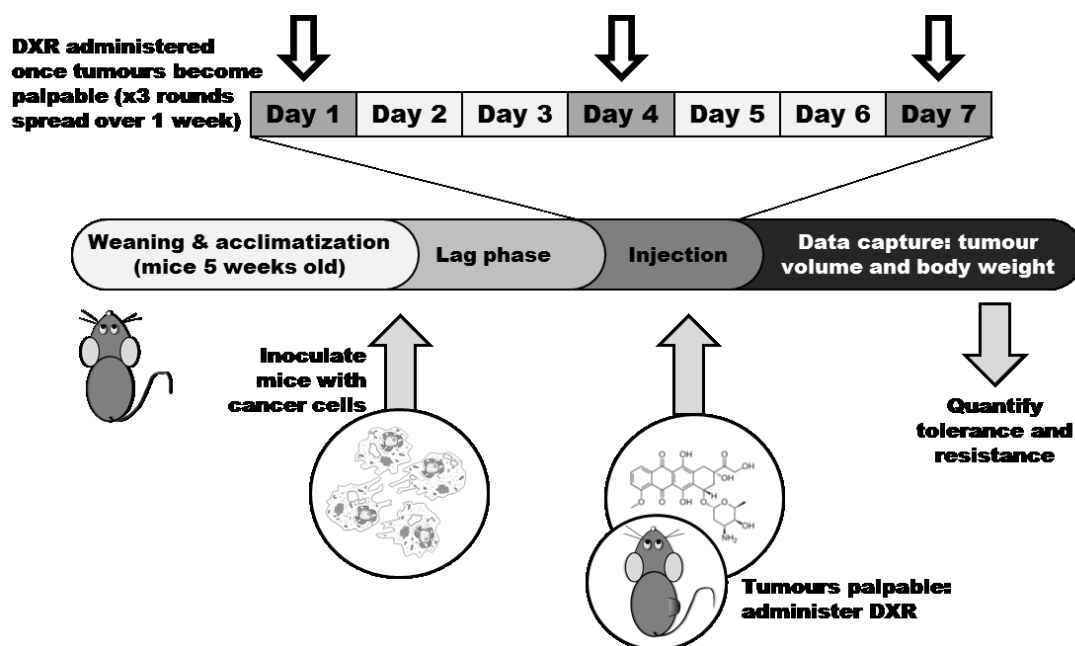
Figure 3.2. Experimental time line. DXR was not administered to mice injected with B16.

3.1.1 Routine cell culture: EO771 and B16

The EO771 cells (a generous gift from Fengzhi Li, Roswell Park Cancer Institute, Buffalo, New York, USA) and B16 cells (kindly provided by Prof. Lester M. Davids, University of Cape

Town, Cape Town, RSA) were maintained in similar conditions. Glutamax-DMEM (Celtic Molecular Diagnostics, Cape Town, South Africa) was supplemented with 10% foetal bovine serum (Sigma Chemical Co., St Louis, MO, USA). Cells grown as monolayer were incubated at 37°C in a humidified atmosphere (95% air and 5% CO_2) in T75 flasks (Greiner Bio One, Germany) to ~80% confluence. Cells were split (1:3) by washing cells in pre-warmed (37°C) Hanks balanced salt solution (HBSS) before incubating cells with 4 ml trypsin/EDTA (Sigma Chemical Co., St Louis, MO, USA) at 37°C for 7 minutes.

3.1.2 Animal husbandry

Weaning-age (4-5 weeks old) female C57BL/6 mice, reared under specified-pathogen-free conditions, were obtained from University of Cape Town's Research Animal Facility. Acquired mice were housed at the Animal Unit, Stellenbosch University, in individually ventilated cages (6-8 mice in a cage) at 22°C under 12-h light/dark cycle. Mice were allowed a one week acclimatisation period before being subjected to experimental procedures, with ad lib access to food and tap water. Ethical clearance had already been obtained for this project from the Research Ethics Committee: Animal Care and Use of Stellenbosch University (SU-ACUM13-00027).

3.1.3 Mice inoculation with EO771 and B16 cancer cells

The protocol that was implemented in this study was adapted from (Ewens et al., 2006), in which Matrigel™ was used instead of HBSS, and was performed for both EO771 and B16 cells. Matrigel™ consists of a range of extracellular proteins and growth factors that are derived from Engelbreth-Holm-Swarm mouse tumour cells (Fridman et al., 2012). Though Matrigel™ is not necessary for the engraftment of either B16 or EO771 cancer cells this procedure is often deployed as it is argued that it more accurately recapitulates the extracellular context of cancer cells.

Both the EO771 (mammary adenocarcinoma) and the B16 cell line (melanoma) are derived from C57BL/6 background and readily form tumours in these mice. For the purpose of inoculating mice with cancer cells, cells were grown to ~70% confluence to ensure the cells were in an exponential growth phase. Cells were trypsinised, centrifuged, and re-suspended in ice-cold mixture (1:1) of PBS and Matrigel™ (9.2 mg/ml protein, BD Biosciences) at 2.5×10^6

cells/ml in sterile 1.5 ml Eppendorf tubes. Since Matrigel™ congeals above 4°C (Fridman et al., 2012), cell suspension was kept on ice continuously after re-suspension.

There are a number of benefits associated with subcutaneous (s.c.) injection as opposed to injection into the mammary fat pad (i.e. orthotopic transplantation). Firstly, subcutaneously injected cancer cells seldom metastasise (Workman et al., 2010). Thus, subcutaneous injection would avoid the stochastic nature of metastasis and also decrease morbidity as well as mortality. In addition, tumours that grow subcutaneously can continuously be monitored, and tumour volume can be measured directly. Finally, EO771 are adenocarcinoma of the mammary gland, whereas B16 are melanomas. Thus 'orthotopic' transplants for EO771 would not recapitulate the native micro-environment of B16 and consequently may introduce the differences in adaptation to micro-environment as a confounding factor. Consequently, the s.c. injections simplified operations, and provided a more standardised model.

Prior to injection, ~0.8 ml of the cell suspension was drawn-up into a syringe, where after a 23-gauge needle was fitted. Each mouse was inoculated subcutaneously at the second inguinal nipple (**Figure 3.3**) with 100 µl cell suspension (i.e. 2.5×10^5 cells). By gently raising the inserted needle, a small subcutaneous 'lacuna' was formed into which the cell suspension was injected. After discharging 100 µl of the cell suspension, the needle was slowly withdrawn in order for the injected Matrigel to be heated up by the body heat of the mice. This caused the Matrigel to become more viscous, thereby minimising leakage once the syringe was retracted. The needle was slowly retracted with a rotating motion.
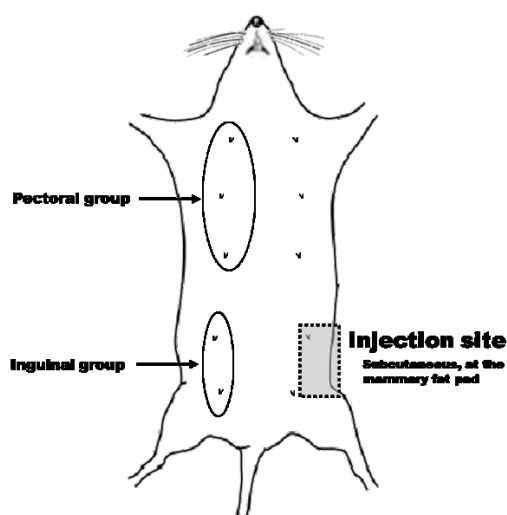
Figure 3.3. Diagram indicating the site of injection. Mice were injected subcutaneously above the second mammary fat pad (left, inguinal group).

3.1.1 Tumour volume and DXR injection

Tumour volume and body weight were measured every second day. Tumour volume was calculated by the formula $1/2 \times (\text{Length} \times \text{Width}^2)$, as measured by digital callipers. Once tumours became palpable (1~2 weeks after inoculation) mice were given three injections of HBSS, or DXR (Doxorubicin hydrochloride, Sigma) over a one week period (i.e. two days between injections, **Figure 3.2**). Dose of DXR to be administered was calculated according to the body weight measured the preceding day, and a stock solution of DXR was diluted in HBSS to produce a final volume of 100 μl.

3.1.2 Endpoints and tissue harvesting

Mice where sacrificed when tumours reached a volume of approximately 400 mm³. First, mice were anesthetised with isoflurane (Safeline Pharmaceuticals), using a 5% (v/v) isoflurane/oxygen mixture for induction, followed by a maintenance mixture of 1.5% isoflurane/oxygen. While the mice were anesthetised, blood samples were obtained through cardiac puncture, and allowed to clot at room temperature (22°C) in a serum clotting tube, followed by certification (1000×g for 15 min). The serum fraction was then aliquoted into 500 μl tubes and immediately frozen at -80°C for later analysis. Muscularis Gastrocnemius (GAS) was harvested, and fixed in neutral-buffered 10% formalin solution (Sigma, HT501128). Liver tissue was washed in ice-cold Hank's balanced salt solution. While submerged in buffer, excess blood from the liver lobes was removed by rapidly compressing and releasing (i.e. by the repeated 'squishing' of liver lobes) with pliers, before the liver lobes were snap-frozen in liquid nitrogen an stored at -80°C.

3.2 Muscle cross-sectional area

After fixing GAS muscle in formalin, muscle samples were placed in an embedding cassette and embedded with paraffin wax (see Appendix I) using TISSUE TEK III (model 4640B, Miles Laboratories Inc, Napervile, IL). Embedded samples were mounted on a rotary microtome (Reichert Jung, Heidelberg, Austria) and sectioned at 5 μm thickness. Sections were then dewaxed in preparation for haematoxylin and eosin (H&E) staining (Appendix I). After allowing sections to be air-dried, a mounting medium was added and a coverslip was placed over the sections. Images of the muscle cross-sectional area (MCA) was taken on a Nikon

Eclipse E400 microscope equipped with a Nikon DXM1200 colour at ×20 magnification. The MCA was calculated using *ImageJ* software (**Figure 3.4**).
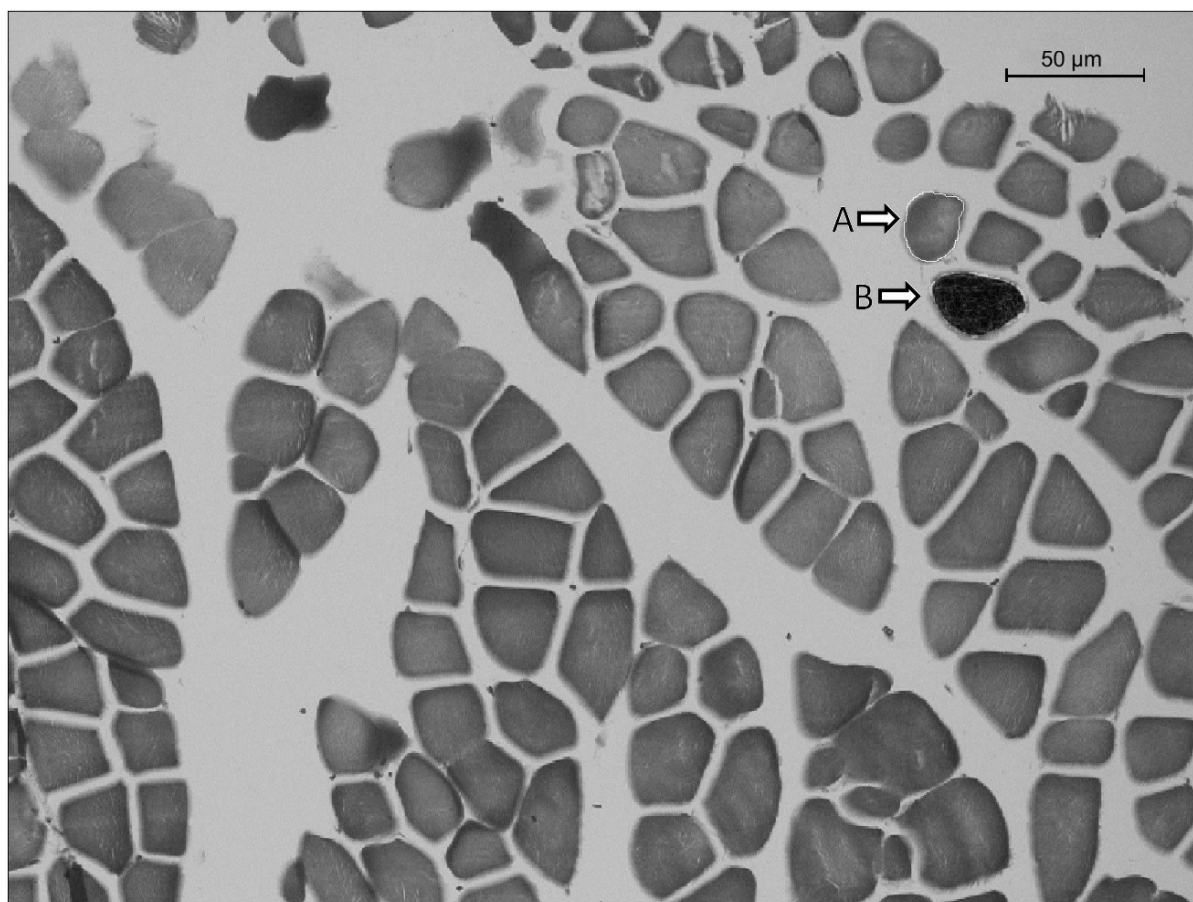
Figure 3.4. Histological cross-section of gastrocnemius muscle. (A**) After calibrating the pixel distance to the scale, the 'Freehand' tool was used to outline the perimeter of muscle cross-section. (**B**) Double counting was avoided by marking measured fibres using the 'Find Edges' function.**

Though mouse muscles exhibit predominantly glycolytic fibre types, the GAS muscle consists of mixed fibres, thus providing a more general effect of DXR, and avoiding any effect that may be attributed to fibre type. Due to the small size of the GAS muscle of the mice, and the fact that a small section of muscle was harvested for a parallel study, a representative histological section was not available for all mice. As a result, the counted fibres were pooled, with the tumour control (TC) group having n = 513 fibres counted, for low-dose (LD), n = 550, and for high dose (HD), n = 323 fibres. Muscle cross-sectional area was calculated in 'pixel-area', standardised to the pixel distance of the scale bar, and expressed in arbitrary units.

3.3   Statistical analysis

Statistical analysis was performed in R (version 3.3), using a variety of software packages including *ggplot2*, *psych*, and *car*. To compare slopes, an updated one-way ANCOVA model was implemented (using Fisher's LSD post hoc test) which included an interaction term between the covariate and predictor variable: for resistance Time:Group and for tolerance, log(tumour volume):Group interaction terms were used. Significance in the interaction terms signify a violation of the assumption that regression slopes are homogenous (i.e. slopes are significantly different).[1] In cases where comparisons between two groups were conducted, analysis was performed as previously described (Paternoster et al., 1998), according to the formula:

$$Z = \frac{b_1 - b_2}{\sqrt{(SEb_1)^2 + (SEb_2)^2}}$$

where b_1 and b_2 represent the regression coefficients (i.e. slopes) and similarly, SEb_1 and SEb_2 the respective standard deviation associated with each groups. The homogeneity of variance was tested using Levene's test, whereas the Shapiro-Wilk test was used to test whether data conformed to a normal distribution. Where applicable, a robust ANOVA was conducted using the *WRS2* package (confidence intervals calculated by 2000 bootstrap samples, and samples means 10% trimmed). For all tests, a p-value of < 0.05 was considered significant.

3.4   The effect of DXR on resistance of mice to EO771

Resistance was measured by fitting a regression line with logged tumour volume (mm³) as a function of time (**Figure 3.5**). As evident from the regressions summary, the slope of tumour control (TC: 0.0988) is shallower than the low concentration DXR group (LD: 0.1346), with the high concentration DXR group being steepest (HD: 0.145). Surprisingly, this suggests that DXR treatment increased tumour growth.

---

[1] Details of this approach are provided by Fields, Miles and Zoë in *Discovering statistics using R* (Chapter 11, pp 483-484).

DXR (Resistance)
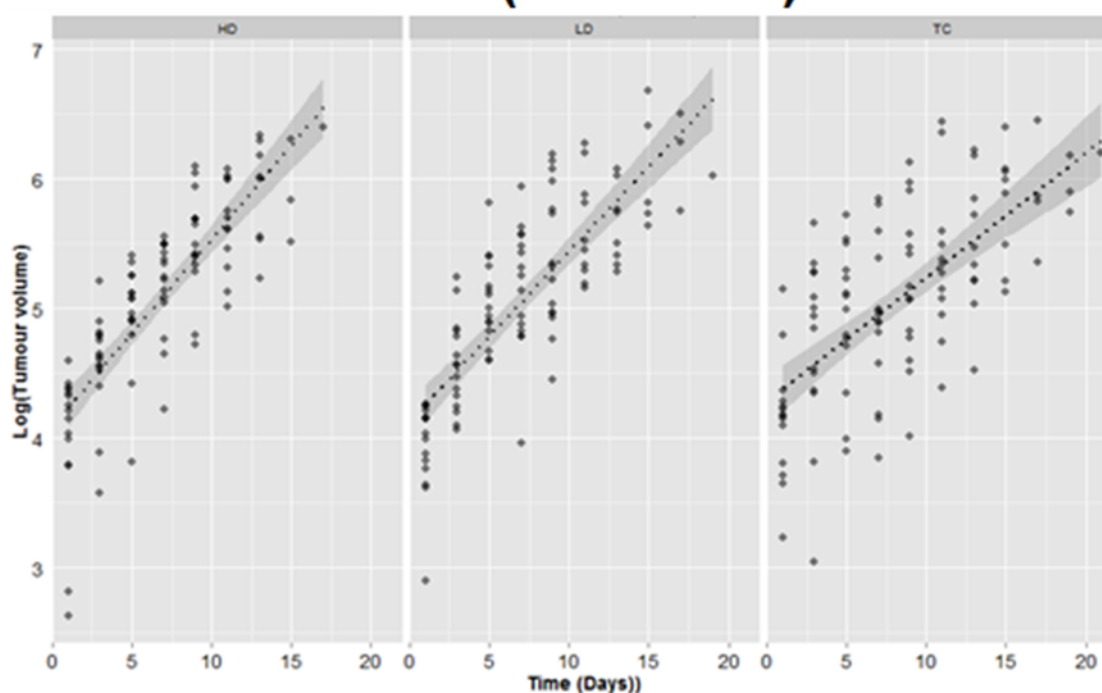
Regression summary: Resistance (DXR)

Group TC		Std. Error	t value	p value	
Intercept:	**4.27254**	0.10695	39.948	<2e-16	***
Slope:	**0.09883**	0.01189	8.309	4.36E-13	***
R²	**0.4036**				

F-statistic: 69.03 on 1 and 102 DF, p-value: 4.357e-13

Group LD		Std. Error	t value	p value	
Intercept:	**4.11566**	0.08351	49.28	<2e-16	***
Slope:	**0.13455**	0.01001	13.44	<2e-16	***
R²	**0.646**				

F-statistic: 180.7 on 1 and 99 DF, p-value: < 2.2e-16

Group HD		Std. Error	t value	p value	
Intercept:	**4.08985**	0.8363	48.9	<2e-16	***
Slope:	**0.14493**	0.011	13.79	<2e-16	***
R²	**0.6613**				

F-statistic: 189.4 on 1 and 97 DF, p-value: < 2.2e-16

Figure 3.5. Linear regression model of logged tumour volume plotted against time. HD: high dose group; LD: low dose group; TC: tumour control. All mice were inoculated with EO771 cancer cells.

Next, a test for homogeneity of regression slopes was performed to investigate if there were any differences in slopes between groups. This analysis indicated that the slopes were indeed significantly (Time:Group, p< 0.001) different (**Figure 3.6**).

Homogeneity of slopes: Resistance (DXR)

Response: Log(TV)	Σ Squares	Df	F value	p value	
Intercept:	442.430	1	1883.600	< 2.2e-16	***
Time	35.030	1	149.152	< 2.2e-16	***
Group	0.540	2	1.147	0.318957	
Time:Group	2.380	2	5.061	0.006894	**

Figure 3.6. Homogeneity of regression slopes. The Time:Group interaction is significant, indicating a violation of the assumption of homogeneity of regression slopes (i.e. slopes are significantly different).

In conclusion, these observations indicate, unexpectedly, that the DXR significantly *increased* tumour growth. Interestingly, DXR had previously been shown to enhance tumour motility and metastatic potential in another mouse mammary carcinoma, the 4T1 cancer cells, as well as in human MDA-MB-231 cancer cells (Bandyopadhyay et al., 2010). Evidence suggests that DXR might mediate this effect by upregulating transforming growth factor-beta (TGF-β) signalling in cancer cells. Similarly, others (Formelli et al., 1986) have noted that B16 cells repeatedly selected for DXR resistance occasionally demonstrated an "enhancement in metastasis formation not associated with an increase in survival time", suggesting that underlying cellular mechanisms by which cells undergo adaptation to doxorubicin may also have an impact on tumour growth.

Collectively, these results suggest a cell-autonomous mechanism by which DXR may enhance tumour growth: TGF-β is also known to play a role in the ability of cells to manipulate their micro-environment and enhance metastatic potential (Massagué, 2008). In addition, as tumour cells 'spread out', competition among cells for resources will be relaxed, consequently enhancing the growth potential of cancer cells. However, it is also possible that DXR may promote cancer growth via its impact on the host. As an example, tissue damage caused by DXR may promote the release of growth factors in order to initiate tissue repair. It is also possible that DXR may increase tumour growth by inhibiting the immune system directly, as monocytes/macrophages are known to "represent a major target of doxorubicin" (Krysko et al.,

2011). Similarly, DXR may have a negative impact on other immune cell such as NK cells, thus promoting tumour growth by preventing immune surveillance.

3.5   The effect of DXR on tolerance of mice to EO771

In order to assess the effect of DXR on tolerance of mice to EO771 tumour cells, a regression curve was fitted to a plot with body weight as response variable and tumour volume as predictor variable (both tumour volume and body weight were log-transformed) (**Figure 3.7**). Implementing the same statistical analysis as discussed above, it was found that slopes were indeed significantly ($p < 0.01$) different. The tumour control group (TC) exhibited a positive regression coefficient whereas both DXR groups (LD and HD) presented negative slopes.

Of note, the R^2 values are very low, indicating that tumour volume had little predictive effect on health status. This would suggest that most of the effect on health status may relate to the group to which mice had been assigned (i.e. depending on whether mice received DXR or not). Indeed, EO771 tumours did not induce weight loss (as indicated by the positive slope of the TC group), indicating that these tumours were well tolerated. Also, only the TC group exhibited a significant slope. However, pooling TC and HD groups, and comparing the slopes from pooled samples to TC (i.e. comparing mice that received DXR versus tumour control) demonstrated a significant ($Z = 23.886$, $p < 0.01$) difference between mice receiving DXR and the TC group.
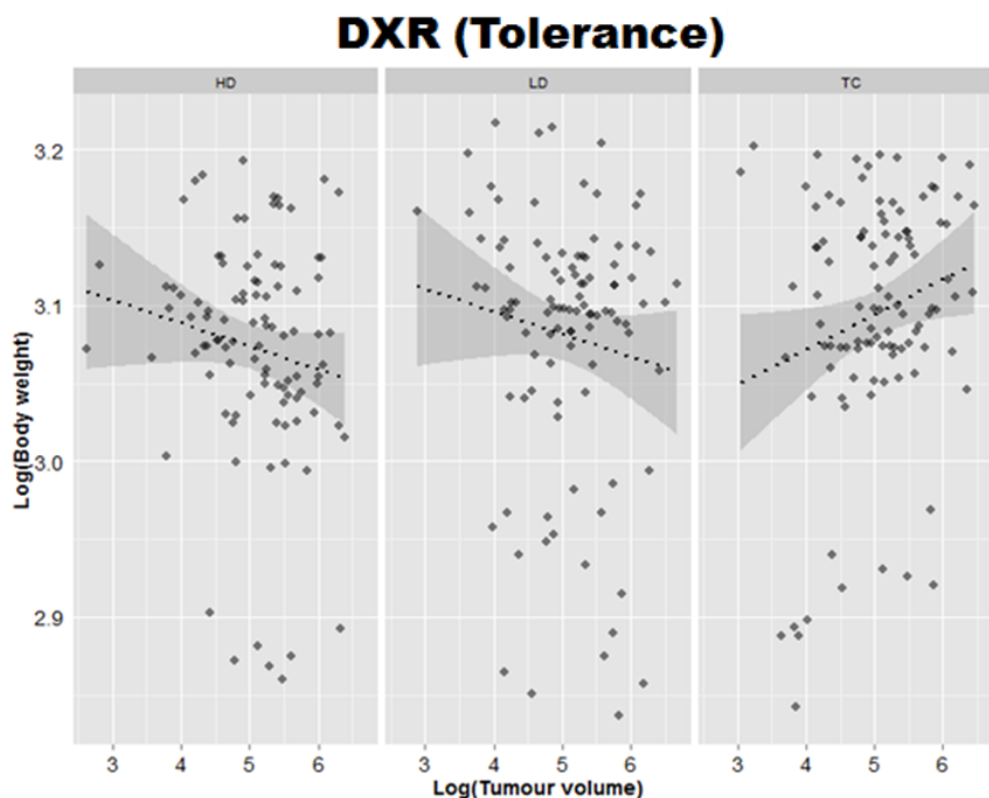
DXR (Tolerance)

Regression summary: Tolerance (Dox)

Group TC		Std. Error	t value	p value	
Intercept:	**2.98132**	0.05295	56.306	<2e-16	***
Slope:	**0.02259**	0.01041	2.169	0.0324	*
R²	**0.0441**				

F-statistic: 4.705 on 1 and 102 DF, p-value: 0.03239

Group LD		Std. Error	t value	p value	
Intercept:	**3.15425**	0.05757	54.794	<2e-16	***
Slope:	**-0.01454**	0.01124	-1.294	0.199	
R²	**0.01663**				

F-statistic: 1.674 on 1 and 99 DF, p-value: 0.1987

Group HD		Std. Error	t value	p value	
Intercept:	**3.147542**	0.050106	62.82	<2e-16	***
Slope:	**-0.014753**	0.009772	-1.51	0.134	
R²	**0.02296**				

F-statistic: 2.279 on 1 and 97 DF, p-value: 0.1344

Figure 3.7. Linear regression model of the logged tumour volume plotted against time. HD: high dose group; LD: low dose group; TC: tumour control. Only the TC slope (i.e. regression coefficient) was significant.

Since pathology may manifest in the absence of any discernible decrease in body weight, MCA was determined as a secondary measure of tolerance. As expected, TC had a higher average MCA in comparison to mice in the HD group. However the difference between TC and LD was not significant (p = 0.248).
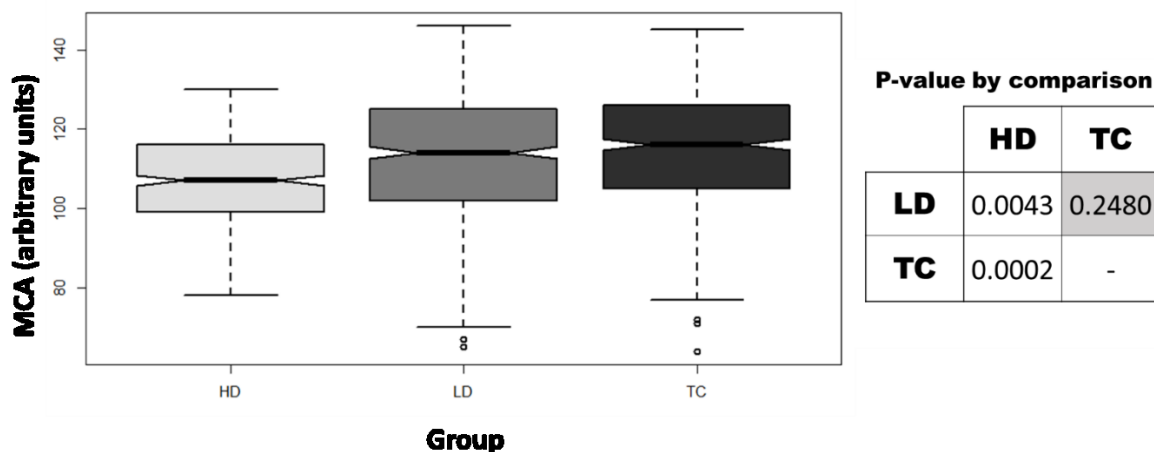
Figure 3.8. The muscle cross sectional area (MCA) in EO771 tumour bearing mice treated with low and high dose DXR. HD: high dose group; LD: low dose group; TC: tumour control.

The results from the MCA thus partially support the tolerance measured by body weight. As expected, mice receiving a high dose of DXR exhibited a significantly lower MCA than the other groups. The lack of significance between the LD and TC groups (despite the decrease in tolerance slopes) may be explained by the fact that data demonstrated large variance. In particular, the site of tumour inoculation might have induced another source of variance: as the tumour grew, the gait of the mice might have altered, resulting in the mice shifting workload on to the unimpeded leg. In turn, a higher work load might have led to muscle hypertrophy and a subsequent increase in MCA.

3.6   Resistance of mice to B16 and EO771

The same statistical analyses were performed to test the tolerance and resistance of C57BL/6 mice against the two syngeneic cancer cell lines, EO771 and B16. As illustrated below (**Figure 3.9**), the B16 cells (M) grew much faster than EO771 (TC). Quantitatively, the mice exhibited lower resistance to B16 (slope of 0.2591) compared to EO771 (slope of 0.0998). In addition to differences in slopes, R^2 was also higher for B16 tumours than EO771 (0.72 vs 0.40). The comparatively lower R^2 for EO771 cells could imply that tumour growth is only partially

predicted by time, and is more influenced by other factors. As an example, B16 cancer cells may be more effective in controlling their local environment, whereas EO771 cells may be more dependent on random factors (e.g. proximity to arteries for blood supply).
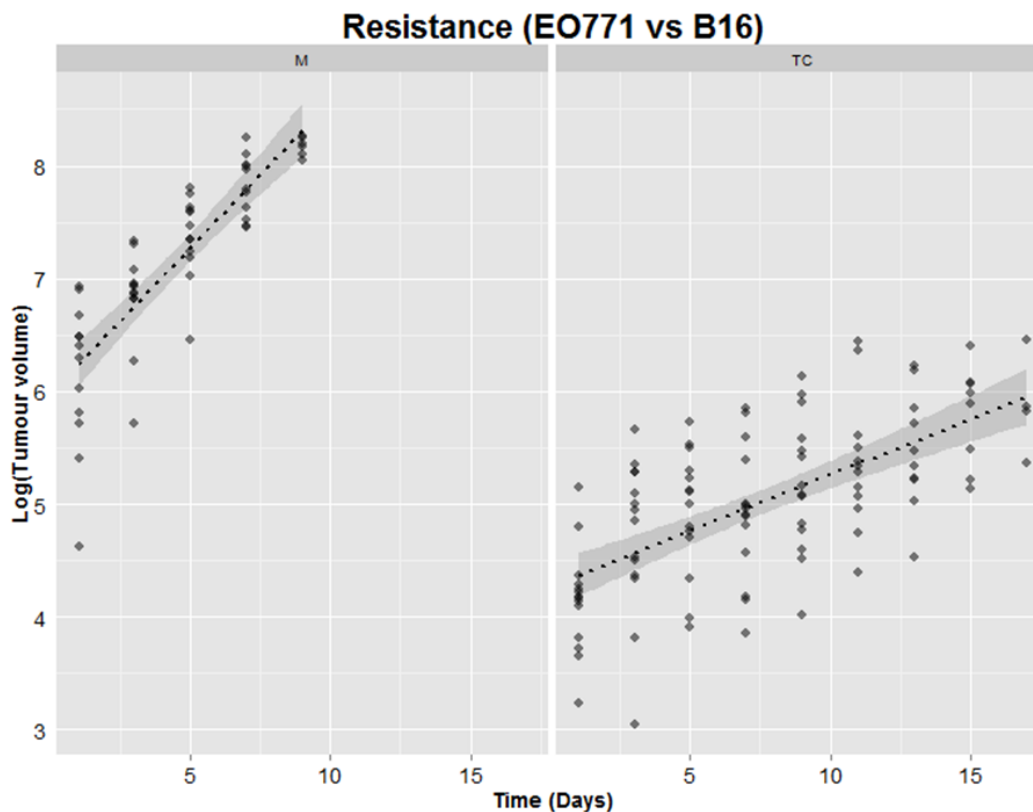
Regression summary: Resistance (EO771 vs B16)

Group TC		Std. Error	t value	p value	
Intercept:	**4.27254**	0.10695	39.948	<2e-16	***
Slope:	**0.09883**	0.01189	8.309	4.36E-13	***
R²	**0.4036**				

F-statistic: 69.03 on 1 and 102 DF, p-value: 4.357e-13

Group M		Std. Error	t value	p value	
Intercept:	**5.9841**	0.11908	50.25	<2e-16	***
Slope:	**0.25917**	0.02281	11.36	1.38E-15	***
R²	**0.7169**				

F-statistic: 3.071 on 1 and 51 DF, p-value: 0.08572

Figure 3.9. Linear regression model of log tumour volume plotted against time. M: B16; TC: (tumour control) EO771.

3.7 Tolerance of mice to B16 and EO771

Mice inoculated with B16 cells demonstrated a significantly lower tolerance compared to mice bearing EO771 tumours (**Figure 3.10**): Mice bearing EO771 tumours exhibited a positive growth (slope = 0.02259), whereas B16 tumours induced weight loss (B16 = -0.02109). The larger body weight (i.e. higher intercept on the y axis) of the TC group (EO771 mice) resulted from the vastly reduced lag phase before tumours become measurable: since all inoculated mice were young (4-5 weeks old) and still growing, a shorter lag time in the B16 resulted in these mice being measured at a younger age (and thus lower initial body weight). Hence, the discrepancy between intercepts (i.e. initial body weights) reflects the ±two weeks of additional growth that the TC group underwent before tumours became measurable.
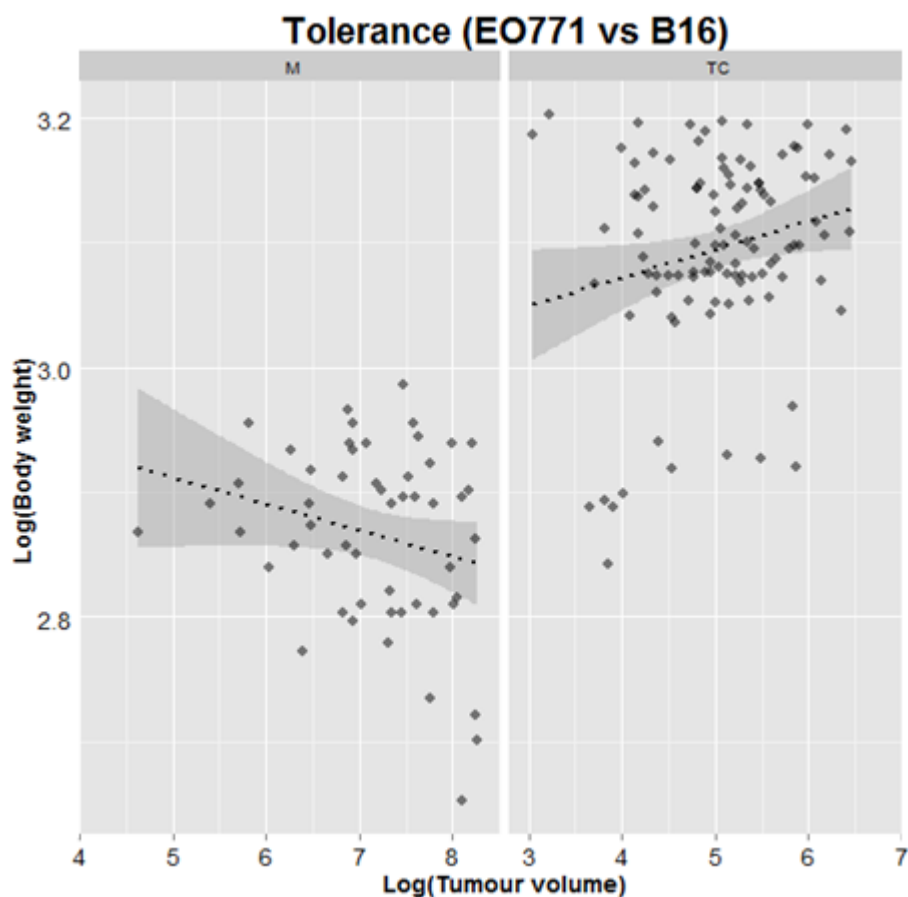
Regression summary: Tolerance (EO771 vs B16)

Group TC		Std. Error	t value	p value	
Intercept:	**2.98132**	0.05295	56.306	<2e-16	***
Slope:	**0.02259**	0.01041	2.169	0.0324	*
R²	**0.0441**				

F-statistic: 4.705 on 1 and 102 DF, p-value: 0.03239

Group M		Std. Error	t value	p value	
Intercept:	**3.01724**	0.08664	34.826	<2e-16	***
Slope:	**-0.02109**	0.01204	-1.752	0.0857	.
R²	**0.05679**				

F-statistic: 3.071 on 1 and 51 DF, p-value: 0.08572

Figure 3.10. Linear regression model of log tumour volume plotted against time. TC: tumour control EO771 cancer cells. M: B16 melanoma cells. The slope of the M group is not significant.

However, quantifying tolerance by differences in MCA did not reveal a significant difference between B16 and EO771 cancer cells (**Figure 3.11**).

MCA
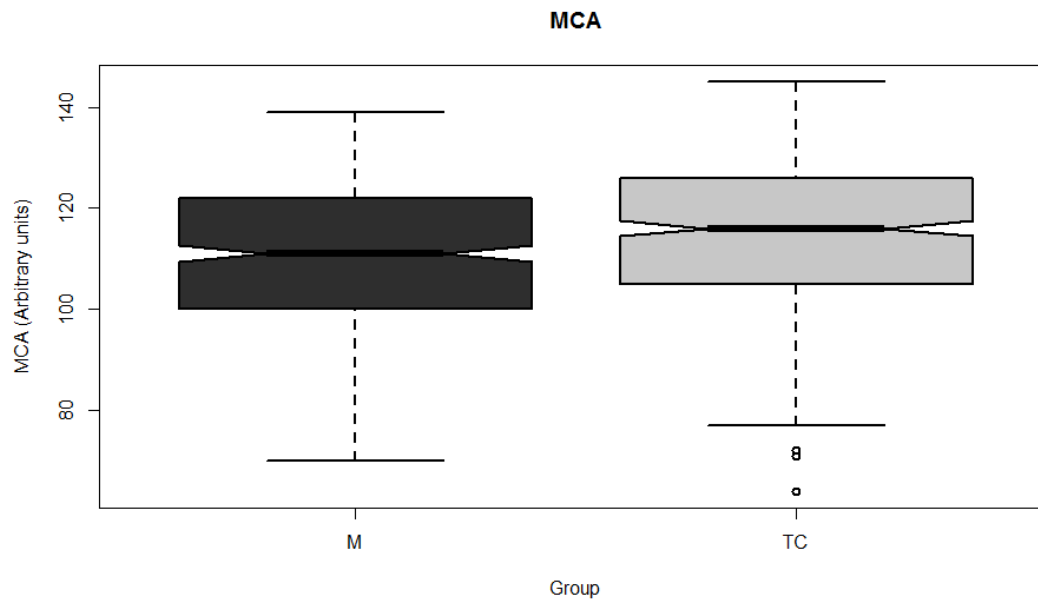
Figure 3.11. The muscle cross sectional area (MCA) in mice bearing EO771 and B16 tumours. M: Melanoma (B16 tumour cells); TC: tumour control (EO771 tumour cells).

At first glance, the lower tolerance of mice to B16 cells may be attributed to the observation that these mice are also less resistant to this cancer cell line, suggesting that a form of metabolic exhaustion may be driving pathology. Yet, the R^2 values are very low (i.e. the correlation between body weight and tumour volume is low, an observation also noticed for EO771 tumours). This may suggest that it is not tumour volume as such that is driving the decline in health, but rather the *type* of tumour. In turn, this would suggest that B16 cells induce pathology (weight loss) through mechanisms that are influenced by the noxious phenotype of the tumour and not only tumour load. However, the slopes for B16-bearing mice are not significant, and similarly, the MCA did not differ significantly.

3.8   Discussion

3.8.1   Effect of DXR on tolerance and resistance

The first notable finding of the current study is the observation that DXR enhanced tumour growth (**Figure 3.5**). Though this result is counter-intuitive, DXR has previously been shown to enhance tumour motility and metastatic potential in another mouse mammary carcinoma, the 4T1 cancer cells, as well as in human MDA-MB-231 cells (Bandyopadhyay et al., 2010). Similarly, it was previously (Formelli et al., 1986) demonstrated that B16 cells repeatedly

selected for doxorubicin resistance eventually developed an "enhancement in metastasis formation not associated with an increase in survival time", suggesting that the underlying cellular mechanism by which cells undergo adaptation to doxorubicin may also have an impact on tumour growth. Thus, although our results are unexpected, similar findings have been observed in both human and mouse cancer cells.

DXR may enhance tumour growth through either its effect on cancer cells (i.e. virulence), or by altering host physiology in a manner that is more conducive to tumour growth (i.e. resistance). A virulence mechanism by which DXR may enhance tumour growth is through the up-regulation of TGF-β signalling in cancer cells (Bandyopadhyay et al., 2010). TGF-β is known to play a role in the ability of cells to manipulate their micro-environment and enhance metastatic potential (Massagué, 2008). In addition, as tumour cells 'spread out', competition among cells for resources will be relaxed, consequently enhancing the growth potential of cancer cells. However, DXR may also have an impact on the micro- or macro-environment (i.e. affect host resistance). As a plausible example, tissue damage caused by cytotoxic DXR may result in the subsequent release of growth factors to promote tissue repair. Similarly, it is also possible that DXR could increase tumour growth by inhibiting the immune system directly, as monocytes/macrophages are known to "represent a major target of doxorubicin" (Krysko et al., 2011). It is thus not possible to conclude if DXR decreased resistance (i.e. inhibited host ability to attenuate tumour growth) or enhanced tumour virulence (enhance cancer cells ability to growth within host).

Regressing tumour volume against time (**Figure 3.5**) resulted in a higher R^2 value of mice receiving DXR (R^2 = 0.661 in high dose and 0.646 in low does DXR) compared to the TC group (R^2 = 0.404), suggesting that in mice receiving DXR, time were a better predictor of tumour growth. This might imply that DXR eliminated other sources of variance that might impact on tumour growth (i.e. additional sources of variance that predict tumour growth other than time). The underlying biological reason for this is unclear. However, DXR-induced tissue damage may result in the release of systemic growth factors that promote tissue repair. In turn, the release of growth factors may not only promote tumour growth, but allow a tumour to grow at the maximum rate, and thus, a more consistent rate. Similarly, systemic factors may decrease dependency on the tumour micro-environment (e.g. the infiltration of immune cells, the release

of danger signals by ischaemic and dying cells), thus removing a stochastic element of tumour development (e.g. the proximity to major blood vessels, or the formation of necrotic centres).

Not only does a reduction of muscle mass carry great prognostic value (Martin et al., 2013), but DXR has also been shown to induce a loss of extensor digitorum longus muscle mass in mice receiving 20 mg/kg DXR – a dose similar to the HD group (Gilliam et al., 2009). Thus, as expected, administration of DXR resulted in lower tolerance slopes. However, this difference only reached significance after pooling results from both high- and low-dose DXR groups. Also, a lower MCA was only observed for mice receiving a high dose of DXR. The fact that MCA did not completely correlate with tolerance slopes (i.e. that LD and HD had similar tolerance slopes, as measured by body weight, but HD exhibited lower MCA compared to LD) indirectly suggests that a decrease in body weight does not completely correlate with a decrease in muscle mass.

This small discrepancy between MCA and tolerance slopes may result from a number of factors. Firstly, the decrease in body weight is not only dependent on a decrease in muscle mass, but may also result from the depletion of glycogen or fat stores, a decrease in bone mineral density, or atrophy of other organ systems. Secondly, it is also possible that a more pronounced decrease in body weight in HD mice is 'masked' by weight gained from pathological manifestations. As an example, an accumulation of fluids, e.g. ascites resulting from liver, kidney or heart failure, may mask a decrease in body weight. However, no overt signs of pathology were observed in the mice during tissue harvesting. Thirdly, it should be noted that a decrease in muscle mass and muscle quantity does not necessarily correlate with a decrease in MCA. As an example, in response to muscle damage caused by DXR, muscle fibres may split – a process that promotes the expansion of muscle mass by hyperplasia (instead of hypertrophy). Here, smaller muscle fibres may in fact represent a form of adaptation and not pathology. Also, DXR may affect different fibre types differently. For example, (Hydock et al., 2011) found that in rats, DXR exerted a more pronounced adverse effect of muscle function in soleus muscle, which consist of more oxidative fibre types compared to GAS. Finally, it could be deduced that the myotoxicity effect of DXR may be counteracted by the increase in 'resistance training' of the muscle, as the tumour caused the mice to shift their weight to the non-tumour-bearing side (i.e. their right side), as mentioned earlier. Since the position and dimensions of growth differ from one tumour to another, mice would also vary in the extent to

which body weight is shifted onto the right hind limb and consequently, the effect of muscle loading. This introduces another source of variance in the data set, dampening the effect.

3.8.2   Comparative tolerance and resistance between B16 and EO771 tumours

Tumours developing from B16 cells grew at a greater pace than those that developed from EO771. Consequently, fewer data points were recorded for regression analysis. Nevertheless, the resistance slope for B16 was significantly higher. Interestingly, despite fewer data points, the linear model fitted the M group more accurately compared to the TC group (R^2 for TC group 0.4 vs 0.7 for M group). This may suggest that the growth trajectory of EO771 cells is more stochastic, depending on factors other than time. The biological basis for this more 'predictable' growth of B16 cells is not clear, but as mentioned, it may suggest that B16 cells are more able to control the micro environment, thus ensuring consistent growth.

With regard to tolerance, B16 appear to be less tolerant, though the slope of the regression line was not significant. Similarly, a decrease in MCA was also not significant between tumour control (TC, EO771 cells) and melanoma (M, B16 cells) groups. The non-significance may relate to the fact that, due to the rapid growth of B16 tumours, fewer data points were recorded for regression analysis. Further complicating interpretation of results, B16-bearing mice were sacrificed at a younger age (due to rapid tumour growth), rendering a direct comparison between EO771 and B16 in terms of tolerance more difficult. As an example, age of the mice may influence the distribution of muscle fibre types, and, since muscle fibre type also relates to MCA, age may alter the MCA independent of tumour load. Also, in young, growing mice, tolerance may manifest as a lack of growth, rather than a negative slope. This would suggest that mice are indeed even less tolerant to B16 tumours than predicted.

3.9   Conclusion

In conclusion, it was found that as a result of the lower tolerance associated with DXR, together with the fact that DXR enhances tumour growth, DXR therapy was not effective in our mice model system. This finding illustrates the efficacy of implementing the T/R framework in exposing the driver of pathology as manifesting from low resistance or low tolerance, but also points out a number of surprising findings, and highlights some challenges. Although the result from MCA does corroborate the results from T/R slopes, this effect may be even more

pronounced in different muscle types. This observation also raises the possible problem that may emerge when different metrics of tolerance exhibit contradicting results. A major challenge in comparing T/R of different cancer cells is that cancer cells grow at different rates, and subsequently any comparison must also take into account that mice will be sacrificed at different ages. The problem is particularly acute when comparisons are being made between full-grown versus juvenile mice. Age-matches controls for each group may not be practical, but using fully grown mice may at least avoid the complication of interpreting results.

We hypothesised that the higher R^2 value of mice receiving DXR may be explained by the systemic release of growth factors, resulting in maximum (and therefore constant) tumour growth. Systemic factors may also hint at the possible mechanism of pathology. As an example, inflammatory cytokines may cause muscle atrophy. In this regard, implementing a multiplex system (Luminex™ assay), the changes in different serum cytokines/growth factors was measured, but results obtained for seven out of the eight growth factors/cytokines were below the detectable range (data not shown) and discarded.

As an alternative, we focused on the pathology of DXR as mediated by altered hepatic function. Most research has focused on the well-established cardio-toxicity of DXR (Octavia et al., 2012). However, DXR also exhibits hepatotoxicity (Kalender et al., 2005) suggesting that liver damage may contribute to the manifestation of pathology. In addition, rapidly dividing tumour cells may increase metabolic load on the liver. In this regard, pathology may manifest as a form of 'metabolic exhaustion' – particular relevant in young mice that are still growing. Consequently, the remainder of the research investigated the manifestation of pathology as a result of DXR treatment, focusing on the liver. However, the surprising observation that DXR can induce tumour growth could also suggest that cancer cell phenotype may be altered by DXR in a manner that would promote tumour growth. The following chapter focuses on the effect of DXR on cancer cell growth.

3.10   Reference List

Bandyopadhyay, A., Wang, L., Agyin, J., Tang, Y., Lin, S., Yeh, I., De, K., and Sun, L. (2010). Doxorubicin in combination with a small TGF-beta inhibitor: a potential novel therapy for metastatic breast cancer in mouse models. PloS One *5,* e10365.

Ewens, A., Luo, L., Berleth, E., Alderfer, J., Wollman, R., Hafeez, B.B., Kanter, P., Mihich, E., and Ehrke, M.J. (2006). Doxorubicin plus interleukin-2 chemoimmunotherapy against breast cancer in mice. Cancer Res. *66,* 5419-5426.

Formelli, F., Rossi, C., Supino, R., and Parmiani, G. (1986). In vivo characterization of a doxorubicin resistant B16 melanoma cell line. Br. J. Cancer *54,* 223-233.

Fridman, R., Benton, G., Aranoutova, I., Kleinman, H.K., and Bonfil, R.D. (2012). Increased initiation and growth of tumor cell lines, cancer stem cells and biopsy material in mice using basement membrane matrix protein (Cultrex or Matrigel) co-injection. Nat. Prot. *7,* 1138-1144.

Gilliam, L.A., Ferreira, L.F., Bruton, J.D., Moylan, J.S., Westerblad, H., St Clair, D.K., and Reid, M.B. (2009). Doxorubicin acts through tumor necrosis factor receptor subtype 1 to cause dysfunction of murine skeletal muscle. J. Appl. Physiol. (1985) *107,* 1935-1942.

Hydock, D.S., Lien, C.Y., Jensen, B.T., Schneider, C.M., and Hayward, R. (2011). Characterization of the effect of in vivo doxorubicin treatment on skeletal muscle function in the rat. Anticancer Res. *31,* 2023-2028.

Kalender, Y., Yel, M., and Kalender, S. (2005). Doxorubicin hepatotoxicity and hepatic free radical metabolism in rats: the effects of vitamin E and catechin. Toxicology *209,* 39-45.

Krysko, D.V., Kaczmarek, A., Krysko, O., Heyndrickx, L., Woznicki, J., Bogaert, P., Cauwels, A., Takahashi, N., Magez, S., and Bachert, C. (2011). TLR-2 and TLR-9 are sensors of apoptosis in a mouse model of doxorubicin-induced acute inflammation. Cell Death Differ. *18,* 1316-1325.

Martin, L., Birdsell, L., Macdonald, N., Reiman, T., Clandinin, M.T., McCargar, L.J., Murphy, R., Ghosh, S., Sawyer, M.B., and Baracos, V.E. (2013). Cancer cachexia in the age of obesity: skeletal muscle depletion is a powerful prognostic factor, independent of body mass index. J. Clin. Oncol. *31,* 1539-1547.

Massagué, J. (2008). TGFβ in cancer. Cell *134,* 215-230.

Octavia, Y., Tocchetti, C.G., Gabrielson, K.L., Janssens, S., Crijns, H.J., and Moens, A.L. (2012). Doxorubicin-induced cardiomyopathy: from molecular mechanisms to therapeutic strategies. J. Mol. Cell. Cardiol. *52,* 1213-1225.

Paternoster, R., Brame, R., Mazerolle, P., and Piquero, A. (1998). Using the correct statistical test for the equality of regression coefficients. Criminology *36,* 859.

Workman, P., Aboagye, E., Balkwill, F., Balmain, A., Bruder, G., Chaplin, D., Double, J., Everitt, J., Farningham, D., and Glennie, M. (2010). Guidelines for the welfare and use of animals in cancer research. Br. J. Cancer *102,* 1555-1577.

Chapter 4

The unexpected finding that DXR increased tumour growth promoted subsequent analyses to elucidate the underlying cell signalling events implicated in this phenomena. Here, findings from western blot analyses are provided.

4.1   Introduction

Doxorubicin (DXR) exerts its cytotoxic effect via a number of mechanisms. One key mechanism is the binding and inactivation of DNA topoisomerase II, resulting in covalently bound topoisomerase to DNA, resulting in single and double strand breaks in DNA (Tewey et al., 1984). In turn, DNA damage initiates the DNA damage response, and ultimately induces apoptosis (Li et al., 2016). It has also been noted that, although DXR preferentially binds to topoisomerase II (Zhang et al., 2012), DXR-induced cardiotoxicity might be mediated by inhibition of mitochondrial topoisomerase (Khiati et al., 2014). Cardiac tissue maintains high levels of oxidative respiration, with a corresponding high level of mitochondrial content. The DXR-mediated cardiotoxicity might thus directly relate to the increased mitochondrial damage inflicted by DXR on mitochondrial topoisomerase (Khiati et al., 2014). In addition to cardiotoxicity, DXR also adversely affects other rapidly dividing cells, and myeloid toxicity resulting in neutropenia as well as anaemia has long been noted (Dessypris et al., 1986).

However, it is generally acknowledged that DXR also mediates its toxic effects through topoisomerase-independent mechanisms (Gewirtz, 1999; Mukhopadhyay et al., 2009). Another key mediator of DXR-associated toxicity includes oxidative stress resulting from radical formation (Doroshow and Davies, 1986). However, anti-oxidants as well as iron chelating agents have thus far not been effective in attenuating the toxic effects of DXR (Ghigo et al., 2016). Recently, it has been shown that DXR, intercalating with DNA, can result in histone eviction, resulting in a deregulated transcriptome (Pang et al., 2013). A deranged transcriptome might indeed impose a novel form of cellular stress, yet it remains to be explained why such a mechanism would be particularly toxic to cardiac tissue. In this regard, it has been noted that mitochondrial DNA (mtDNA), though lacking histones, also interact with proteins that protect mtDNA against radiation and free radicals (Guliaeva et al., 2006). It is thus tempting to

speculate that the intercalation of DXR with DNA that results in histone eviction might similarly inhibit the binding of protective proteins to the mtDNA, which rendering mtDNA more susceptible to oxidative stress.

It is likely that a combination of these toxic effects might be at play, or that one mechanism predominates in certain cellular contexts (Kato et al., 2000). The range of mechanisms by which DXR mediates its toxicity might also explain why DXR is used to treat a vast array of both solid and haematological malignancies. Yet, the fact that DXR is effective against many cancers, in conjunction with the diverse mechanism of toxicity, renders the finding that DXR enhanced tumour growth all the more surprising.

From a tolerance/resistance perspective, DXR could promote tumour growth by either decreasing host resistance, or by enhancing tumour virulence. As an example, DXR might enhance tumour growth by adversely affecting immune cells, compromising the host's ability to eliminate cancer cells through immune editing. However, such a hypothesis is not easily testable, given the complex nature of measuring immune surveillance and the anti-cancer activity of the immune system. Alternatively, DXR may alter cancer-intrinsic processes that may promote tumour growth. In this chapter, efforts to evaluate the effect of DXR on cancer virulence (i.e. the ability of DXR to promote tumour growth by enhancing cell-intrinsic mechanisms) are reported.

4.2   Cell Signalling

4.2.1   Apoptotic signalling

Apoptosis can be initiated via either intrinsic or extrinsic pathways (**Figure 4.1**). The extrinsic pathway is often activated by immune cells, e.g. cytotoxic T cells, as well as Natural Killer cells (Wilson et al., 2009) or signalling effectors such as Tumour Necrosis Factor (TNF) (Wang and El-Deiry, 2003). In contrast, the intrinsic pathway is typically activated by cell stress such as DNA damage, oxidative stress, or as part of the endoplasmic reticulum (ER) stresses (unfolded protein response), and is characterised by the important role played by the release of key mitochondrial proteins such as cytochrome C (Cyt C) (Fulda and Debatin, 2006).

Intrinsic activation of p38 protein kinase (by various cell stressors such as DNA damage) results in the activation of p53 (Bulavin et al., 1999). In turn, p53 regulates the expression of

the pro-apoptotic proteins, Bid (Sax et al., 2002) and Bax (Chipuk et al., 2004). Similarly, p53 can also induce apoptosis via a transcription-independent mechanism, including the direct activation of Bax [(Basu and Haldar, 1998; Chipuk et al., 2004), which promotes mitochondrial permeability and the formation of the apoptosome. The intrinsic and extrinsic pathways also intersect. Caspase 8, activated by the extrinsic pathway, can cleave cytosolic Bid, rendering the activated truncated Bid (tBid) (Li et al., 1998). The truncated Bid translocates from the cytosol to the mitochondria where it mediates the release of Cyt C (Tan et al., 2014). Once released, Cyt C forms a complex with caspase 9 and Apaf-1, known as the apoptosome, which subsequently activates executioner caspases (caspase 3, 6 and 7), and ultimately induces apoptosis (Cain et al., 2002; Garrido et al., 2006). In addition, these executioner caspases can also be activated through proteolytic cleavage of caspase 12 (Liu et al., 2014) or caspase 8 (Fernandes-Alnemri et al., 1996).
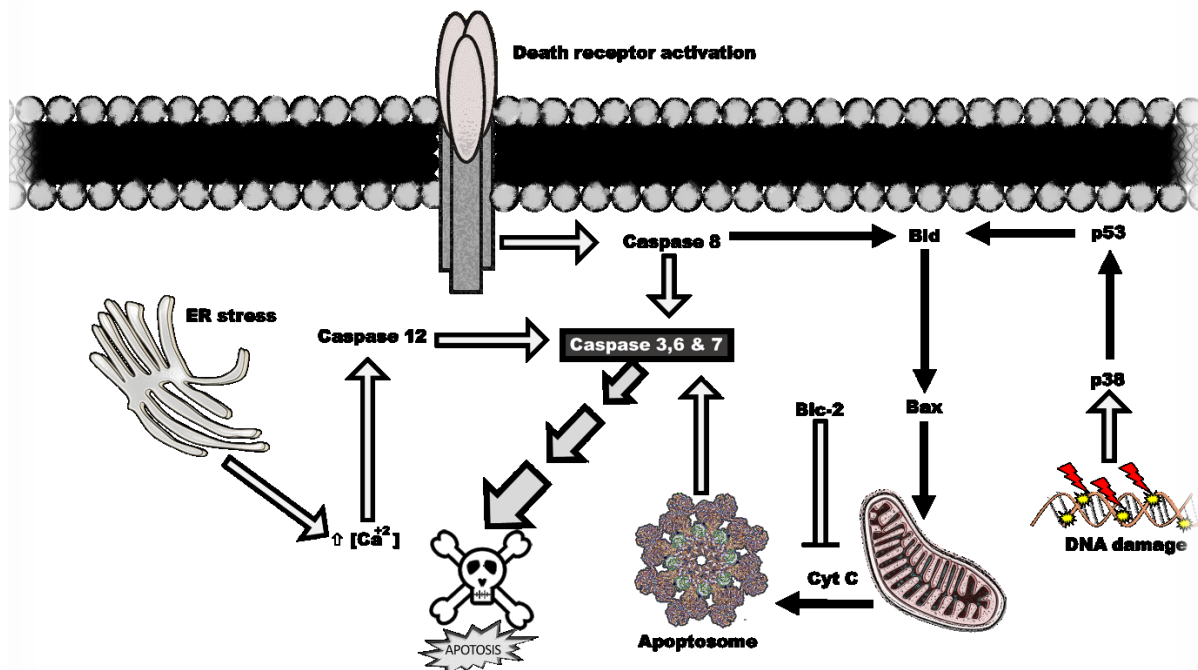
Figure 4.1. The intrinsic and extrinsic pathways of apoptosis. Various intrinsic stressors such as DNA damage, ROS or ER stress induce apoptosis via the intrinsic pathway, where death receptor activation (e.g. by TNF) induces apoptosis through the extrinsic pathway.

Since an increase in tumour growth could be mediated by a decrease in cell death, cell death pathway proteins such as the cleavage (i.e. activation) of various caspases (3, 8 and 9) as well as initiators (e.g. p38 and caspase 12) of the apoptotic pathway are investigated in the current study. The expression of Bcl-2 was also assessed, since this protein is often upregulated during

cell stress and prevents the induction of apoptosis through the inhibition of Cyt C being released from the mitochondria (Cory et al., 2003). Furthermore, Bcl-2 is also and occasionally associated with the development of chemo-resistance (Sartorius and Krammer, 2002).

4.2.2 Cell growth and pro-survival signalling

The raf/MAPK/ERK and PI3K/PTEN/Akt/mTOR pathways play a key role in promoting cell growth and proliferation (**Figure 4.2**). Indeed, altered expression or mutations of genes involved in these pathways are often associated with both cancer development and chemo-resistance (Steelman et al., 2011). As an example, the application of mTOR inhibitors in treating certain tumours has also been proposed (Pópulo et al., 2012). Similarly, most tumours exhibit mutations in signalling proteins which occur upstream of ERK (Samatar and Poulikakos, 2014). Also, activation of Akt signalling pathways antagonises various mediators of apoptosis (Avan et al., 2016). It is thus likely that altered expression and activation status of key proteins involved in these pathways may explain the observed DXR resistance and tumour growth observed in mice in our study.
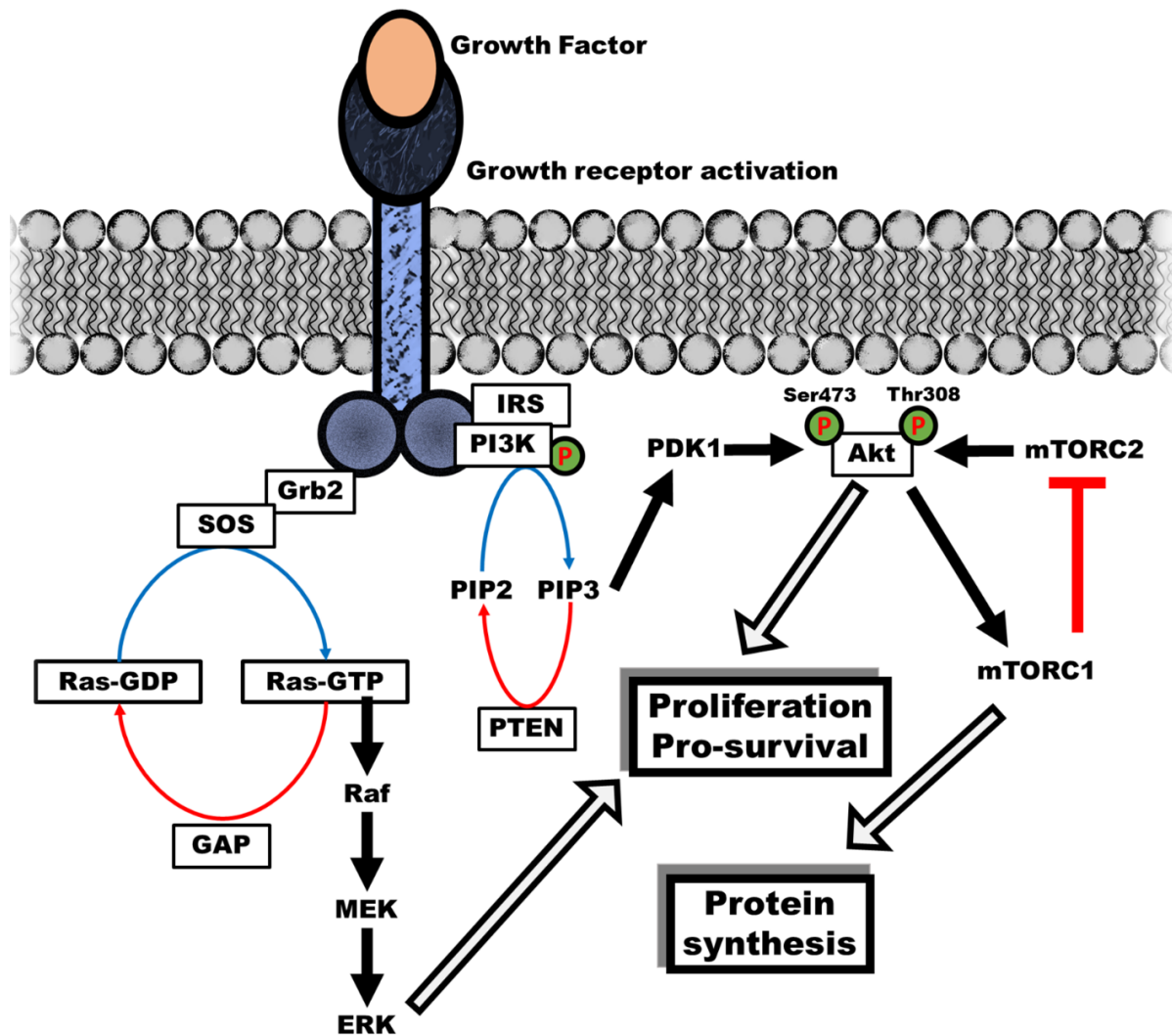
Figure 4.2. Cell-signalling pathways involved in cell growth and proliferation.

External stimuli such as growth factors (GF) bind to the receptor tyrosine kinase (RTK) where after subsequent receptor auto-phosphorylation creates binding sites that then recruit IRS, an adaptor protein for phosphoinositide 3-kinase (PI3K). Activated PI3K mediates the phosphorylation of phosphatidylinositol (4,5)-bisphosphate (PIP$_2$) to generate membrane-bound phosphatidylinositol (3,4,5)-trisphosphate (PIP$_3$). Pleckstrin homology (PH) domains in Akt and phosphoinositide dependent protein kinase-1 (PDK1) recognize PIP$_3$ and translocate to the membrane. In turn, PDK1 phosphorylates the activation loop of Akt on the threonine residue, thus partially activating Akt (Hemmings and Restuccia, 2012). Subsequent phosphorylation of Akt on the serine residue by mTORC2 (mechanistic target of rapamycin complex 2) fully activates Akt, which initiates downstream mitogenic cell-signalling events, and antagonises cell-death pathways (Avan et al., 2016; Manning and Cantley, 2007)

Furthermore, Akt activates mTORC1 which upregulates biosynthetic pathways (Avan et al., 2016; Manning and Cantley, 2007).

Similarly, GF binding activates RTK auto-phosphorylation, generating binding sites for the SHC and GRB2 adaptor molecules that recruit SOS, the RasGEF (GTPases exchange factor) to the membrane. SOS catalyses Ras GTP exchange and Ras-GTP then recruits Raf to the membrane, where it gets activated (Weber et al., 2001). Raf activates MEK and MEK activates ERK via activation loop phosphorylation (Sasaki et al., 2003). The activated ERK translocates to the nucleus where it regulates the expression of various proteins including proteins involved in cell proliferation (Lidke et al., 2010; Zhang and Liu, 2002).

Key regulators which oppose these signalling cascades include Jun amino-terminal kinases (JNK) and Phosphatase and tensin homolog (PTEN). The activity of PTEN is controlled on various levels including transcriptionally (methylation status, miRNAs or the presence of transcription factors), by posttranslational modifications and various interactions with other proteins (Song et al., 2012). PTEN is a well-established anti-cancer protein which is often mutated or inactive in various types of cancers (Cully et al., 2006). This function is also signified by the fact that other anti-apoptotic proteins such as p53 plays a key role in the transcription of this protein (Stambolic et al., 2001). Mechanistically, PTEN antagonises the PI3K-Akt pathway by catalysing the hydrolysis of PIP_3 to PIP_2, thereby opposing the function of PI3K (Georgescu, 2010).

JNK can exert contrasting effects, depending on the cellular context. Earlier studies have implicated JNK as a key mediator of the cellular stress response. This is also exemplified by JNK's alternative name – stress-activated protein kinase. Indeed, inflammatory cytokines such as TNF are known to activate the JNK-signalling pathway (Liu et al., 1996). In line with JNK's function during cellular stress, JNK rapidly inhibits protein synthesis (Banerjee and Kyriakis, 1994). JNK can also antagonise the mutagenic-signalling cascades by inhibiting the Akt-signalling pathway (Sunayama et al., 2005). Furthermore, constitutive activation of JNK can lead to the induction of apoptosis through both transcriptionally dependent and independent mechanisms (Chen et al., 1996; Donovan et al., 2002; Donovan et al., 2002; Shen and Liu, 2006). In fruit flies the activation of JNK can act as a switch between signalling cascades, moving from apoptotic to mutagenic pathways (Ryoo et al., 2004). Similarly, in cancer cells lacking PTEN, an upregulation of both JNK and Akt promote cell proliferation, and the

anchorage-independent growth of cancer cells (Vivanco et al., 2007). The ultimate function of JNK activation is thus dependent on the cell type, and in particular with reference to an oncological context, dependent on the genomic lesions carried by the cancer cells.

4.3   Study outline

Western blot analysis was conducted on key signalling proteins in order to identify the signalling circuits activated in tumours in response to DXR (**Figure 4.3**). For each group (either tumour control, mice receiving low dose DXR, or mice receiving high dose DXR) a total of 8 mice were randomly selected.
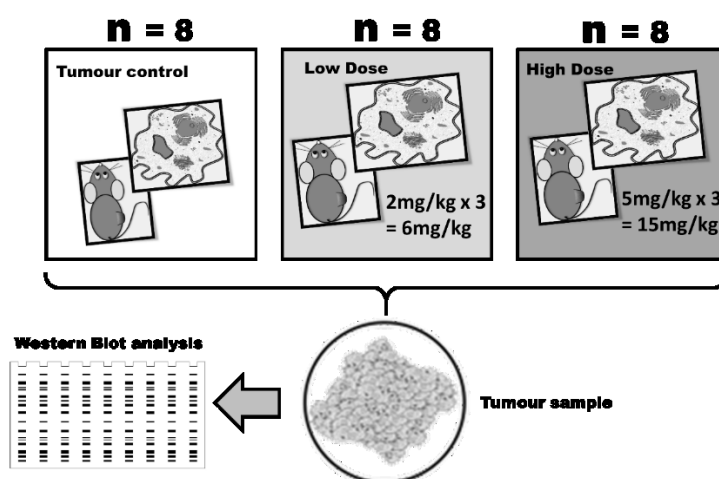
Figure 4.3. Study design to identify key singling proteins in tumour samples. Tumour samples from 8 mice in each group were subjected to Western Blot analysis.

4.4   Materials and methodology

Harvested cancer tissue was thawed on ice and lysed by adding radioimmunoprecipitation assay (RIPA) buffer (0.1% SDS, 5 mM EGTA, 5 mM EDTA, 65 mM Tris, NP-40, 1% Na-deoxycholate and 154 mM NaCl at pH 7.4), freshly supplemented with protease and phosphatase inhibitors (Aprotinin, Leupeptin and Benzamidine at 1 µg/ml, and NaF, Na_3VO_4 and PMSF at 1 mM). Tissue samples were subsequently homogenised (KineMatica Polytron™ PT2100 homogeniser, Fisher Scientific), and left on ice for 2 hours prior to being centrifuged (12000 rpm for 20 min) at 4°C, where after the supernatant was collected and stored at -80°C for later analysis.

Protein concentration was determined using the Bradford method (Bradford, 1976). Briefly, a ×5 stock solution (500 mg G-250 Coomassie Brilliant Blue dissolved in a solution consisting of 250 ml 95% ethanol and 500 ml phosphoric acid, filled to 1L with distilled water) was diluted to a ×1 stock solution and filtered to remove any undissolved Coomassie particles. A standard curve was generated from a two-fold serial dilution (blank, followed by a 2-20 µg protein gradient) of 100 µl bovine serum albumin (BSA, Roche) added to 900 µl Bradford reagent. Protein samples (5 µl each) were diluted in distilled water (95 µl), where after Bradford reagent (900 µl) was added. The protein concentration was spectrometrically determined by measuring the absorbance spectra at a wavelength of 595 nm (Cecil CE 2021 spectrophotometer, Cecil Instruments). Proteins samples above the linear absorbance range were diluted with RIPA buffer.

Protein lysates were denatured with Laemli's sample buffer (working solution consisting of 5% beta-mercaptoethanol, 4% SDS, 10% glycerol, 0.03% bromophenol blue and 62.5 mM Tris, pH 6.8) prior to sodium dodecyl sulfate polyacrylamide gel electrophoresis (SDS-PAGE). Based on Bradford protein quantification results, samples were diluted with Laemli's sample buffer to 50 µg of total protein. Samples were frozen at -80 °C. These samples were later thawed on ice, vortexed, and heated to 95°C for 5 minutes before use. The molecular weights of bands were established from the BLUeye Prestained Protein Ladder (Genedirex). After loading the samples, gels were run for 10 min at 100 V, where after the voltage was increased (150 V) and samples were run until the dye-front approached the end of the gel (~90 minutes) in Tris/Glycine/SDS running buffer (Bio-Rad). Proteins were separated using a TGX Stain-Free FastCast™ Acrylamide kit (12% acrylamide gel, Bio-Rad).

Protein was referred to a membrane using Trans-Blot® Turbo™ RTA Mini PVDF Transfer Kits (Bio-Rad) according to the manufacturer's specifications: PVDF membranes were submerged in methanol (100%) for 10 seconds, and subsequently incubated, along with blotting paper, in transfer buffer (supplied with kit) for 2 min. Proteins were transferred to the membrane on a Trans-Blot Turbo Transfer System (Bio-Rad) for 10 minutes (25V, 2.5 A). After transferring the proteins onto membranes, the proteins were fixed by bathing membranes in 100% methanol where after they were air-dried. Membranes were subsequently re-submerged in methanol and washed in TBS-T (tris-buffer saline: 20 mM tris, 137 mM NaCl, 0.1%Tween-20 and pH 7.6).

The TGX Stain-Free FastCast™ gels are infused with trihalo compounds which interact with tryptophan amino acids, which then provide a fluorescent signal at the 300 nm wavelength and provides a means for quantifying total protein content, and allow the subsequent normalisation of protein content. Visualisation of total protein was performed using the ChemiDoc™ MP System (Bio-Rad) by exposing gels to UV light for 150 seconds.

Membranes were incubated in 5% skimmed milk (diluted with TBS-T) for 1 hour in order to avoid non-specific binding of antibodies on the membrane, and subsequently rinsed in TBS-T to remove excess milk. Primary antibody incubation was performed overnight at 4°C (see **Table 4.1** for summary of antibodies used). Following incubation, membranes were again washed with TBS-T and incubated with the secondary antibody at room temperature for 1 hour. Membranes were washed again before being developed using Clarity™ ECL Substrate (Bio-Rad) on the ChemiDoc™ MP system.

Table 4.1. Primary and secondary antibodies used in this study.

Primary Antibody (1° AB)	Molecular weight (kDa)	Vendor	Catalogue #	Species	1° AB Dilution	2° AB Dilution
PTEN	54	Cell Signalling	9559	Rabbit	1:1000	1: 10 000
p-PTEN (Ser380)	54	Cell Signalling	9551	Rabbit	1:1000	1: 10 000
PI3K p85	85	Abcam	ab86714	Mouse	1:1000	1: 10 000
p-PI3Kp85 (Tyr458)	85	Elabscience	ENP0224	Rabbit	1:1000	1: 10 000
Akt	60	Abcam	ab32505	Rabbit	1:1000	1: 10 000
p-Akt (Ser473)	60	Cell Signalling	4060	Rabbit	1:1000	1:10 000
p-Akt (Thr308)	60	Cell Signalling	9275	Rabbit	1:1000	1:10 000
PDK1	58-68	Cell Signalling	3062	Rabbit	1:1000	1: 10 000
p-PDK1 (Ser241)	58-68	Cell Signalling	3061	Rabbit	1:1000	1: 10 000
mTOR	289	Abcam	ab51089	Rabbit	1:1000	1:5000
p-mTOR (Ser2448)	289	Abcam	ab84400	Rabbit	1:1000	1:5000
cRaf	74	Cell Signalling	9422	Rabbit	1:1000	1: 10 000
p-cRaf (Ser259)	74	Cell Signalling	9421	Rabbit	1:1000	1: 10 000
ERK1/ERk2	42, 44	Cell Signalling	4695	Rabbit	1:1000	1: 10 000
p-ERK1/ERK2 (Thr202/Tyr204)	42,44	Cell Signalling	4370	Rabbit	1:1000	1: 10 000
p38	43	Cell Signalling	9212	Rabbit	1:1000	1: 10 000
p-p38 (Thr180/Tyr182)	43	Cell Signalling	9211	Rabbit	1:1000	1: 10 000
JNK	46, 54	Cell Signalling	9252	Rabbit	1:1000	1: 10 000
p-JNK (Thr183/Tyr185)	46, 54	Cell Signalling	9251	Rabbit	1:1000	1: 10 000
Bcl-2	26	Santa Cruise	130308	Mouse	1:1000	1:5000
Caspase 9	51	Cell Signalling	9508	Mouse	1:1000	1: 10 000
Caspase 8	57	Abcam	ab25901	Rabbit	1:1000	1: 10 000
c-Caspase 8	18	Abcam	ab25901	Rabbit	1:1000	1: 10 000
Caspase 3	35	Cell Signalling	9665	Rabbit	1:1000	1: 10 000
c-Caspase 3	17, 19	Cell Signalling	9664	Rabbit	1:1000	1: 10 000

Normalisation of protein content was conducted on Bio-Rad Image Lab™ software (version 5.1) and exported to Microsoft Excel. Groups were compared using a one-way ANOVA followed by Bonferroni post hoc comparison for significant ($p < 0.05$) changes between groups

compared. Statistical analysis was performed in *GraphPad Prism* (version 5.0) and R using the *car* package.

4.5   Results: Pro-survival signalling

4.5.1   cRaf phosphorylation

DXR did not significantly alter cRaf phosphorylation between groups: There was no significant increase in total or phosphorylated cRaf, and similarly, no increase in the ratio between p-cRaf and total cRaf (**Figure 4.4**).

Figure 4.4. The effect of low and high DXR concentration on cRaf protein phosphorylation status. (A) Phosphorylated-cRaf1 (p-cRaf) (B) Total cRaf expression. (C) Ratio between p-cRaf and total cRaf was not significant different between groups (Control: 1.0 ± 0.17; LD-DXR: 1.13 ± 0.17; HD-DXR: 1.09 ± 0.2). Results are expressed as mean ± SEM.

4.5.1   ERK phosphorylation

The ratio between total and p-ERK was significantly different between the HD-DXR and control groups (Control: 1.0 ± 0.16; LD-DXR: 1.58 ± 0.16; HD-DXR: 1.71 ± 0.18), as demonstrated by the significant increase in the p-ERK:ERK ratio in the HD-DXR group (**Figure 4.5**).

Figure 4.5. The effect of low and high DXR concentrations on ERK protein phosphorylation status. (A) Phosphorylated-ERK (p-ERK). (B) Total ERK expression. (C) Ratio between p-ERK and total ERK. Results are expressed as mean ± SEM.

4.5.2   p38 MAPK

There was no significant increase in total or phosphorylated p38, and similarly, no increase in the ratio between p-p38 and total p38 (**Figure 4.6**) (Control: 1.0 ± 0.17 versus HD group: 1.27 ± 0.25).

Figure 4.6. The effect of low and high DXR concentration on p38 protein phosphorylation status. (A) Phosphorylated-p38 (p-p38). (B) Total p38 expression. (C) Ratio between p-p38 and total p38. Results are expressed as mean ± SEM.

4.5.3   JNK

There was no significant increase in either total or phosphorylated JNK, and similarly, no increase in the ratio between p-JNK and total JNK (**Figure 4.7**): DXR did not significantly alter JNK phosphorylation between groups (Control: 1.0 ± 0.47 versus HD group: 0.9 ± 0.41).
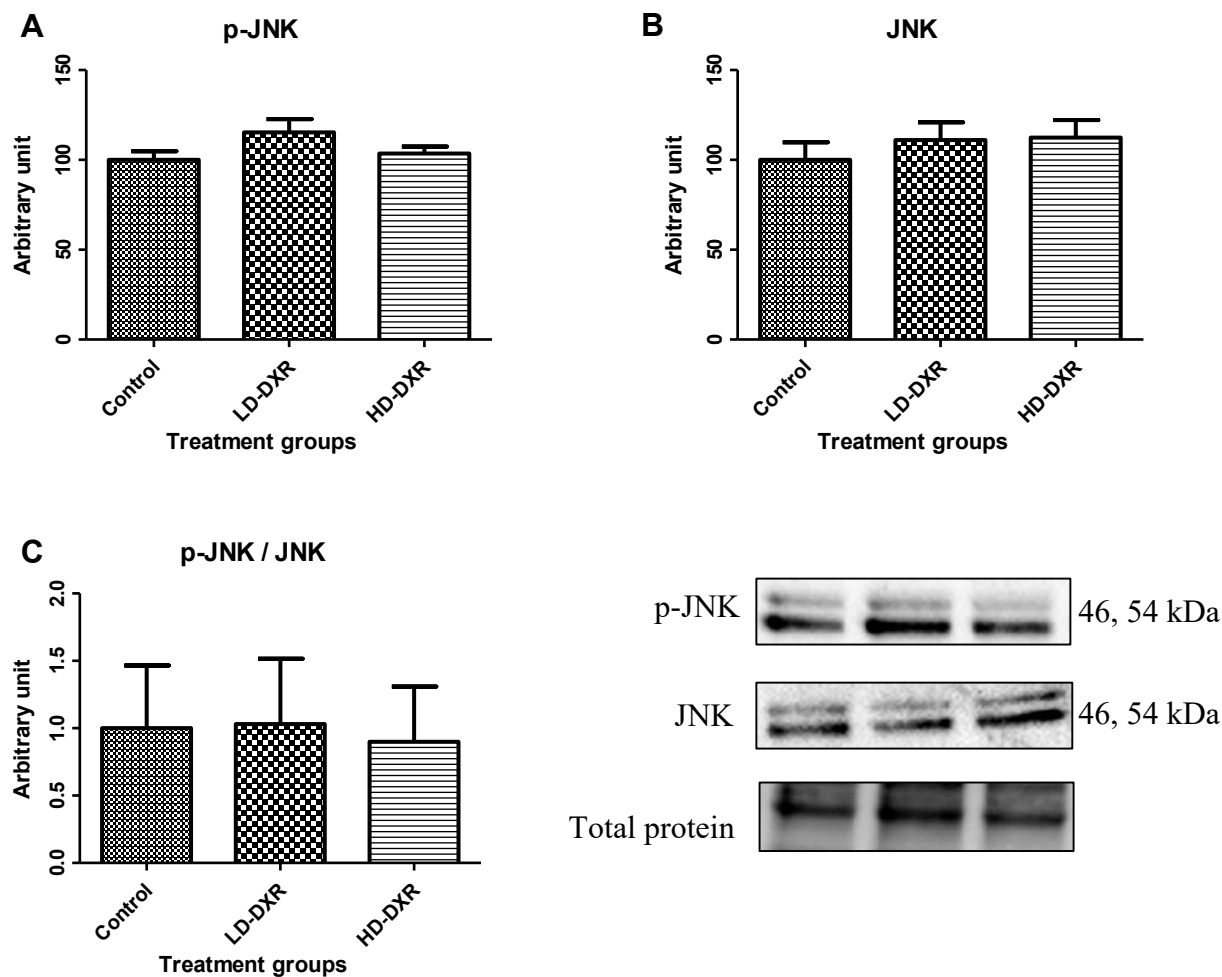
Figure 4.7. The effect of low and high DXR concentration on JNK protein phosphorylation status. (A) Phosphorylated-JNK (p-JNK). (B) Total JNK expression. (C) Ratio between p-JNK and total JNK. Results are expressed as mean ± SEM.

4.5.4 PTEN

There was no significant increase in either total or phosphorylated PTEN (Control: 1.0 ± 0.05 versus HD group: 1.12 ± 0.07) and similarly, no increase in the ratio between p-PTEN and total PTEN (**Figure 4.8**).
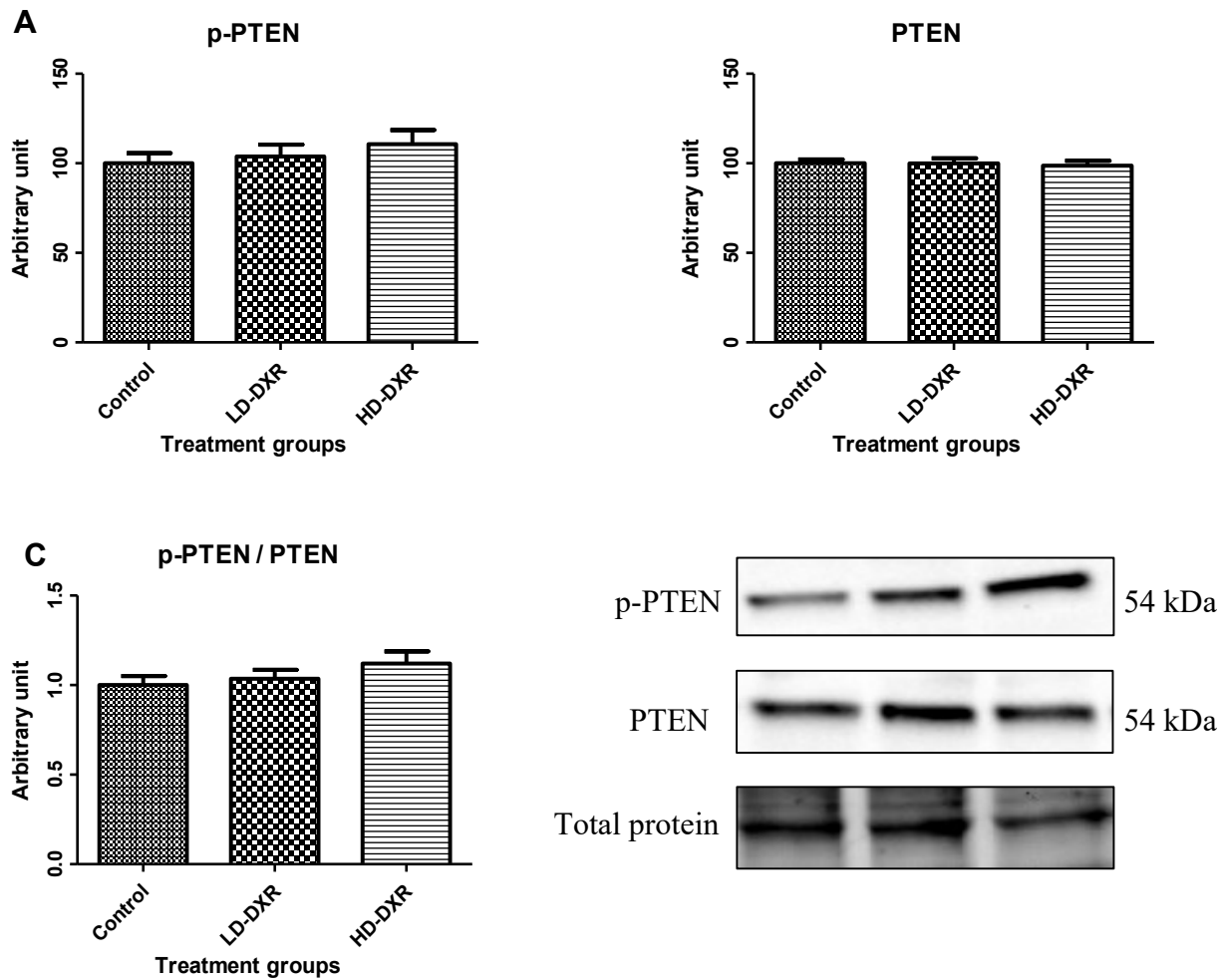
Figure 4.8. The effect of low and high DXR concentration on PTEN protein phosphorylation status. (A) Phosphorylated-PTEN (p-PTEN). (B) Total PTEN expression. (C) Ratio between p-PTEN and total PTEN. Results are expressed as mean ± SEM.

4.5.5   PI3Kp85

There was no significant increase in either total or phosphorylated PI3Kp85, despite a slight increase in the HD group (Control: 1.0 ± 0.1 versus HD group: 1.2 ± 0.27). Similarly, no increase in the ratio between p- PI3Kp85 and total PI3Kp85 was observed (**Figure 4.9**).
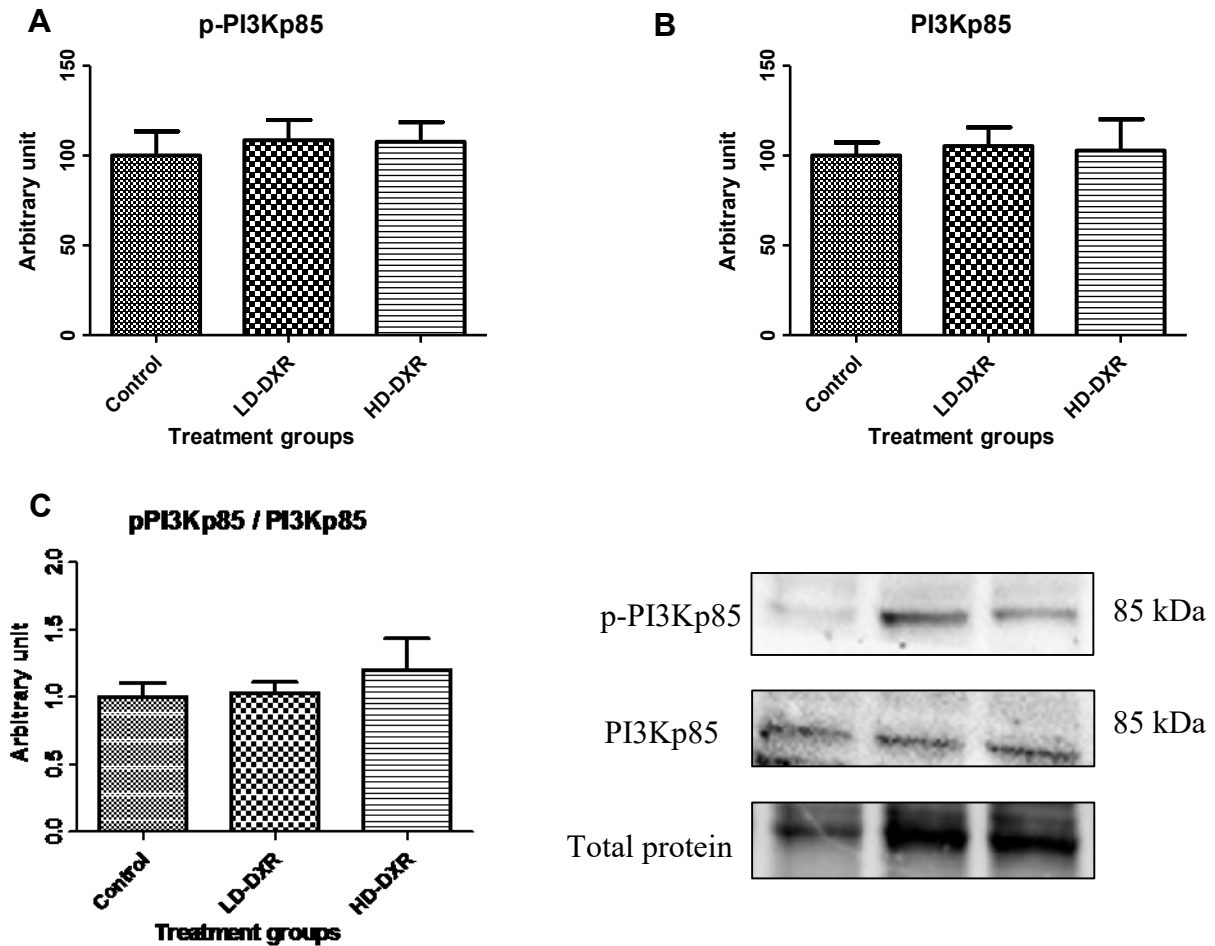
Figure 4.9. The effect of low and high DXR concentration on PI3Kp85 protein phosphorylation status. (A) Phosphorylated-PI3Kp85 (p-PI3Kp85). (B) Total PI3Kp85 expression. (C) Ratio between p-PI3Kp85 and total PI3Kp85. Results are expressed as mean ± SEM.

4.5.6 PDK1

Despite a slight decrease in the HD group (Control: 1.0 ± 0.11 versus HD group: 0.96 ± 0.11), DXR did not significantly alter PDK1 phosphorylation status (**Figure 4.10**).
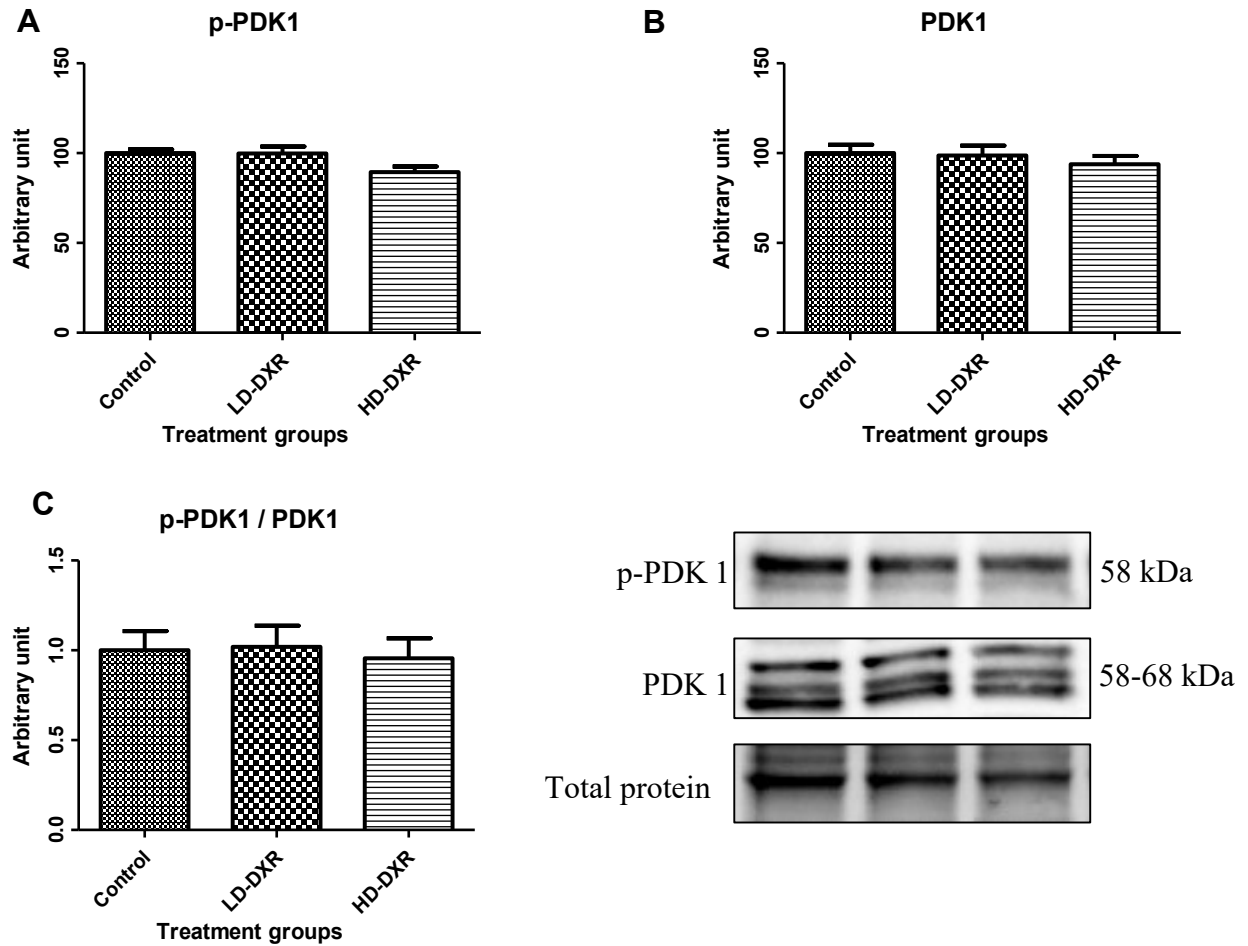
Figure 4.10. The effect of low and high DXR concentration on PDK1 protein phosphorylation status. (A) Phosphorylated-PDK1 (p-PDK1). (B) Total PDK1 expression. (C) Ratio between p-PTEN and total PDK1. Results are expressed as mean ± SEM.

4.5.1 Akt (phosphorylated at thr308)

Despite a slight increase in the HD group (Control: 1.0 ± 0.2 versus HD group: 1.74 ± 0.44), no significant difference in phosphorylation (thr308) was observed (**Figure 4.11**).
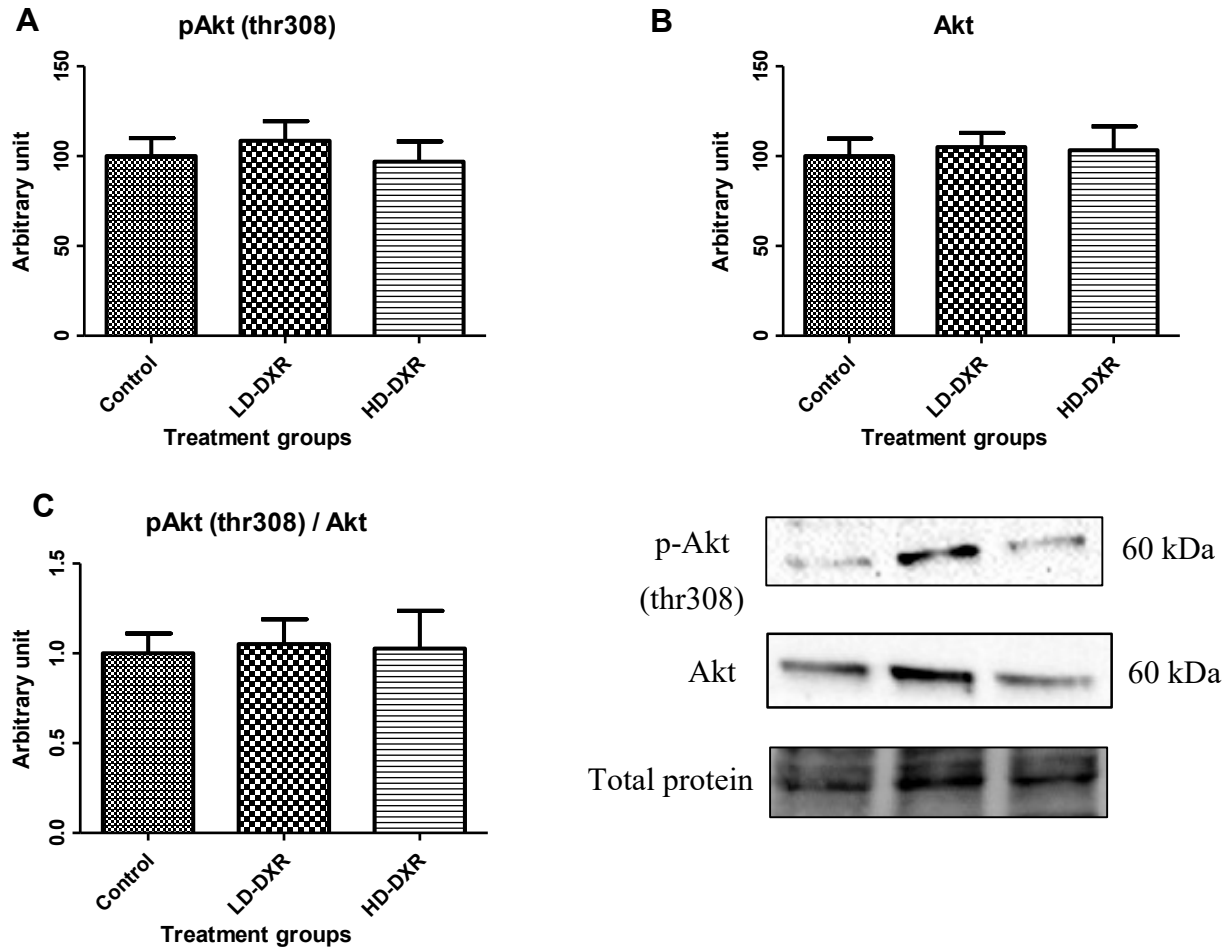
Figure 4.11. The effect of low and high DXR concentration on Akt protein phosphorylation status (thr308). (A) Phosphorylated Akt (thr308). (B) Total Akt expression. (C) Ratio between p-Akt (thr308) and total Akt. Results are expressed as mean ± SEM.

4.5.2 Akt (phosphorylated at ser473)

DXR did not significantly alter Akt phosphorylation (ser473) between groups (**Figure 4.12**), as a slight increase in the phosphorylation of Akt remained non-significant (Control: 1.0 ± 0.2 versus HD group: 1.74 ± 0.44).
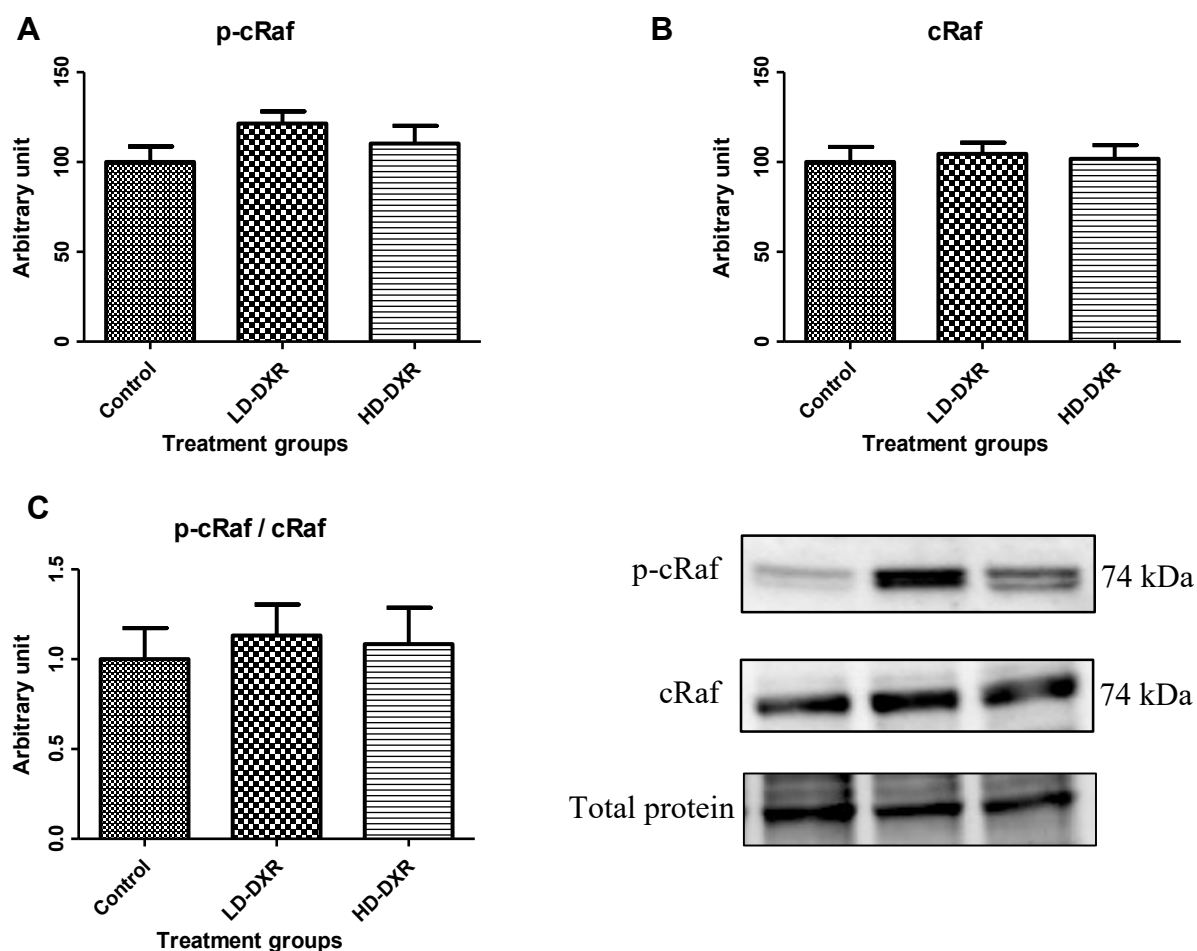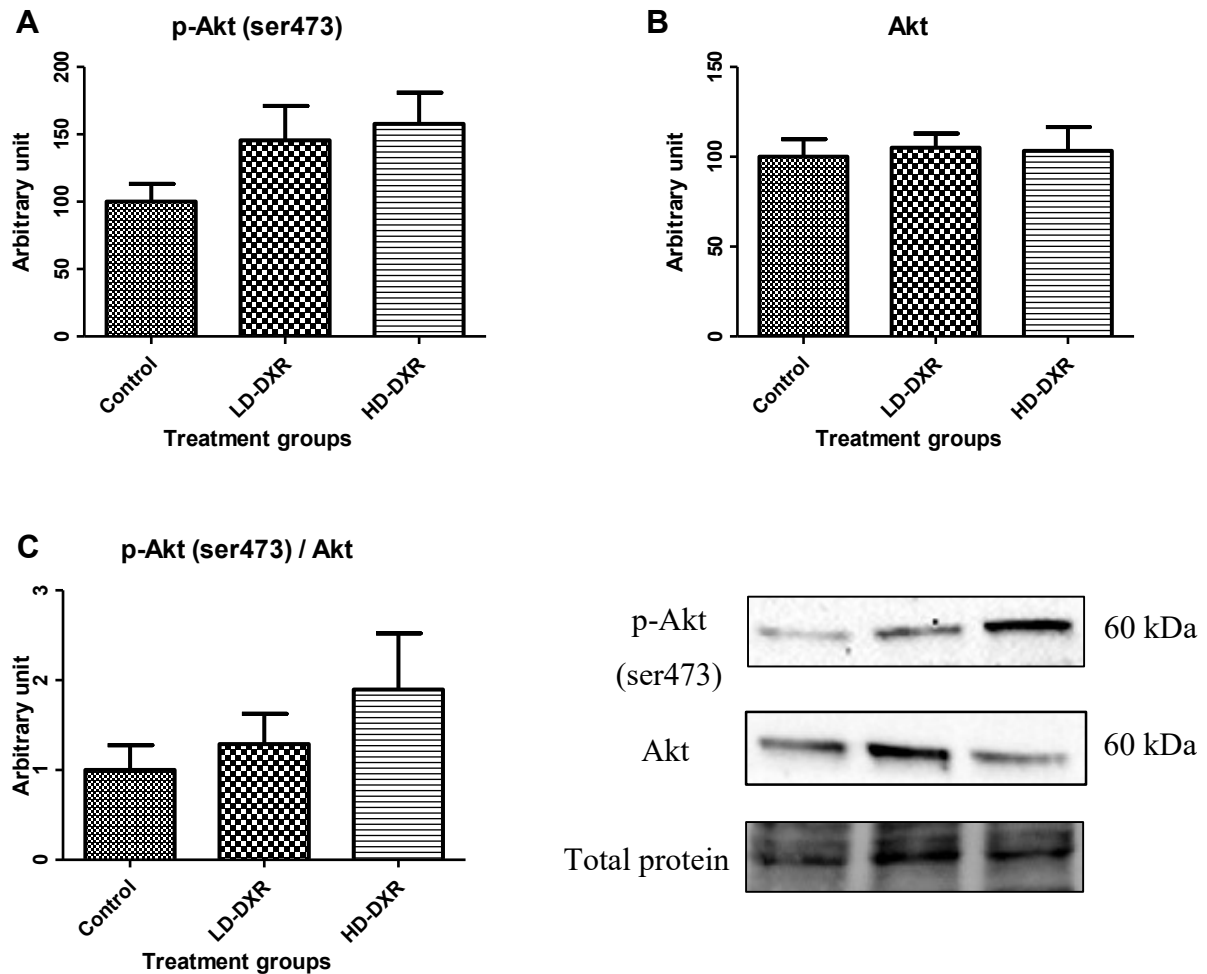

Figure 4.12. The effect of low and high DXR concentration on Akt protein phosphorylation status (ser473). (A) Phosphorylated Akt (ser473). (B) Total Akt expression. (C) Ratio between p-Akt (ser473) and total Akt. Results are expressed as mean ± SEM.

4.5.3 mTOR

There were no significant differences in either total or phosphorylated mTOR, and correspondingly, also no increase in the ratio between p-mTOR and total mTOR (**Figure 4.13**), despite a slight increase in the LD group (Control: 1.0 ± 0.38 versus LD group: 1.18 ± 0.24). .
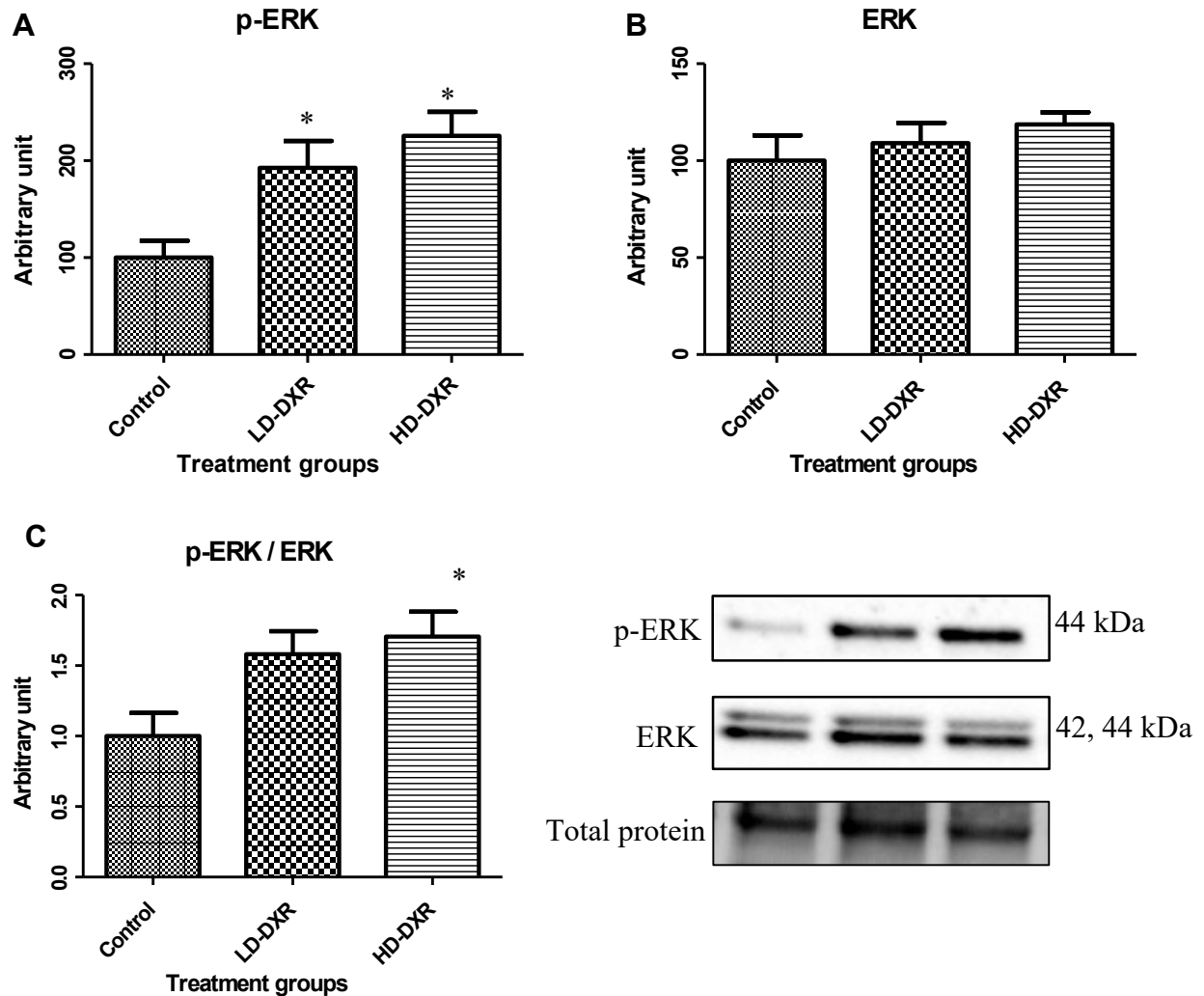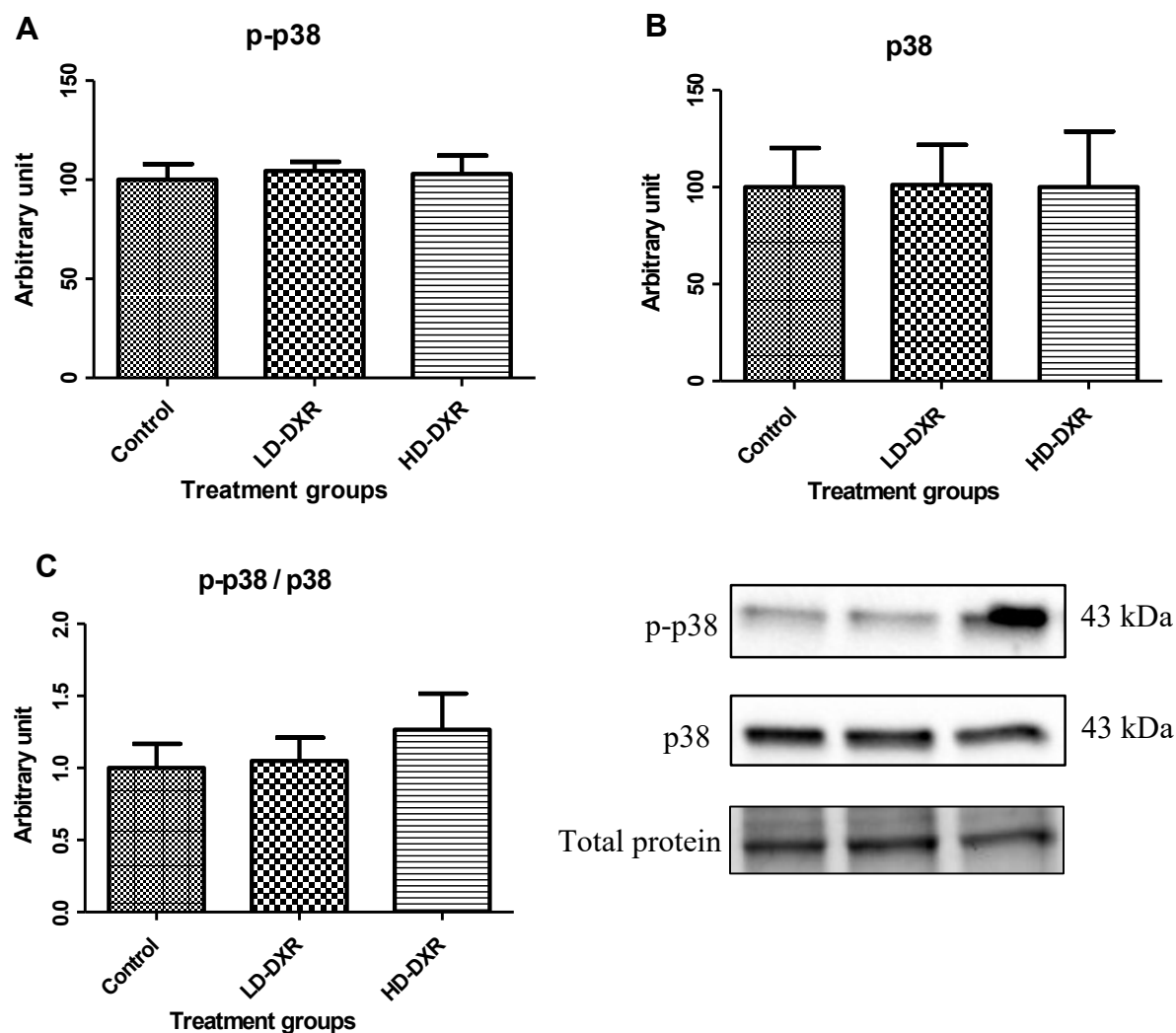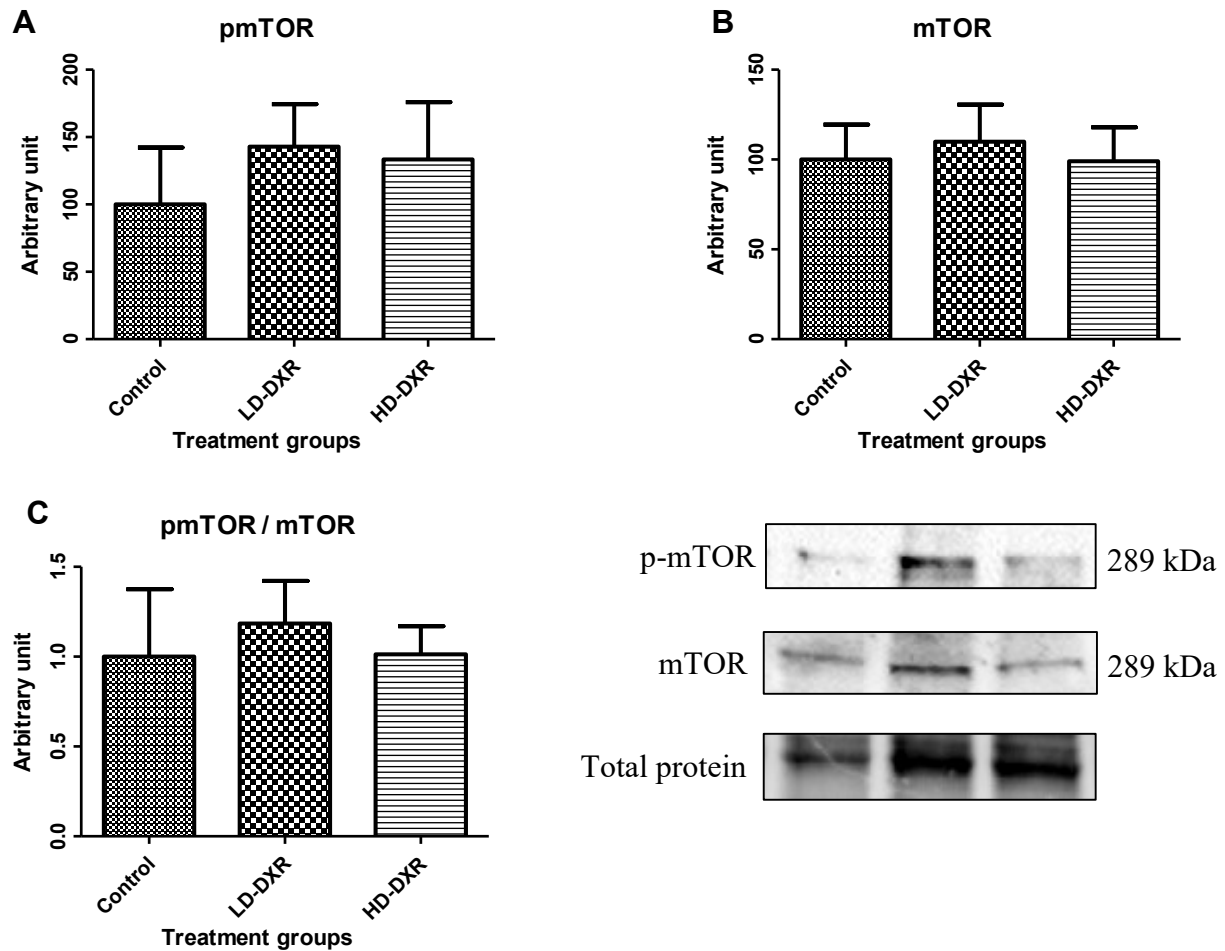

Figure 4.13. The effect of low and high DXR concentration on mTOR protein phosphorylation status. (A) Phosphorylated-mTOR. (B) Total mTOR expression. (C) Ratio between p-mTOR and total mTOR. Results are expressed as mean ± SEM.

4.5.4 Bcl-2

There were no significant differences in the expression of Bcl-2 between groups (**Figure 4.14**) (Control: 100.0 ± 12.5; LD group: 94.62 ± 9.16; HD group: 84.46 ± 13.09).
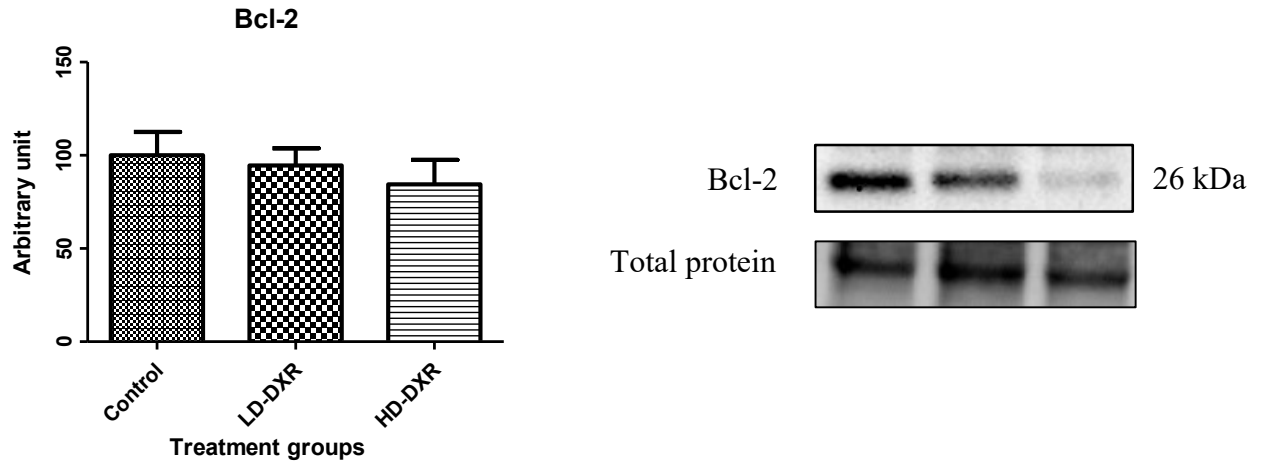
Figure 4.14. The effect of low and high DXR concentration on Bcl-2 expression. Results are expressed as mean ± SEM.

4.6 Results: Apoptotic markers

4.6.1 Caspase 9

Expression of caspase 9 was not significantly different between groups (**Figure 4.15**) (Control: 100.0 ± 12.08; LD group: 115.4 ± 10.81; HD group: 108.3 ± 8.87).
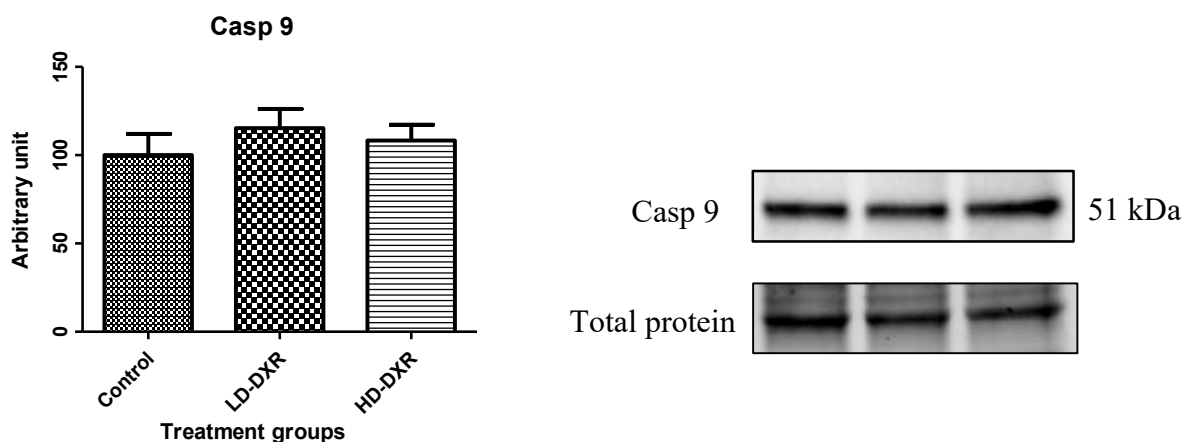
Figure 4.15. The effect of low and high DXR concentration on caspase 9 expression. Results are expressed as mean ± SEM.

4.6.2   Caspase 8

DXR did not significantly alter the ratio between cleaved and un-cleaved caspase 8 between groups (**Figure 4.16**). This is despite a dramatic (almost 5-fold) increase in the HD group above the control group, which is most likely due to the high SEM in the HD group (Control: 1.0 ± 0.14; LD group: 2.04 ± 0.89; HD group: 5.78 ± 2.95).
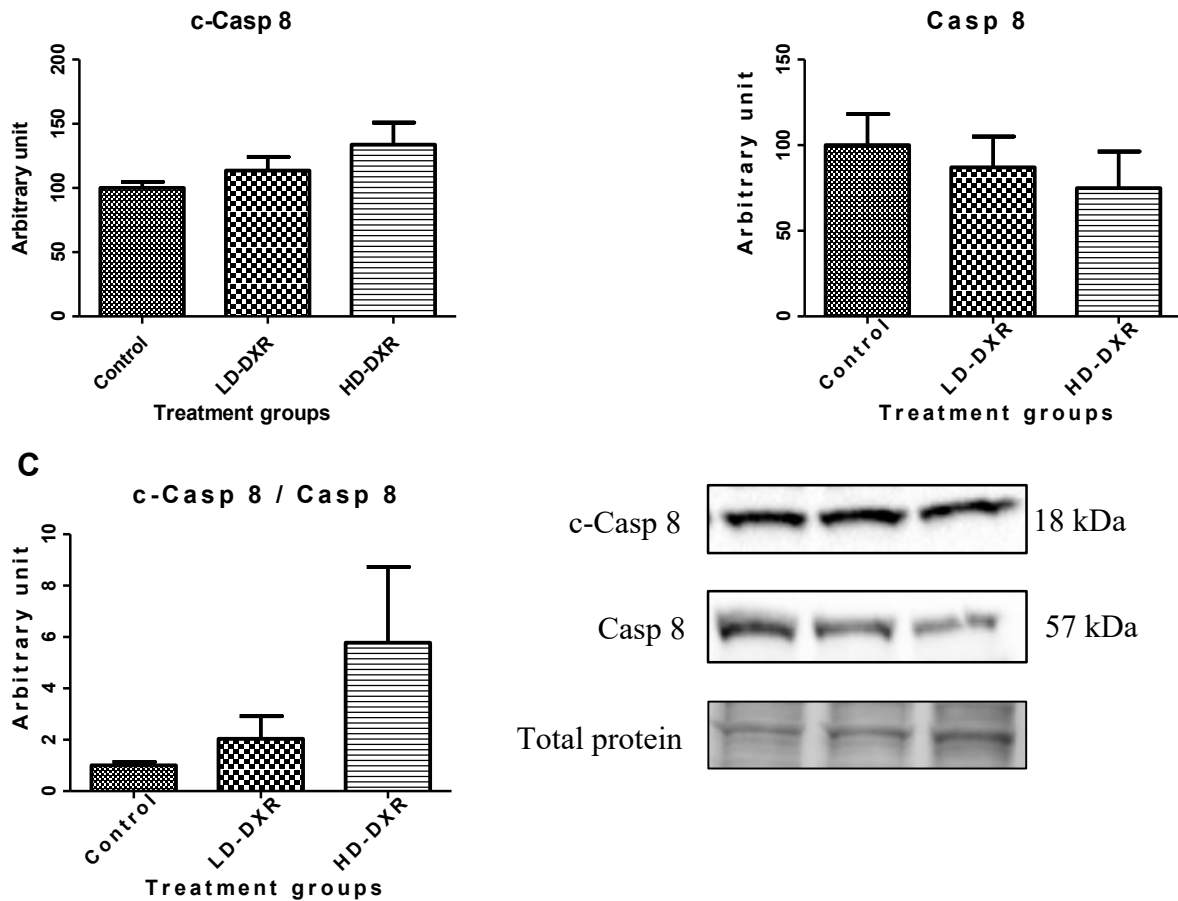
Figure 4.16. The effect of low and high DXR concentration on caspase 8 cleavage. Results are expressed as mean ± SEM.

4.6.3   Caspase 3

There was no significant difference in the ratio between total and cleaved caspase 3 between groups (**Figure 4.17**).
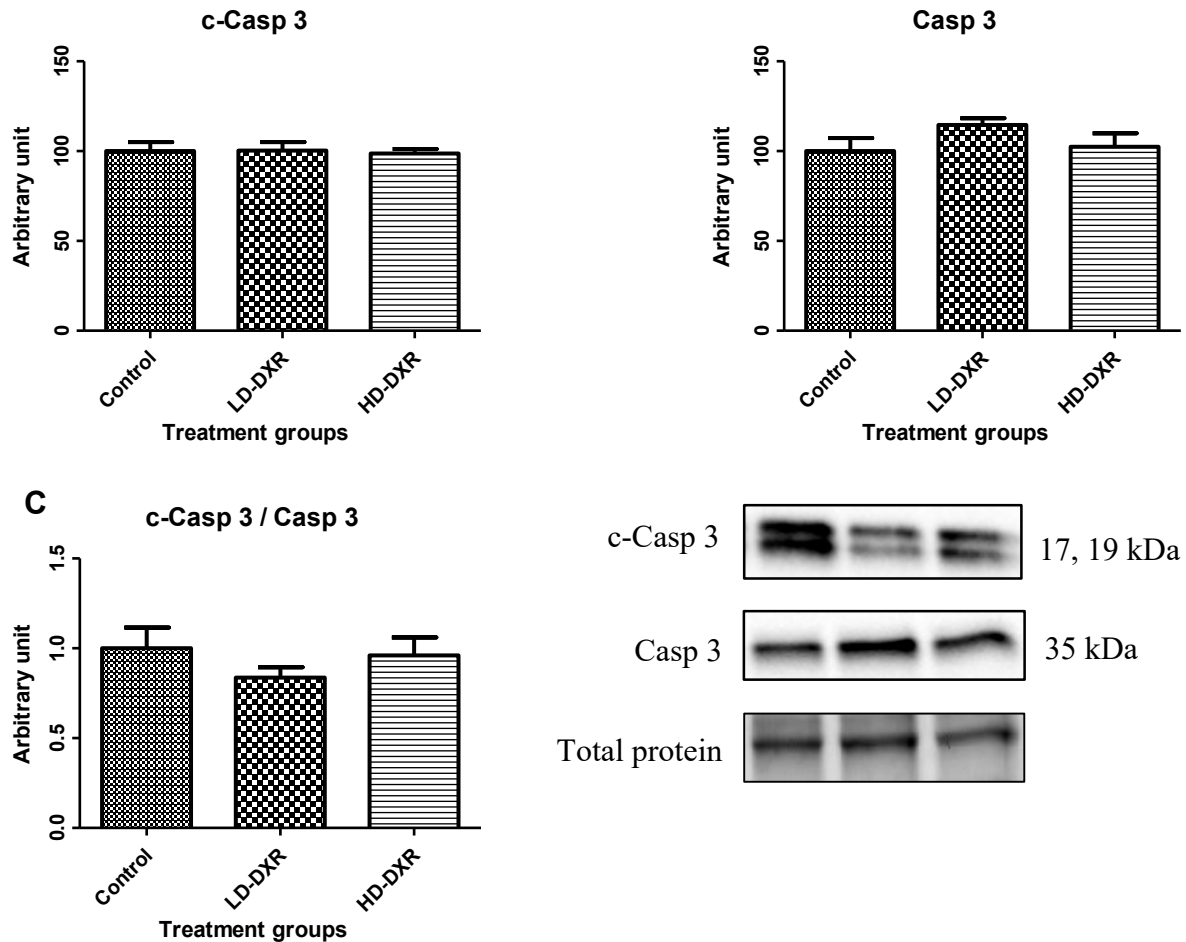
Figure 4.17. The effect of low and high DXR concentration on caspase 3 cleavage. Results are expressed as mean ± SEM.

4.7   Discussion

Although various trends were evident, the only significant change that was observed relates to the increase in ERK phosphorylation (**Figure 4.5**). The lack of significance (e.g. caspase 8 – **Figure 4.16**) is likely because of the greater variance in the data set, as well as the fact that Bonferoni is a conservative post hoc test. Caspase 8 activation is mediated via the extrinsic pathway by factors such as TNF (Beaudouin et al., 2013) or immune cell activation (Waring

and Müllbacher, 1999). TNF might be increased as a result of DXR-induced tissue damage, or might be expressed by tumour cells as a result of the hostile micro-environment (e.g. hypoxic tumour centres resulting from rapid cell division outpacing vascularisation). However, none of the other caspases showed evidence of an increase in cleavage (a marker for the induction of apoptosis), suggesting that DXR did not increase cell death.

ERK, as a member of the mitogen-activated protein kinase super family, antagonises apoptotic signals and promotes cell division (Mebratu and Tesfaigzi, 2009). The downstream targets of ERK are diverse: ERK1/2 regulates more than 600 proteins (Steelman et al., 2011). ERK phosphorylation is induced by growth factors which might be derived from different sources. As an example, cancer cells induce the paracrine release of various growth factors by stromal cells (Caplan and Dennis, 2006). Similarly, cancer cells themselves can also release trophic factors in an autocrine fashion (Hoelzinger et al., 2007). Alternatively, following tissue damage resulting from DXR, an increase in circulating growth factors might occur to promote tissue repair. In this regard, attempts were made to measure various serum markers using a Luminex Bead-based Multiplex Assay platform. Unfortunately, results were below the detectable range, likely as a result of experimental error[2].

The mechanism by which DXR promotes tumour growth is thus not clear. One possibility is that DXR compromised the immune system of mice, resulting in lower levels of immune surveillance. Indeed, the fact that mice exhibited lower tolerance toward DXR demonstrated the susceptibility of mice to DXR. Accordingly, the DXR reduced host resistance by eliminating immune cells that would otherwise induce cancer cell death. However, this argument is not supported by the fact that apoptotic signalling was not observed. Alternatively, cell-autonomous mechanisms in cancer cells might explain the increased tumour growth. The inability of DXR to induce apoptosis might be a result of an increased expression of efflux proteins. As an example, the over-expression of ABC transporters, known to export xenobiotic compounds such as DXR (Elliott and Al-Hajj, 2009), is a known mechanism of drug resistance in cancer cells. This would imply that DXR did not directly alter cancer cell growth since intra-

---

[2] Samples were analysed on the same day as samples from another study, which also generated data below the standard curve, suggesting experimental or assay failure rather than a legitimate decrease in serum markers.

cellular DXR concentrations would be low. However, chemoresistance does no directly explain the increase in tumour growth. Rather, tumour growth might be promoted by the release of growth factors after DXR has been cleared or it might have resulted from an increase in serum nutrients which might promote cell growth. Collectively, these observations indicate that DXR did not alter apoptotic pathways, but could decrease resistance as host reasons to DXR-mediate tissue injury. Growth factors released during the resolution phase could have led to the activation of ERK pathway in tumour cells, promoting tumour growth, thereby explaining lower resistance.

4.8   Reference List

Avan, A., Narayan, R., Giovannetti, E., and Peters, G.J. (2016). Role of Akt signaling in resistance to DNA-targeted therapy. World. J .Clin. Oncol. *7,* 352.

Banerjee, P., and Kyriakis, J.M. (1994). The stress-activated protein kinase subfamily of c-Jun kinases. Nature *369,* 156-160.

Basu, A., and Haldar, S. (1998). The relationship between BcI2, Bax and p53: consequences for cell cycle progression and cell death. Mol. Hum. Reprod. *4,* 1099-1109.

Beaudouin, J., Liesche, C., Aschenbrenner, S., Hörner, M., and Eils, R. (2013). Caspase-8 cleaves its substrates from the plasma membrane upon CD95-induced apoptosis. Cell Death Differ. *20,* 599-610.

Bradford, M.M. (1976). A rapid and sensitive method for the quantitation of microgram quantities of protein utilizing the principle of protein-dye binding. Anal. Biochem. *72,* 248-254.

Bulavin, D.V., Saito, S., Hollander, M.C., Sakaguchi, K., Anderson, C.W., Appella, E., and Fornace, A.J.,Jr. (1999). Phosphorylation of human p53 by p38 kinase coordinates N-terminal phosphorylation and apoptosis in response to UV radiation. Embo J. *18,* 6845-6854.

Cain, K., Bratton, S.B., and Cohen, G.M. (2002). The Apaf-1 apoptosome: a large caspase-activating complex. Biochimie *84,* 203-214.

Caplan, A.I., and Dennis, J.E. (2006). Mesenchymal stem cells as trophic mediators. J. Cell. Biochem. *98,* 1076-1084.

Chen, Y.R., Meyer, C.F., and Tan, T.H. (1996). Persistent activation of c-Jun N-terminal kinase 1 (JNK1) in gamma radiation-induced apoptosis. J. Biol. Chem. *271,* 631-634.

Chipuk, J.E., Kuwana, T., Bouchier-Hayes, L., Droin, N.M., Newmeyer, D.D., Schuler, M., and Green, D.R. (2004). Direct activation of Bax by p53 mediates mitochondrial membrane permeabilization and apoptosis. Science *303,* 1010-1014.

Cory, S., Huang, D.C., and Adams, J.M. (2003). The Bcl-2 family: roles in cell survival and oncogenesis. Oncogene *22,* 8590-8607.

Cully, M., You, H., Levine, A.J., and Mak, T.W. (2006). Beyond PTEN mutations: the PI3K pathway as an integrator of multiple inputs during tumorigenesis. Nat. Rev. Cancer *6,* 184-192.

Dessypris, E.N., Brenner, D.E., and Hande, K.R. (1986). Toxicity of doxorubicin metabolites to human marrow erythroid and myeloid progenitors in vitro. Cancer Treat. Rep. *70,* 487-490.

Donovan, N., Becker, E.B., Konishi, Y., and Bonni, A. (2002). JNK phosphorylation and activation of BAD couples the stress-activated signaling pathway to the cell death machinery. J. Biol. Chem. *277,* 40944-40949.

Doroshow, J.H., and Davies, K.J. (1986). Redox cycling of anthracyclines by cardiac mitochondria. II. Formation of superoxide anion, hydrogen peroxide, and hydroxyl radical. J. Biol. Chem. *261,* 3068-3074.

Elliott, A.M., and Al-Hajj, M.A. (2009). ABCB8 mediates doxorubicin resistance in melanoma cells by protecting the mitochondrial genome. Mol. Cancer. Res. *7,* 79-87.

Fernandes-Alnemri, T., Armstrong, R.C., Krebs, J., Srinivasula, S.M., Wang, L., Bullrich, F., Fritz, L.C., Trapani, J.A., Tomaselli, K.J., Litwack, G., and Alnemri, E.S. (1996). In vitro activation of CPP32 and Mch3 by Mch4, a novel human apoptotic cysteine protease containing two FADD-like domains. Proc. Natl. Acad. Sci. U. S. A. *93,* 7464-7469.

Fulda, S., and Debatin, K. (2006). Extrinsic versus intrinsic apoptosis pathways in anticancer chemotherapy. Oncogene *25,* 4798-4811.

Garrido, C., Galluzzi, L., Brunet, M., Puig, P., Didelot, C., and Kroemer, G. (2006). Mechanisms of cytochrome c release from mitochondria. Cell Death & Differentiation *13,* 1423-1433.

Georgescu, M. (2010). PTEN tumor suppressor network in PI3K-Akt pathway control. Genes Cancer *1,* 1170-1177.

Gewirtz, D. (1999). A critical evaluation of the mechanisms of action proposed for the antitumor effects of the anthracycline antibiotics adriamycin and daunorubicin. Biochem. Pharmacol. *57,* 727-741.

Ghigo, A., Li, M., and Hirsch, E. (2016). New signal transduction paradigms in anthracycline-induced cardiotoxicity. Biochim Biophys. Acta. *1863,* 1916-1925.

Guliaeva, N.A., Kuznetsova, E.A., and Gaziev, A.I. (2006). Proteins associated with mitochondrial DNA protect it against the action of X-rays and hydrogen peroxide. Biofizika *51,* 692-697.

Hemmings, B.A., and Restuccia, D.F. (2012). PI3K-PKB/Akt pathway. Cold Spring Harb Perspect. Biol. *4,* a011189.

Hoelzinger, D.B., Demuth, T., and Berens, M.E. (2007). Autocrine factors that sustain glioma invasion and paracrine biology in the brain microenvironment. J. Natl. Cancer Inst. *99,* 1583-1593.

Kato, S., Burke, P.J., Fenick, D.J., Taatjes, D.J., Bierbaum, V.M., and Koch, T.H. (2000). Mass spectrometric measurement of formaldehyde generated in breast cancer cells upon treatment with anthracycline antitumor drugs. Chem. Res. Toxicol. *13,* 509-516.

Khiati, S., Dalla Rosa, I., Sourbier, C., Ma, X., Rao, V.A., Neckers, L.M., Zhang, H., and Pommier, Y. (2014). Mitochondrial topoisomerase I (top1mt) is a novel limiting factor of doxorubicin cardiotoxicity. Clin. Cancer Res. *20,* 4873-4881.

Li, H., Zhu, H., Xu, C., and Yuan, J. (1998). Cleavage of BID by caspase 8 mediates the mitochondrial damage in the Fas pathway of apoptosis. Cell *94,* 491-501.

Li, Z., Pearlman, A.H., and Hsieh, P. (2016). DNA mismatch repair and the DNA damage response. DNA Repair *38,* 94-101.

Lidke, D.S., Huang, F., Post, J.N., Rieger, B., Wilsbacher, J., Thomas, J.L., Pouyssegur, J., Jovin, T.M., and Lenormand, P. (2010). ERK nuclear translocation is dimerization-independent but controlled by the rate of phosphorylation. J. Biol. Chem. *285,* 3092-3102.

Liu, Z., Hsu, H., Goeddel, D.V., and Karin, M. (1996). Dissection of TNF receptor 1 effector functions: JNK activation is not linked to apoptosis while NF-κB activation prevents cell death. Cell *87,* 565-576.

Liu, H., Wang, Z., and Nowicki, M.J. (2014). Caspase-12 mediates carbon tetrachloride-induced hepatocyte apoptosis in mice. World J. Gastroenterol. *20,* 18189-18198.

Manning, B.D., and Cantley, L.C. (2007). AKT/PKB signaling: navigating downstream. Cell *129,* 1261-1274.

Mebratu, Y., and Tesfaigzi, Y. (2009). How ERK1/2 activation controls cell proliferation and cell death: Is subcellular localization the answer? Cell Cycle *8,* 1168-1175.

Mukhopadhyay, P., Rajesh, M., Batkai, S., Kashiwaya, Y., Hasko, G., Liaudet, L., Szabo, C., and Pacher, P. (2009). Role of superoxide, nitric oxide, and peroxynitrite in doxorubicin-induced cell death in vivo and in vitro. Am. J. Physiol. Heart Circ. Physiol. *296,* 1466-83.

Pang, B., Qiao, X., Janssen, L., Velds, A., Groothuis, T., Kerkhoven, R., Nieuwland, M., Ovaa, H., Rottenberg, S., and van Tellingen, O. (2013). Drug-induced histone eviction from open chromatin contributes to the chemotherapeutic effects of doxorubicin. Nat. Commun. *4,* 1908.

Pópulo, H., Lopes, J.M., and Soares, P. (2012). The mTOR signalling pathway in human cancer. Int. J. Mol. Sci. *13,* 1886-1918.

Ryoo, H.D., Gorenc, T., and Steller, H. (2004). Apoptotic cells can induce compensatory cell proliferation through the JNK and the Wingless signaling pathways. Dev. Cell. *7,* 491-501.

Samatar, A.A., and Poulikakos, P.I. (2014). Targeting RAS–ERK signalling in cancer: promises and challenges. Nat. Rev. Drug. Discov. *13,* 928-942.

Sartorius, U.A., and Krammer, P.H. (2002). Upregulation of bcl-2 is involved in the mediation of chemotherapy resistance in human small cell lung cancer cell lines. Int J Cancer *97,* 584-592.

Sasaki, A., Taketomi, T., Kato, R., Saeki, K., Nonami, A., Sasaki, M., Kuriyama, M., Saito, N., Shibuya, M., and Yoshimura, A. (2003). Mammalian Sprouty4 suppresses Ras-independent ERK activation by binding to Raf1. Nat. Cell Biol. *5,* 427-432.

Sax, J.K., Fei, P., Murphy, M.E., Bernhard, E., Korsmeyer, S.J., and El-Deiry, W.S. (2002). BID regulation by p53 contributes to chemosensitivity. Nat. Cell Biol. *4,* 842-849.

Shen, H., and Liu, Z. (2006). JNK signaling pathway is a key modulator in cell death mediated by reactive oxygen and nitrogen species. Free Radic. Biol. Med. *40,* 928-939.

Song, M.S., Salmena, L., and Pandolfi, P.P. (2012). The functions and regulation of the PTEN tumour suppressor. Nat. Rev. Mol. Cell Bio. *13,* 283-296.

Stambolic, V., MacPherson, D., Sas, D., Lin, Y., Snow, B., Jang, Y., Benchimol, S., and Mak, T. (2001). Regulation of PTEN transcription by p53. Mol. Cell *8,* 317-325.

Steelman, L.S., Chappell, W.H., Abrams, S.L., Kempf, R.C., Long, J., Laidler, P., Mijatovic, S., Maksimovic-Ivanic, D., Stivala, F., Mazzarino, M.C.*, et al.* (2011). Roles of the Raf/MEK/ERK and PI3K/PTEN/Akt/mTOR pathways in controlling growth and sensitivity to therapy-implications for cancer and aging. Aging *3,* 192-222.

Sunayama, J., Tsuruta, F., Masuyama, N., and Gotoh, Y. (2005). JNK antagonizes Akt-mediated survival signals by phosphorylating 14-3-3. J. Cell Biol. *170,* 295-304.

Tan, C., Lu, Y., Ji, L., and Mao, Z. (2014). Metallomics insights into the programmed cell death induced by metal-based anticancer compounds. Metallomics *6,* 978-995.

Tewey, K.M., Rowe, T.C., Yang, L., Halligan, B.D., and Liu, L.F. (1984). Adriamycin-induced DNA damage mediated by mammalian DNA topoisomerase II. Science *226,* 466-468.

Vivanco, I., Palaskas, N., Tran, C., Finn, S.P., Getz, G., Kennedy, N.J., Jiao, J., Rose, J., Xie, W., and Loda, M. (2007). Identification of the JNK signaling pathway as a functional target of the tumor suppressor PTEN. Cancer Cell *11,* 555-569.

Wang, S., and El-Deiry, W.S. (2003). TRAIL and apoptosis induction by TNF-family death receptors. Oncogene *22,* 8628-8633.

Waring, P., and Müllbacher, A. (1999). Cell death induced by the Fas/Fas ligand pathway and its role in pathology. Immunol. Cell Biol. *77,* 312-317.

Weber, C.K., Slupsky, J.R., Kalmes, H.A., and Rapp, U.R. (2001). Active Ras induces heterodimerization of cRaf and BRaf. Cancer Res. *61,* 3595-3598.

Wilson, N.S., Dixit, V., and Ashkenazi, A. (2009). Death receptor signal transducers: nodes of coordination in immune signaling networks. Nat. Immunol. *10,* 348-355.

Zhang, S., Liu, X., Bawa-Khalfe, T., Lu, L., Lyu, Y.L., Liu, L.F., and Yeh, E.T. (2012). Identification of the molecular basis of doxorubicin-induced cardiotoxicity. Nat. Med. *18,* 1639-1642.

Zhang, W., and Liu, H.T. (2002). MAPK signal pathways in the regulation of cell proliferation in mammalian cells. Cell Res. *12,* 9-18.

Chapter 5

Both tumour load and chemotherapy are likely to impact on host tolerance and resistance. Given the cardinal role played by the liver in energy homeostasis, immunomodulation functions and detoxification of xenobiotic, efforts were directed at investigating the effects of tumour load (EO771 vs B16) and chemotherapy on hepatic autophagy and cell death/survival markers.

5.1 Introduction

Various anatomical features, unique to the liver, highlight the key role of the liver as a major 'filtering' organ. While the hepatic arteries provide oxygenated blood, the liver also receives blood via the portal vein which derives its blood supply directly from the gastrointestinal tract. The portal system thus ensures that any substrate ingested is first 'filtered' by the liver before entering systemic circulation. Also, the liver exhibits a low blood pressure as a result of various hepatic sinusoids, where the slow blood flow provides more time for liver cells to clear toxins and foreign bodies. In fact, the liver can contain approximately a quarter of the total cardiac output in humans (Dhainaut et al., 2001). Consequently, the liver plays a key role in metabolising xenobiotics: the liver expresses a battery of enzymes capable of metabolising noxious substrates into less noxious compounds (Shimada, 2006). The liver also performs housekeeping functions such as the synthesis of various biological compounds for both local and systemic supply, as well as the removal of excess metabolites. Moreover, recent evidence indicates that the liver, as opposed to the spleen, might represent the primary organ for the removal of damaged erythrocytes (Theurl et al., 2016). The liver also represents the major site for vitamin A storage (Blomhoff et al., 1990).

Another housekeeping function of the liver is the production of primary bile acids by hepatocytes, which play an indisputably critical role in the digestion of lipids and the absorption of hydrophobic vitamins in micelles. Bile acids are formed by conjugating an amino acid, such as taurine, to a cholic acid (a steroid moiety). The polarity and hydrophobicity of the bile acid is thus dependent on the moiety conjugated to cholic acid. Hence, the consequence that dietary fats has an impact on the type of bile acid produced. As an example, long chain fatty acids are

more likely to induce the secretion of more hydrophobic bile acids since these fatty acids are less water soluble than short chain fatty acids. Interestingly, the amphiphilic nature of bile acids makes it possible for these molecules to disrupt bacterial membranes (Taranto et al., 2006), suggesting that bile might also play a role in preventing bacterial overgrowth of the small intestine. Conversely, the differential ability of certain bacteria to metabolise bile salts has also been implicated in the ontology of dysbiosis between host and intestinal biota. As an example, in mice, the introduction of a diet rich in milk fats stimulates the increased production of taurine-conjugated bile salts, which in turn promotes the growth of anaerobic bacteria, *Bilophila wadsworthia*, which use the sulphur in taurine as a terminal electron acceptor (Devkota et al., 2012). Also, biliary excretion of various xenobiotics can represent a major route for the systemic clearance of toxins. As an example, in an isolated perfused rat liver model system, almost a third of DXR was cleared by the biliary secretion of unmodified DXR (Ballet et al., 1987). Finally, bile salts, either modified by intestinal biota, or unmodified entering circulation (being very effectively reabsorbed post-prandially), can bind to various nuclear receptors and influence a host of cell types (recently reviewed elsewhere (Kuipers et al., 2014; Li and Chiang, 2013). Bile secretion thus has an impact on the population of intestinal biota, nutrient absorption and clearance of xenobiotics, and it influences immune and metabolic parameters by binding to nuclear receptors.

The liver also has an important immunological function. Kupffer cells in the liver represent the largest population of tissue-resident macrophages (Dhainaut et al., 2001). In response to inflammatory stimuli, the liver represents a major site for the production of cytokines, initial phase proteins and various pro-thrombotic factors (Dhainaut et al., 2001). However, the liver has also been shown to play a role in clearance of such inflammatory mediators (Andus et al., 1991). In fact, Kupffer cells also play a crucial role in clearance of bacteria (Katz et al., 1991) and inflammatory mediators such as lipopolysaccharides (LPS) (Mathison and Ulevitch, 1979). As an example, impairment in liver function decreases the ability of the liver to clear bacteria (Ashare et al., 2009). Similarly, two hours following a 90% hepatecomy, rats demonstrated bacteraemia (Wang et al., 1993). It should however be noted that an increase in bacteria entering circulation is not only a result of decreased liver clearance, but also results from an increase in the growth of bacteria in the small intestine (Wang et al., 1993). Also, others (Cani et al., 2009) have shown that inflammatory mediators could increase gut permeability and enhance bacterial translocation, suggesting that the accumulation of bacteria is not only a result

of decreased clearance, but also due to an increase in bacteria translocation as a result of increased gut permeability.

As a major site for glycogen storage, along with an extensive capacity for gluconeogenesis, the liver plays a key role in glucose homeostasis (Pilkis and Granner, 1992). The role of the liver in maintaining energy homeostasis is particularly relevant during an infection, or in response to an inflammatory stimulus in general, as the elevated blood glucose during severe infections is largely driven by gluconeogenesis in the liver (Dahn et al., 1995; Hirasawa et al., 2009). In turn, elevated glucose levels play a key adaptive role: in the mitochondrial matrix of rapidly dividing cells (e.g. cancerous as well as non-transformed cells such as rapidly proliferating immune cells), glucose is converted to acetyl-CoA which is subsequently fluxed into biosynthetic pathways (Vander Heiden et al., 2009). This observation is also supported by the finding that the differentiation of monocytes into mature macrophages is inhibited by the inactivation of fatty acid biosynthetic pathways (Ecker et al., 2010). In turn, fatty acid synthesis drives the production of phospholipids, which is required for mature macrophages to perform immune functions (e.g. increased phospholipids for the formation of filopodia as well as various organelles such as lysosomes) (Ecker et al., 2010). Finally, tissue rich in phagocytic cells such as the liver, spleen and lung consistently show an increase in glucose uptake in a rat caecal ligation and puncture model of sepsis (Maitra et al., 2000), demonstrating the increase glucose utilisation of immune cells during a bacterial challenge. These observations also illustrate the important role of maintaining elevated glucose levels during immune cell activation. The key role of the liver in supplying glucose during an infection is exemplified by the observation that primary hepatic dysfunction results in a decrease in glucose levels and the development of lactic acidosis (Dhainaut et al., 2001).

Patients in intensive care invariably exhibit a range of anomalous hepatic functional parameters (Jenniskens et al., 2016). Some of them might represent manifestations of pathology (i.e. pathogenicity) whereas other changes in liver function might in fact be directed to tolerance during the challenge, or aimed at resisting an infection. For example, an increase in glucose levels has been observed to be an "independent risk factor for increased hospital mortality" (Krinsley, 2003). Yet, hyperglycaemia might not be a cause of mortality, but might rather reflect a more severe infection. Likewise, other anomalies in liver function might not necessarily reflect pathology, but an adaptive response. As an example, hyperbilirubinemia has

similarly been described as "a common complication of sepsis" and a predictor of mortality during sepsis (Zhai et al., 2009). Yet, bilirubin is a potent antioxidant and could play an important role in protecting cells against oxidative stress (Jansen and Daiber, 2012). In this regard, the T/R framework might be applied in order to elucidate the physiological relevance of various 'anomalous' liver functional parameters.

Various operational aspects of the liver discussed are likely to play a role in response to DXR and tumour load. Rapidly dividing cancer cells might induce lactic acidosis (Sillos et al., 2001). Disrupted vascular architecture of tumours might induce anaemia as more blood becomes pooled in the poorly formed vascular bed (Nagy et al., 2009). Necrotic centres might provide a constant supply of sterile inflammatory mediators as intracellular content is spilled into the extracellular milieu (Lotze and Tracey, 2005; Trautmann, 2009). Similarly, DXR has been shown to increase release of inflammatory cytokines such as prostaglandin E_2, and interleukin 1β and 8 (Kang et al., 2013). Accordingly, targeting cytokine-signalling cascades has been proposed as a potential intervention for limiting the toxic effect of DXR (Wong et al., 2013). Thus, in addition to the role of the liver in metabolising DXR (Le Bot et al., 1988) and the excretion of DXR via bile flow (Ballet et al., 1987), the liver may also play a key role in altering metabolic parameters in response to DXR-induced cytokine release.

Both tumour load and DXR are thus likely to impose stress on the hepatic system. Regarding the critical role of the liver in managing the challenge posed by DXR and tumour load, a reduction of liver operational capacity will have a great impact on the host's ability to tolerate tumour load and DXR. Accordingly, the aim of this study was to investigate the role of tumour load on key hepatic proteins involved in cell survival as well as autophagy, a generic cell stress response, in an attempt to explain the observed difference between B17 and EO771 cells.

5.2   Molecular markers

Autophagy is a generic cellular stress response that is upregulated in response to a variety of cellular insults (Kroemer et al., 2010). Autophagy has been implicated in the removal of damaged proteins (Kroemer et al., 2010) as well as defective cellular organelles such as mitochondria (Ward et al., 2016). Since DXR has been implicated in oxidative stress, which results in protein and organelle damage (Zhou et al., 2001), it is likely that autophagy may play a pivotal role in mediating host tolerance to chemotherapeutic agents such as DXR.

Autophagy plays an indispensable role in energy homeostasis by supplying cells with nutrients from the breakdown of non-essential cellular components (Kuma et al., 2004). Autophagy is also involved in the mobilisation of stored fat (Ward et al., 2016) and glycogen (Zirin et al., 2013). Rapidly dividing cells could introduce low-level energy stress which might become compounded by the toxic effects of DXR.

Autophagy has also been implicated as a mechanism for cell death, though such claims have caused considerable controversy. The role of autophagy in response to cell stress implies that autophagy is often upregulated parallel to cell-death pathways similarly activated in response to the same stressor. However, a number of observations now implicate autophagy as a legitimate cell-death mechanism ('autosis') at least under certain conditions (Liu and Levine, 2015). Similarly, the consequence of an upregulation of autophagy in response to DXR is controversial with conflicting results being reported (Dirks-Naylor, 2013). As an example, in rats, suppression of autophagy with 3-methyladenine increased cardiovascular performance after a DXR challenge, implicating autophagy in the development of cardiovascular disease (Lu et al., 2009). Conversely, in mice, inhibition of autophagy with bafilomycin resulted in increased mortality, whereas induction of autophagy with rapamycin attenuated the development of cardio-toxicity (Sishi et al., 2013). The role of autophagy is thus not fully understood.

Autophagy also plays a key role in modulating inflammatory pathways, where it has been implicated in the secretion of activated Il-1β as well as the degradation of pro-Il-1β (Harris et al., 2011). Similarly, autophagy has also been implicated in the degradation of inflammasomes (Yuk and Jo, 2013). Since the liver hosts a large population of tissue-resident macrophages (Kupffer cells), it is likely that autophagy might play a key role in either increasing or attenuating inflammatory signalling pathways. Finally, hepatic autophagy might also have an important function in removing translocated bacteria, or LPS entering circulation (Katz et al., 1991; Mathison and Ulevitch, 1979).

Taken together, these observations demonstrate a number of cellular activities by which hepatic autophagy may impact on host tolerance and resistance (**Figure 5.1**). DXR treatment could damage mitochondria, induce the production of radicals which subsequently damage proteins. Since DXR damage rapidly dividing cells, including the rapidly dividing stem cells forming the intestinal epithelium (Dekaney et al., 2009), it is possible that translocated bacteria might

enter circulation where the liver may play an important function in removing pathogens as well as noxious factors such as LPS. In addition, removal of apoptotic bodies formed by liver cells destroyed by DXR could prevent secondary apoptosis and subsequent inflammation. Autophagic activity might also be implicated in an inflammatory signalling context, by targeting the inflammasome for degradation, or through the non-canonical secretion of inflammatory mediators such as IL-1β. In addition, the role of autophagy in mobilising energy-rich substrates also suggests that this pathway might have an impact on host resistance, since an increase in circulating nutrients might fuel tumour growth.
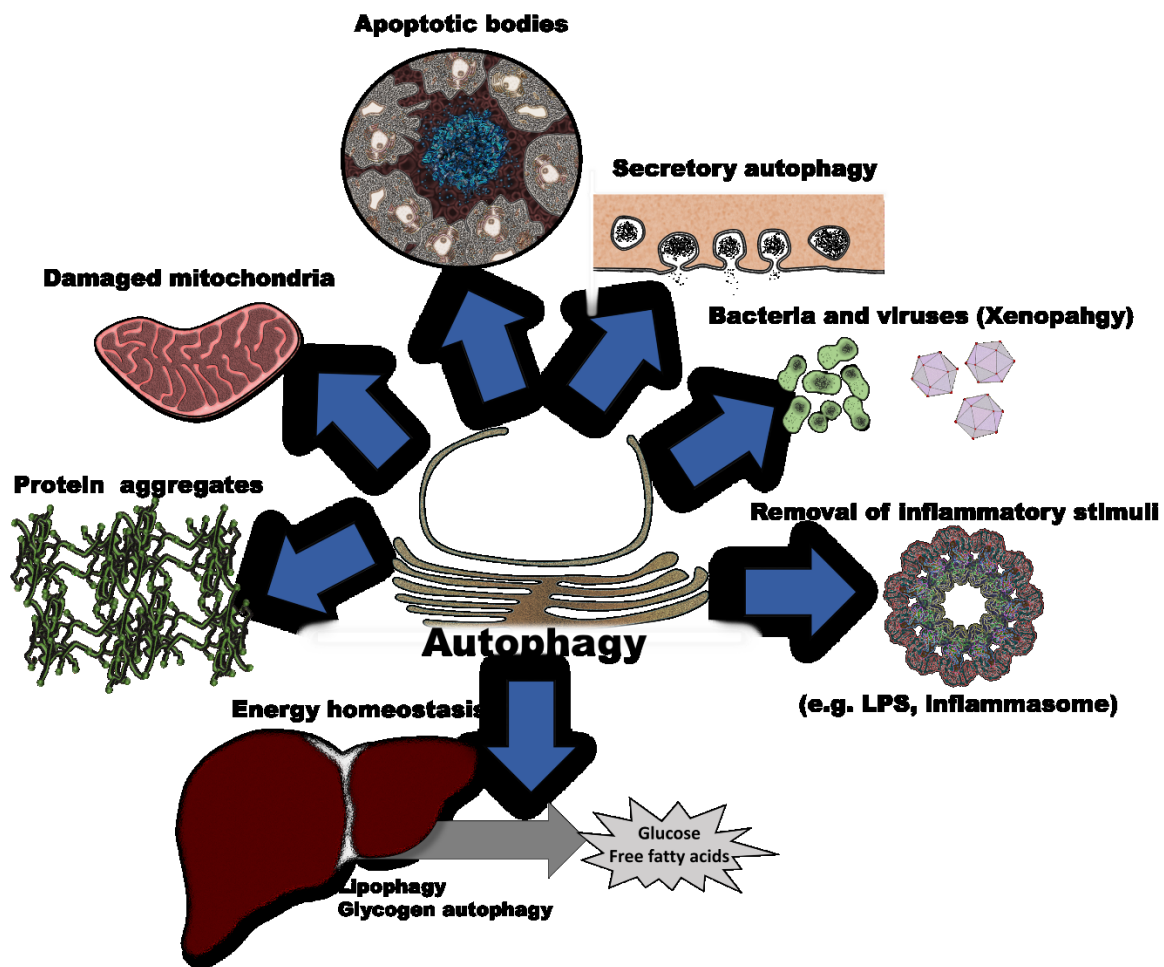
Figure 5.1. Hepatic autophagy plays a major role in a number of physiological functions.

In the current study two accepted markers for autophagy activity, p62 and LC3B-II were assessed (**Figure 5.2**). LC3 is cleaved by ATG4 (autophagy-related gene 4) forming LC3-1. In turn, cytosolic LC3-I is activated by ATG7 cleavage of a small peptide fragment and subsequent lipidation, rendering the active LC3B-II protein witch is membrane-bound, and in

turn, is recruited to the autophagosomal membrane (Tanida et al., 2008). The scaffold protein p62 can bind to both ubiquitin (Ub) and LC3, thus designating ubiquitinated proteins for autophagy degradation (Komatsu et al., 2007). Also, western blot analysis was conducted in order to investigate the activation status of mTOR (by phosphorylation on Ser2448) since mTOR activation is a strong suppressor of autophagy (Kim et al., 2011). Finally, liver damage is also likely to compromise hepatic function, and consequently, pro-survival (e.g. Akt phosphorylation status) as well as pro-apoptotic markers (cleavage of caspase 3 and PARP) were also assessed by western blot analysis.
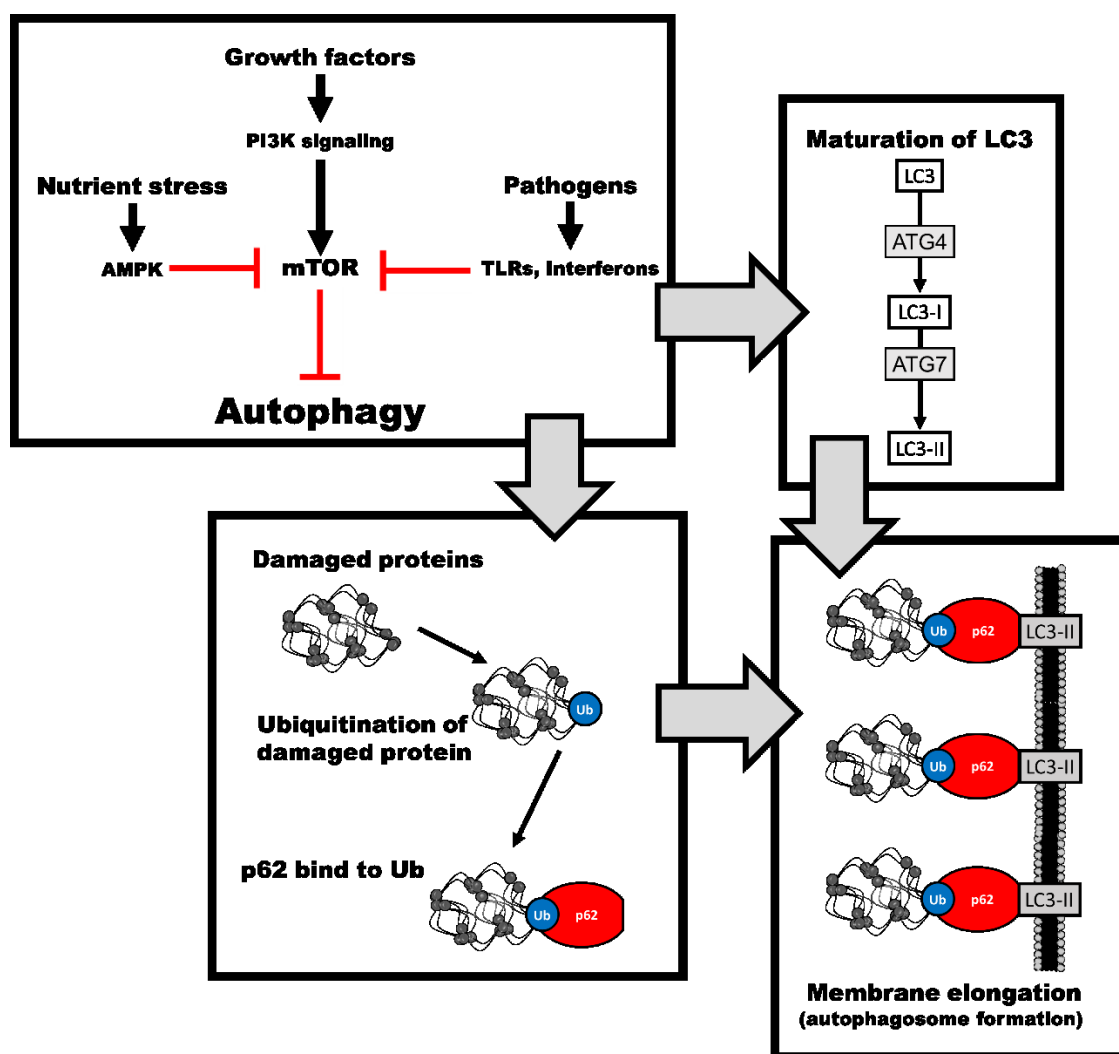
Figure 5.2. Both p62 and LC3 play indispensable roles in autophagy.

5.3   Study outline

As outlined in Chapter 3, mice were divided into six groups (**Figure 5.3**), in order to (a) evaluate the effect of DXR on liver parameters in mice bearing EO771 tumours, and (b) to determine the effect of B16 versus EO771 tumours on liver function. For western blot analysis, liver samples were pooled[3]: for each group consisting of 12 mice, three liver samples were randomly pooled in order to generate four pooled samples for each group.
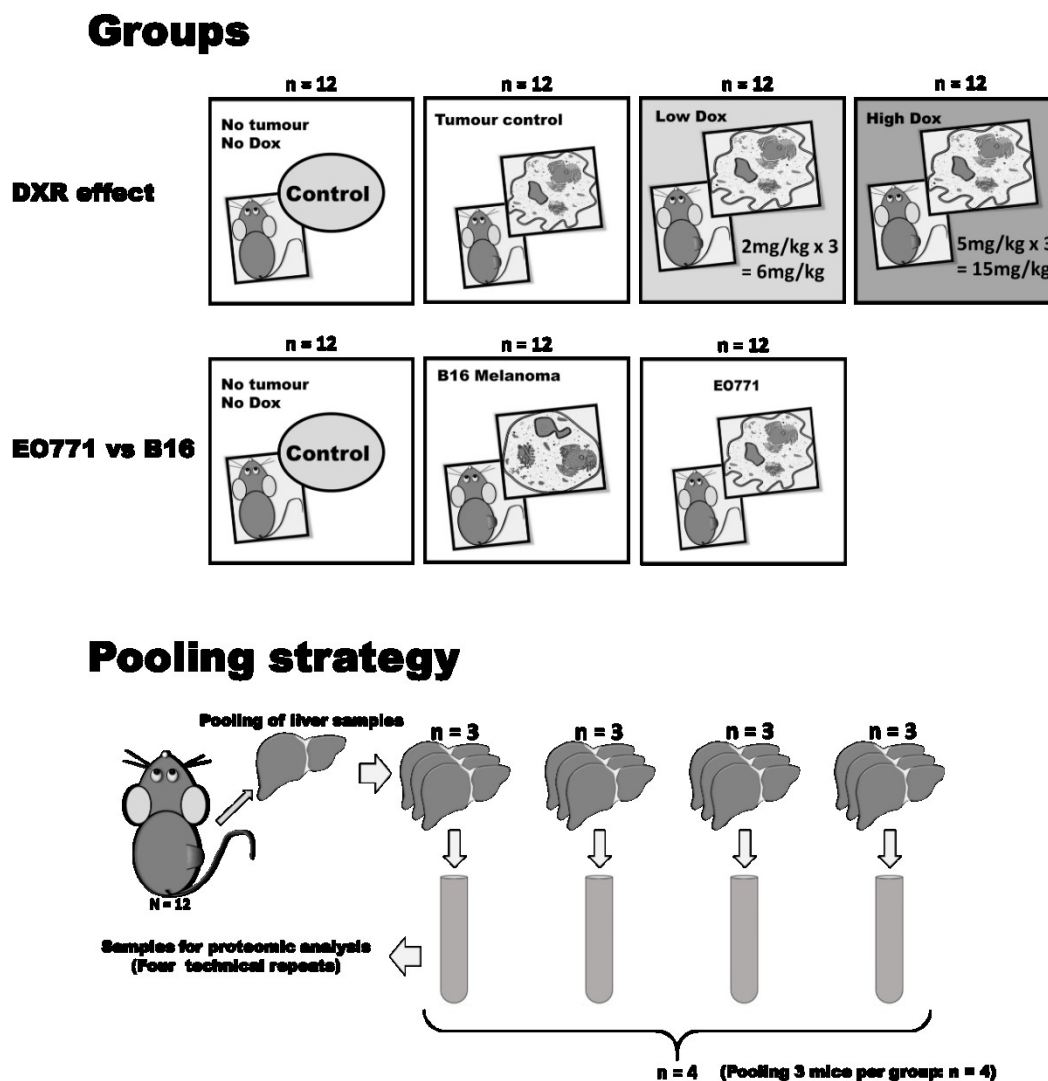
Figure 5.3. Study design. Liver samples from 12 mice in each groups were pooled (3 mice per sample) and subsequently used for western blot analyses.

---

[3] Detailed motivation for pooling samples is detailed in Chapter 6.

5.4   Materials and methodology

Harvested liver samples were thawed on ice and lysed by adding lysis buffer (**Table 5.1**). Tissue samples were subsequently homogenised (KineMatica Polytron™ PT2100 homogeniser, Fisher Scientific), and left on ice for 2 hours prior to being centrifuged (12 000 rpm for 20 min) at 4°C, where after the supernatant was collected and stored at -80°C for later analyses.

Table 5.1. Constituents of lysis buffer used for western blot analysis.

	Stock	10 ml	20 ml	30 ml	50 ml
20 mM Tris-HCl	200 mM	1 ml	2 ml	3 ml	-
1 mM EGTA	10 mM				
1 mM EDTA	100 mM	100 µl	200 µl	300 µl	500 µl
150 mM NaCl	1 M	1.5 ml	3 ml	4.5 ml	7.5 ml
1 mM β-glycerophosphate	-	0.002 g	0.004 g	0.006 g	0.01 g
2.5 mM tetra-Na-Pirophosphate	-	0.01 g	0.02 g	0.03g	0.05 g
1 mM Na_3VO_4	10 mM	1 ml	2 ml	3 ml	5 ml
50 µg/ml PMSF	100 mM	30 µl	60 µl	90 µl	150 µl
10 µg/ml Leupeptin	-	10 µl	20 µl	30 µl	50 µl
10 µg/ml Aprotinin	-	10 µl	20 µl	30 µl	50 µl
0.1% SDS	10%	100 ul	2 ml	3 ml	5 ml

Protein concentrations were determined using the Bradford method (Bradford, 1976). Briefly, a ×5 stock solution [500 mg G-250 Coomassie Brilliant Blue dissolved in a solution consisting of 250 ml 95% ethanol and 500 ml phosphoric acid (filled to 1L with distilled water)] was diluted to a ×1 stock solution and filtered to remove any undissolved Coomassie particles. A standard curve was generated from a two-fold serial dilution (blank, followed by a 2-20 µg protein gradient) of 100 µl bovine serum albumin (BSA, Roche) added to 900 µl Bradford reagent. Protein samples (5 µl each) were diluted in distilled water (95 µl), where after Bradford reagent (900 µl) were added. The protein concentration was spectrophotometrically determined by measuring the absorbance spectra at 595 nm (Cecil CE 2021 spectrophotometer, Cecil Instruments). Protein samples above the linear absorbance range were diluted with RIPA buffer.

Protein lysates were denatured with Laemli's sample buffer (working solution consisting of 5% beta-mercaptoethanol, 4% SDS, 10% glycerol, 0.03% bromophenol blue and 62.5 mM Tris, pH 6.8) prior to sodium dodecyl sulphate polyacrylamide gel electrophoresis (SDS-

PAGE). Based on Bradford protein quantification results, samples were diluted with Laemli's sample buffer to 50 μg of total protein. Samples were frozen at -80°C. These samples were later thawed on ice, vortexed and heated to 95°C for 5 minutes before use. Molecular weights of bands where established from BLUeye Prestained Protein ladder (Genedirex). After loading the samples, gels were run for 10 minutes at 100 V, where after the voltage was increased (150 V) and samples run until the dye-front approached the end of the gel (~90 minutes) in Tris/Glycine/SDS running buffer (Bio-Rad). Proteins were separated using a TGX Stain-Free FastCast™ Acrylamide kit (12% acrylamide gel, Bio-Rad).

Proteins were transferred to a membrane using Trans-Blot® Turbo™ RTA Mini PVDF Transfer Kits (Bio-Rad) according to the manufacturer's specifications: PVDF membranes were submerged in methanol (100%) for 10 seconds, and subsequently incubated, along with blotting paper, in transfer buffer (supplied with kit) for 2 minutes. Proteins were transferred to the membrane on a Trans-Blot Turbo Transfer System (Bio-Rad) for 10 minutes (25V and 2.5 A). After transferring proteins onto membranes, proteins were fixed by bathing membranes in 100% methanol where after it was air-dried. Membranes were subsequently re-submerged in methanol and washed in TBS-T (tris-buffer saline: 20 mM tris, 137 mM NaCl, 0.1%Tween-20 and pH 7.6)

The TGX Stain-Free FastCast™ gels are infused with trihalo-compounds which interact with tryptophan amino acids, which then provide a fluorescent signal at the 300 nm wavelength, and provide a means for quantifying total protein content, and allow the subsequent normalisation of protein content. Visualisation of total protein was performed using the ChemiDoc™ MP System (Bio-Rad) by exposing gels to UV light for 150 seconds.

Membranes were incubated in 5% skimmed milk (diluted with TBS-T) for one hour in order to avoid non-specific binding of antibodies on the membrane, and subsequently rinsed in TBS-T to remove excess milk. Primary antibody incubation was performed overnight at 4°C (see **Table 5.2** for summary of antibodies used). Following incubation, membranes were again washed with TBS-T and incubated with the secondary antibody at room temperature for 1 hour. Membranes were washed again before being developed using Clarity™ ECL Substrate (Bio-Rad) on the ChemiDoc™ MP system.

Table 5.2 Primary and secondary antibodies used.

Primary Antibody (1° AB)	Molecular weight (kDa)	Vendor	Catalogue #	Species	1° AB Dilution	2° AB Dilution
p62	62	Cell Signalling	8025	Rabbit	1:1000	1:10 000
mTOR	289	Abcam	ab51089	Rabbit	1:1000	1:5000
p-mTOR (Ser2448)	289	Abcam	ab84400	Rabbit	1:1000	1:5000
Caspase 3	35	Cell Signalling	9665	Rabbit	1:1000	1:10 000
c-Caspase 3	17, 19	Cell Signalling	9664	Rabbit	1:1000	1:10 000
Akt	60	Abcam	ab32505	Rabbit	1:1000	1:10 000
p-Akt (Ser473)	60	Cell Signalling	4060	Rabbit	1:1000	1:10 000
p-Akt (Thr308)	60	Cell Signalling	9275	Rabbit	1:1000	1:10 000
PARP	116	Abcam	ab191217	Rabbit	1:1000	1:10 000
c-PARP	89	Cell Signalling	9541	Rabbit	1:1000	1:10 000
LC3B-II	14,16	Cell Signalling	3868	Rabbit	1:1000	1:10 000

Normalisation of protein content was conducted on Bio-Rad Image Lab™ software (version 5.1) and exported to Microsoft Excel. Groups were compared using a one-way ANOVA followed by Bonferroni post hoc comparison for significant ($p < 0.05$) changes between groups compared. Statistical analysis was performed in GraphPad Prism (version 5.0). Significance among groups compared are indicated with by '*' for significant with regard to control; '#' for significant with regard to B16, and '$' for significance resulting from comparison with the tumour/EO771 group.

5.5 Results: Effect of DXR on liver

5.5.1 Markers of autophagy

a) Expression of p62

There were no significant differences in the expression of p62 between groups (Control: 1 ± 0.16; Tumour: 1.22 ± 0.05; LD-DXR: 1.10 ± 0.23; HD-DXR: 1.11 ± 0.17) (**Figure 5.4**).
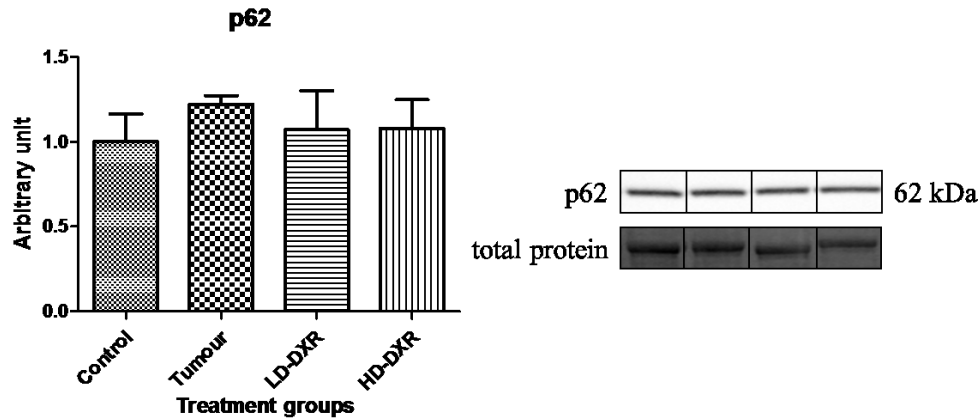
Figure 5.4. The effect of low and high DXR concentrations on p62 expression. Results are expressed as mean ± SEM.

b) LC3B-II

Tumour-bearing mice exhibited a marked increase in LC3B-II, being significantly higher (p >0.05) than in mice receiving no DXR, or high dose DXR (Control 1 ± 0.18; Tumour 2.45 ± 0.36; LD-DXR 1.73 ± 0.35; HD-DXR 1.13 ± 0.18) (**Figure 5.5**).
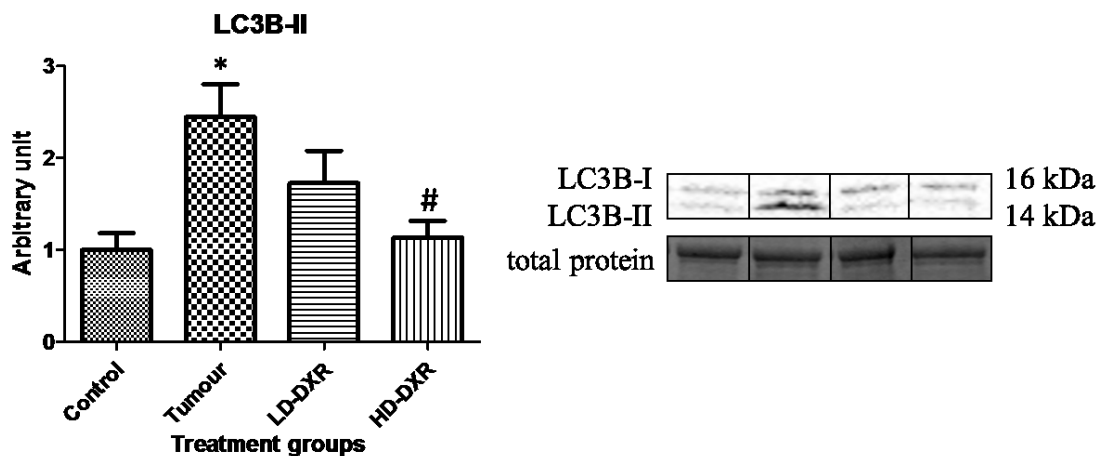
Figure 5.5. The effect of low and high DXR concentrations on LC3B-II. Results are expressed as mean ± SEM (*: significant with regard to Control; #: significant with regard to Tumour group)

5.5.2 Markers of cell growth and proliferation

a) Akt (phosphorylated at Ser473)

There was no significant difference in the phosphorylation status of Akt between groups (**Figure 5.6**).
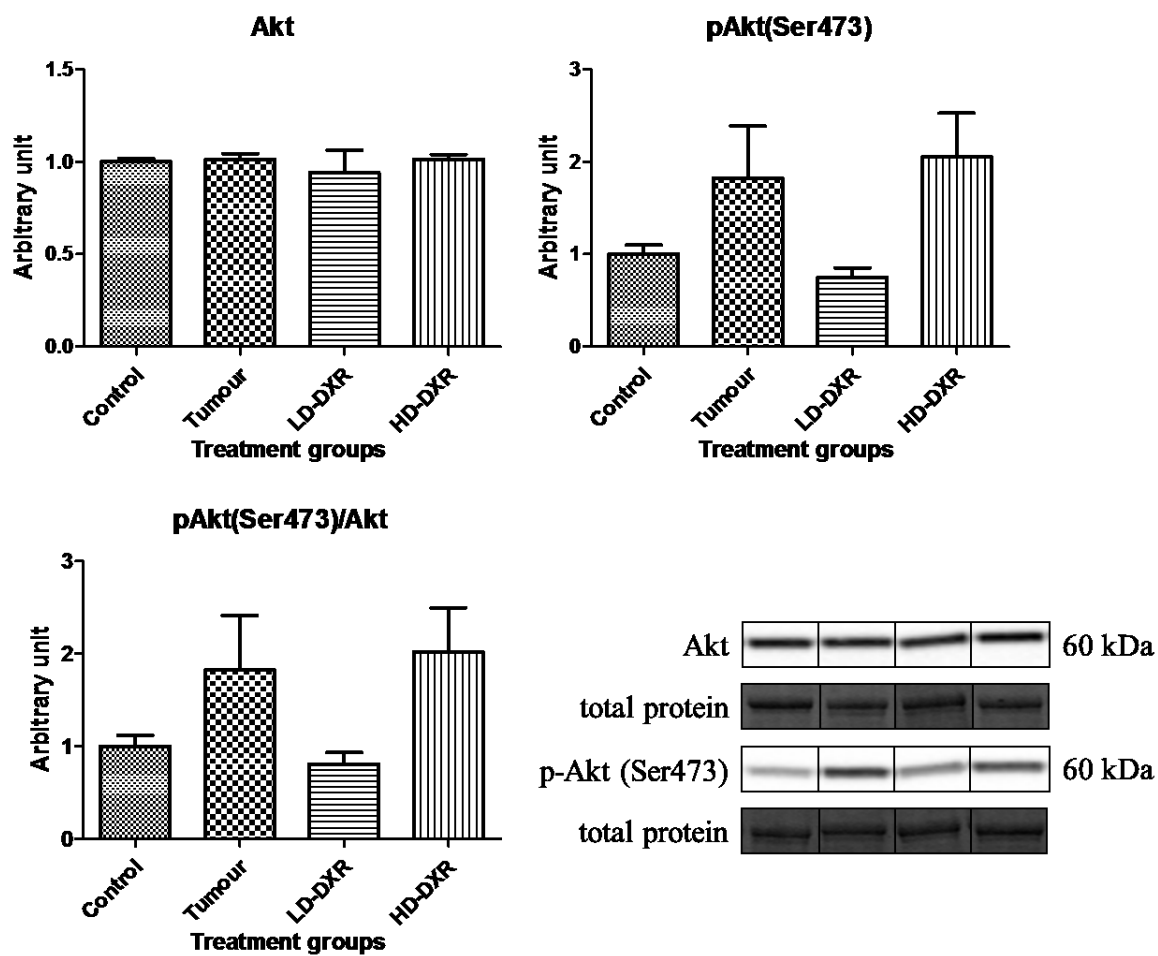
Figure 5.6. The effect of low and high DXR concentrations on Akt(Ser473) phosphorylation. Results are expressed as mean ± SEM.

b) Akt (phosphorylated at Thr308)

There were no significant differences in the phosphorylation status of Akt between groups (**Figure 5.7**).
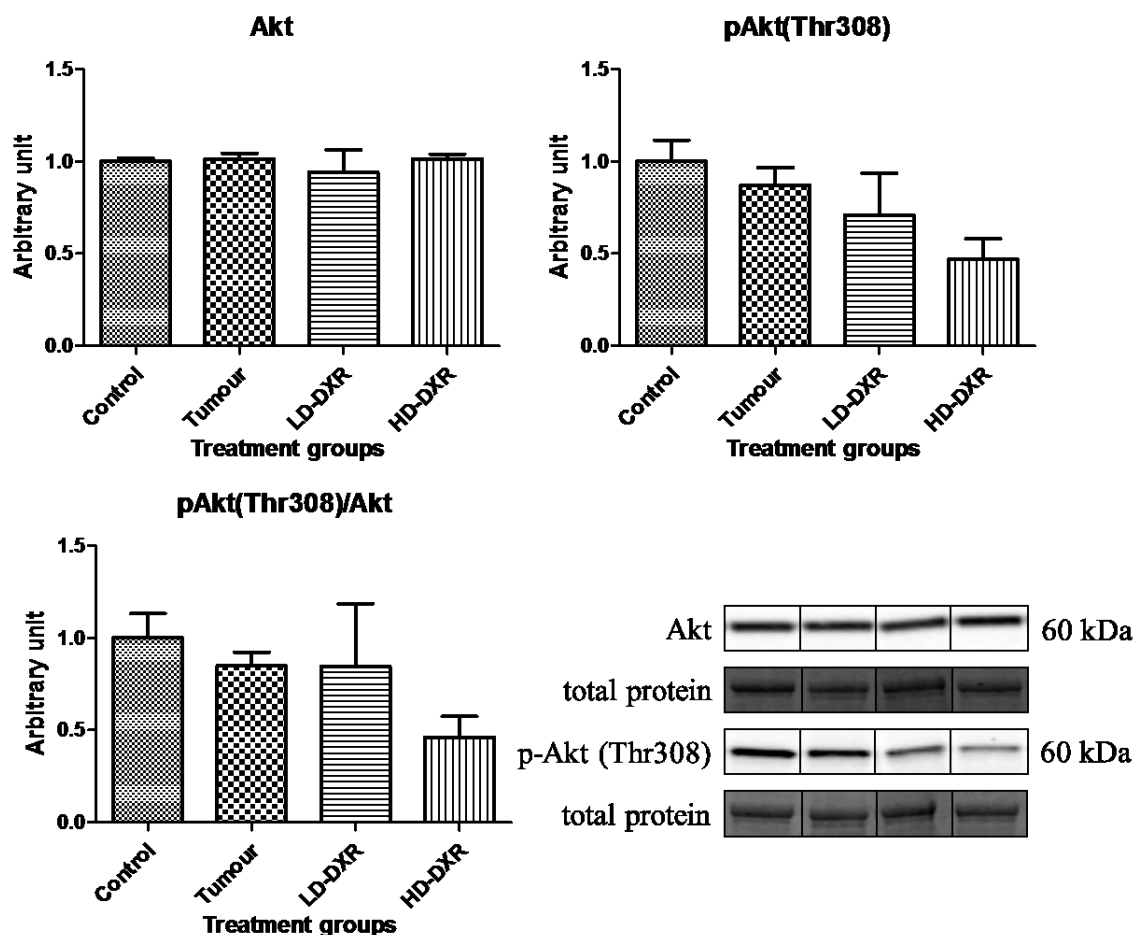
Figure 5.7. The effect of low and high DXR concentrations on the phosphorylation status of Akt(Thr308). Results are expressed as mean ± SEM.

c) Phosphorylation of mTOR

Tumour-bearing mice not receiving DXR exhibited a significant (p >0.05) increase in mTOR phosphorylation status compared to tumour-bearing mice receiving DXR (**Figure 5.8**). Low-dose DXR exhibited a decrease in mTOR phosphorylation compared to control, however, the ratio between total and phosphorylated mTOR increased in both groups receiving DXR (Control: 1.0 ± 0.13; Tumour: 1.52 ± 0.09; LD-DXR: 0.89 ± 0.13; HD-DXR: $0.84. \pm 0.18$).
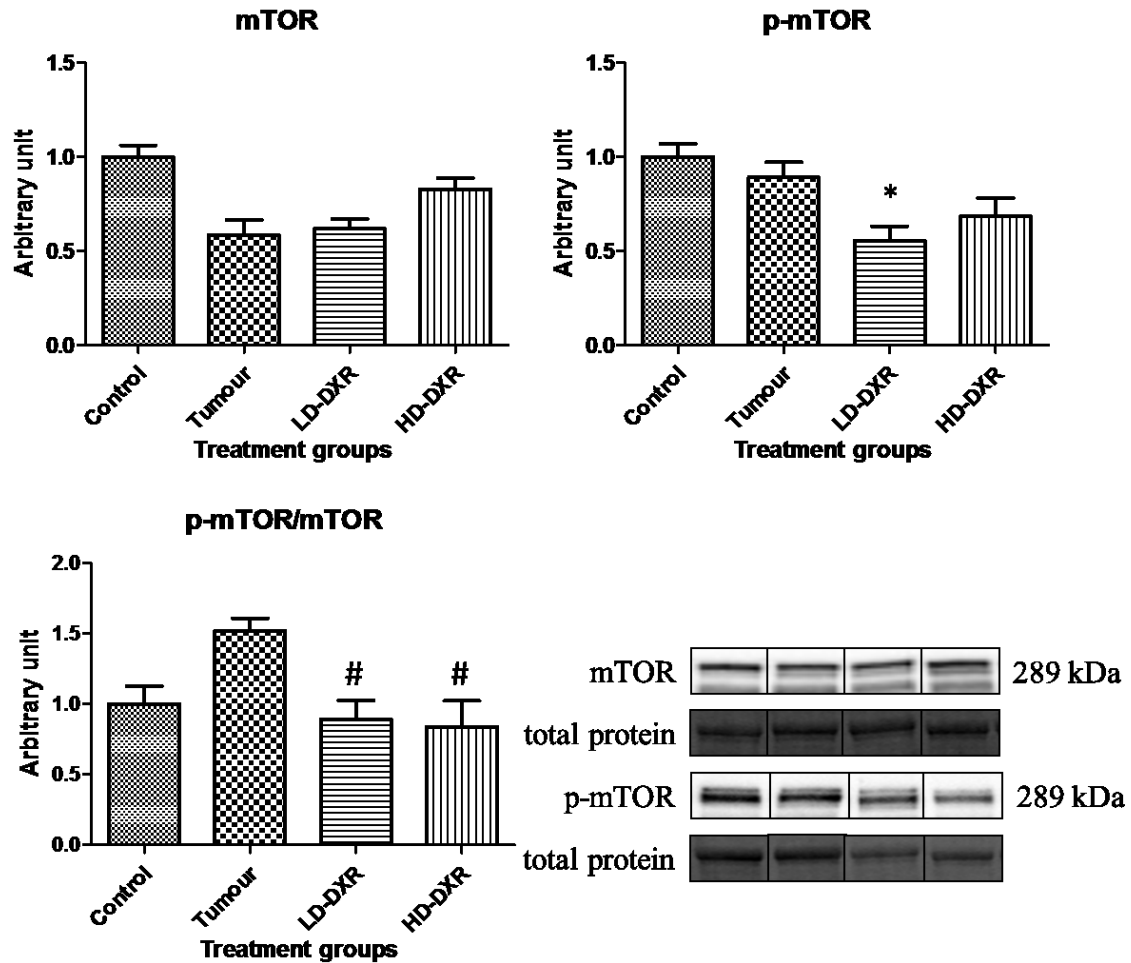
Figure 5.8. The effect of low and high DXR concentrations on mTOR phosphorylation. Results are expressed as mean ± SEM (*: significant with regard to Control; #: significant with regard to Tumour group)

5.5.3   Markers for apoptosis

a) Caspase 3 cleavage

Tumour-bearing mice not receiving DXR exhibited a significant increase ($p < 0.05$) in caspase 3 cleavage (Control: 1.0 ± 0.19; Tumour: 3.52 ± 0.63; LD-DXR: 2.4 ± 0.57; HD-DXR: 2.47 ± 0.24) (**Figure 5.9**).
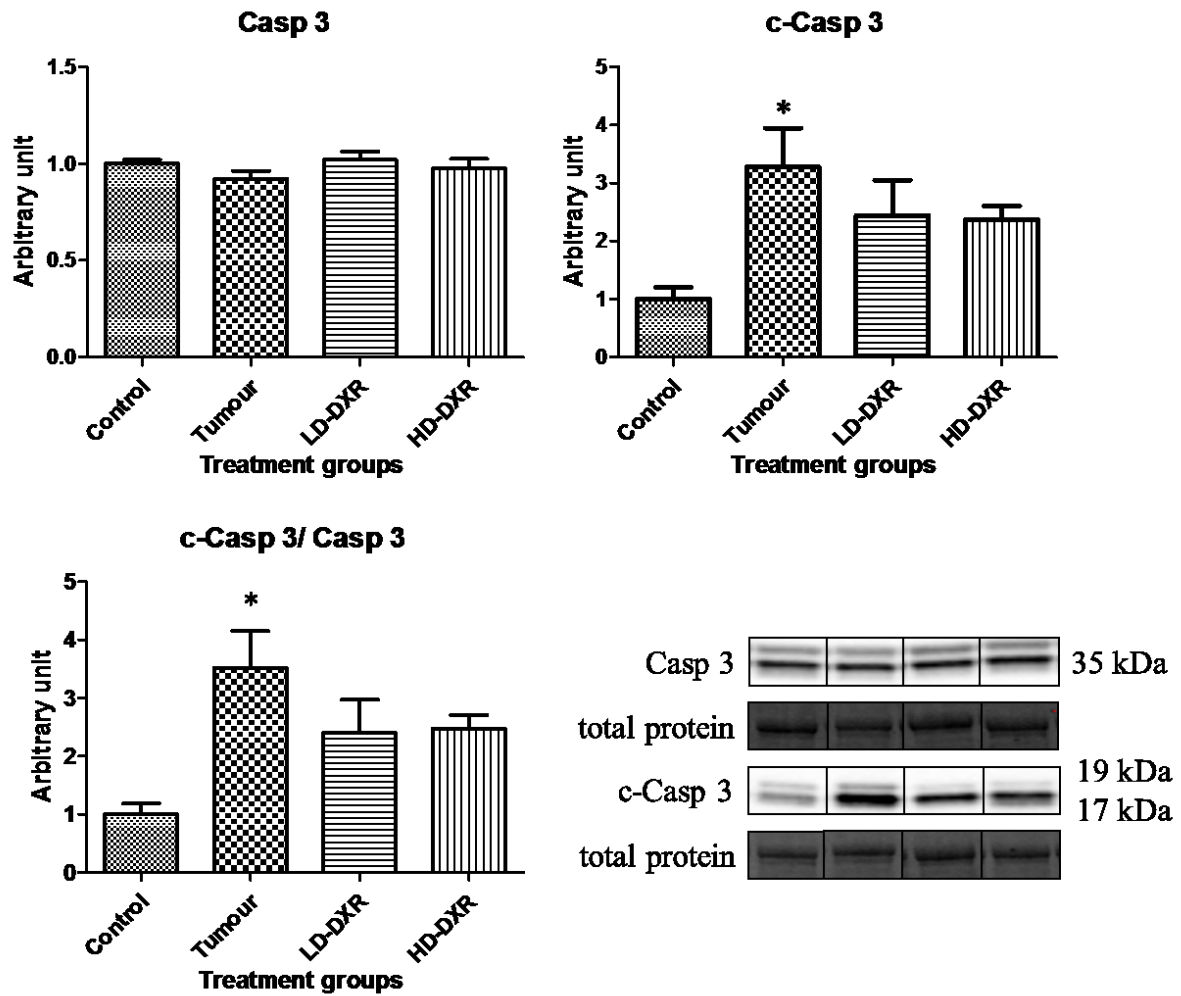
Figure 5.9. The effect of low and high DXR concentrations on caspase 3 cleavage. Results expressed as mean ± SEM. (*: significant with regard to Control)

b) PARP

Groups did not differ significantly with regard to cleavage of PARP (**Figure 5.10**).
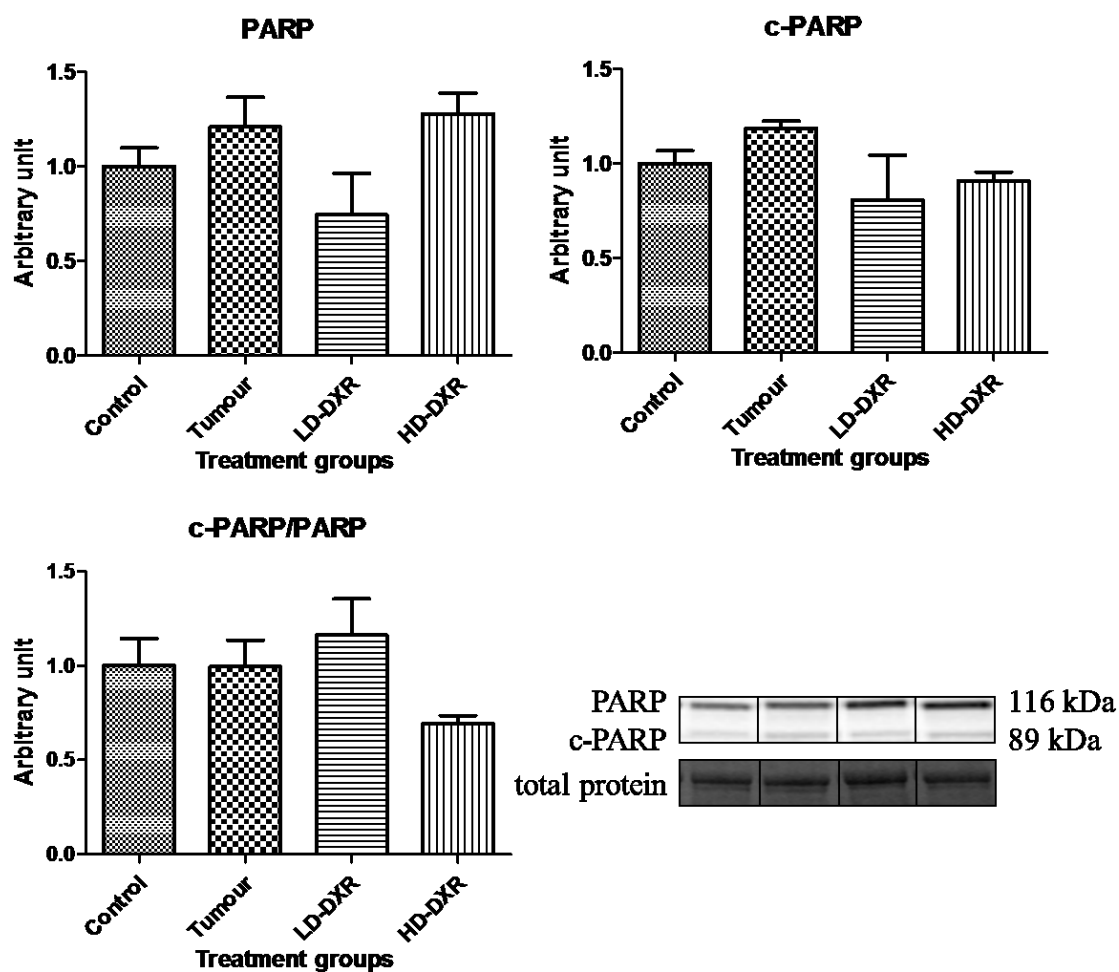
Figure 5.10. The effect of low and high DXR concentration on PARP cleavage. Results expressed as mean ± SEM.

5.6   Results: Comparison between B16 and EO771 tumours

5.6.1   Markers of autophagy

a) Expression of p62

Mice bearing B16 tumours exhibited a marked increase in p62 expression (Control: 1 ± 0.15; EO771: 1.27 ± 0.14; B16: 2.49 ± 0.14) (**Figure 5.11**).
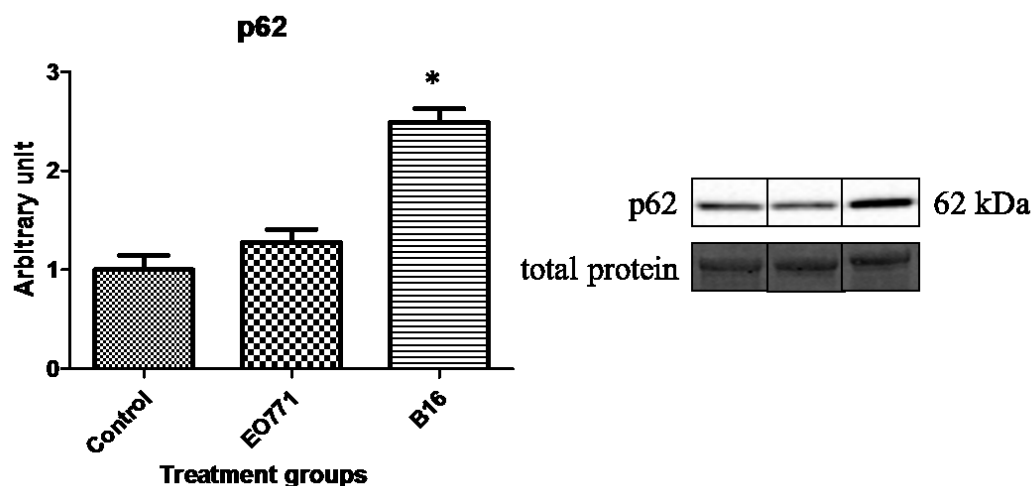
Figure 5.11. The effect of tumour type on p62 expression. Results are expressed as mean ± SEM. (*: significant with regard to Control)

b) LC3B-II

Mice bearing B16 tumours exhibited levels of LC3B-II significantly higher than both EO771 and B16 (Control: 1 ± 0.23; EO771: 1.48 ± 0.37; B16: 2.97 ± 0.17) (**Figure 5.12**).
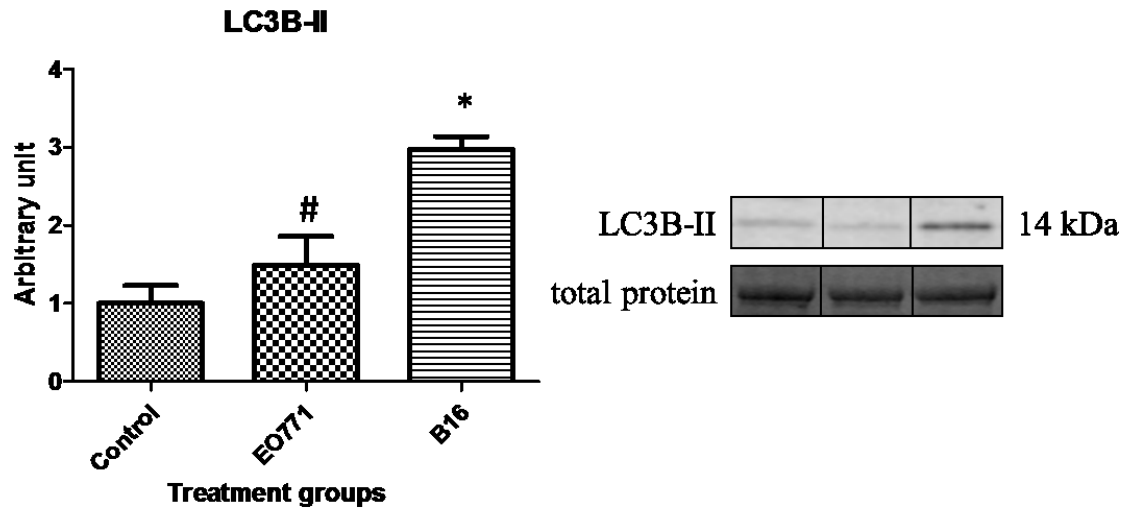
Figure 5.12. The effect of tumour type on LC3B-II. Results expressed as mean ± SEM (*: significant with regard to Control; #: significant with regard to B16 tumour group)

5.6.2   Markers of cell growth and proliferation

c) Akt (phosphorylated at Ser473)

Though there was a significant difference in Akt expression (**Figure 5.13**), a marked increase in phosphorylation of Akt (Ser 473) in mice bearing EO771 tumours which were significantly higher in EO771 compared to either control or B16 mice (Control: 1 ± 0.18; EO771: 4.01 ± 0.95; B16: 0.24 ± 0.11).
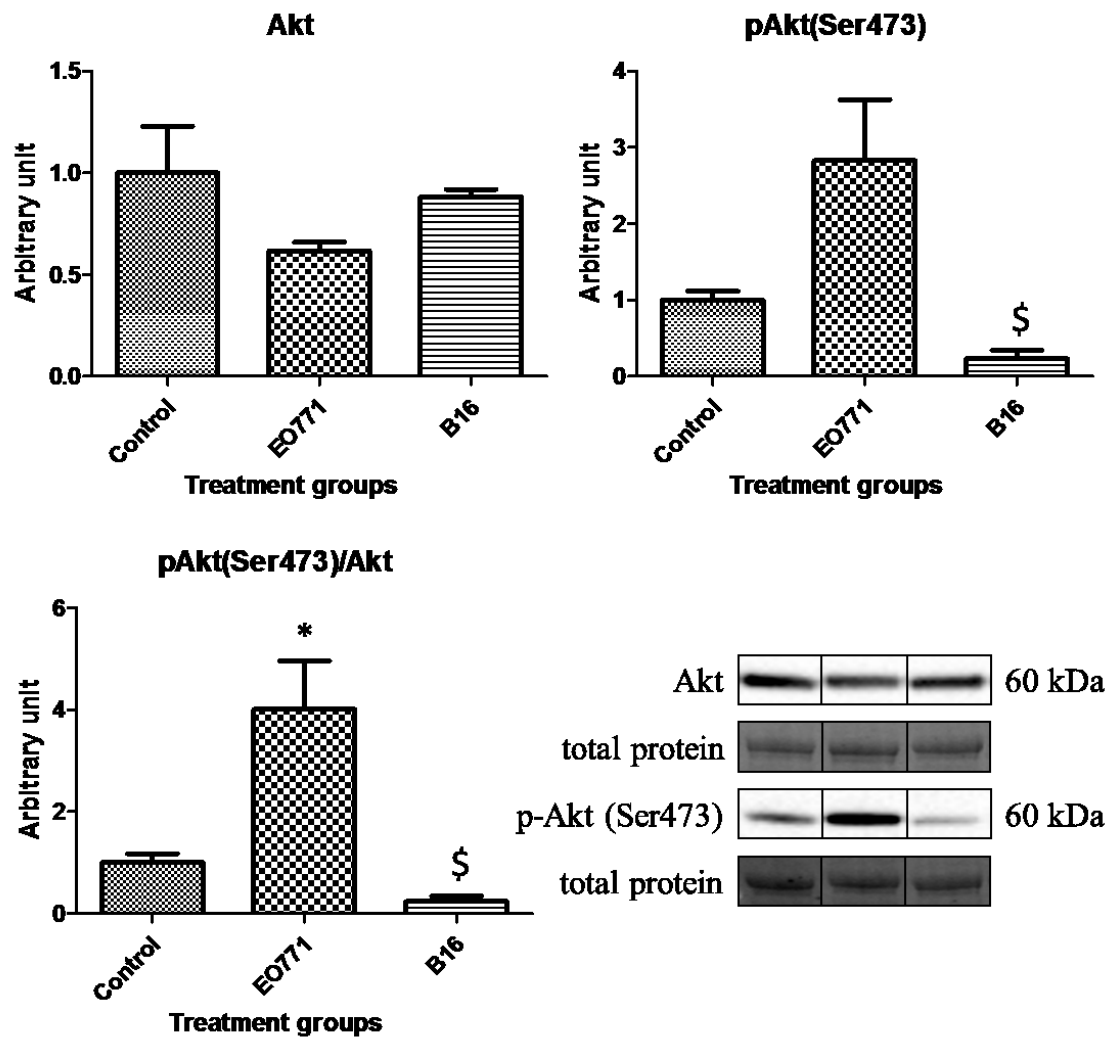
Figure 5.13. The effect of tumour type on Akt(Ser473) phosphorylation. Results are expressed as mean ± SEM. (*: significant with regard to control; \$: significant with regard to EO771 tumour group).

d) Akt (phosphorylated at Thr308)

There was no significant differences in the phosphorylation status of Akt (Thr308) between groups (**Figure 5.14**).
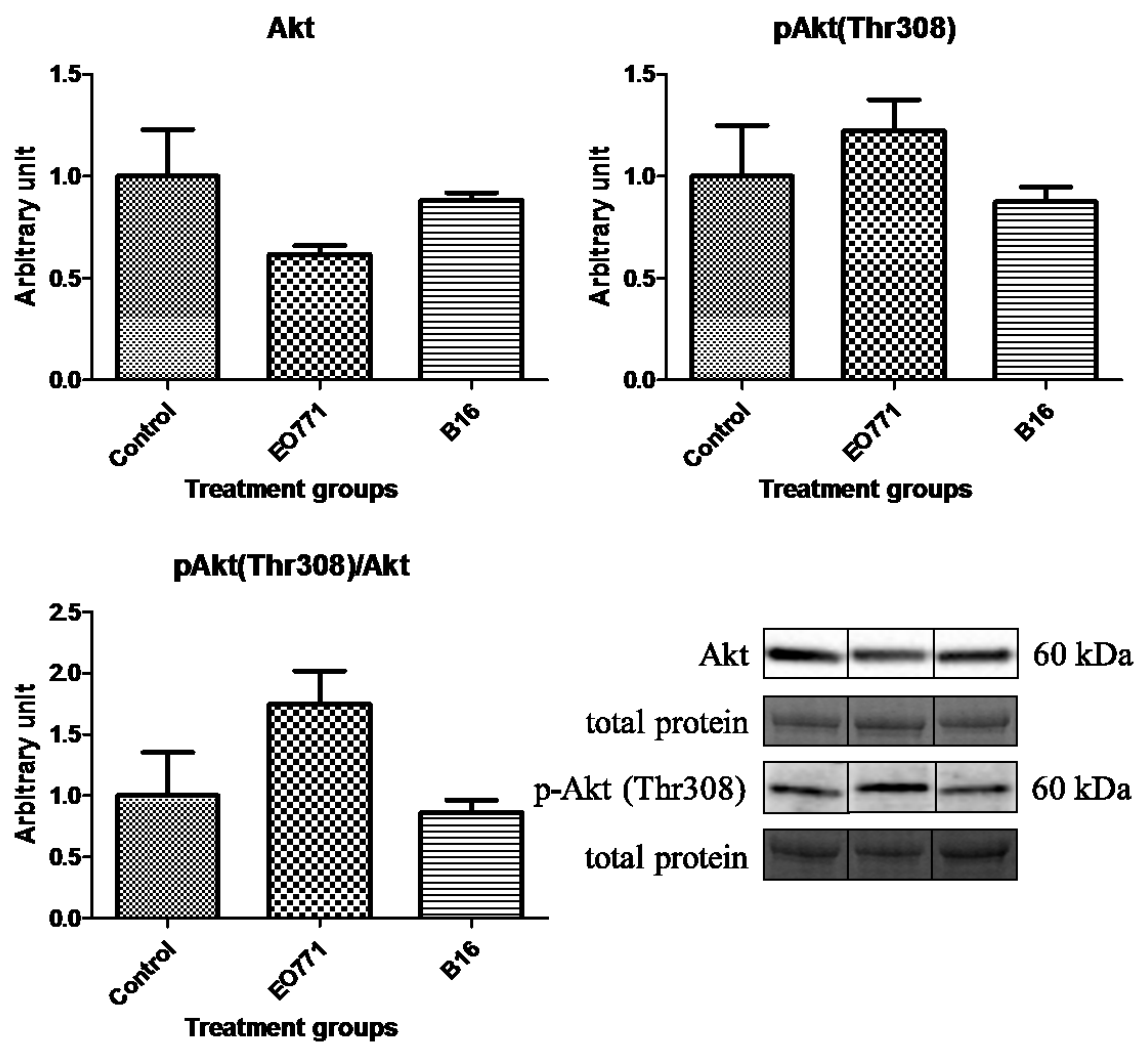
Figure 5.14. The effect of tumour type on Akt(Thr308) phosphorylation. Results ae expressed as mean ± SEM.

c) Phosphorylation of mTOR

Neither EO771 nor B16 tumours differed significantly from the control mice (**Figure 5.15**). However, mice bearing EO771 tumours exhibited lower expression of mTOR compared to mice with B16 tumours (Control: 1 ± 0.15; EO771: 1.27 ± 0.14; B16: 2.49 ± 0.14).
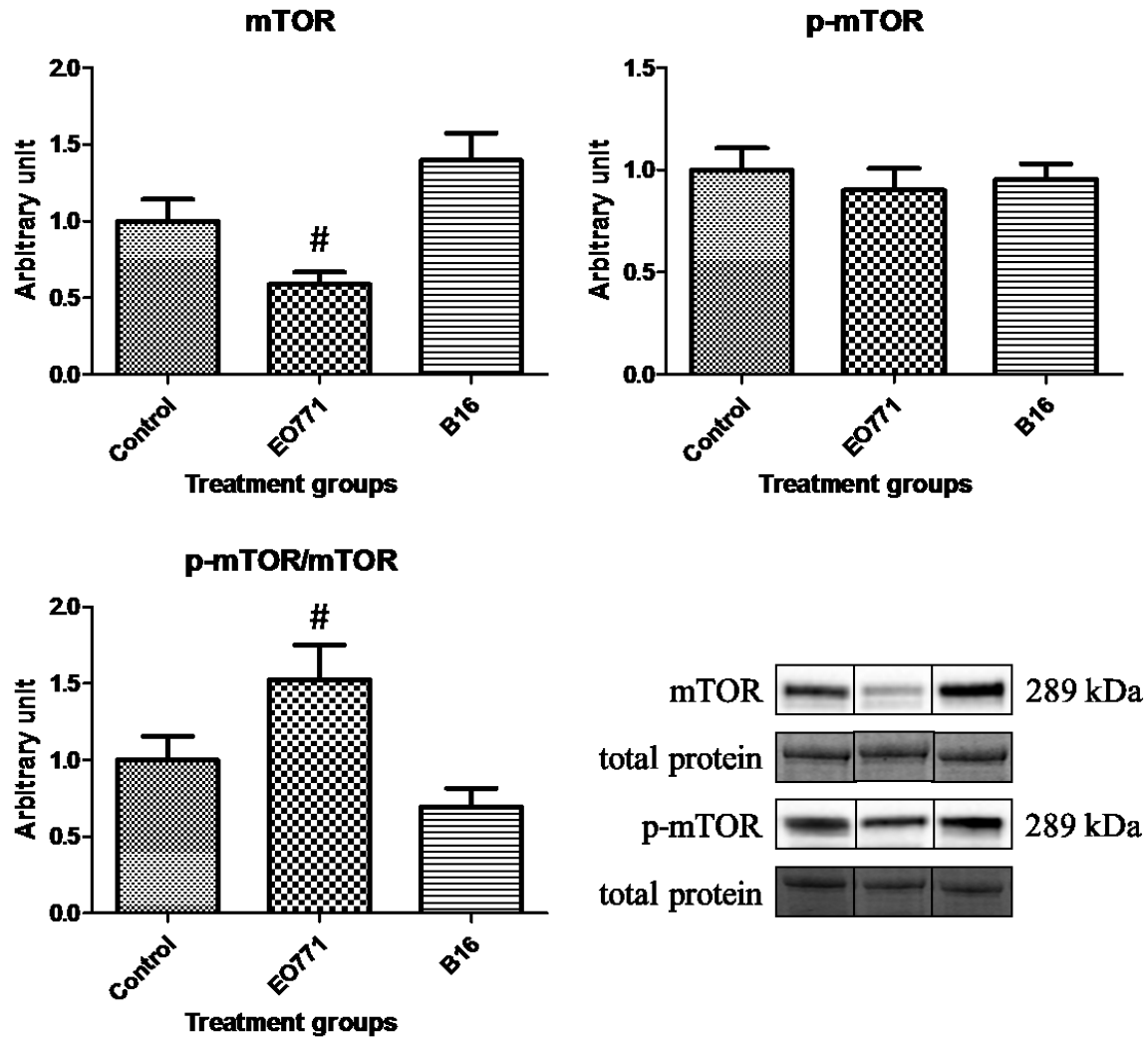

Figure 5.15. The effect of tumour type on mTOR phosphorylation. Results are expressed as mean ± SEM (#: significant with regard to B16 tumour group).

5.6.3 Markers for apoptosis

a) Caspase 3 cleavage

Caspase 3 levels were comparable between groups (**Figure 5.16**). Compared to EO771, B16 tumours exhibited a significant decrease in caspase 3 cleavage (Control: 1 ± 0.27; EO771: 0.98 ± 0.06; B16: 0.41 ± 0.04).
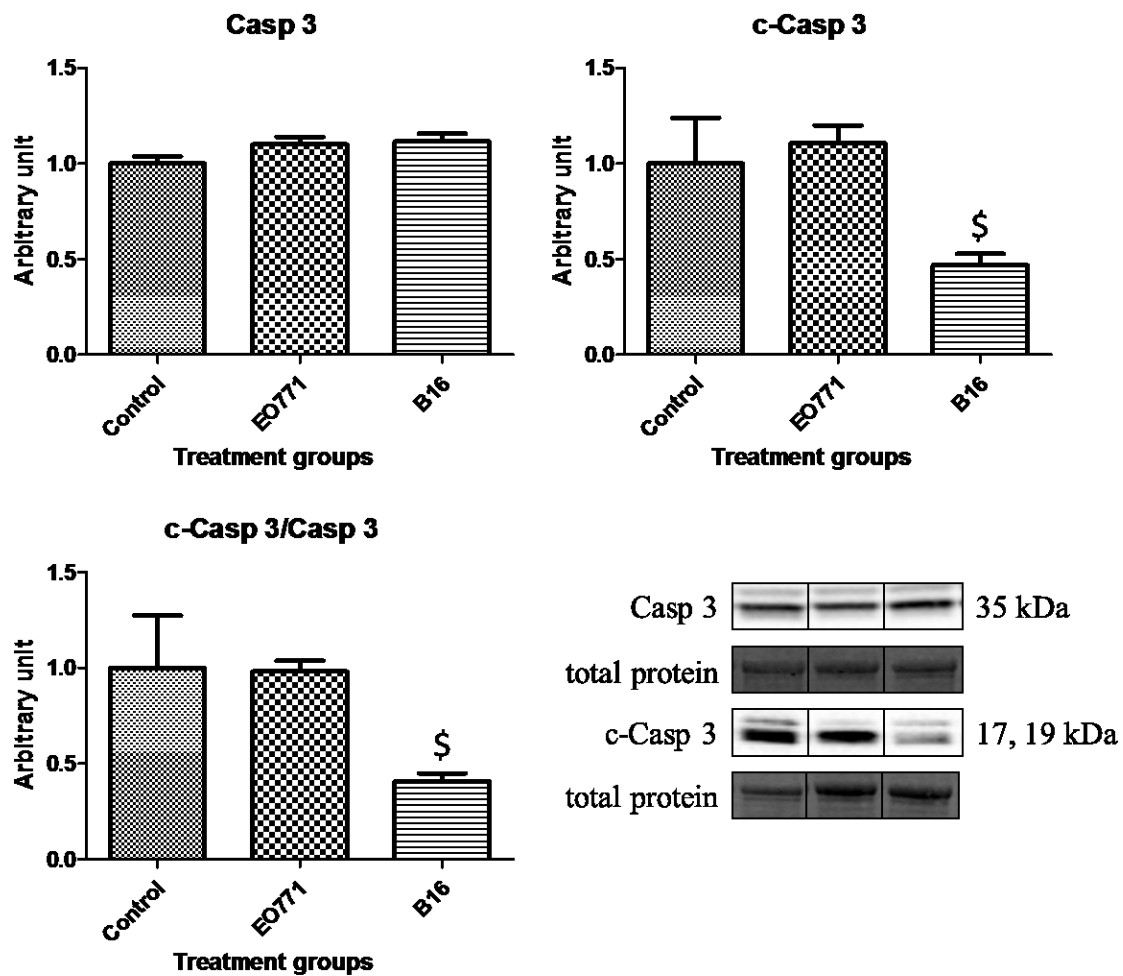
Figure 5.16. The effect of tumour type on caspase 3 cleavage. Results expressed as mean ± SEM. ($: significant with regard to EO771 tumour group).

b) PARP

Although PARP expression was significantly higher in EO771 mice compared to B16 and control mice (Control: 1 ± 0.2; EO771: 2.71 ± 0.14; B16: 1.29 ± 0.08), no significant differences were observed in the ratio between total and cleaved PARP (**Figure 5.17**)
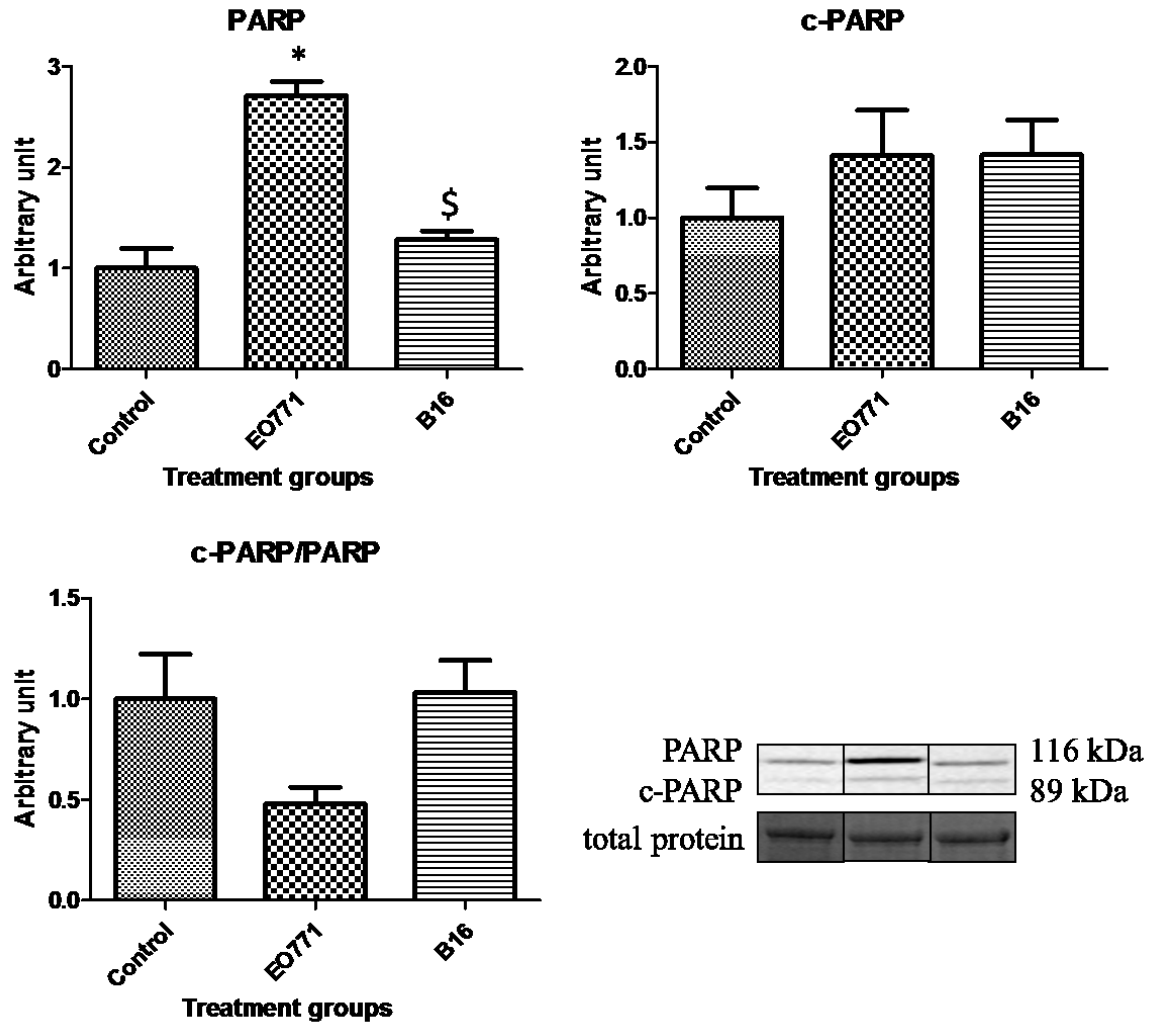
Figure 5.17. The effect of tumour type on PARP cleavage. Results are expressed as mean ± SEM. (*: significant with regard to Control; $: significant with regard to EO771 tumour group)

5.7   Comparison between DXR groups

The phosphorylation status of mTOR (**Figure 5.8**) indicated that the mice bearing EO771 tumours exhibited higher p-mTOR/mTOR ratio, suggesting that the activated mTOR might inhibit autophagy in tumour bearing mice. This is somewhat unexpected since, higher metabolic demand placed on mice as a result of tumour load could be expected to increase hepatic autophagy. However, DXR groups with significantly lower p-mTOR/mTOR ratio (compared to tumour groups) would suggest that the DXR challenge re-introduced the need to upregulate autophagy. However, autophagy is also regulated by mTOR- independent mechanism (Chen et al., 2016). As such, these results should be viewed in context of other findings.

Indeed an increase in LC3B-II observed in tumour groups (**Figure 5.5**) could suggest an increase in autophagic activity. This interpretation would contradict results from p-mTOR/mTOR (**Figure 5.8**) ratio which was elevated in the tumour group and suggest a decrease of autophagy. Alternatively, an increase in LC3B-II could also occur if the pool of autophagic vesicles are increased, but degradation of vesicle are not increased (i.e. if autophagic flux was not increased). This raises concerns regarding the reason why autopahgic flux would be inhibited by DXR. Finally, p62 levels did not differ between groups (**Figure 5.11**). Since p62 is degraded with the phagosome vesicle content, an increase in p62 might indicate an increase in vesicle formation, or a decrease in vesicle degradation. The observation that p62 did not change is consistent with an interpretation that autoaphgic flux did not increase. Taken together, immunoblotting results are inconclusive with regards to autophagic activity.

Activated mTOR does not only inhibit autophagy, but also induce a host of anabolic processes reflective of growth and proliferation (McCarthy and Esser, 2010). Mice receiving DXR might undergo liver damage, with would decrease the activity of mTOR. However, this interpretation is challenged by other results. Firstly, Akt activation did not differ between groups (**Figure 5.13 & 5.14**). Moreover, only the tumour group (not receiving DXR) demonstrated a significant increase in the apoptotic marker, cleaved caspase 3 (**Figure 5.9**). It is hard to reconcile an increase in mTOR activity (which is anabolic signalling cascade) in context of an elevated apoptotic marker. Similarly, it is unclear why mice receiving DXR would have lower cleaved caspase 3 compared to mice inoculated with only tumour cells. However, it should be noted

that cleaved PARP did not differ between groups (**Figure 5.15**). Thus, apoptosis is inferred from a single marker and should be treated with caution.

In conclusion, the immunoblotting results are largely inconclusive. It should be noted that the liver is metabolically dynamic tissue and highly responsive to feed-fasting cycles (Komatsu et al., 2005). In this regard, it is possible that the cellular content of structures involved in autophagy is comparative between groups, but that autophagic processes are implemented in different ways. As an example, autophagic proteins used to mobilise glycogen might also be up regulated in response to DXR-induced stress. Extending the range of proteins evaluated might resolve discrepancies observed between groups.

5.8   Comparison between cancer types

Interestingly, both p62 (**Figure 5.11**) and LC3B-II (**Figure 5.12**) was significantly elevated in the B16 melanoma group. While LC3B-II levels might suggest an increase in autophagosomal pool size, the increase in p62 would imply a failure to degrade these vesicles. In other words, these results are suggestive of lysosomal dysfunction. It is tempting to speculate that a compromised autophagy apparatus might contribute to the low tolerance observed in mice bearing B16 tumours (Chapter 3). Indeed, lysosomal failure ~~are~~ is usually associated with an increase in cell death (Loos and Engelbrecht, 2009). However, this interpretation is not supported by the observation that caspase 3 cleavage was lower in the B16 group compared to the EO771 group (**Figure 5.16**), and that PARP cleavage was not significantly different between groups (**Figure 5.15**). Another context where LC3B-II is increased with p62 is during pathogen subversion of autophagy processes (van Niekerk et al., 2016): Many viruses, bacteria and protozoans inhibit lysosomal fusion with autophagic vesicles, since these pathogens make use of the vesicles to avoid immune detection. Although mice did not show any overt signs of infection, this possibility cannot be ruled out.

Prosurvival signaling (Akt phosphorylation) did not differ significantly: although Akt phosphorylation on Ser473 was significantly higher in the EO771 group (**Figure 5.12**), phosphorylation at Thr308 was not significantly elevated. Similarly, though PARP levels was significantly elevated in EO771 group, cleaved PARP was not (**Figure 5.14**), and possibly related to non-apoptotic function of these uncleaved proteins (Schwerk and Schulze-Osthoff, 2003). However, B16 mice exhibit suppressed levels of cleaved caspase 3 (**Figure 5.16**). Since

B16 cancer cells also exhibited the lowest tolerance (Chapter 3), this observation would suggest that increased apoptosis might be reflective of increased liver pathology. In conclusion, the main finding of this study was that mice bearing B16 tumours might exhibit signs of dysfunctional autophagy, since p62 and LC3B-II where concomitantly elevated, suggesting that lysosomal function and degradation of vesicle content could not be executed.

5.9   Conclusion

Comparison between groups receiving DXR did not demonstrate an expected increase in autophagy: although LC3B-II was elevated in the tumour group compared to DXR, no other marker indicated an increase in autophagy. The elevated p-mTOR/mTOR ratio in the tumour group compared to DXR might be reflective of increased cell proliferation or protein synthesis rather than an inhibition of autophagy. This interpretation would describe the lower p-mTOR/mTOR ratio in mice receiving DXR compared to tumour group as a result of cellular stress (i.e. in mice receiving DXR, cells disengaging anabolic activities usually activated by suppressing mTOR activation). Yet, this interpretation is not corroborated by increased caspase 3 cleavage in the tumour group as it is not clear why cells expressing apoptotic markers, would activate mTOR signalling.

In contrast, there was suggestive evidence that mice bearing B16 tumours might exhibit signs of a compromised autophagic process. The increase in LC3B-II suggest an increase in vesicle formation, whereas the elevated p62 imply that vesicle content (and the p62 inside the vesicle) does not undergo degradation, thus suggesting an inability of lysosomal vesicles to fuse with autophagosomes. Regarding the various functions of autophagy (**Figure 5.1**), an inability to fully execute the entire autophagic process to completion could explain the lower tolerance in mice bearing B16 tumours.

Measuring autophagy with western blotting is challenging as it provides a 'snap shot' of a dynamic process. In this regard, transgenic mice models have been introduced to measure autophagic activity *in vivo* (Castillo et al., 2013). Also, only a few proteins playing an executioner role (i.e. not induction) was measured and it is therefrom not possible to point out the purpose of autophagy in these cells. As an example, autophagic machinery upregulated in response to nutritional stress (fasting) might be subsequently repurposed for other functions such as cell-autonomous defence against pathogens (van Niekerk et al., 2016). Thus, high basal

levels of autophagy in both control and DXR groups might be comparable, suggesting autophagy is not an important response to a DXR challenge. Yet, this does not preclude the possibility that autophagy was differentially implemented in pursuit of diverging needs (clearance of damaged mitochondria in DXR groups, versus mobilisation of energy rich substrate in control groups). Expanding the range of proteins investigated might highlight such differences. In this regard, a study was subsequently conducted making use of a proteomic analysis (Chapter 6) in order to resolve the ambiguous results obtained in this chapter.

5.10   Reference List

Andus, T., Bauer, J., and Gerok, W. (1991). Effects of cytokines on the liver. Hepatology *13,* 364-375.

Ashare, A., Stanford, C., Hancock, P., Stark, D., Lilli, K., Birrer, E., Nymon, A., Doerschug, K.C., and Hunninghake, G.W. (2009). Chronic liver disease impairs bacterial clearance in a human model of induced bacteremia. Clin Transl Sci. *2,* 199-205.

Ballet, F., Vrignaud, P., Robert, J., Rey, C., and Poupon, R. (1987). Hepatic extraction, metabolism and biliary excretion of doxorubicin in the isolated prefused rat liver. Cancer Chemother. Pharmacol. *19,* 240-245.

Blomhoff, R., Green, M.H., Berg, T., and Norum, K.R. (1990). Transport and storage of vitamin A. Science *250,* 399-404.

Bradford, M.M. (1976). A rapid and sensitive method for the quantitation of microgram quantities of protein utilizing the principle of protein-dye binding. Anal. Biochem. *72,* 248-254.

Cani, P.D., Possemiers, S., Van de Wiele, T., Guiot, Y., Everard, A., Rottier, O., Geurts, L., Naslain, D., Neyrinck, A., Lambert, D.M., Muccioli, G.G., and Delzenne, N.M. (2009). Changes in gut microbiota control inflammation in obese mice through a mechanism involving GLP-2-driven improvement of gut permeability. Gut *58,* 1091-1103.

Castillo, K., Valenzuela, V., Matus, S., Nassif, M., Oñate, M., Fuentealba, Y., Encina, G., Irrazabal, T., Parsons, G., and Court, F. (2013). Measurement of autophagy flux in the nervous system in vivo. Cell. Death Dis. *4,* e917.

Chen, X., Li, M., Li, L., Xu, S., Huang, D., Ju, M., Huang, J., Chen, K., and Gu, H. (2016). Trehalose, sucrose and raffinose are novel activators of autophagy in human keratinocytes through an mTOR-independent pathway. Sci. Rep. *6,* 28423.

Dahn, M.S., Mitchell, R.A., Lange, M.P., Smith, S., and Jacobs, L.A. (1995). Hepatic metabolic response to injury and sepsis. Surgery *117,* 520-530.

Dekaney, C.M., Gulati, A.S., Garrison, A.P., Helmrath, M.A., and Henning, S.J. (2009). Regeneration of intestinal stem/progenitor cells following doxorubicin treatment of mice. Am. J. Physiol. Gastrointest. Liver Physiol. *297,* G461-70.

Devkota, S., Wang, Y., Musch, M.W., Leone, V., Fehlner-Peach, H., Nadimpalli, A., Antonopoulos, D.A., Jabri, B., and Chang, E.B. (2012). Dietary-fat-induced taurocholic acid promotes pathobiont expansion and colitis in Il10-/-mice. Nature *487,* 104-108.

Dhainaut, J., Marin, N., Mignon, A., and Vinsonneau, C. (2001). Hepatic response to sepsis: interaction between coagulation and inflammatory processes. Crit. Care. Med. *29,* S42-S47.

Dirks-Naylor, A.J. (2013). The role of autophagy in doxorubicin-induced cardiotoxicity. Life Sci. *93,* 913-916.

Ecker, J., Liebisch, G., Englmaier, M., Grandl, M., Robenek, H., and Schmitz, G. (2010). Induction of fatty acid synthesis is a key requirement for phagocytic differentiation of human monocytes. Proc. Natl. Acad. Sci. U. S. A. *107,* 7817-7822.

Harris, J., Hartman, M., Roche, C., Zeng, S.G., O'Shea, A., Sharp, F.A., Lambe, E.M., Creagh, E.M., Golenbock, D.T., Tschopp, J.*, et al.* (2011). Autophagy controls IL-1beta secretion by targeting pro-IL-1beta for degradation. J. Biol. Chem. *286,* 9587-9597.

Hirasawa, H., Oda, S., and Nakamura, M. (2009). Blood glucose control in patients with severe sepsis and septic shock. World J Gastroenterol *15,* 4132-4136.

Jansen, T., and Daiber, A. (2012). Direct antioxidant properties of bilirubin and biliverdin. Is there a role for biliverdin reductase? The Role of Bile Pigments in Health and Disease: Effects on Cell Signaling, Cytotoxicity and Cytoprotection 150.

Jenniskens, M., Langouche, L., Vanwijngaerden, Y., Mesotten, D., and Van den Berghe, G. (2016). Cholestatic liver (dys) function during sepsis and other critical illnesses. Intensive Care Med. *42,* 16-27.

Kang, S., Chess-Williams, R., Anoopkumar-Dukie, S., and McDermott, C. (2013). Induction of inflammatory cytokines and alteration of urothelial ATP, acetylcholine and prostaglandin E 2 release by doxorubicin. Eur. J. Pharmacol. *700,* 102-109.

Katz, S., Jimenez, M.A., Lehmkuhler, W.E., and Grosfeld, J.L. (1991). Liver bacterial clearance following hepatic artery ligation and portacaval shunt. J. Surg. Res. *51,* 267-270.

Kim, J., Kundu, M., Viollet, B., and Guan, K. (2011). AMPK and mTOR regulate autophagy through direct phosphorylation of Ulk1. Nat. Cell Biol. *13,* 132-141.

Komatsu, M., Waguri, S., Koike, M., Sou, Y., Ueno, T., Hara, T., Mizushima, N., Iwata, J., Ezaki, J., and Murata, S. (2007). Homeostatic levels of p62 control cytoplasmic inclusion body formation in autophagy-deficient mice. Cell *131,* 1149-1163.

Komatsu, M., Waguri, S., Ueno, T., Iwata, J., Murata, S., Tanida, I., Ezaki, J., Mizushima, N., Ohsumi, Y., Uchiyama, Y*., et al.* (2005). Impairment of starvation-induced and constitutive autophagy in Atg7-deficient mice. J. Cell Biol. *169,* 425-434.

Krinsley, J.S (2003). Mayo Clin. Proc. *78*, 1471-1478

Kroemer, G., Mariño, G., and Levine, B. (2010). Autophagy and the integrated stress response. Mol. Cell *40,* 280-293.

Kuipers, F., Bloks, V.W., and Groen, A.K. (2014). Beyond intestinal soap -bile acids in metabolic control. Nat. Rev. Endocrinol. *10,* 488-498.

Kuma, A., Hatano, M., Matsui, M., Yamamoto, A., Nakaya, H., Yoshimori, T., Ohsumi, Y., Tokuhisa, T., and Mizushima, N. (2004). The role of autophagy during the early neonatal starvation period. Nature *432,* 1032-1036.

Le Bot, M.A., Bégué, J.M., Kernaleguen, D., Robert, J., Ratanasavanh, D., Airiau, J., Riché, C., and Guillouzo, A. (1988). Different cytotoxicity and metabolism of doxorubicin, daunorubicin, epirubicin, esorubicin and idarubicin in cultured human and rat hepatocytes. Biochem. Pharmacol. *37,* 3877-3887.

Li, T., and Chiang, J.Y. (2013). Nuclear receptors in bile acid metabolism. Drug Metab. Rev. *45,* 145-155.

Liu, Y., and Levine, B. (2015). Autosis and autophagic cell death: the dark side of autophagy. Cell Death Differ. *22,* 367-376.

Loos, B., and Engelbrecht, A. (2009). Cell death: a dynamic response concept. Autophagy *5,* 590-603.

Lotze, M.T., and Tracey, K.J. (2005). High-mobility group box 1 protein (HMGB1): nuclear weapon in the immune arsenal. Nat. Rev. Immunol. *5,* 331-342.

Lu, L., Wu, W., Yan, J., Li, X., Yu, H., and Yu, X. (2009). Adriamycin-induced autophagic cardiomyocyte death plays a pathogenic role in a rat model of heart failure. Int. J. Cardiol. *134,* 82-90.

Maitra, S.R., Wojnar, M.M., and Lang, C.H. (2000). Alterations in tissue glucose uptake during the hyperglycemic and hypoglycemic phases of sepsis. Shock *13,* 379-385.

Mathison, J.C., and Ulevitch, R.J. (1979). The clearance, tissue distribution, and cellular localization of intravenously injected lipopolysaccharide in rabbits. J. Immunol. *123,* 2133-2143.

McCarthy, J.J., and Esser, K.A. (2010). Anabolic and catabolic pathways regulating skeletal muscle mass. Curr. Opin. Clin. Nutr. Metab. Care *13,* 230-235.

Nagy, J., Chang, S., Dvorak, A., and Dvorak, H. (2009). Why are tumour blood vessels abnormal and why is it important to know&quest. Br. J. Cancer *100,* 865-869.

Pilkis, S.J., and Granner, D. (1992). Molecular physiology of the regulation of hepatic gluconeogenesis and glycolysis. Annu. Rev. Physiol. *54,* 885-909.

Schwerk, C., and Schulze-Osthoff, K. (2003). Non-apoptotic functions of caspases in cellular proliferation and differentiation. Biochem. Pharmacol. *66,* 1453-1458.

Shimada, T. (2006). Xenobiotic-metabolizing enzymes involved in activation and detoxification of carcinogenic polycyclic aromatic hydrocarbons. Drug Metabolism and Pharmacokinetics *21,* 257-276.

Sillos, E.M., Shenep, J.L., Burghen, G.A., Pui, C., Behm, F.G., and Sandlund, J.T. (2001). Lactic acidosis: a metabolic complication of hematologic malignancies. Cancer *92,* 2237-2246.

Sishi, B.J., Loos, B., van Rooyen, J., and Engelbrecht, A. (2013). Autophagy upregulation promotes survival and attenuates doxorubicin-induced cardiotoxicity. Biochem. Pharmacol. *85,* 124-134.

Tanida, I., Ueno, T., and Kominami, E. (2008). LC3 and Autophagy. Autophagosome and Phagosome 77-88.

Taranto, M.P., Perez-Martinez, G., and de Valdez, G.F. (2006). Effect of bile acid on the cell membrane functionality of lactic acid bacteria for oral administration. Res. Microbiol. *157,* 720-725.

Theurl, I., Hilgendorf, I., Nairz, M., Tymoszuk, P., Haschka, D., Asshoff, M., He, S., Gerhardt, L.M., Holderried, T.A., and Seifert, M. (2016). On-demand erythrocyte disposal and iron recycling requires transient macrophages in the liver. Nat. Med. *22,* 945-951.

Trautmann, A. (2009). Extracellular ATP in the immune system: more than just a "danger signal". Sci. Signal. *2,* pe6.

van Niekerk, G., Loos, B., Nell, T., and Engelbrecht, A. (2016). Autophagy—A free meal in sickness-associated anorexia. Autophagy *12,* 727-734.

Vander Heiden, M.G., Cantley, L.C., and Thompson, C.B. (2009). Understanding the Warburg effect: the metabolic requirements of cell proliferation. Science *324,* 1029-1033.

Wang, X., Soltesz, V., Andersson, R., and Bengmark, S. (1993). Bacterial translocation in acute liver failure induced by 90 per cent hepatectomy in the rat. Br. J. Surg. *80,* 66-71.

Ward, C., Martinez-Lopez, N., Otten, E.G., Carroll, B., Maetzel, D., Singh, R., Sarkar, S., and Korolchuk, V.I. (2016). Autophagy, lipophagy and lysosomal lipid storage disorders. Biochim Biophys Acta. *1861,* 269-284.

Wong, J., Smith, L.B., Magun, E.A., Engstrom, T., Kelley-Howard, K., Jandhyala, D.M., Thorpe, C.M., Magun, B.E., and Wood, L.J. (2013). Small molecule kinase inhibitors block the ZAK-dependent inflammatory effects of doxorubicin. Cancer Biol. Ther. *14,* 56-63.

Yuk, J., and Jo, E. (2013). Crosstalk between autophagy and inflammasomes. Mol. Cells *36,* 393-399.

Zhai, R., Sheu, C.C., Su, L., Gong, M.N., Tejera, P., Chen, F., Wang, Z., Convery, M.P., Thompson, B.T., and Christiani, D.C. (2009). Serum bilirubin levels on ICU admission are associated with ARDS development and mortality in sepsis. Thorax *64,* 784-790.

Zhou, S., Palmeira, C.M., and Wallace, K.B. (2001). Doxorubicin-induced persistent oxidative stress to cardiac myocytes. Toxicol. Lett. *121,* 151-157.

Zirin, J., Nieuwenhuis, J., and Perrimon, N. (2013). Role of autophagy in glycogen breakdown and its relevance to chloroquine myopathy. PLoS Biol *11,* e1001708.

Chapter 6

Based on the inconclusive results from western blot analyses, subsequent proteomic analyses were performed. This chapter outline key findings from bioinformatics analyses implementing a gene ontology approach to describe biological relevance of deferentially regulated proteins between groups of mice.

6.1 Proteomic study design

Two key technical challenges in proteomics analysis are the complexity of the protein sample (i.e. the range of proteins expressed by tissue/cell sample) and the dynamic range (i.e. variability in the expression range) of proteins. As an example, protein abundance in plasma samples can vary across a 10^{12}-fold range, whereas the sensitivity of most proteomic platforms is within three to four orders of magnitude (Wasinger et al., 2013). Inter-sample variation can thus be substantial, and rapidly inflate variance and decrease statistical power. To address this concern, liver samples were pooled prior to proteomic analysis in order to 'level out' inter-mice variability: for each group, three mouse liver samples were randomly pooled, forming four samples which were submitted for proteomic analysis (**Figure 6.1**). Thus, from a total of 12 mice, 4 samples (containing liver samples from three mice) were used for proteomic analysis.
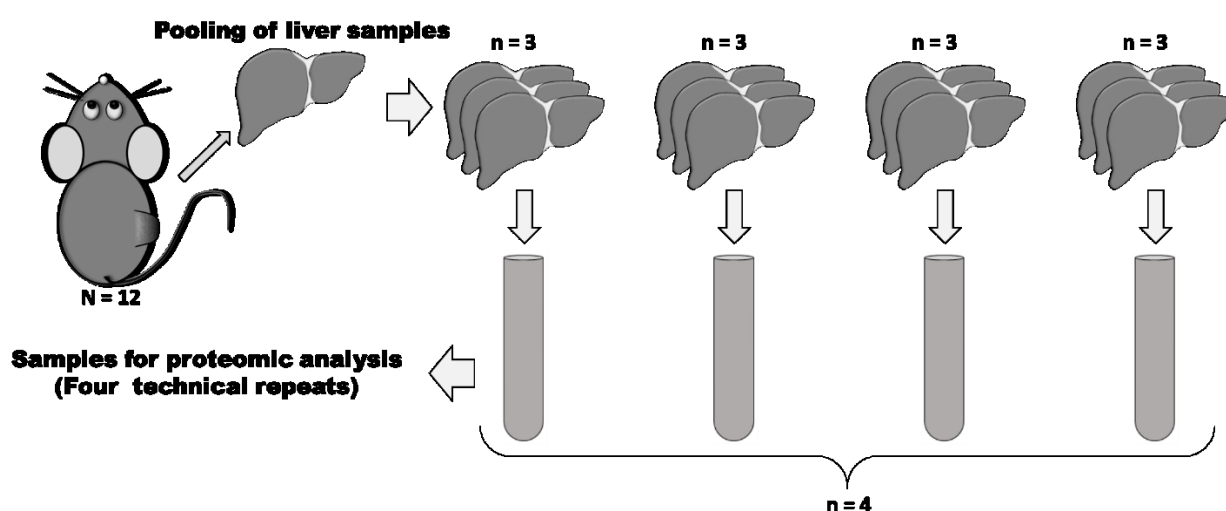
Figure 6.1. Pooling of liver samples.

Snap-frozen liver samples were wrapped in tin foil (pre-cooled in liquid nitrogen) and crushed between two spoons (also pre-cooled). It is not practical to add identical amounts of liver samples since water vapour condenses on frozen tissue samples, increasing the weight. Therefore, a similar, but not exact amount of liver samples were pooled. It was not desirable to re-generate batches of pooled liver samples, since the representative amount of liver tissue each mouse contributed would differ between batches. Thus, the same samples were used for both western blot and proteomic analyses. This facilitated comparison between analytic platforms (western blot and proteomic results). Pooled-liver samples were sonicated in lysis buffer (**Table 6.1**) and frozen at -80°C until analysed.

Table 6.1. Constituents of lysis buffer used for proteomic analysis.

	Stock	10 ml	20 ml	30 ml	50 ml
20 mM Tris-HCl	200 mM	1 ml	2 ml	3 ml	-
1 mM EGTA	10 mM				
1 mM EDTA	100 mM	100 µl	200 µl	300 µl	500 µl
150 mM NaCl	1 M	1.5 ml	3 ml	4.5 ml	7.5 ml
1 mM β-glycerophosphate	-	0.002 g	0.004 g	0.006 g	0.01 g
2.5 mM tetra-Na-Pirophosphate	-	0.01 g	0.02 g	0.03g	0.05 g
1 mM Na_3VO_4	10 mM	1 ml	2 ml	3 ml	5 ml
50 µg/ml PMSF	100 mM	30 µl	60 µl	90 µl	150 µl
10 µg/ml Leupeptin	-	10 µl	20 µl	30 µl	50 µl
10 µg/ml Aprotinin	-	10 µl	20 µl	30 µl	50 µl
0.1% SDS	10%	100 ul	2 ml	3 ml	5 ml

Finally, an attempt was made to compare our results to published data. Unfortunately, no study has yet performed either proteomic or transcriptomic analysis on mouse liver following DXR treatment. However, published data is available for HepG2 cells exposed to DXR. These cells are a human-derived hepatocellular carcinoma that was treated with DXR (Hammer et al., 2010). This publicly available proteomic data was also analysed using (where applicable) the same set of analytic procedures employed in the bioinformatics pipeline.

6.2 Mass spectrometry

Liquid chromatography mass spectrometry was performed by the Centre for Proteomic & Genomic Research (CPGR), an ISO 9001:2008 certified facility. Analysis was performed using a Dionex Ultimate 3000 nano-HPLC system followed by peptide analysis on a Q-Exactive quadrupole-Orbitrap mass spectrometer (Thermo Fisher Scientific, USA) in positive ion mode.

Relative quantification of protein abundance was performed using the Progenesis QI (Nonlinear, UK) software suit. Identified peptides were matched to proteins in the UniProt database using Byonic algorithm (Proteinmetrics, San Carlos, CA, USA; version PMI-Byonic-Com:v2.5.6). Proteins were included if at least two unique peptides were observed for a corresponding protein. A minimal 2-fold change in protein abundance with a significance threshold of $p < 0.05$ (ANOVA) was used as the cut-off criterion for inclusion in the final list of regulated proteins. Principal component analysis was used to identify outliers (analysis part of service provided by CPGR). Since four liver samples were run, outliers identified were omitted, thus, for some groups n = 3 and not 4.

6.3 Proteomic results

Regulated protein samples that adhered to the selection criteria (see preceding section) are tabulated in Appendix I. Protein abundance was normalised to control mice (i.e. no tumour or DXR). Briefly, mice bearing EO771 tumours exhibited 143 differentially regulated proteins, low dose DXR 176 and high dose 145, and mice with B16 melanoma exhibited 186 regulated proteins. Proteomic results from the published study (Hammer et al., 2010) revealed 85 regulated proteins. It is likely that this lower protein abundance results from the fact that liver samples are complex, consisting of multiple cell types, as well as from the fact that in vivo systems are more complex (a more dynamic environment than typical for monocultured cells) and are thus expected to provide a more complex data set with greater variation.

The end product of proteomic analysis is a long list of regulated proteins and not very useful. Subsequent analysis includes a bioinformatics approach to identify sets of regulated proteins involved in a particular biological function (i.e. enrichment analysis). To ascertain meaning from the proteomic profile, a gene ontology (GO) approach was implemented in our research.

6.4 Gene ontology approach

The Gene Ontology Consortium oversees a collaborative effort to assign a standardised functional description to genes and their protein products. These 'functional descriptions' are divided into three different domains (ontologies): (1) *biological process*, (2) *cellular components* and (3) *molecular function*. A cellular component is part of a cell such as an organelle or part of another structure (e.g. ribosomal subunit being part of a ribosome). The

molecular function refers to a molecular 'action' such as binding or catalysing substrates. In contrast, a biological process describes a series of events (e.g. a ribosomal protein is involved in the biological process 'translation'). Of note, gene ontology (GO) does not describe biological entities such as a protein or a metabolic pathway, but focuses on the characteristics and functionality of a gene or the protein product. Thus, as an example, an enzyme is not an ontology, but the enzymatic *function* is. Similarly, a 'cellular component' is defined by the cellular structure into which the component fits, and not by the component itself. Therefore, 'cytochrome c' is not an ontology, but a 'component of electron transport chain' is an ontology.

These GO terms are arranged in a hierarchical manner (**Figure 6.2**), with parent terms carrying less detail than the child term. As an example, the term 'cellular response to gamma radiation' is more detailed than 'cellular response to ionizing radiation' since gamma radiation is simply one source of ionising radiation. Thus, child terms are more informative than parent terms.
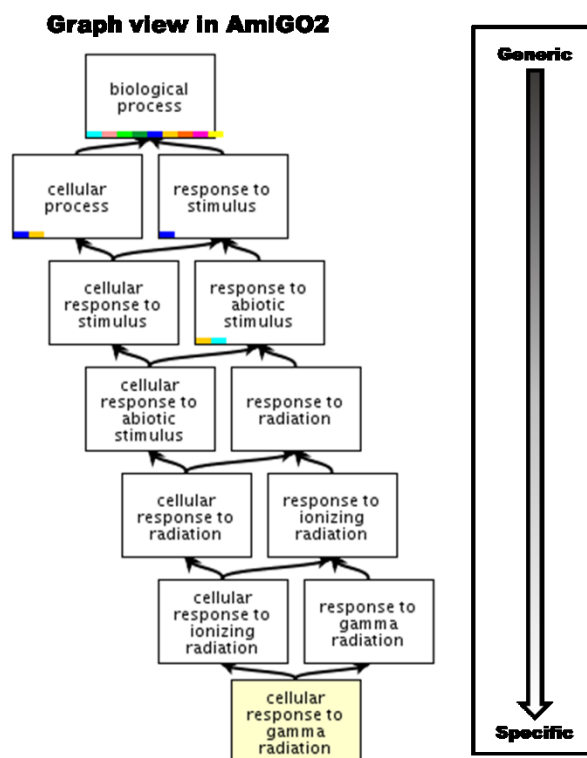
Figure 6.2. GO terms exhibits a hierarchical ordering, with parent terms being more general (i.e. being less informative) than child terms.

The interaction between GO terms is defined in a manner similar to the way in which a GO term itself is defined. Thus, GO does not only attempt to collapse complex interaction into a

simple hierarchy; rather, GO terms are semantically expressed (**Figure 6.3**) by 'controlled vocabularies' that describe the relationship between GO terms. As an example, the relationship between GO terms often takes on the form 'X *is a* Y', where X might be a 'response to stimulus' and Y a 'response to abiotic stimulus'. In this example, a response to a stimulus is a type of response that includes a response to abiotic factors. The edge connecting the parent term ('response to stimulus') with the child term ('response to abiotic stimulus') is logically defined by the '*is a*' relationship. Various interactions are possible (e.g., '*part of*' or '*has part*') with varying levels of detail.
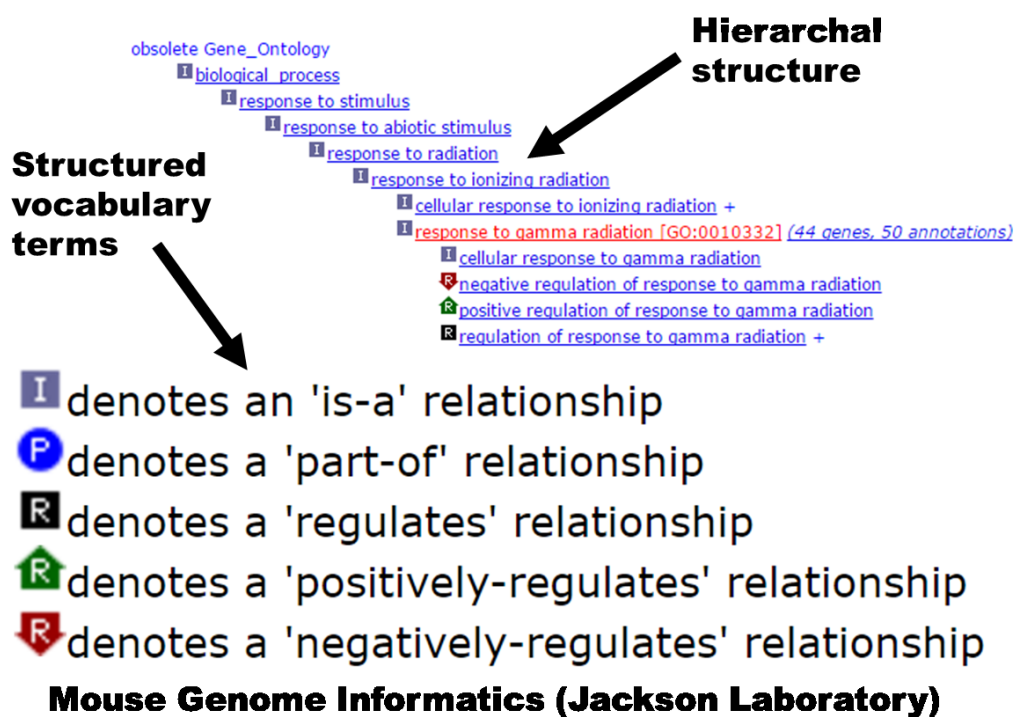
Figure 6.3 Semantic similarity between GO terms (generated in AmiGO2).

The interaction between GO terms can give rise to complex graphs since 'many-to-many' interactions are possible (**Figure 6.4**). Firstly, one parent term can have multiple child terms (**Figure 6.4A** – dark grey box). Here, the parent term 'protein binding' maps to multiple specific child terms ('enzyme binding', 'calcium dependent protein binding', 'receptor binding' etc.) Similarly (**Figure 6.4B** – light grey box), the child term 'G-protein coupled receptor binding' has two parent terms ('glutamate receptor binding' and 'G-protein coupled

receptor binding'). Thus, topologically, GO terms can be described as nodes that are connected by semantic operators such as 'is a' or 'part of' which represent the edges to the graph.
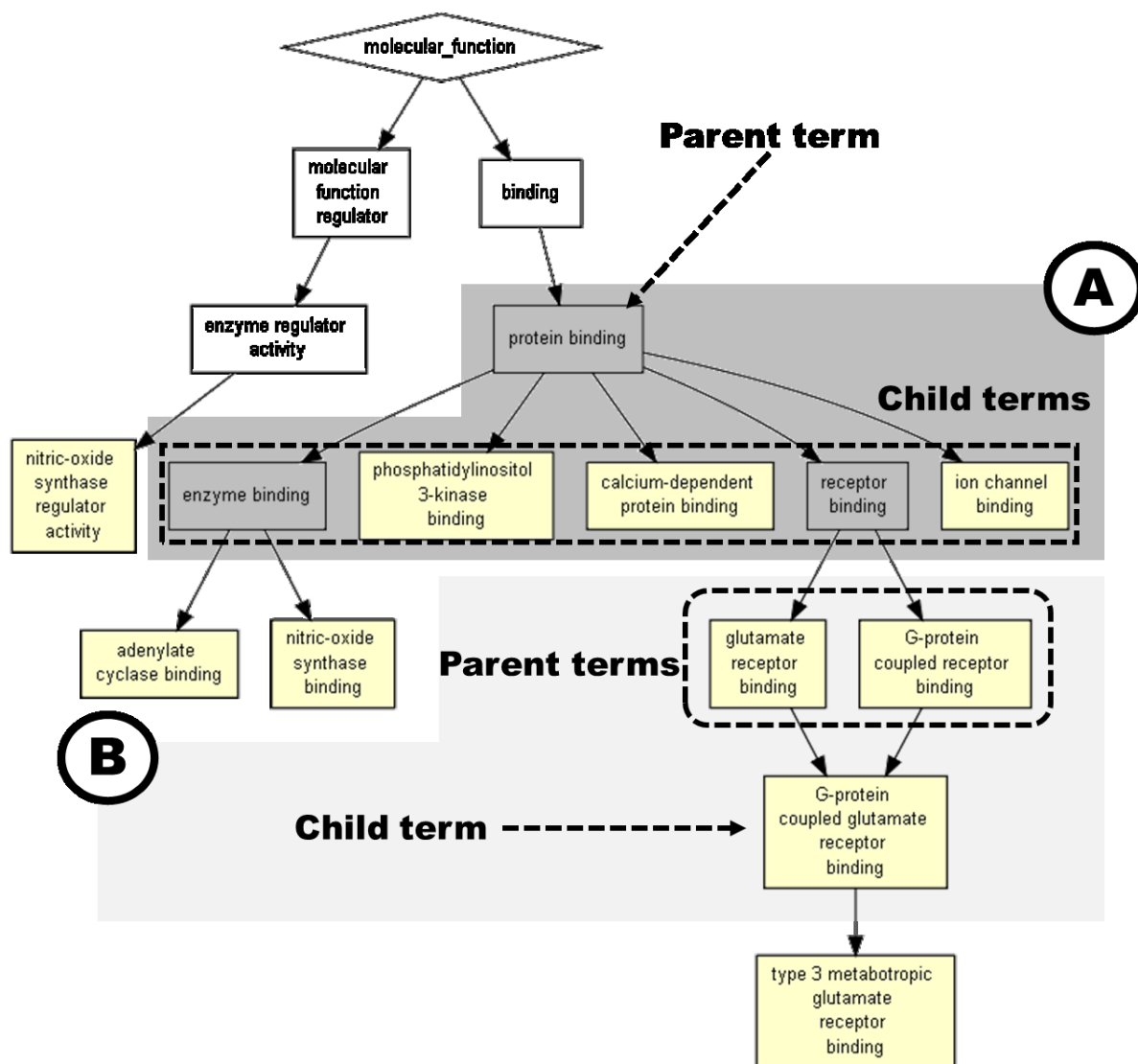
Figure 6.4. Interaction between GO terms gives rise to a directed acyclic graph (generated with GOrila).

The GO approach thus allows for complex descriptions of biologically relevant processes. There are currently ~35 000 GO terms with ~65 000 term-term interactions (Dutkowski et al., 2013) from which graphs of varying degrees of complexity can be generated. In turn, a variety of freely available packages are available for analysing lists of GO terms, including FatiGO (Al-Shahrour et al., 2004), GOrila (Eden et al., 2009), agriGO (Du et al., 2010), AmiGO

(Carbon et al., 2009), GoMiner (Zeeberg et al., 2003), and BiNGO (Maere et al., 2005). In this study, GO analysis is primarily reported from REVIGO which make use of the 'semantic similarity' between GO terms to collapse GO terms into 'the most informative common ancestor' for a set of GO terms (Supek et al., 2011).

6.5 Bioinformatics pipeline

For each group, the list of regulated proteins was divided into 'up-' (i.e. expressed higher in intervention group than control group) and 'down-' (i.e. protein levels are lower in intervention group compared to control) regulated proteins. Lists were then submitted to DAVID (*Database for Annotation, Visualization and Integrated Discovery*) version 6.8, a freely available online analytic tool set for bioinformatics analyses (Huang et al., 2009). Among the various functionalities provided by DAVID are the assignment of GO terms, with corresponding p-values (Benjamini-Hochberg corrected for multiple testing), to a list of proteins. The list of GO terms, with their corresponding p-values, was then submitted to REVIGO. REVIGO implements the user-supplied p-value to collapse GO terms into clusters that remove redundancies (e.g. overlap between parent and child terms). The data presented is then depicted in various graphic formats. Data is inspected according to the three ontologies (biological process, cellular component and molecular function).

REVIGO often provides clusters of GO terms that require more detailed analysis. In performing the enrichment analysis, a number of additional recourses were used (**Figure 6.5**). DAVID provides easy access to the KEGG (*Kyoto Encyclopedia of Genes and Genomes*) and the Reactome Pathway Browser where the role of a group of proteins assigned a given GO term can be inspected within the context of a metabolic or signalling pathway. DAVID also provides a 2-D viewer were protein-protein interactions within a group can be inspected. BioVenn was used to identify sets of GO terms that are unique to an intervention group, or shared across all groups. Also, most platforms only accommodate a set number of gene/protein identifiers. In particular, a UniProt database was used to convert UniProt accession numbers to a number of alternative formats compatible with BioVenn (e.g. Ensembl gene identifiers).

Figure 6.5 Basic outline of enrichment analyses.

Unless stated otherwise, all analyses were performed using default settings. A notable exception was analysis on HepG2 cells, where inclusion criteria and selection parameters were more relaxed. This is because HepG2 cells are not formally analysed, but mainly used as a broad reference. As an example, GO enrichment analyses have indicated the upregulation of proteins not typically associated with the liver (e.g. proteins involved with sarcomeres). Here, a comparison between the proteomes of liver samples and published data on HepG2 cells assisted with the interpretation of data.

In total, analyses were performed on five samples sets: High dose DXR (HD), Low dose DXR (LD), tumour control (T), B16 melanoma (M) and published data for HepG2 cells. For each group, proteins were classified as up- or downregulated, resulting in 10 lists of regulated proteins (5 groups × up- or downregulated = 10). These 10 sets were subsequently analysed according to three ontologies: biological process, cellular components and molecular function. Thus, a total of 30 analyses were performed. In the following section, a detailed overview of the analytic procedure and data interpretation is provided. This overview is followed by a brief description of each group and a review of the main differences and similarities between groups.

6.6 Effect of high dose DXR on the hepatic proteome

Despite the large number of GO terms identified as downregulated, REVIGO collapsed most of the GO terms into few clusters. Only ontology terms downregulated include biological processes (**Figure 6.6**). The size of the nodes ('bubbles') describes the specificity of the terms: large nodes imply less specific terms (i.e. the larger the node, the more GO terms are collapsed within it). Nodes (GO terms) are connected via edges that are based on the hierarchical relationship between GO terms. The shade of red represents the significance of the term ('deep red' more significant). However, all nodes are significant (-log[p-value] > 1.3 which translates to p-value less than 0.05).
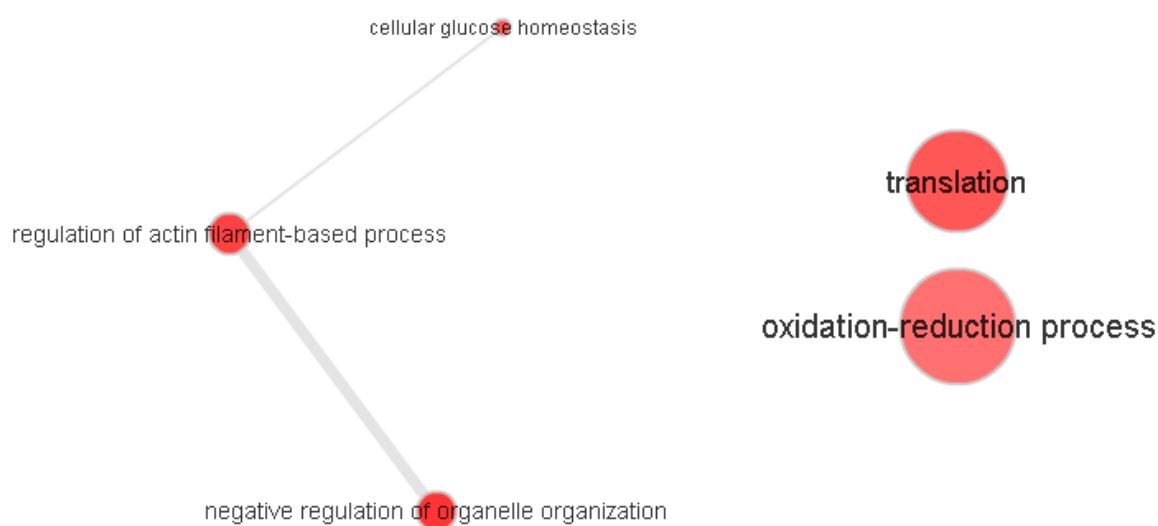
Figure 6.6 Biological processes downregulated in HD group.

A downregulation in various biological processes observed in REVIGO was also observed by Functional Annotation Clustering (FAC) in DAVID. As an example, a decrease in cytoskeletal processes ('regulation of actin filament-based process') was again observed to cluster together in DAVID (**Figure 6.7**), despite the fact that the two software environments make use of different clustering algorithms. The observation that cytoskeletal processes ('regulation of actin filament-based process') are downregulated might have a number of implications. As an example, an upregulating of cytoskeletal functions might also reflect the infiltration of various cells into damaged liver. This might include mobilised hepatic stellate cells, as well as immune cells (Amieva and Furthmayr, 1995).

Figure 6.7 2-D viewer in DAVID of proteins (horizontal) and their functional relationship (vertical) involved in cytoskeletal organisation (downregulated). Notice, DAVID uses a different clustering algorithm from REVIGO, and also does not distinguish between different ontologies (e.g. biological process or a cellar component).

However, altered cytoskeletal activity might also reflect a number of additional cellular activities and events, including energy homeostasis. As an example, actin plays a role in trafficking of organelles as well as organelle structures and also in mitochondrial fission/fusion events (De Vos et al., 2005; Wu et al., 2011). Thus, altered expression in proteins involved in mediating cytoskeletal structure may in fact signify altered mitochondrial function, and consequently have an impact on cellular energy homeostasis. In this regard, a downregulation of proteins implicated in cellular glucose homeostasis might in fact relate to altered mitochondrial structure and functionality. However, DAVID did not specifically cluster proteins involved in glucose homeostasis. Similarly, the node 'cellular glucose homeostasis' identified in REVIGO is small, indicating few GO terms are included by the category cellular glucose homeostasis. Nevertheless, the observation that cytoskeletal elements ('regulation of actin filament-based process') share functionality with organelle organisation ('negative regulation of organelle organisation'), in conjunction with the observation that metabolic components are downregulated ('cellular glucose homeostasis') could imply alterations in

mitochondrial fission/fusion events. Mitochondrial alteration may account for altered glucose metabolism as well as an alternation in organelle size: mitochondrial stress, such as oxidative stress, results in altered fission/fusion dynamics (Wu et al., 2011).

The oxidation-reduction processes might also at first seem to be related to energy homeostasis since oxidative respiration is a typical process that also involves an oxidation-reduction process. This is also partially corroborated by Functional Annotation Clustering (FAC) in DAVID (**Figure 6.8**). As an example, *Hao1* (hydroxyacid oxidase 1) has been implicated in metabolism of phytanic acid (a fatty acid) which cannot be metabolised in β-oxidation but undergoes α-oxidation exclusively in peroxisomes (Jones et al., 2000). The relevance of a downregulation of hydroxyacid oxidase 1 is not clear. Phytanic acid can be produced by bacterial fermentation, suggesting that a downregulation might imply a decrease in bacteria-derived phytanic acid. Interestingly, *Sept11* that was also downregulated (**Figure 6.7**) has previously been implicated in cell-autonomous defence against invading pathogens (Mostowy et al., 2009). Collectively, the downregulation of these proteins suggests a possible shift in the interaction between the host and intestinal biota. As an example, damage to the intestinal lining caused by DXR-induced toxicity (Dekaney et al., 2009) might result in gut permeability which might increase circulating lipopolysaccharides (LPS). Since the liver performs a filtering function, increased circulating LPS might induce an upregulation of defence mechanisms in hepatocytes. The role of *Phyhd1* (Phytanoyl-CoA Dioxygenase Domain Containing 1) is also not obvious, in part because the protein function is not fully understood: no study has detailed the function of this protein since its initial discovery from a mouse cDNA library (Strausberg et al., 2002).

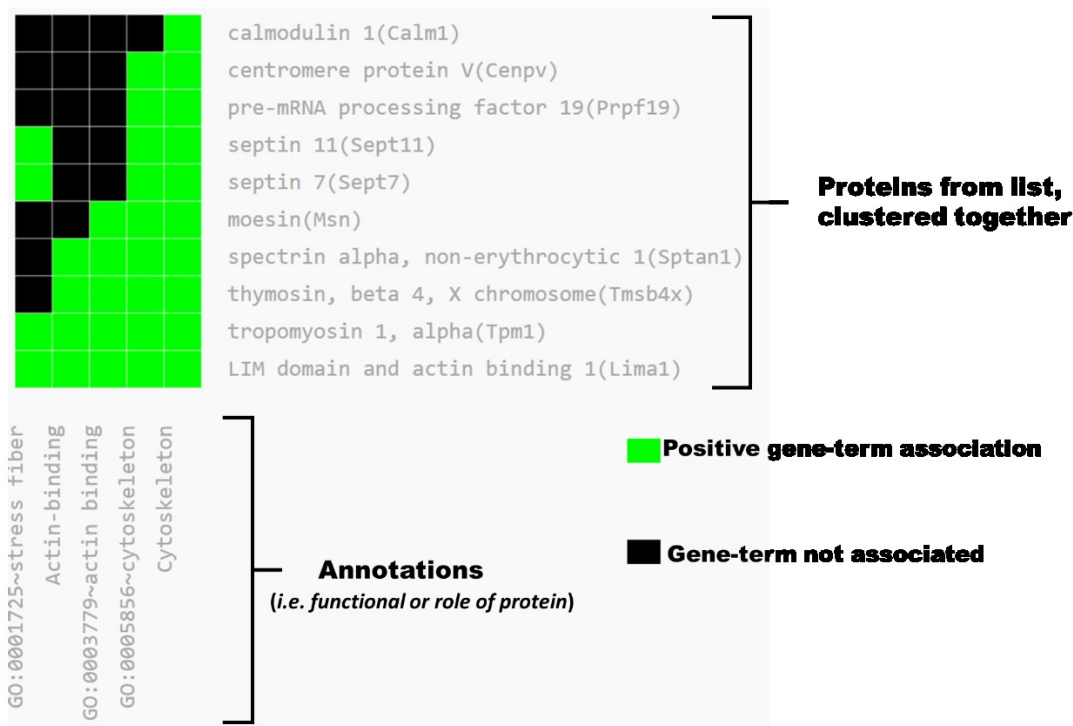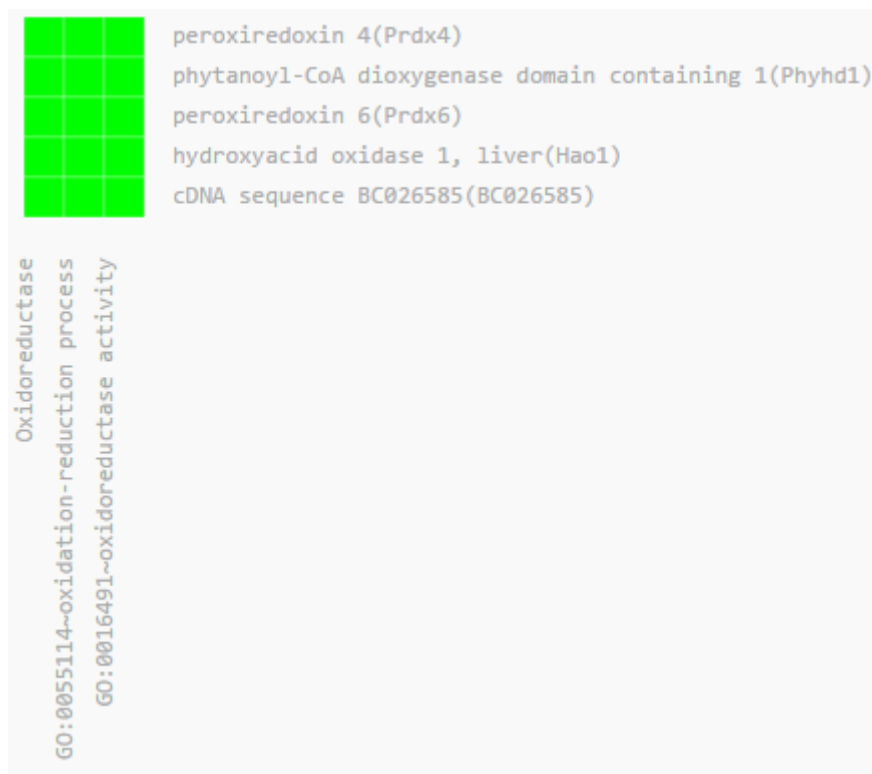**Figure 6.8. 2-D viewer in DAVID of proteins (horizontal) and their functional relationship (vertical) involved in oxidation/reduction processes downregulated.**

However, in addition to identifying metabolic proteins, FAC also identified a number of genes suggesting that a decrease in oxidation-reduction processes might also include, unexpectedly, a decrease in antioxidant capacity such as lower levels of *Prdx6* (encoding peroxiredoxin 6, also known as antioxidant protein 2). The antioxidant activity of *Prdx6* is exemplified by the observation that mice lacking *Prdx6* exhibit higher levels of protein oxidation (Wang et al., 2003). Similarly, peroxiredoxin 4 has also been implicated in ROS scavenging (Nabeshima et al., 2013). Consequently, a decrease of peroxiredoxin 6 is surprising in light of the fact that DXR is widely believed to induce ROS production (Injac and Strukelj, 2008; Nayak et al., 2013).

One possibility for the observed decrease in proteins involved in radical scavenging is that this observation represents a 'refractory response' that occurs after a dramatic upregulation of antioxidant capacity in response to the initial DXR-induced oxidative damage. Following the clearance of DXR, antioxidant capacity needs to be re-equilibrated, since ROS also plays a role in a number of important cell-signalling events (Schieber and Chandel, 2014). In addition, it is of interest that supplementation with antioxidants as well as iron chelators (iron generates more

reactive radical species from H_2O_2 via Fenton reactions) has failed to provide protection against DXR (Šimůnek et al., 2009). In fact, mitochondrial-derived H_2O_2 results in the oxidation of PTEN, which results in an increase in Akt-signalling pathways (Connor et al., 2005). This suggests that a decrease in radical scavenging proteins might be a response to optimise and re-equilibrate radical signalling in the context of tissue repair processes.

6.7 Upregulation of proteins induced by high dose DXR

In contrast to the number of downregulated GO terms, a number of biological processes were upregulated in response to DXR (**Figure 6.9**). Many of these nodes represent biological activities involved in catabolic processes such as macromolecule catabolism and proteolysis. An increase in proteolytic processes might be placed in context of nutrient deprivation: DXR, like many other chemotherapeutic agents, likely induced a decrease in feeding behaviour, necessitating the breakdown of proteins for gluconeogenesis in the liver. Alternatively, higher proteolytic activity might result from the need to degrade proteins damaged by free radical damage post DXR treatment. Also of interest, certain GO terms assigned to downregulated proteins were also present in the set of upregulated proteins. As an example, oxidation-reduction processes were both downregulated and upregulated.
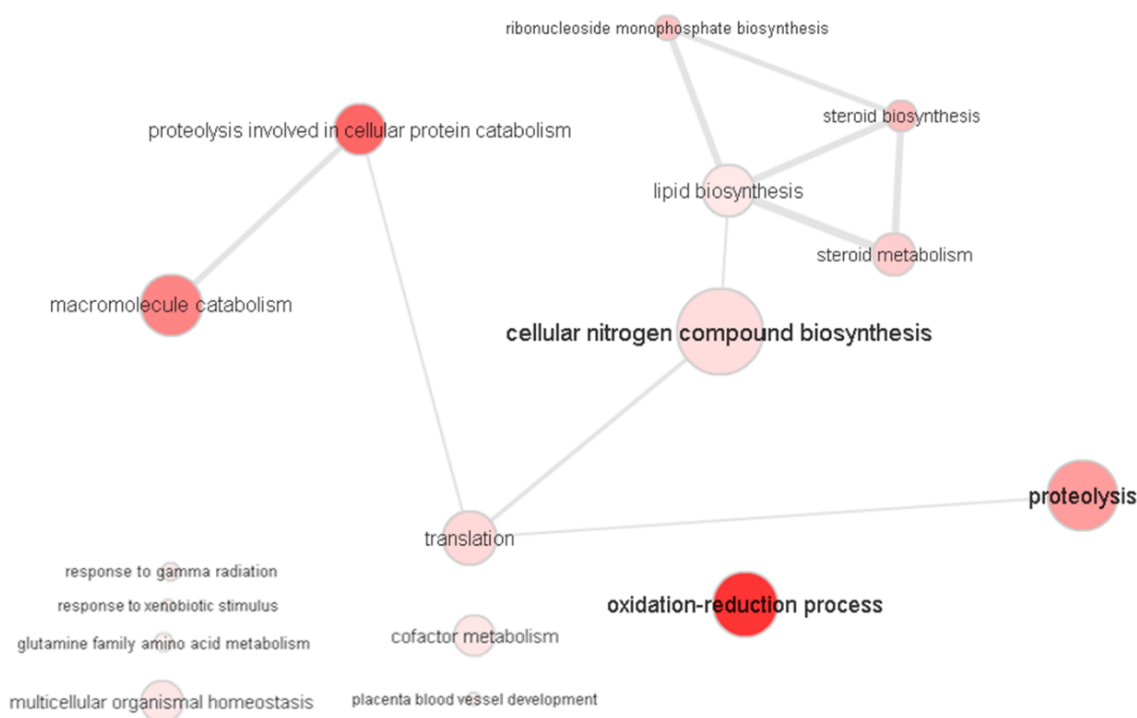
Figure 6.9. Biological processes upregulated in the HD group (HD: High dose DXR).

The observation that GO terms assigned to downregulated proteins again appear in the set of upregulated proteins, appears contradictory. However, many GO terms are generic, including proteins that might perform the same biological function, but in vastly deferent contexts. As an example, proteolytic reactions are not only relevant to catabolic processes but also play a cell signaling role (e.g. cleaving PARP). Similarly, the seeming paradoxical observation that similar processes are both up- and downregulated (e.g. as observed for oxidation-reduction processes) can be explained by the fact that these reactions are activated in different contexts. This is also exemplified in the data for upregulated proteins (**Figure 6.10**). In particular, many of the proteins implicated in 'oxidation-reduction processes' play detoxification roles or are involved in biosynthetic pathways, whereas the downregulated 'oxidation-reduction processes' (**Figure 6.8**) were enriched for proteins implicated in radical scavenging.

Of note, however, is that certain radical scavenging proteins (e.g. glutathione peroxidase (Lei, 2002)) were indeed upregulated. The reason why certain antioxidant mechanisms are upregulated, whereas others are simultaneously downregulated is unclear. One possibility might be that different antioxidant mechanisms are invoked, based on the origin and species of radicals produced (e.g. H_2O_2 versus OH^-). As a plausible example, excessive mitochondrial ROS might need to be curbed, while minimising the impact on cytosolic ROS that might play various cell-signalling functions (Ray et al., 2012).

Figure 6.10. 2-D viewer in DAVID of proteins involved in oxidation/reduction processes. Biological function (horizontally) and their functional relationship (vertical).

An upregulation of ribonucleoside monophosphate biosynthesis (**Figure 6.9**) may suggest a form of nucleotide stress, since ribonucleotide inosine 5'-monophosphate is a purine precursor of Guanosine 5'-monophosphate (GMP) and adenosine 5'-monophosphate (AMP). DXR causes a halt in replication by inhibiting topoisomerase (Tewey et al., 1984). In this regard, a stalled replication process might activate a response similar to nucleotide depletion (Zeman and

Cimprich, 2014). This would suggest that an upregulating of proteins involved in purine biosynthesis might reflect a response to replication stress induced by nucleotide depletion. Alternatively, an increase in nucleotide production might demonstrate a physiological adaptation: after the removal of the DXR insult, replication of cells takes place in order to replace damaged tissue which might increase the systemic demand for nucleotides (used in RNA and DNA). As an example, the myelo-suppressive effects of DXR have long been appreciated (Bally et al., 1990), suggesting that the replacement of hepatocytes following DXR might increase the demand for nucleotides. Finally, extracellular ATP and ADP have a well-established role in immune signalling (Idzko et al., 2014), whereas cyclic AMP and GMP play various cell-signalling roles (Fajardo et al., 2014). The significance of an increase in nucleotide synthesis can have a number of implications.

An upregulating of steroid metabolism as well as lipid biosynthesis was also observed with FAC analysis (**Figure 6.11**). One plausible explanation is that these activities might include that replicating cells require more steroids to be incorporated into membranes. This narrative is in line with the preceding argument that nucleotide synthesis might be upregulated to accommodate tissue expansion of certain organ systems. However, all proteins are reasonably central in the biosynthesis pathway (**Figure 6.12**), rendering it impossible to exclude other possibilities (e.g. the use of steroids as hormone precursors or in the synthesis of bile acids). The fact that DXR can damage intestinal lining (Dekaney et al., 2009), as well as its immune-suppressive effect (Hui-Chou et al., 2012) might cause the expansion and invasion of intestinal biota that is usually regulated by the immune system (Maynard et al., 2012). Since bile acids exhibit anti-microbial properties (Sung et al., 1993), an increase in bile acids might represent a strategy to prevent bacterial overgrowth in DXR treated (i.e. immune-compromised) mice. Finally, the biliary excretion of DXR represents an important route through which the body may remove this noxious substance (Ballet et al., 1987). Thus, an increase in bile flow might represent a strategy to enhance the clearance of DXR.
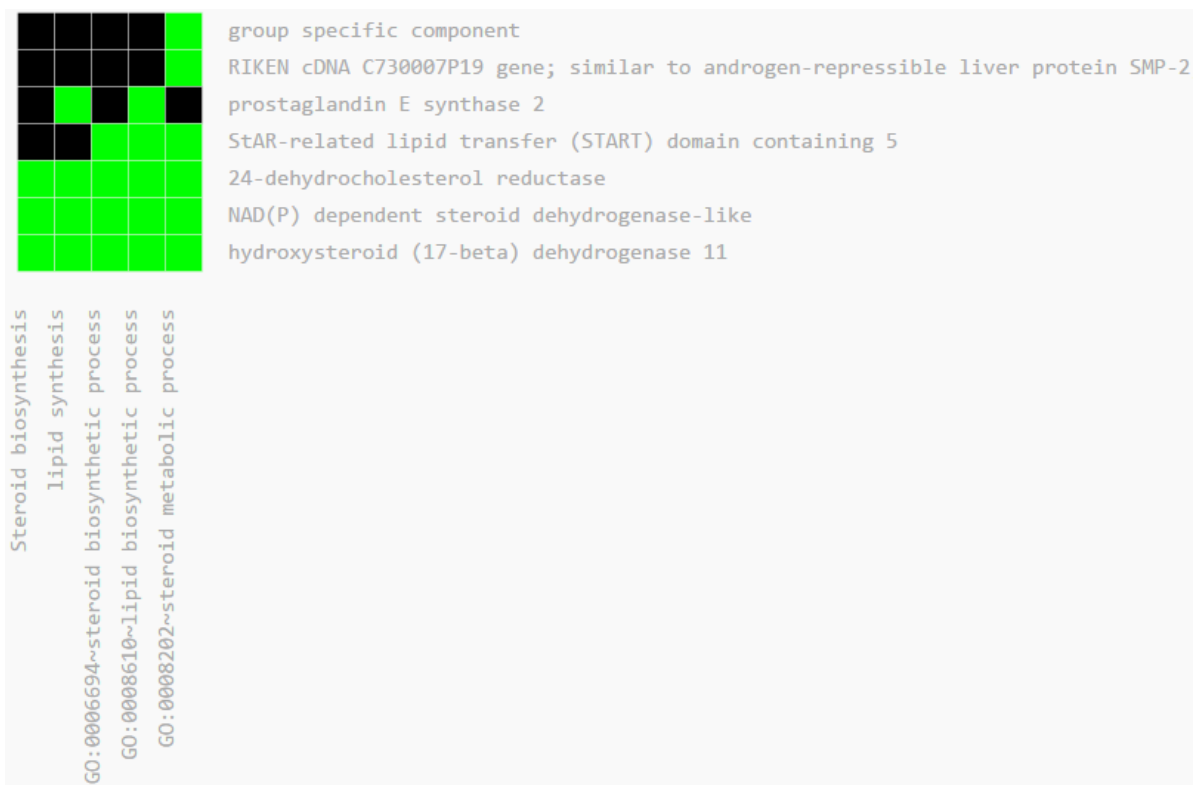
Figure 6.11. 2-D viewer in DAVID of proteins involved in lipid and steroid biosynthesis. Biological function (horizontally) and their functional relationship (vertical).
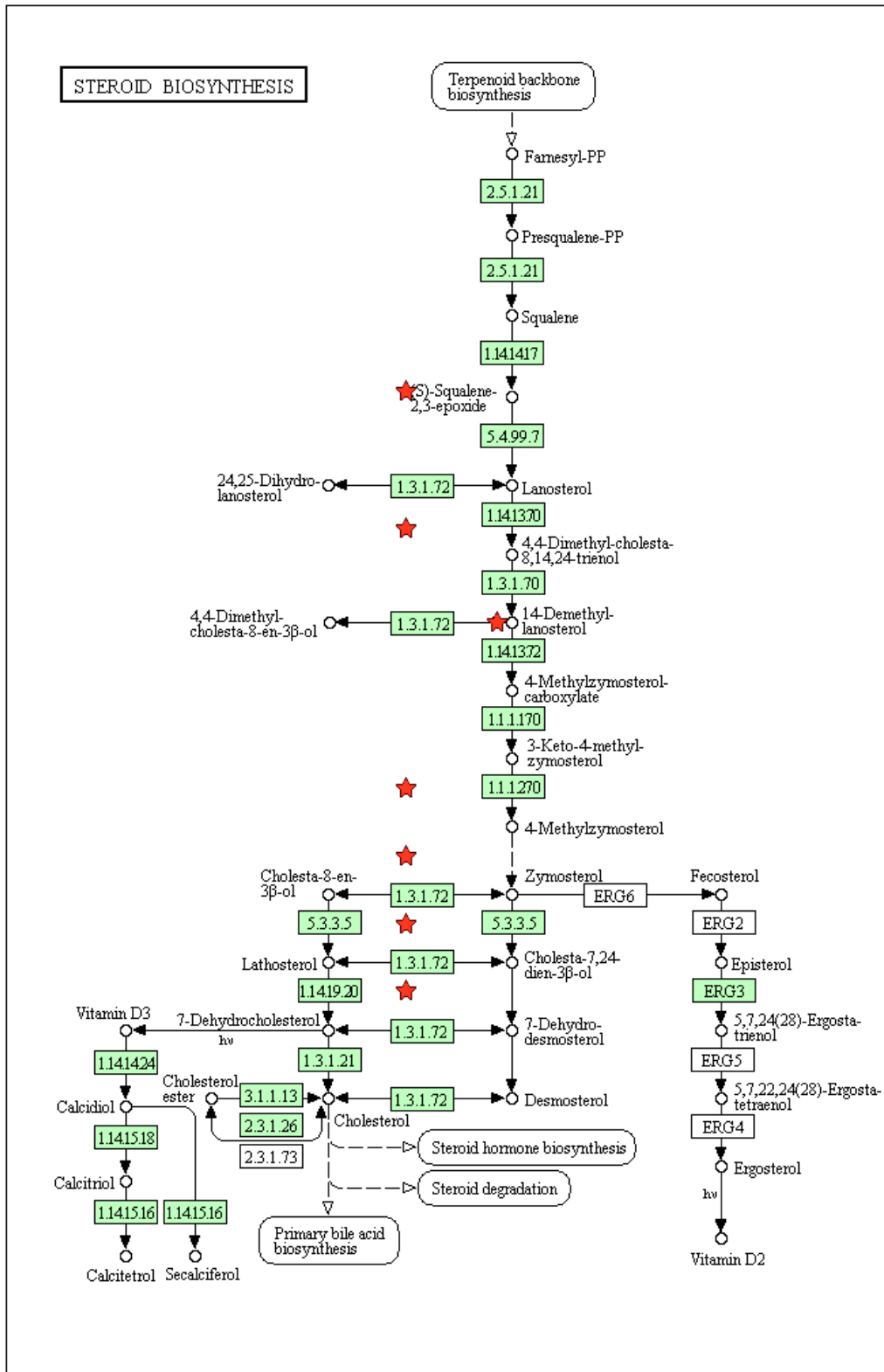
Figure 6.12. Proteins involved in xenobiotic metabolism. Upregulated proteins are indicated by red stars (★). Diagram from KEGG (diagram abridged). Numbers indicate proteins, according to International Union of Biochemistry and Molecular Biology Enzyme Nomenclature.

Finally, it is also interesting that both catabolic and anabolic processes are upregulated (Figure 6.10). As an example, proteolysis and macromolecular catabolism is upregulated, whereas cellular nitrogen compound biosynthesis is also co-currently upregulated. Furthermore, these cellular activities are functionally integrated, with nodes being either directly or indirectly linked with edges (i.e. have functional components). This might seem to invoke a possible futile cycle, with both catabolic and anabolic processes operating simultaneously in the same tissue. However, cells are capable of spatially partitioning biological processes. A key example is the activation of autophagy (a process long appreciated to be involved in catabolic functions) along with the upregulation of biosynthetic pathways (Kaur and Debnath, 2015; Narita et al., 2011). The need to activate catabolic and anabolic processes simultaneously is also relevant to the liver. As an example, during an inflammatory insult, the liver is involved in catabolic processes (e.g. gluconeogenesis from proteins) as well as in the synthesis of immune modulators and effectors (initial phase proteins and thrombotic factors) (Robinson et al., 2016).

The upregulation of proteins involved in xenobiotic metabolism (**Figure 6.9**) was confirmed by FCA. Interestingly, two proteins upregulated, xanthine dehydrogenase and guanine monophosphate synthase (indicated as 1.17.32 and 6.3.52 respectively in **Figure 6.13**) are involved in the metabolism of azathioprine (brand name Imuran, used as an immune suppressor) which, like DXR, exerts a therapeutic effect by halting DNA replication in rapidly dividing immune cells (Nielsen et al., 2001). Similarly, a protein (UDP-glucuronosyltransferase 1-9, indicated as 2.4.1.17) involved in irinotecan (also an anti-cancer agent that, like DXR, inhibits topoisomerase) was also upregulated (2.4.1.17). Collectively, the upregulating of these enzymes is likely reflective of the hepatic processing of DXR.
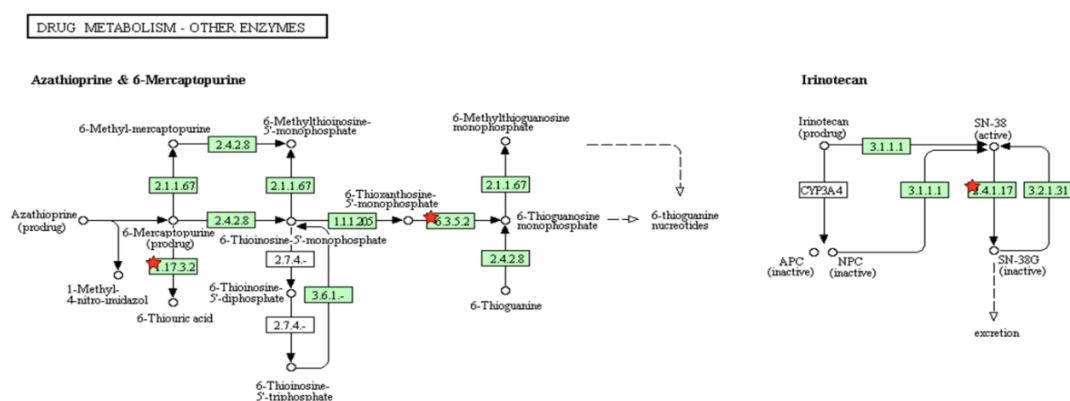
Figure 6.13. Proteins involved in xenobiotic metabolism. Upregulated proteins are indicated by red stars (★).

The upregulation of GO terms associated with cellular components (**Figure 6.14**) supports the interpretation that DXR treatment results in an alteration in cellular metabolism, including increasing protein catabolism, as well as altered mitochondrial function. As an example, components of the proteasome complex were upregulated, whereas numerous mitochondrial proteins were also upregulated. There is also evidence of vesicle formation or an increase in vesicle trafficking (e.g. proteins involved in the formation of membrane envelopes, as well as endoplasmic reticulum). The upregulating of cytoskeletal proteins ('regulation of actin filament-based processes' – **Figure 6.6**) might suggest an increase in vesicle trafficking. In turn, an increase in vesicle trafficking may also reflect biological processes. As an example, damaged mitochondria may 'bud off' (i.e. undergo mitochondrial fission) and subsequently be sequestered in autophagic vesicles prior to fusion with lysosomal vesicles (Twig et al., 2008). However, proteins involved in autophagic processes were not upregulated in our sample, a result also confirmed by western blot analyses (Chapter 5).
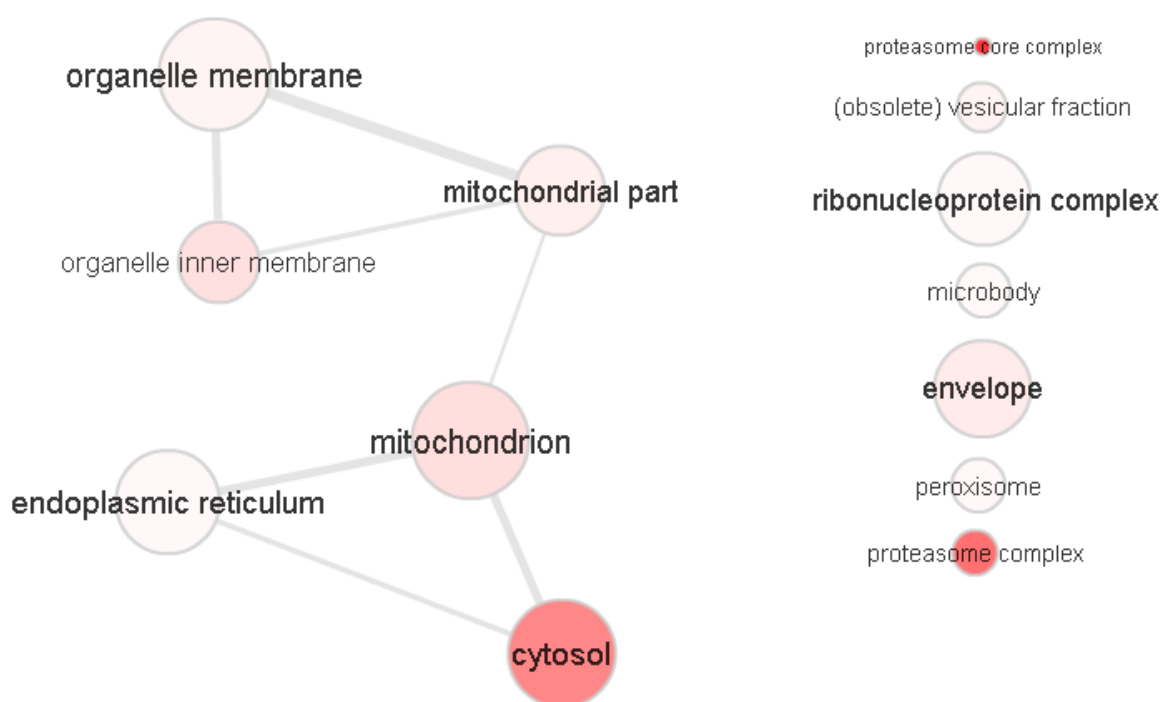
Figure 6.14. Cellular components upregulated in the HD group. Components described as obsolete (e.g. 'vesicular fraction') are components that form structures in other species (in this case, yeast cells). In REVIGO, GO terms were specified to be derived from mice, and are thus designated as 'obsolete' if GO term is relevant to a different organism (e.g. yeast).

Similarly, the upregulation of processes involved in detoxification and synthesis of cholesterol is also supported by the observation that elements contributing to microbody formation were

upregulated. Microbodies are peroxisomes and glyoxysomes which play a role in α- and β-oxidation, processing of radicals, and detoxification of xenobiotics (Faust and Kovacs, 2014). Though peroxisomes are also formed from ER components (Ma et al., 2011), the upregulating of ER processes did not share elements with peroxisomes (i.e. there were no edges connecting GO terms in the node 'endoplasmic reticulum' with node 'microbody' – **Figure 6.14**).

Inspection of GO terms associated with molecular function (**Figure 6.15**) affirmed the preceding observations that catabolic processes such as the proteasomal pathway might be upregulated, and that mitochondrial remodelling was taking place. GO terms involved in electron transport, as well as cofactor binding suggest that mitochondrial activity was indeed altered. Also, proteins with peptidase activity were similarly upregulated, supporting the role of catabolic processes. Yet, there was an increase in protein components of ribosomes, contrasting with the finding that processes involved in translation were downregulated (**Figure 6.6**). The significance of this finding is not clear.
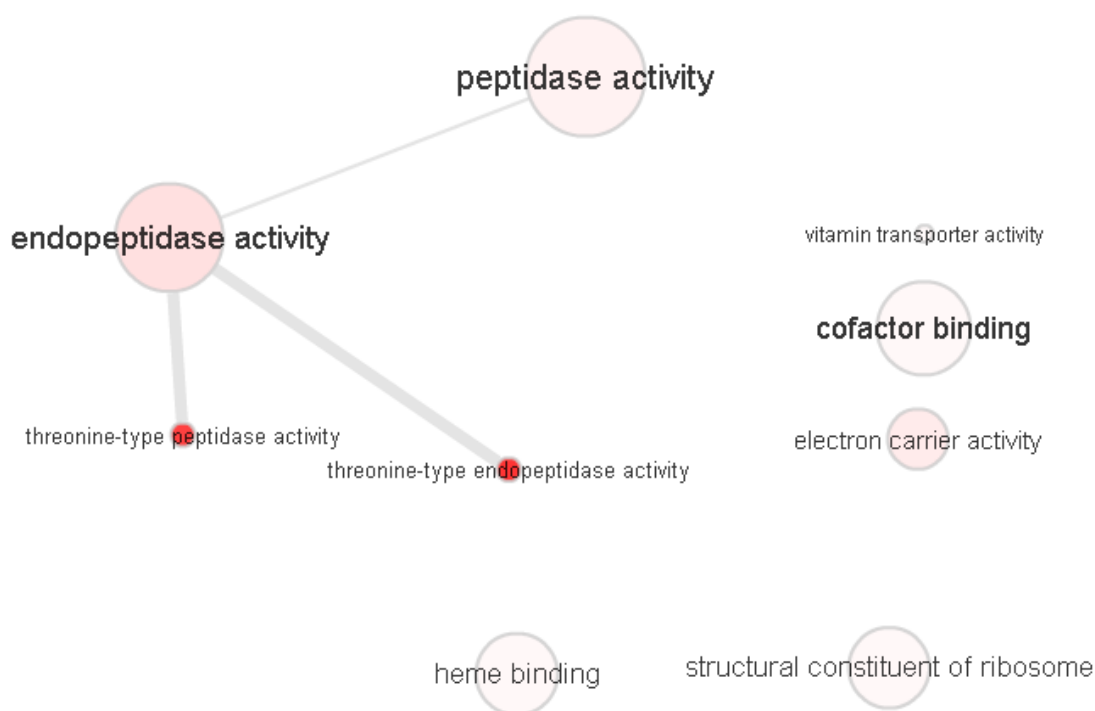
Figure 6.15. **Molecular functions upregulated in the HD group (HD: High dose DXR).**

6.8 Summary: High DXR group

Many observations, such as the increased expression of proteins involved in the detoxification of xenobiotics in the HD group, were as expected. Similarly, the response to gamma radiation

might correspond to the fact that many chemotherapeutic agents, including DXR, can lead to 'radiation recall', inducing tissue damage similar to exposure to radiation (Burris and Hurtig, 2010). Alterations in mitochondrial fission and fusion activities in response to DXR have also previously been reported (Ashley and Poulton, 2009). However, the relevance of some findings is less obvious. An interesting observation is the concurrent up- and downregulation of certain proteins involved in radical scavenging. This might suggest the need to scavenge particular radical species, or the special compartmentalisation of radicals (e.g. the need to decrease mitochondria-derived ROS, while saving cytosolic ROS to perform normal functions). This, in turn, raises the possibility of exploring tolerance therapies that aim to either target particular ROS species, or compartmentalise the distribution of antioxidants.

The unexpected impact of the host's intestinal biota on the chemotherapeutic outcome has only recently been appreciated (Karin et al., 2014). This is likely also true in the context of DXR. The immune system plays a key role in managing the composition of intestinal biota (Kato et al., 2014; Lee and Mazmanian, 2010), and conversely, the immune system is also altered by the intestinal biota (Bauer et al., 2006). Since DXR attenuates the host's immune system (Bhinge et al., 2012), it is likely that the relationship between the host and intestinal biota would be affected. In fact, proteomic results indicated a number of regulated processes that might have an impact on host-symbiont interactions. As an example, an increase in bile flow (possible consequence of increase steroid metabolism) might prevent bacterial overgrowth in DXR-treated (i.e. immune-compromised) mice. The reduction of hydroxyl-acid oxidase 1, necessary for the metabolism of bacteria-derived phytanic acid, suggests that bacteria are either not fermenting substrate, or that the bacterial load in the intestines is low. Similarly, Septin-11, known to play a role in host defence against bacteria was also observed. It remains to be seen how populations of intestinal biota are altered in response to chemotherapy, and more importantly, what the consequence and effect may be of a 're-negotiated' equilibrium between the host and its symbionts.

Interestingly, only a few immune-modulating agents such as cytokines were observed. A possible reason for this is an interplay between two factors. Firstly, immune modulators such as cytokines are often small and usually only present in low quantities. Being small, a cytokine would generate fewer peptides compared to larger proteins; being low in abundance only confounds the low counts of cytokine-derived peptides. The second factor is the pooling of

mouse liver samples. Mice were sacrificed based on tumour size, and not according to the date on which DXR was administered. Consequently, the liver proteome of some mice would exhibit an acute response to DXR, whereas other mice might exhibit a liver proteome reflective of a 'resolution phase' where tissue repair is taking place (e.g. mice that received DXR earlier, but were sacrificed at a later date). Some observations in the proteomic results support this argument, such as the increased expression of proteins involved in vascularisation ('placental blood vessel development' – **Figure 6.9**) while the response to xenobiotics was concurrently elevated.

Nonetheless, the proteomic data highlighted a number of unexpected pathways activated in the HD groups. As an example, higher cholesterol synthesis might suggest that these compounds might play an important role during the resolution phase, post chemotherapy. However, many of the observations might not relate to the effect of DXR, but may result from the tumour. As an example, increased glycolysis in tumour cells might increase the hepatic clearance of lactate, thus explaining the observed increase in proteins involved in glucose homeostasis (**Figure 6.6**). It is thus import to compare the HD group to the tumour group (T) in order to make these kinds of distinctions. In the following section, a comparison between groups is presented. Details of data analysis have been omitted.

6.8.1   Comparison between DXR groups: Procedural outline

The preceding discussion provided an example of how data was analysed. However, proteomic alterations are more insightful if comparisons are drawn between groups. As an example, a comparison between tumour group (T) and the high dose DXR group (HD) could allow for the identification of regulated pathways in response to DXR versus tumour.

After assigning GO terms to regulated proteins, BioVenn was use to generate an area-proportional representation of GO terms that were either unique or shared by intervention groups (**Figure 6.16**). Interestingly, the majority of downregulated proteins were shared between groups, whereas the upregulation of GO terms was unique to each intervention group. This would suggest that downregulation of proteins may represent a more generic response to hepatic stress (arising from DXR or tumour load), whereas the upregulation of proteins resulted from unique responses.
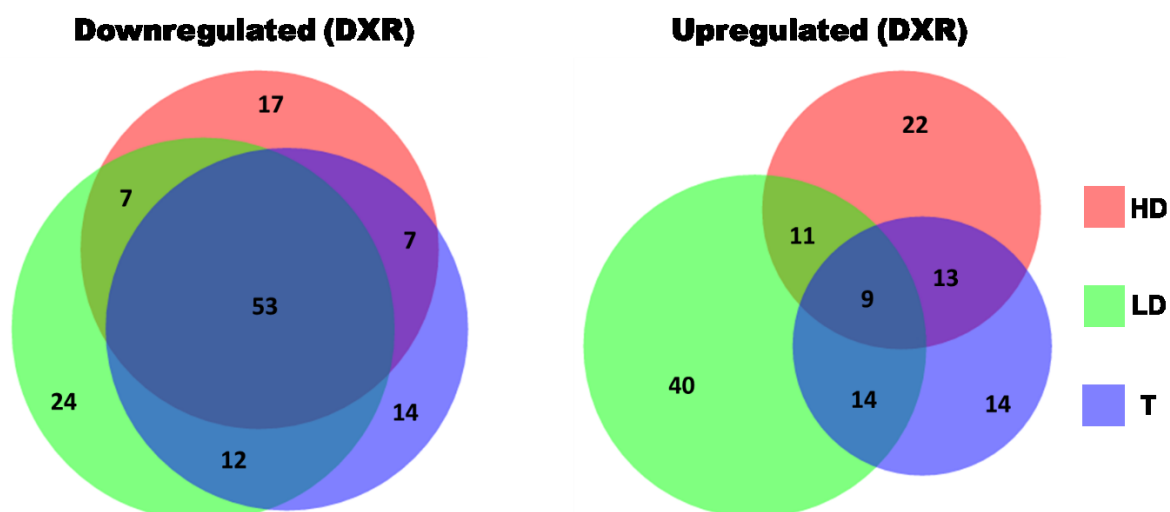
Figure 6.16. Differential enrichment of GO terms between mice receiving DXR. Diagram generated in BioVenn. (HD: High dose Dox; LD: Low dose Dox; T tumour control).

For each group, GO terms were analysed by applying the same procedure as implemented for the HD group. However, since groups are compared (and not simply described), another procedure was introduced: From BioVenn, the GO terms that were identified as unique to each group, or shared universally, were imported to REVIGO. This allowed for identification of processes that were common between groups or unique to a particular group. However, because many GO terms are shared between groups (particular with reference to the downregulated proteins), the p-value for each term was not included, in order to identify processes likely to be implicated. Thus, excluding p-values allowed REVIGO greater scope to collapse GO terms into the most informative common ancestor between GO terms. However, lacking a formal statistical description of significance (i.e. p-value), results cannot be considered definitive. Rather, the goal was to provide a broad overview of processes of interest (i.e. which are universal or specific) that might assist in interpreting results (which are generated for each group in a manner similar to the example for the HD group); therefore, this was an exploratory procedure.

As an example, biological processes that were upregulated highlighted many unique GO terms (**Figure 6.17**). With regards to the previously analysed HD group, many of the processes unique to the HD group were again observed to be uniquely upregulated, including regulation of the cytoskeleton, and organelle organisation. This would suggest that these processes are unique to the HD group. Similar procedures were implemented for the analysis of the other groups.

Biological processes upregulated
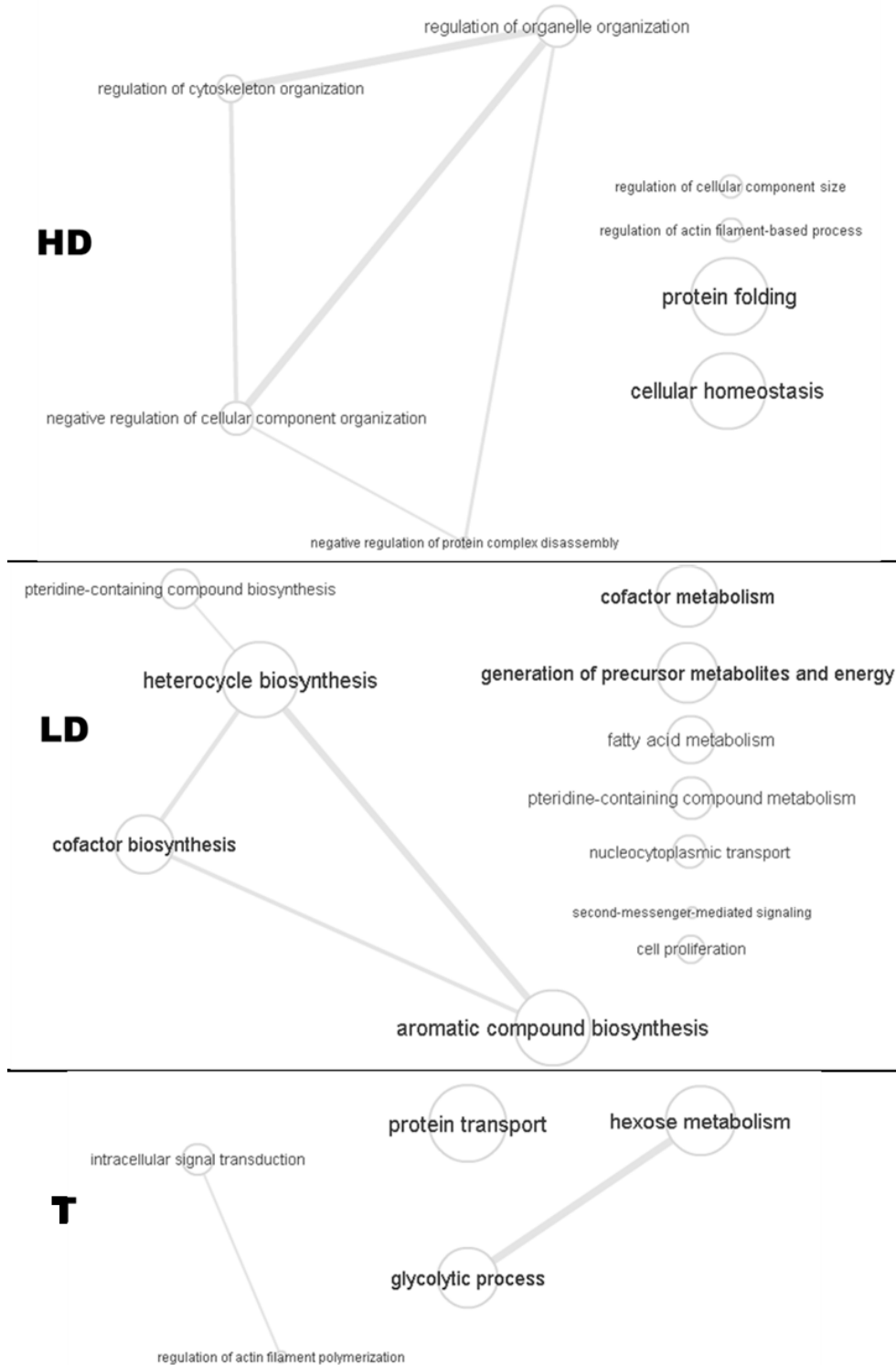
Figure 6.17. **Upregulated GO terms unique to each group (comparison between DXR groups). Nodes are blank to indicate that terms are not assigned significance values. (HD: High dose DXR; LD: Low dose DXR; T: Tumour control).**

6.8.2   Comparison between DXR groups: Results

Both HD and LD had similar underlying trends in the enrichment of GO terms. As an example, the LD group, like the HD group, demonstrated alteration of mitochondrial architecture (**Figure 6.18**). However, many of the similarities are not directly evident. As an example, instead of cytoskeletal processes, contractile fibres collapsed into 'sarcomere' and 'contractile fibre'. These results might seem strange since sarcomeres are usually associated with contractile tissue such as muscle. However, hepatic stellate cells have previously been shown to express sarcomere proteins (Ogata et al., 1993). Similarly, proteomic analysis of Hep2G cell revealed an upregulation of contractile fibres as well as sarcomeres (**Figure 6.19**). The expression of contractile proteins, in conjunction with the anatomical position of hepatic stellate cells and responsiveness to vasomodulators such as angiotensin II and endothelin I have implicated these cells in the maintenance of vascular tone within the liver (Hellerbrand, 2013). Indeed, the liver contains a large portion of the total blood volume (up to 30%), of which a large fraction can be expelled to maintain systemic blood pressure in case of rapid blood loss (Lautt, 2009). Tumour vasculature is typically chaotic and often results in a haemorrhagic tumour, which cause lower blood pressure. (As a personal observation, this seems particularly true for EO771 tumours.) This might suggest that an increase in contractile fibres may represent a strategy to constrict haptic blood volume. Alternatively, the significance of increased sarcomeric proteins is possibly related to fact that, after liver injury, stellate cells take on a myofibroblast-like phenotype (Hellerbrand, 2013). The increase in contractile proteins might suggest an expansion and activation of these cells in response to liver injury.
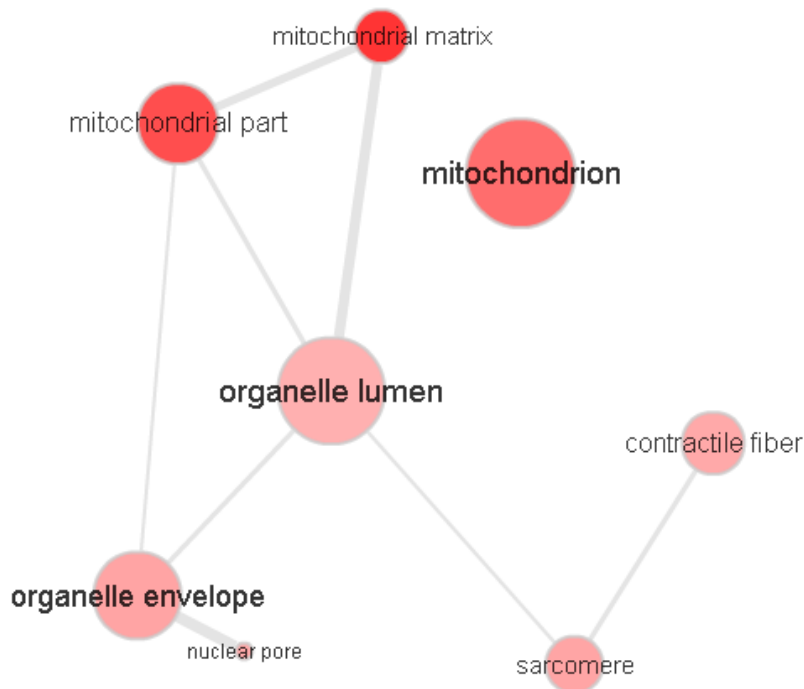
Figure 6.18. **Upregulated GO terms (in LD mice) associated with cellular components.**
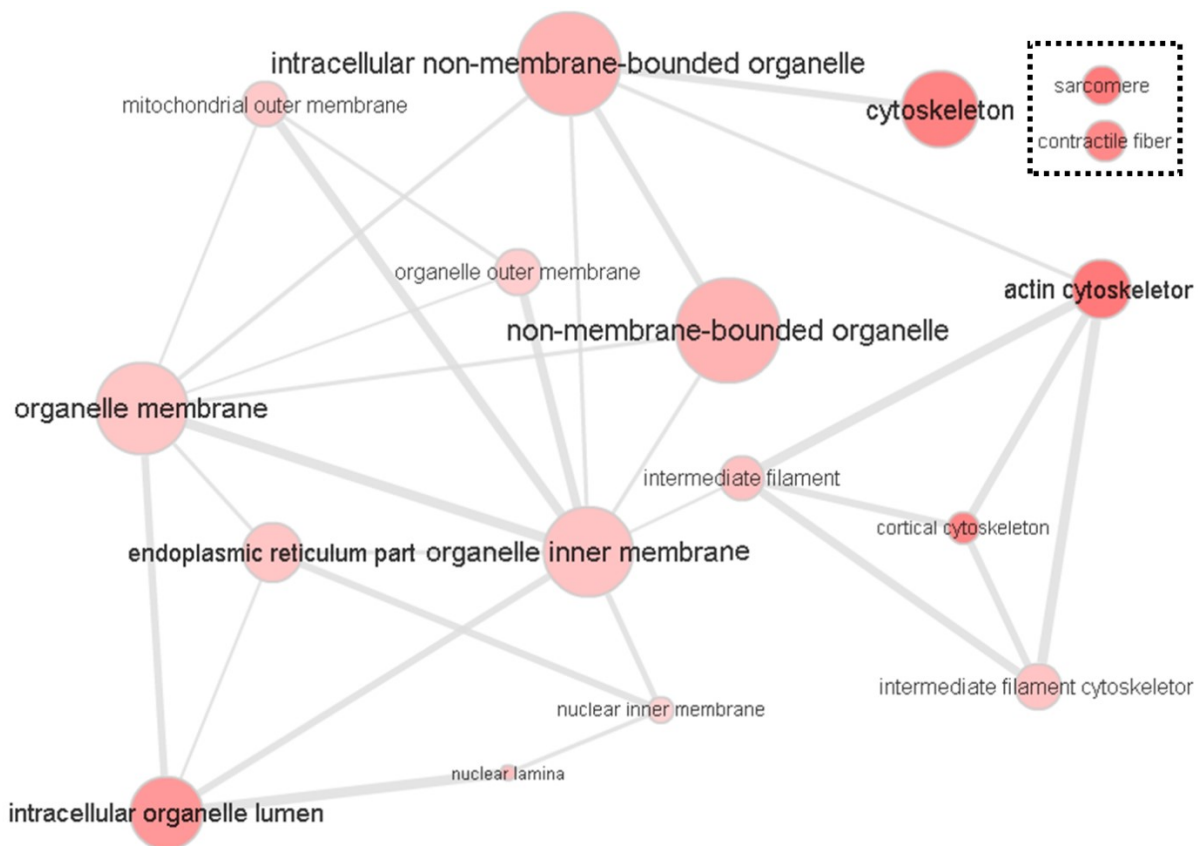
Figure 6.19. **Upregulated GO terms associated with cellular components (Hep2G cell line).**

There was also evidence suggesting that a DXR-detoxification response in the LD group was upregulated. However, instead of collapsing GO terms into 'response to gamma radiation' (as was seen in the HD group), LD GO terms clustered into groups 'cellular response to stress' which was connected to 'response to organic substance' (anthracyclines, of which DXR is one, are all organic compounds). GO terms associated with cholesterol synthesis were not significantly enriched, though there was an increase in lipid metabolism (e.g. upregulation of two-carbon metabolic pathways, which include enzymes that are involved in acetyl-coenzyme A metabolism). Yet, the cytochrome P450 family of enzymes is involved in various detoxification as well as biosynthetic pathways. Some of these enzymes are involved in both fatty acid and cholesterol biosynthesis. As an example, FAC grouped CYP51 with fatty acid biosynthesis (**Figure 6.20**), yet this enzyme has also been implicated in cholesterol biosynthesis as well as in modulating cellular sterol content (Fink et al., 2005). Nevertheless, the HD group exhibited more unique GO terms (**Figure 6.16**), suggesting that the lack of a lower expression of proteins involved in cholesterol metabolism might be a very legitimate difference between LD and HD groups.

Figure 6.20. 2-D viewer in DAVID of proteins (horizontal) and their functional relationship (vertical) involved in fatty acid and lipid metabolism (upregulated).

The tumour control (T) group exhibited a number of GO terms shared with other groups, including antioxidant enzymes (e.g. peroxiredoxin 4), stress proteins such as heat shock proteins (e.g. expression of Hspa1b) and pitrilysin metallepetidase (Pitrm1). A range of metabolic proteins were also upregulated in the T group (**Figure 6.21**). Also similar to the HD and LD groups, a number GO terms identified are mitochondrial components, thus again reflecting an alteration in the metabolic activity in T group (**Figure 6.22**). GO terms unique to the T group suggest that 'glycolytic processes' might have been uniquely upregulated in this group (**Figure 6.17**), though these results are only indirectly supported by the number of regulated GO terms associated with mitochondrial function (**Figure 6.22**). As an example, the observation that pyruvate dehydrogenase complex (PDC) was upregulated, in conjunction with

the possible alteration to mitochondrial function pathways, collectively supports the observation that proteins involved in glycolytic functions might have been upregulated. Similarly, the upregulation of glucokinase (**Figure 6.21**), an enzyme predominantly expressed by hepatocytes and β-cells (Matschinsky, 1990), implicates glucose homoeostasis as being a regulated pathway unique to the T group.
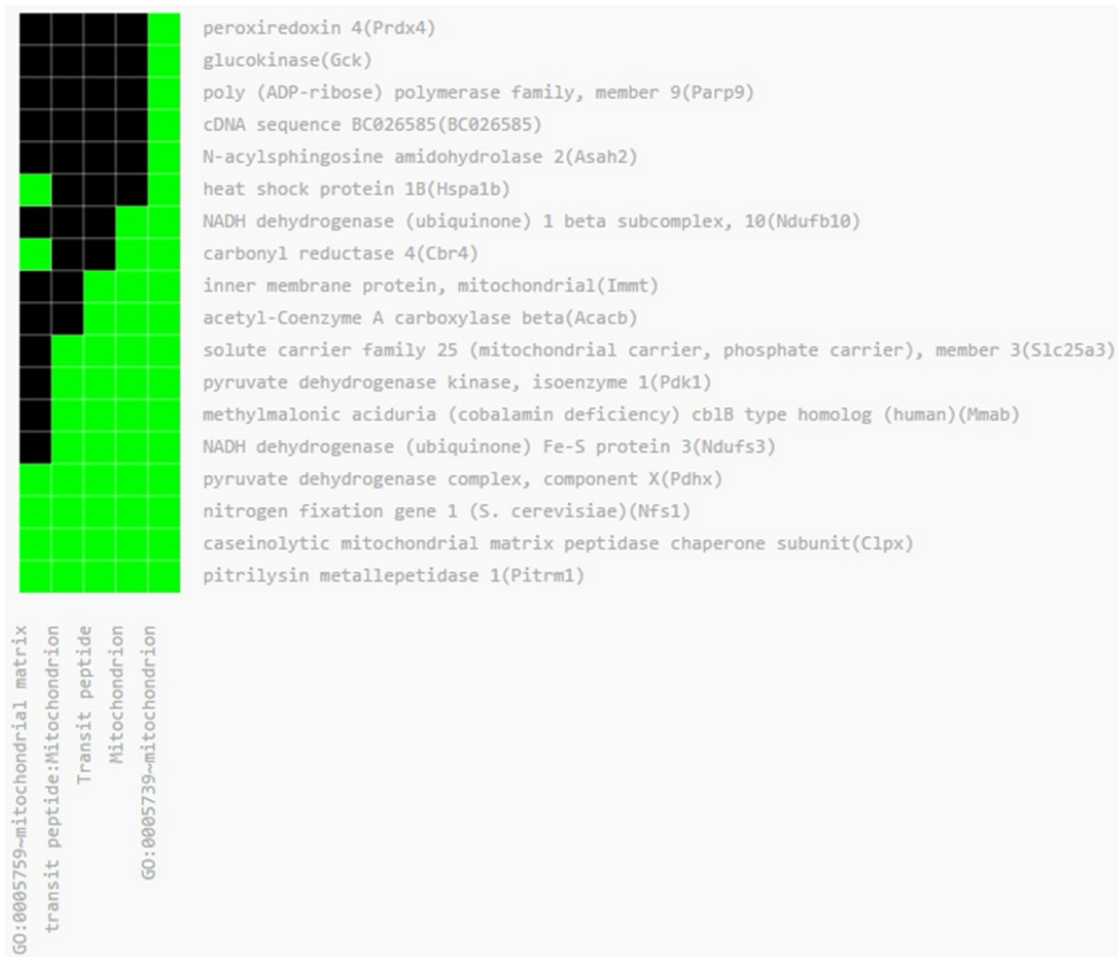
Figure 6.21. 2-D viewer in DAVID of proteins (horizontal) and their functional relationship (vertical) involved in mitochondrial function and structure (upregulated regulated).

Biological processes upregulated
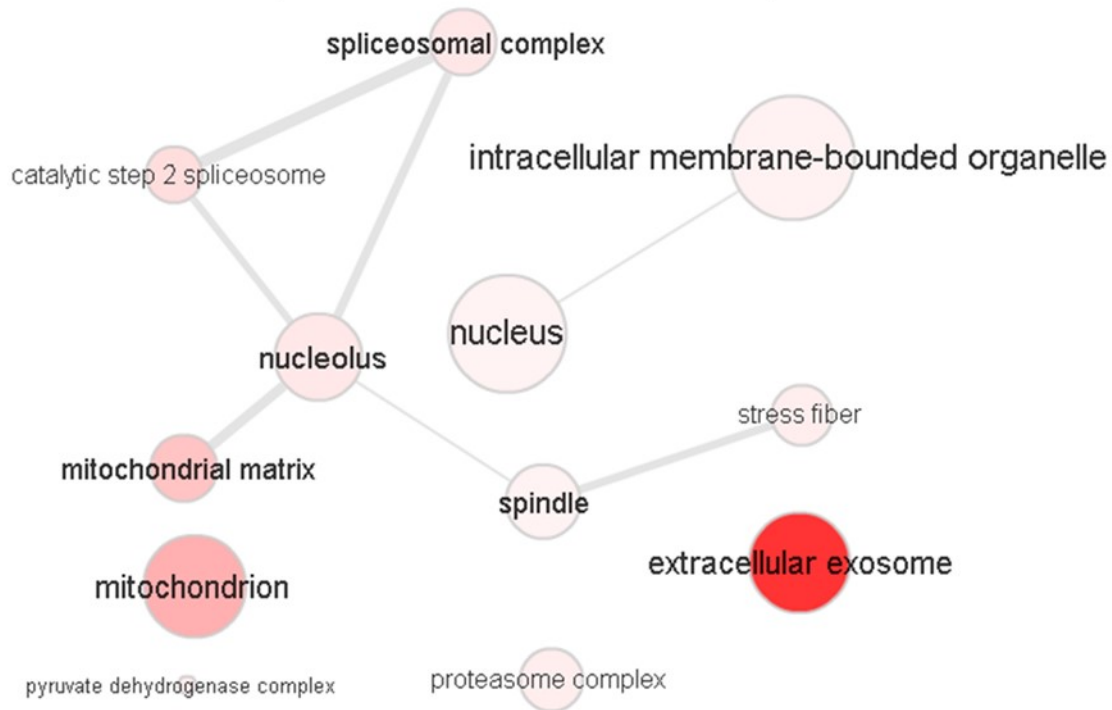
Figure 6.22. Upregulated GO terms associated with biological processes upregulated in the tumour control group.

An upregulation of proteins involved in glucose metabolism can have two effects. The end product of glycolysis is pyruvate, which can be converted to either lactate, or acetyl-coenzyme A. An upregulation of pyruvate dehydrogenase complex may thus play a key role in lactate clearance. In fact, mutations associated with proteins involved in the pyruvate dehydrogenase complex often results in fatal lactic acidosis (Brown et al., 1994; Ferriero et al., 2013). The liver plays an important role in the conversion of lactate back to glucose, a process referred to as the Cori cycle. The fact that two moles of ATP are generated from one mole of glycolysis, compared to the 6 moles of ATP required to recycle glucose, means this process operates at a net loss of 4 moles of ATP. It seems unlikely that hepatocytes would increase glycolysis, thus producing lactate, which is then subsequently recycled back to glucose (a futile cycle). Indeed, since many tumours exhibit high levels of glycolysis despite sufficient oxygen, the so called-Warburg effect (Vander Heiden et al., 2009), it is expected that livers of tumour-bearing mice would experience a higher metabolic burden as a result of the increased recycling of lactate.

Alternatively, acetyl-coenzyme A may enter the citric acid cycle or it can be used in various biosynthetic processes. In fact, many rapidly dividing cells, such as activated immune cells

(Palsson-McDermott and O'neill, 2013; Vander Heiden et al., 2009) or cancer cells (Hatzivassiliou et al., 2005), increase glycolysis (irrespective of oxygen levels) in order to direct metabolic intermediates (e.g. acetyl-coenzyme A) towards biosynthetic processes such as lipid synthesis. This suggests that glycolytic intermediates might be fluxed into biosynthetic pathways. Indeed, a flux of glucose intermediates into biosynthetic pathways is also supported by the upregulation of Acetyl-CoA carboxylase 2 (**Figure 6.21**), which catalyses the conversion of acetyl-CoA to malonyl-CoA, which is subsequently used in fatty acid synthesis (Hardie, 1989; Kim et al., 1989). Collectively, these arguments suggest that the upregulation of proteins implicated in glycolytic functions (**Figure 6.17**) might rather be linked to biosynthetic pathways or the clearance of lactate.

Also of interest was the unique upregulation of proteins involved in exosome formation. These vesicles often contain a variety of cellular cargo, including microRNA that regulates transcription. However, the significance of this finding is not clear, since it is the cargo of these vesicles that determines biological significance. However, it does pose the interesting possibility that such vesicles and their content might be used as markers for liver phenotypic changes (Sato et al., 2016).

6.9 The effect of DXR on the liver proteome of tumour-bearing mice

Most of the downregulated genes were common among all groups. Similarly, many processes that were upregulated between groups exhibited similar molecular functions. As an example, all groups exhibited some form of stress response (upregulation of heat shock proteins, and certain enzymes implicated in radical scavenging activities). However, at least some of the observed processes were unique to each group. The observation that downregulated proteins appear to be shared suggests that a decrease in gene expression is a more generic response to stress, whereas the upregulated genes are unique.

Also of interest was the absence of proteins involved in autophagy. Since DXR is likely to stress hepatocytes, e.g. by the induction of oxidative stress (Injac and Strukelj, 2008; Nayak et al., 2013), it would be expected that a generic stress response such as an upregulation of autophagy should be evident, yet this was not the case, a result also observed with immunoblotting (Chapter 5). One possibility is that autophagy was already elevated, and

subsequently 'repurposed' from a metabolic function, to a stress response. Mice have a high metabolic rate, and are very dependent on autophagy during fasting periods. In fact, mice lacking key autophagic proteins do not survive the postnatal feed-fasting cycles (Liu et al., 2013). Hence, it is possible that control mice exhibited high basal levels of autophagy. This might explain the lack of listed autophagic proteins: during DXR-challenge, the autophagic machinery might be 'repurposed' to deal with damaged organelles. Thus, autophagy might indeed play a key role in managing the consequence of DXR despite the absence of autophagy proteins. Alternatively, the liver, as a key regulator of energy homeostasis, might not increase autophagy as a defence mechanism. In the context of DXR-induced cardiotoxicity, a recent review (Dirks-Naylor, 2013) pointed out that many studies implicate an upregulation of autophagy in cardiac tissue as promoting the pathology. Thus, not increasing autophagy above basal levels might promote tolerance in hepatocytes.

All groups also expressed various proteins associated with contractile function. This might include activities such as vesicle transport, original structural changes, cell division, and the contractile function of hepatic stellate cells (possible in response to a decrease in blood volume). Similarly, in the T group, the observed upregulation of proteins involved in spindle formation might suggest an increase in cell proliferation, though proteins involved in cell growth, proliferation or cell cycle regulation were not identified.

All groups exhibited alterations in proteins involved in mitochondrial function and alteration in metabolic activities. A number of enzymes implicated in glycolysis may in fact play the key function of fluxing metabolic intermediates towards biosynthetic processes. As an example, liver proteomes of mice in the T group exhibited an increase in lipid synthesis. In mice receiving DXR, biosynthesis was possibly channelled more towards cholesterol synthesis, though anabolic processes such as an upregulation of proteins involved in the proteasomal pathway was observed. The relevance of an increased expression of cholesterol is not clear, since the position of the enzymes in this pathway was not close enough to an end product to identify the main role of synthesised cholesterol. Cholesterol is a key component of cell membranes, and consequently, all cells are capable of synthesising cholesterol. In the liver, cholesterol plays a role in the formation of bile. If DXR induced a loss of appetite, a decrease in the demand for bile would be expected. However, an increase in bile production during DXR treatment might be followed by an upregulating of cholesterol-synthesising enzymes in order

to meet the renewed increase in the demand for bile acids. High synthesis of cholesterol might also decrease DXR tolerance, since chronic hypercholesterolemia is associated with pathology beyond arteriosclerosis. As an example, higher cholesterol may impair membrane function, altering the flow of ions in cardiac myocytes (Wu et al., 1995). Clearly, the significance of cholesterol production during DXR treatment needs to be further investigated.

Proteomic results also highlight mechanisms that might have an impact on the interaction between host and intestinal biota. Not only is bile acids' amphiphilic molecule capable of disrupting microbial membranes (Begley et al., 2005), but the conjugation of amino acids to cholesterol can also have an impact on the composition of intestinal populations. The amino acids to which bile is bound influences the polarity of bile, with the result that dietary fat influences the species of bile acids secreted (i.e. the amino acid to which the cholesterol is conjugated). As an example, mice receiving milk-derived fat secrete bile acids conjugated to taurine (a sulfonic acid), which promotes the growth of certain anaerobic bacteria (Devkota et al., 2012). Mechanistically, these bacteria are adapted to metabolising bile, and in particular, liberating the sulphur from taurine and using it as a terminal electron acceptor (instead of oxygen). Therefore, altering not only the volume but also the composition of bile acids may be a strategy to select for, or against, certain strains of intestinal bacteria.

Some of the data hints at a possible role of intestinal biota in mediating host tolerance in the HD group. This is inferred from the downregulation of *Sept11*. Yet, Septin 11 has also been demonstrated to play a role in establishing cellular architecture. As an example, in rat neurons Septin 11 has been found to play a key role in regulating cytoskeletal structure at the synapses of at GABAergic neurons (Li et al., 2009). Similarly, a related protein, Septin 7, which was also upregulated, played a key role in mice during meiosis (Li et al., 2012) – another process implicated in cellular structure and motility. This would suggest that the upregulating of Septin 11 might not be directly linked to immune function, but possibly related to cellular architecture.

The upregulation of proteins involved in nucleotide synthesis in the HD group remains to be established. Since nucleotides such as cyclic GMP and ATP play various roles in intracellular signalling functions, whereas extracellular nucleotides have an important function in mediating inflammatory signalling (Riteau et al., 2010). It therefore appears as if an upregulation of nucleotides might have an impact on various signalling events. Nucleotides are also important in transcription and cell replication as they form building blocks of RNA/DNA. This suggests

that an upregulation in nucleotide synthesis might play a role in tissue repair. It is also possible that nucleotide precursors could be exported for biosynthetic application in peripheral tissue such as bone marrow or intestinal epithelium cells that undergo rapid cell division. In fact, certain cancers have a higher demand for phosphorus precisely because these cancers have more nucleotides (Elser et al., 2006). Collectively, these observations suggest the possibility that higher nucleotide synthesis might drive both tolerance (e.g. replenishing tissue damaged by DXR) and resistance (explaining the enhanced tumour growth in the HD group).

Finally, in comparing mouse liver proteome to the proteome of Hep2G human liver carcinoma cells, very similar trends were demonstrated in the protein expression in response to DXR (**Figure 6.23**). This includes an upregulation of proteins involved in lipid and cholesterol synthesis, mitochondrial alterations (particularly in context of apoptosis) and cytoskeletal or contractile proteins. A notable exception includes the higher activation of Ras-signalling activity in HepG2 cells, which possibly reflects the cancerous nature of these cells. The comparison also indicated that our data exhibited fewer enriched GO terms, as well as that metabolic pathways were generally identified by fewer representative proteins: for most metabolic pathways, only a handful of proteins were upregulated in our data set compared to that of HepG2 cells. In fact, this is illustrated by the well-connected nodes in the graph for HepG2 cells (**Figure 6.23**). Consequently, our data set provided few opportunities to identify a definitive metabolic processes activated in a given intervention group.
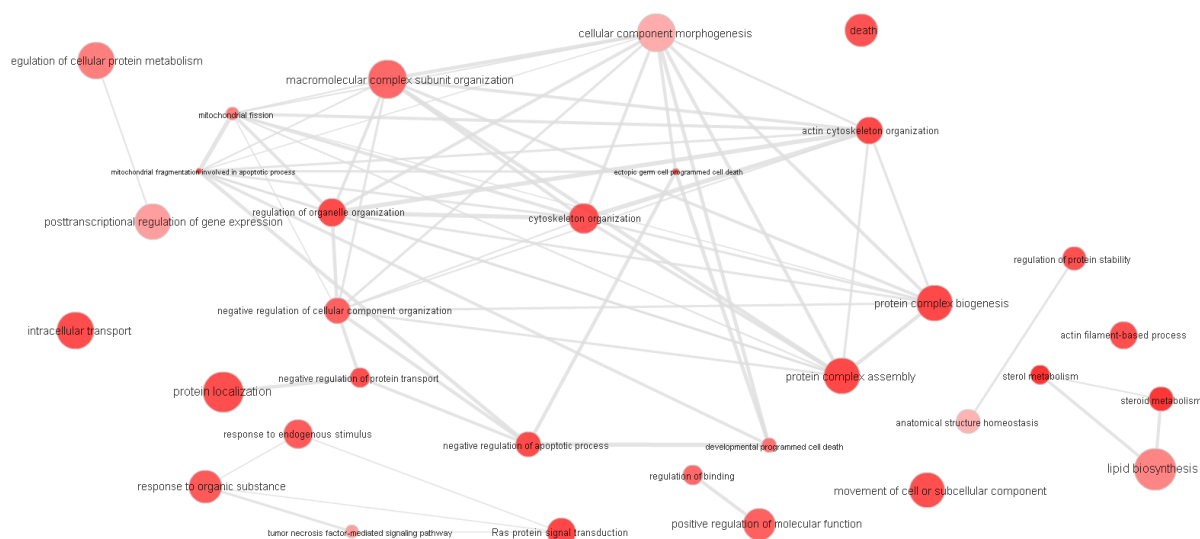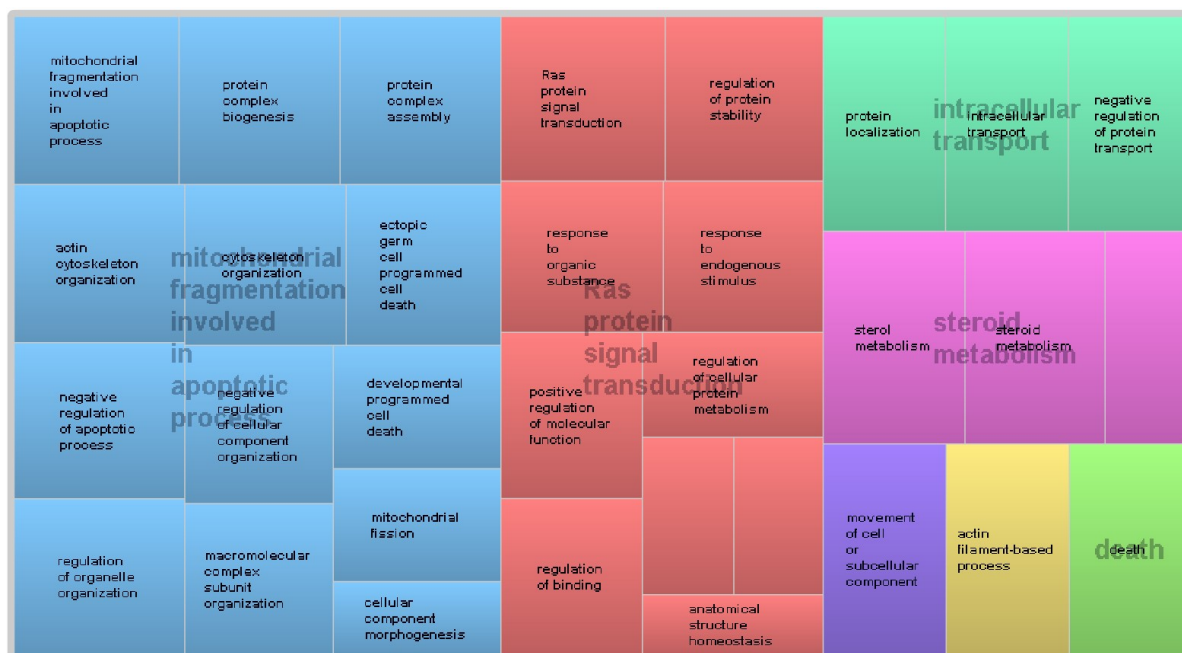
Figure 6.23. TreeMap (top) and graph (bottom) of biological processes upregulated in HepG2 cells in reaction to DXR.

The lower yield of informative GO terms, as well as the low connectivity between GO terms (i.e. fewer nodes connected to each other) in our samples compared to HepG2 cells is surprising in light of the fact that liver samples are derived from different cells (endothelium, hepatic stellate cells, Kupffer cells and hepatocytes), and are thus expected to be more complex (and give rise to more potential protein-protein interactions). A number of reasons may be put forward in this regard to explain the lower connectivity between GO terms, as well as the lower yield of significant GO terms. First, cell culture conditions are expected to be more stable,

giving rise to lower variance in data and thus rendering results more significant. Secondly, for the proteomic study on HepG2 cells, the authors (Hammer et al., 2010) considered a 1.2-fold protein increase/decrease as selection threshold, whereas the current study implemented a more conservative 2-fold increase. Consequently, the data set for HepG2 cells was expected to contain more proteins since the selection criteria were lower.

6.10   Comparison between EO771 and B16 mice

A comparison between GO terms unique to and shared by B16 (M: melanoma cells) and EO771 (T: EO771 breast cancer cells) revealed a number of GO upregulated terms unique to each group, whereas downregulated terms shared more GO terms (**Figure 6.24**). Comparisons between T and M groups were subsequently analysed in a manner similar to the groups following DXR treatment.
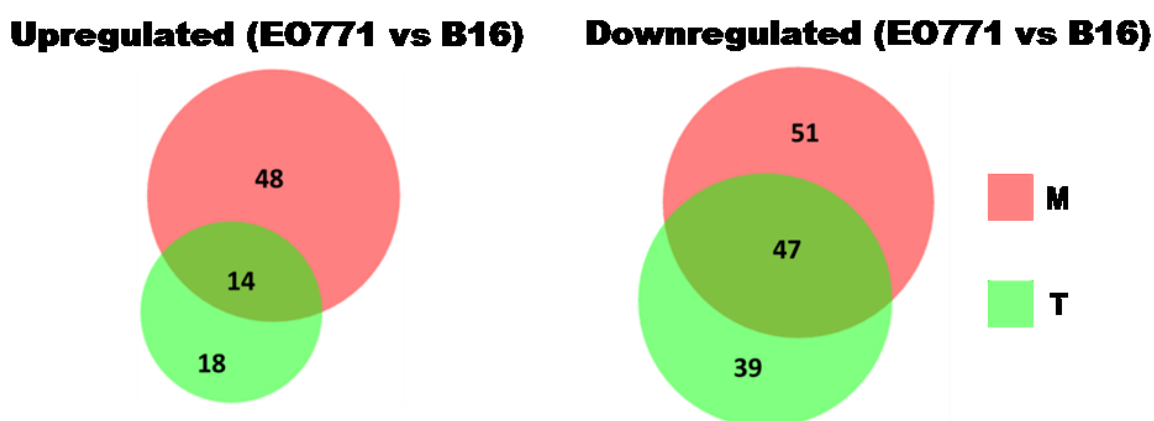
Figure 6.24. Differential enrichment of GO terms between groups. M: B16 melanoma; T: EO771 breast cancer cells. Diagram generated in BioVenn.

Of note is that a number of downregulated proteins are not completely understood. As an example, a number of proteins involved in the transfer of methyl groups were observed (**Figure 6.25**). These include histamine n-methyltransferase (Hnmt) which plays a role in histamine clearance in the brain, kidney and liver of mice (Kitanaka et al., 2002). Indolethylamine n-methyltransferase has been implicated in the metabolism of xenobiotics (which is unexpected since these mice did not receive DXR) as well as neuro-transmitters (Thompson et al., 1999), whereas AS3MT has been found to play a role in the metabolism of inorganic arsenic into methylated metabolites (Thomas et al., 2007). The downregulation of these proteins in mice bearing B16 tumours is not clear.

histamine N-methyltransferase(Hnmt)

indolethylamine N-methyltransferase(Inmt)

arsenic (+3 oxidation state) methyltransferase(As3mt)

Figure 6.25. **2-D viewer in DAVID of proteins (horizontal) and their functional relationship (vertical) involved in methyltransferase processes downregulated.**

However, a number of proteins involved in vitamin A (retinoic acid -RA) metabolism were upregulated (**Figure 6.26**). Hepatic stellate cells (HSC) represent a major storing site for RA, but are also involved in various other activates, ranging from the deposition of connective tissue to the expression of key immune regulators (Weiskirchen and Tacke, 2014). The altered metabolism of RA results from an increased activation of HSC, and the subsequent 'metabolic retooling' that takes place in these cells, or in response to external stimuli.

Alteration in retinoic acids (RA) metabolism is likely to have far-reaching effects since retinoid metabolites perform pleiotropic functions in cell-signalling roles. Some of the key transcriptional targets or RA-metabolites include the retinoic acid receptor (RAR), the retinoic x receptor (RXR) and peroxisome proliferator activated receptors (PPAR) (Al Tanoury et al., 2013). The diverse role of RA-metabolites is exemplified by the observation that retinoids can both inhibit and promote cell growth. As an example, the anti-proliferative effect of retinoids has been used in treating malignancies (Altucci and Gronemeyer, 2001; Di Masi et al., 2015);

yet, in contrast, retinoids have also been shown to promote cell proliferation in certain cancers (Perri et al., 2010).
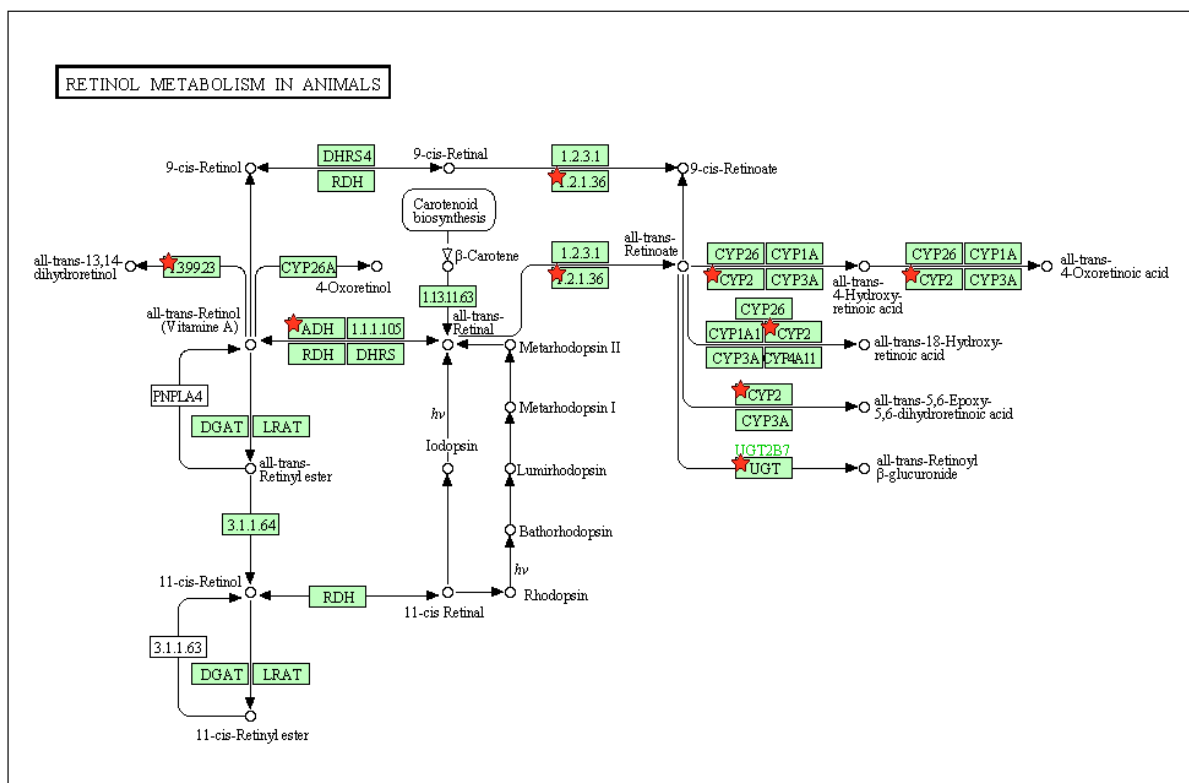
Figure 6.26. Proteins involved in retinoid metabolism. Upregulated proteins are indicated by red stars (★). Diagram from KEGG (diagram abridged). Numbers indicate proteins, according to the International Union of Biochemistry and Molecular Biology Enzyme Nomenclature.

In previous *in vitro* studies, it was shown that all-trans retinoic acids can suppress melanin production and cell proliferation in B16 cells (Niles, 2003; Sato et al., 2008). Thus, an upregulation in proteins involved in retinoic metabolism would suggest an inhibitory effect on B16 cancer cells. Yet, B16 tumours were the most rapidly growing tumours in the current study, casting doubt on any direct effect of elevated RA. Alternatively, RA might promote tumour growth indirectly via its role on glucose homeostasis. As an example, 9-cis-retinoic acid inhibits the secretion of insulin in response to glucose in mouse islet cells (Kane et al., 2010). Insulin itself is an anabolic hormone, suggesting that a decrease in this hormone might similarly impede cell growth. Also, though 9-cis-retinoic acid was indeed formed in the metabolic path of regulated enzymes, most metabolic pathways resulted in the formation of all-trans retinoic acids. It is thus not clear if altered glucose homeostasis resulted in the increase in B16 cell growth.

By another indirect mechanism, RA might exert a tumour-promoting effect by altering the immune system. As an example, RA induces apoptosis in antigen-presenting cells such as dendritic cells (Geissmann et al., 2003), suggesting that this might lower the immunogenic profile of cancer cells. Similarly, RA plays a role in regulatory T-cell development (Benson et al., 2007). An increase in regulatory T-cells might enhance the immune tolerance to cancerous cells, thus promoting tumour growth. However, it should be noted that RA plays a key role in the normal immune system (Pino-Lagos et al., 2008; Semba, 1994; Smith and Hayes, 1987) and that many of the immune-regulatory effects might be dose-dependent.

6.11   Conclusion

Many proteins were generically regulated between groups. These include ribosomal proteins, various peptidase and catabolic enzymes, and various proteins involved in cytoskeletal architecture and cell motility. Similarly, mitochondrial proteins were also among the GO terms most enriched. Furthermore, proteins that take part in various interactions with vitamins were also enriched. GO terms such as 'cofactor binding' or 'cofactor metabolism' often refer to proteins that bind to vitamins. As an example, thiamine (vitamin B1) metabolites are key cofactors of mitochondrial enzymes involved in energy homeostasis. However, many of these GO terms depicting interaction with vitamins (e.g. 'vitamin transport activity' – see e.g. **Figure 6.15**) also include reference to vitamin A metabolism. This distinction was not always obvious in REVIGO, but became more apparent after performing FCA in DAVID.

Since the liver performs various metabolic functions, it was challenging to identify a putative mechanism by which T/R could be influenced. This is exemplified by the increase in steroid metabolism observed in the HD group. Cholesterol moieties can be incorporated into the membrane of rapidly dividing cancer cells, decreasing host resistance. Cholesterol also has an important function in bile formation, with an increase in bile flow promoting the clearance of DXR (decreasing DXR might increase tolerance). Finally, the increase in bile flow might be an epiphenomenon of no consequence: an increase in feeding that occurs after prolonged suppression of appetite in response to DXR might necessitate an upregulation of proteins involved in bile formation. Similarly, an upregulation of nucleotide metabolism is also unclear. Nevertheless, the fact that steroid and nucleotide metabolism could affect various T/R circuits suggests that these systems might play a key role on the disease trajectory.

In summary, it was found that tumour burden repeatedly upregulates proteins involved in metabolic activities. It is likely that mice are able to cope well with the additional metabolic demands imposed by tumour load, as demonstrated by the higher tolerance in mice bearing EO771 tumours. In addition to the direct toxic effects of DXR, the fact that DXR also compromises mitochondrial function might render mice more vulnerable to tumour load. In particular, the effect of DXR on mitochondrial activity might limit the 'metabolic flexibility' of mice.

The higher metabolism of vitamin A is unexpected and difficult to explain. Retinoic acid usually exerts a cytostatic effect, and induce cell differentiation. This is in contrast to the hyper-growth observed in B16 tumours. The various RA-metabolites could have an impact on different tissue types, promoting tumour growth indirectly. However, the broad activity of RA-metabolites renders it difficult to identify a putative mechanism by which tumour growth would be enhanced. It is possible that B16 cells release factors that induce the transcription of enzymes involved in RA metabolism, and that the release of RA is in fact a manifestation of pathology (e.g. a cytostatic effect on liver cells might render mice less tolerant to tumour burden). However, in the absence of any supporting evidence, this remains pure conjecture.

6.12　Reference List

Al Tanoury, Z., Piskunov, A., and Rochette-Egly, C. (2013). Vitamin A and retinoid signaling: genomic and nongenomic effects. J. Lipid Res. *54,* 1761-1775.

Al-Shahrour, F., Diaz-Uriarte, R., and Dopazo, J. (2004). FatiGO: a web tool for finding significant associations of Gene Ontology terms with groups of genes. Bioinformatics *20,* 578-580.

Altucci, L., and Gronemeyer, H. (2001). The promise of retinoids to fight against cancer. Nature Reviews Cancer *1,* 181-193.

Amieva, M.R., and Furthmayr, H. (1995). Subcellular localization of moesin in dynamic filopodia, retraction fibers, and other structures involved in substrate exploration, attachment, and cell-cell contacts. Exp. Cell Res. *219,* 180-196.

Ashley, N., and Poulton, J. (2009). Anticancer DNA intercalators cause p53-dependent mitochondrial DNA nucleoid re-modelling. Oncogene *28,* 3880-3891.

Ballet, F., Vrignaud, P., Robert, J., Rey, C., and Poupon, R. (1987). Hepatic extraction, metabolism and biliary excretion of doxorubicin in the isolated prefused rat liver. Cancer Chemother. Pharmacol. *19,* 240-245.

Bally, M.B., Nayar, R., Masin, D., Cullis, P.R., and Mayer, L.D. (1990). Studies on the myelosuppressive activity of doxorubicin entrapped in liposomes. Cancer Chemother. Pharmacol. *27,* 13-19.

Bauer, E., Williams, B.A., Smidt, H., Verstegen, M.W., and Mosenthin, R. (2006). Influence of the gastrointestinal microbiota on development of the immune system in young animals. Curr. Issues Intestinal Microbiol. *7,* 35-52.

Begley, M., Gahan, C.G., and Hill, C. (2005). The interaction between bacteria and bile. FEMS Microbiol. Rev. *29,* 625-651.

Benson, M.J., Pino-Lagos, K., Rosemblatt, M., and Noelle, R.J. (2007). All-trans retinoic acid mediates enhanced T reg cell growth, differentiation, and gut homing in the face of high levels of co-stimulation. J. Exp. Med. *204,* 1765-1774.

Bhinge, K.N., Gupta, V., Hosain, S.B., Satyanarayanajois, S.D., Meyer, S.A., Blaylock, B., Zhang, Q., and Liu, Y. (2012). The opposite effects of doxorubicin on bone marrow stem cells versus breast cancer stem cells depend on glucosylceramide synthase. Int. J. Biochem. Cell Biol. *44,* 1770-1778.

Brown, G.K., Otero, L.J., LeGris, M., and Brown, R.M. (1994). Pyruvate dehydrogenase deficiency. J. Med. Genet. *31,* 875-879.

Burris, H.A.,3rd, and Hurtig, J. (2010). Radiation recall with anticancer agents. Oncologist *15,* 1227-1237.

Carbon, S., Ireland, A., Mungall, C.J., Shu, S., Marshall, B., Lewis, S., AmiGO Hub, and Web Presence Working Group. (2009). AmiGO: online access to ontology and annotation data. Bioinformatics *25,* 288-289.

Connor, K.M., Subbaram, S., Regan, K.J., Nelson, K.K., Mazurkiewicz, J.E., Bartholomew, P.J., Aplin, A.E., Tai, Y.T., Aguirre-Ghiso, J., Flores, S.C., and Melendez, J.A. (2005). Mitochondrial H2O2 regulates the angiogenic phenotype via PTEN oxidation. J. Biol. Chem. *280,* 16916-16924.

De Vos, K.J., Allan, V.J., Grierson, A.J., and Sheetz, M.P. (2005). Mitochondrial function and actin regulate dynamin-related protein 1-dependent mitochondrial fission. Curr. Biol. *15,* 678-683.

Dekaney, C.M., Gulati, A.S., Garrison, A.P., Helmrath, M.A., and Henning, S.J. (2009). Regeneration of intestinal stem/progenitor cells following doxorubicin treatment of mice. Am. J. Physiol. Gastrointest. Liver Physiol. *297,* G461-70.

Devkota, S., Wang, Y., Musch, M.W., Leone, V., Fehlner-Peach, H., Nadimpalli, A., Antonopoulos, D.A., Jabri, B., and Chang, E.B. (2012). Dietary-fat-induced taurocholic acid promotes pathobiont expansion and colitis in Il10-/-mice. Nature *487,* 104-108.

Di Masi, A., Leboffe, L., De Marinis, E., Pagano, F., Cicconi, L., Rochette-Egly, C., Lo-Coco, F., Ascenzi, P., and Nervi, C. (2015). Retinoic acid receptors: from molecular mechanisms to cancer therapy. Mol. Aspects Med. *41,* 1-115.

Dirks-Naylor, A.J. (2013). The role of autophagy in doxorubicin-induced cardiotoxicity. Life Sci. *93,* 913-916.

Du, Z., Zhou, X., Ling, Y., Zhang, Z., and Su, Z. (2010). agriGO: a GO analysis toolkit for the agricultural community. Nucleic Acids Res. *38,* W64-70.

Dutkowski, J., Kramer, M., Surma, M.A., Balakrishnan, R., Cherry, J.M., Krogan, N.J., and Ideker, T. (2013). A gene ontology inferred from molecular networks. Nat. Biotechnol. *31,* 38-45.

Eden, E., Navon, R., Steinfeld, I., Lipson, D., and Yakhini, Z. (2009). GOrilla: a tool for discovery and visualization of enriched GO terms in ranked gene lists. BMC Bioinformatics *10,* 1.

Elser, J., Kyle, M., Smith, M., and Nagy, J. (2006). Biological stoichiometry in human cancer. PloS One *2,* e1028-e1028.

Fajardo, A.M., Piazza, G.A., and Tinsley, H.N. (2014). The role of cyclic nucleotide signaling pathways in cancer: targets for prevention and treatment. Cancers *6,* 436-458.

Faust, P.L., and Kovacs, W.J. (2014). Cholesterol biosynthesis and ER stress in peroxisome deficiency. Biochimie *98,* 75-85.

Ferriero, R., Manco, G., Lamantea, E., Nusco, E., Ferrante, M.I., Sordino, P., Stacpoole, P.W., Lee, B., Zeviani, M., and Brunetti-Pierri, N. (2013). Phenylbutyrate therapy for pyruvate dehydrogenase complex deficiency and lactic acidosis. Sci. Transl. Med. *5,* 175ra31.

Fink, M., Ačimovič, J., Režen, T., Tanšek, N., and Rozman, D. (2005). Cholesterogenic lanosterol 14α-demethylase (CYP51) is an immediate early response gene. Endocrinology *146,* 5321-5331.

Geissmann, F., Revy, P., Brousse, N., Lepelletier, Y., Folli, C., Durandy, A., Chambon, P., and Dy, M. (2003). Retinoids regulate survival and antigen presentation by immature dendritic cells. J. Exp. Med. *198,* 623-634.

Hammer, E., Bien, S., Salazar, M.G., Steil, L., Scharf, C., Hildebrandt, P., Schroeder, H.W., Kroemer, H.K., Völker, U., and Ritter, C.A. (2010). Proteomic analysis of doxorubicin-induced changes in the proteome of HepG2cells combining 2-D DIGE and LC-MS/MS approaches. Proteomics *10,* 99-114.

Hardie, D.G. (1989). Regulation of fatty acid synthesis via phosphorylation of acetyl-CoA carboxylase. Prog. Lipid Res. *28,* 117-146.

Hatzivassiliou, G., Zhao, F., Bauer, D.E., Andreadis, C., Shaw, A.N., Dhanak, D., Hingorani, S.R., Tuveson, D.A., and Thompson, C.B. (2005). ATP citrate lyase inhibition can suppress tumor cell growth. Cancer Cell *8,* 311-321.

Hellerbrand, C. (2013). Hepatic stellate cells—the pericytes in the liver. Pflügers Archiv-European Journal of Physiology *465,* 775-778.

Huang, D.W., Sherman, B.T., and Lempicki, R.A. (2009). Systematic and integrative analysis of large gene lists using DAVID bioinformatics resources. Nat Protoc. *4,* 44-57.

Hui-Chou, H.G., Olenczak, J.B., Drachenberg, C.B., Shea, S.M., and Rodriguez, E.D. (2012). Short-term application of doxorubicin chemotherapy immunosuppressive side effects for composite tissue allotransplantation. Ann. Plast. Surg. *68,* 215-221.

Idzko, M., Ferrari, D., and Eltzschig, H.K. (2014). Nucleotide signalling during inflammation. Nature *509,* 310-317.

Injac, R., and Strukelj, B. (2008). Recent advances in protection against doxorubicin-induced toxicity. Technol. Cancer. Res. Treat. *7,* 497-516.

Jones, J.M., Morrell, J.C., and Gould, S.J. (2000). Identification and characterization of HAOX1, HAOX2, and HAOX3, three human peroxisomal 2-hydroxy acid oxidases. J. Biol. Chem. *275,* 12590-12597.

Kane, M.A., Folias, A.E., Pingitore, A., Perri, M., Obrochta, K.M., Krois, C.R., Cione, E., Ryu, J.Y., and Napoli, J.L. (2010). Identification of 9-cis-retinoic acid as a pancreas-specific autacoid that attenuates glucose-stimulated insulin secretion. Proc. Natl. Acad. Sci. U. S. A. *107,* 21884-21889.

Karin, M., Jobin, C., and Balkwill, F. (2014). Chemotherapy, immunity and microbiota--a new triumvirate? Nat. Med. *20,* 126-127.

Kato, L.M., Kawamoto, S., Maruya, M., and Fagarasan, S. (2014). The role of the adaptive immune system in regulation of gut microbiota. Immunol. Rev. *260,* 67-75.

Kaur, J., and Debnath, J. (2015). Autophagy at the crossroads of catabolism and anabolism. Nat. Rev. Mol. Cell Biol. *16,* 461-472.

Kim, K.H., Lopez-Casillas, F., Bai, D.H., Luo, X., and Pape, M.E. (1989). Role of reversible phosphorylation of acetyl-CoA carboxylase in long-chain fatty acid synthesis. Faseb J. *3,* 2250-2256.

Kitanaka, N., Kitanaka, J., Oue, T., Tada, Y., Tanaka, T., and Takemura, M. (2002). Genomic structure of the rat and mouse histamine N-methyltransferase gene. Jpn J Pharmacol. *88,* 85-92.

Lautt, W.W. Paper presented at Colloquium Series on Integrated Systems Physiology: from Molecule to Function.

Lee, Y.K., and Mazmanian, S.K. (2010). Has the microbiota played a critical role in the evolution of the adaptive immune system? Science *330,* 1768-1773.

Lei, X.G. (2002). In vivo antioxidant role of glutathione peroxidase: evidence from knockout mice. Meth. Enzymol. *347,* 213-225.

Li, S., Ou, X., Wei, L., Wang, Z., Zhang, Q., Ouyang, Y., Hou, Y., Schatten, H., and Sun, Q. (2012). Septin 7 is required for orderly meiosis in mouse oocytes. Cell Cycle *11,* 3211-3218.

Li, X., Serwanski, D.R., Miralles, C.P., Nagata, K., and De Blas, A.L. (2009). Septin 11 is present in GABAergic synapses and plays a functional role in the cytoarchitecture of neurons and GABAergic synaptic connectivity. J. Biol. Chem. *284,* 17253-17265.

Liu, Y., Shoji-Kawata, S., Sumpter, R.M.,Jr, Wei, Y., Ginet, V., Zhang, L., Posner, B., Tran, K.A., Green, D.R., Xavier, R.J*., et al.* (2013). Autosis is a Na+,K+-ATPase-regulated form of cell death triggered by autophagy-inducing peptides, starvation, and hypoxia-ischemia. Proc. Natl. Acad. Sci. U. S. A. *110,* 20364-20371.

Ma, C., Agrawal, G., and Subramani, S. (2011). Peroxisome assembly: matrix and membrane protein biogenesis. J. Cell Biol. *193,* 7-16.

Maere, S., Heymans, K., and Kuiper, M. (2005). BiNGO: a Cytoscape plugin to assess overrepresentation of gene ontology categories in biological networks. Bioinformatics *21,* 3448-3449.

Matschinsky, F.M. (1990). Glucokinase as glucose sensor and metabolic signal generator in pancreatic beta-cells and hepatocytes. Diabetes *39,* 647-652.

Maynard, C.L., Elson, C.O., Hatton, R.D., and Weaver, C.T. (2012). Reciprocal interactions of the intestinal microbiota and immune system. Nature *489,* 231-241.

Mostowy, S., Danckaert, A., Tham, T.N., Machu, C., Guadagnini, S., Pizarro-Cerda, J., and Cossart, P. (2009). Septin 11 restricts InlB-mediated invasion by Listeria. J. Biol. Chem. *284,* 11613-11621.

Nabeshima, A., Yamada, S., Guo, X., Tanimoto, A., Wang, K., Shimajiri, S., Kimura, S., Tasaki, T., Noguchi, H., and Kitada, S. (2013). Peroxiredoxin 4 protects against nonalcoholic steatohepatitis and type 2 diabetes in a nongenetic mouse model. Antioxid. Redox Signal. *19,* 1983-1998.

Narita, M., Young, A.R., Arakawa, S., Samarajiwa, S.A., Nakashima, T., Yoshida, S., Hong, S., Berry, L.S., Reichelt, S., Ferreira, M*., et al.* (2011). Spatial coupling of mTOR and autophagy augments secretory phenotypes. Science *332,* 966-970.

Nayak, P.G., Paul, P., Bansal, P., Kutty, N.G., and Pai, K.S.R. (2013). Sesamol prevents doxorubicin-induced oxidative damage and toxicity on H9c2 cardiomyoblasts. J. Pharm. Pharmacol. *65,* 1083-1093.

Nielsen, O., Vainer, B., and Rask-Madsen, J. (2001). The treatment of inflammatory bowel disease with 6-mercaptopurine or azathioprine. Aliment. Pharmacol. Ther. *15,* 1699-1708.

Niles, R.M. (2003). Vitamin A (retinoids) regulation of mouse melanoma growth and differentiation. J. Nutr. *133,* 282S-286S.

Ogata, I., Sáez, C.G., Greenwel, P., de Lourdes Ponce, M., Geerts, A., Leinwand, L.A., and Rojkind, M. (1993). Rat liver fat-storing cell lines express sarcomeric myosin heavy chain mRNA and protein. Cell Motil. Cytoskeleton *26,* 125-132.

Palsson-McDermott, E.M., and O'neill, L.A. (2013). The Warburg effect then and now: from cancer to inflammatory diseases. Bioessays *35,* 965-973.

Perri, M., Pingitore, A., Cione, E., Vilardi, E., Perrone, V., and Genchi, G. (2010). Proliferative and anti-proliferative effects of retinoic acid at doses similar to endogenous levels in Leydig MLTC-1/R2C/TM-3 cells. Biochim Biophys Acta. *9,* 993-1001.

Pino-Lagos, K., Benson, M.J., and Noelle, R.J. (2008). Retinoic acid in the immune system. Ann. N. Y. Acad. Sci. *1143,* 170-187.

Ray, P.D., Huang, B., and Tsuji, Y. (2012). Reactive oxygen species (ROS) homeostasis and redox regulation in cellular signaling. Cell. Signal. *24,* 981-990.

Riteau, N., Gasse, P., Fauconnier, L., Gombault, A., Couegnat, M., Fick, L., Kanellopoulos, J., Quesniaux, V.F., Marchand-Adam, S., and Crestani, B. (2010). Extracellular ATP is a danger signal activating P2X7 receptor in lung inflammation and fibrosis. Am. J. Respir. Crit. Care Med. *182,* 774-783.

Robinson, M.W., Harmon, C., and O'Farrelly, C. (2016). Liver immunology and its role in inflammation and homeostasis. Cell Mol. Immunol. *13*, 267-76

Sato, K., Morita, M., Ichikawa, C., TAKAHASHI, H., and Toriyama, M. (2008). Depigmenting mechanisms of all-trans retinoic acid and retinol on B16 melanoma cells. Biosci. Biotechnol. Biochem. *72,* 2589-2597.

Sato, K., Meng, F., Glaser, S., and Alpini, G. (2016). Exosomes in liver pathology. J. Hepatol. *1*, 213-221

Schieber, M., and Chandel, N.S. (2014). ROS function in redox signaling and oxidative stress. Curr. Biol. *24,* R453-R462.

Semba, R.D. (1994). Vitamin A, immunity, and infection. Clin. Infect. Dis. *19,* 489-499.

Šimůnek, T., Štěrba, M., Popelová, O., Adamcová, M., Hrdina, R., and Geršl, V. (2009). Anthracycline-induced cardiotoxicity: overview of studies examining the roles of oxidative stress and free cellular iron. Pharmacol. Rep. *61,* 154-171.

Smith, S.M., and Hayes, C.E. (1987). Contrasting impairments in IgM and IgG responses of vitamin A-deficient mice. Proc. Natl. Acad. Sci. U. S. A. *84,* 5878-5882.

Strausberg, R.L., Feingold, E.A., Grouse, L.H., Derge, J.G., Klausner, R.D., Collins, F.S., Wagner, L., Shenmen, C.M., Schuler, G.D., Altschul, S.F.*, et al.* (2002). Generation and initial analysis of more than 15,000 full-length human and mouse cDNA sequences. Proc. Natl. Acad. Sci. U. S. A. *99,* 16899-16903.

Sung, J., Shaffer, E., and Costerton, J. (1993). Antibacterial activity of bile salts against common biliary pathogens. Dig. Dis. Sci. *38,* 2104-2112.

Supek, F., Bošnjak, M., Škunca, N., and Šmuc, T. (2011). REVIGO summarizes and visualizes long lists of gene ontology terms. PloS One *6,* e21800.

Tewey, K.M., Rowe, T.C., Yang, L., Halligan, B.D., and Liu, L.F. (1984). Adriamycin-induced DNA damage mediated by mammalian DNA topoisomerase II. Science *226,* 466-468.

Thomas, D.J., Li, J., Waters, S.B., Xing, W., Adair, B.M., Drobna, Z., Devesa, V., and Styblo, M. (2007). Arsenic (3 Oxidation State) Methyltransferase and the Methylation of Arsenicals. Experimental Biology and Medicine (Maywood, NJ) *232,* 3.

Thompson, M.A., Moon, E., Kim, U., Xu, J., Siciliano, M.J., and Weinshilboum, R.M. (1999). Human indolethylamine N-methyltransferase: cDNA cloning and expression, gene cloning, and chromosomal localization. Genomics *61,* 285-297.

Twig, G., Elorza, A., Molina, A.J., Mohamed, H., Wikstrom, J.D., Walzer, G., Stiles, L., Haigh, S.E., Katz, S., Las, G.*, et al.* (2008). Fission and selective fusion govern mitochondrial segregation and elimination by autophagy. Embo J. *27,* 433-446.

Vander Heiden, M.G., Cantley, L.C., and Thompson, C.B. (2009). Understanding the Warburg effect: the metabolic requirements of cell proliferation. Science *324,* 1029-1033.

Wang, X., Phelan, S.A., Forsman-Semb, K., Taylor, E.F., Petros, C., Brown, A., Lerner, C.P., and Paigen, B. (2003). Mice with targeted mutation of peroxiredoxin 6 develop normally but are susceptible to oxidative stress. J. Biol. Chem. *278,* 25179-25190.

Wasinger, V.C., Zeng, M., and Yau, Y. (2013). Current status and advances in quantitative proteomic mass spectrometry. Int. J. Proteomics *2013,* 180605.

Weiskirchen, R., and Tacke, F. (2014). Cellular and molecular functions of hepatic stellate cells in inflammatory responses and liver immunology. Hepatobiliary Surg Nutr *3,* 344-363.

Wu, C., Su, M., Chi, J., Chen, W., Hsu, H., and Lee, Y. (1995). The effect of hypercholesterolemia on the sodium inward currents in cardiac myocyte. J. Mol. Cell. Cardiol. *27,* 1263-1269.

Wu, S., Zhou, F., Zhang, Z., and Xing, D. (2011). Mitochondrial oxidative stress causes mitochondrial fragmentation via differential modulation of mitochondrial fission–fusion proteins. FEBS J. *278,* 941-954.

Zeeberg, B.R., Feng, W., Wang, G., Wang, M.D., Fojo, A.T., Sunshine, M., Narasimhan, S., Kane, D.W., Reinhold, W.C., and Lababidi, S. (2003). GoMiner: a resource for biological interpretation of genomic and proteomic data. Genome Biol. *4,* 1.

Zeman, M.K., and Cimprich, K.A. (2014). Causes and consequences of replication stress. Nat. Cell Biol. *16,* 2-9.

Chapter 7

In this chapter, a brief overview of main findings and future recommendations are provided.

7.1   Introduction

The observation during the First Wold that mustard gas supresses bone marrow eventually led to the first rational cancer therapy for leukemia (Papac, 2001). Subsequent refinement later lead to the development of antimetabolites such as antifolates and fluorouracil which is still used today (Papac, 2001). Decades of basic research resulted in a deeper understanding of basic cancer biology, culminating in the so called era of 'targeted therapy' which targets key biological functions of cancer cells, such as hormone receptors. This approach is exemplified by Trastuzumab (also known as Herceptin), a monoclonal antibody that block human epidermal growth factor receptor 2 (HER2), a tyrosine kinase receptor which is often upregulated in cancer cells (Nahta et al., 2006). However, both targeted therapy, as well as antimetabolites, despite the initial responsiveness, inevitably result in the development of drug resistance in cancer (Holohan et al., 2013).

Interestingly, what have been hailed as "arguably the most exciting advance made in cancer treatment in recent years" (Ribas, 2015), represents a completely different therapeutic approach. These novel therapeutic interventions do not target cancer cells, but rather host cells by targeting and inactivating so called 'immune checkpoint blockers' that are usually activated by cancer cells in order to avoid immune surveillance (Larkin et al., 2015). Though it is to be seen how effective these therapies will prove to be, initial results are promising. If as effective as initial findings suggest (Larkin et al., 2015), this therapy will represent a completely novel approach to cancer: targeting the host instead of cancer.

Similar, the tolerance/resistance (T/R) framework represents an approach that emphasise the role of the host in the developing disease trajectory. The ultimate clinical utility may initially find more application in palliative context or situations where a cure is no longer a realistic clinical goal. However, as support for cancer patients increase, it might become more realistic

to pursue a clinical outcome where people die *with* cancer, and not because of neoplastic infections.

7.2   Main findings

The implementation of the T/R framework within an immunological setting remains an emerging field, and there is continual interest in developing novel tools for quantifying the disease state (Louie et al., 2016). The approach implemented in this study (Chapter 3) was effective in quantifying tolerance and resistance. An interesting observation however was the differences in variance between groups when measuring tolerance: groups receiving DXR exhibited less variance (i.e. clustered closer to the fitted regression line) than the tumour control group. The underlying biological reason for this observation is not clear. This observation also suggests that, whereas traditional hypothesis testing (i.e. comparing means) are undoubtedly insightful, studying the biological origin of differences in variation might also highlight novel aspects that are not usually obtained.

The observation that DXR increased tumour growth (Chapter 3) was unexpected, but also documented by others (Bandyopadhyay et al., 2010). Attempts to explain the origin of this increase (Chapter 4) was however less successful: the only significant result includes the elevated phosphorylation of ERK in groups receiving DXR. Although ERK induce cell growth and proliferation, it is not clear why ERK was activated in mice receiving DXR.

Results from both immunoblotting and liver proteomic analyses were occasionally counter intuitive and difficult to interpret with no definite mechanism identified as a driver for tolerance or resistance. In particular, the absence of autophagic proteins were unexpected. However, the study also highlight novel insight. As an example, the observation that proteins involved in radical scavenging were both up- and down-regulated in mice liver in response to DXR might suggest that DXR toxicity could be mitigated more effectively by using antioxidants that are more selective in the species of radicals they target (thereby possibly sparing adaptive radical signalling). This would explain why 'generic' antioxidant therapies have failed to attenuate DXR-associated cardiopathologies (Štěrba et al., 2013). Gene ontology analyses also suggest that proteins involved in the host-symbiote (i.e. intestinal biota) could be altered in DXR groups. The significance of this finding is not clear. It is possible that DXR adversely affects the host immune system, which may impact on intestinal biota, permitting the expansion of

bacterial strains which are usually constrained by the host's immune system. Alternatively, the results may be an epi-phenomena: if DXR damage the intestinal lining, more bacteria (and bacterial particles such as LPS) might enter circulation. Exposing the liver to bacteria and their components might explain the haptic response. What is evident is that a change in host intestinal biota could greatly impact on host health. Intestinal biota contain far more non-overlaying genes (also referred to as the 'metagenome') that that of the human genome (Cho and Blaser, 2012). Therefore, altering host-microbe interaction is likely to alter microbial population, and with it, the biochemical potentiality contained within the host metagenome.

There is also evidence that cell contractile functioning is altered in liver cells in response to DXR. In line with other observations, this might include an increase in intracellular vesicle trafficking, cell mobility, as well as contraction. With regards to the contraction function, the observation might relate to altered hemodynamics since the liver contains a large fraction of the total blood supply. The observation of altered cholesterol synthesis is also surprising, yet, it was not possible to identify the reason why an increase in cholesterol synthesis would take place in response to DXR. Finally, the observation that B16 tumours increase the expression of a number of enzymes associated with retinoic acids (RA) metabolism is also of interest given the fact that this could alter both tolerance and resistance. As an example, the anti-mitotic effect of certain RA-metabolites (Altucci and Gronemeyer, 2001; Di Masi et al., 2015) could explain the lower tolerance in mice bearing B16 tumours. Similar, RA has been demonstrated to enhance the growth of some cancer cells (Perri et al., 2010), thus potentially explaining increased tumour growth.

7.3   Limitations and future prospects

More metrics of health should have been used to quantify tolerance, particularly markers unique for a given organ as this might have assisted in the identification of putative tolerance mechanisms. As an example, we speculated that the increase in contractile proteins observed in the liver proteome might be a result of decreased blood volume: large tumours are richly vascularised, though the tumour vascular bed itself is chaotic and poorly developed, resulting in hemorrhagic tumours. In this scenario, increased constriction of the liver might redirect blood flow in response to hypovolemia resulting from blood that accumulates in the tumour region. However, it is also possible that DXR-induced cardiotoxicity resulted in poor cardiac

performance, with lower circulatory velocity or some associated decrease in blood flow. According to this narrative, hepatic constriction might be a downstream consequence of cardiac-associated pathology.

It is also advisable to make use of adult mice that are not growing as this simplify interpretation of a tolerance metric that makes use of body weight. Tolerance could still be measured in growing individuals, manifesting as a 'failure to thrive'. However, since resistance differ greatly between EO771 and B16 groups (B16 growing faster than EO771 tumours), the increase in body weight (a metric for tolerance) in EO771 might reflect the longer time the mice spend growing (and subsequently higher body mass). Also, there is evidence that a host often exhibits different tolerance to a pathogen, depending on life history (e.g. age) of the host (Sears et al., 2015). As an example, small pox is usually well tolerated if contracted during childhood, but often lead to complications in adults. Similarly, the tolerance exhibited by an adult versus juvenile mice could markedly differ.

Also, the use of different inoculation media, e.g. Matrigel® or Hanks' Balanced Salt solution would undoubtedly also impact on tumour growth. One advantage of using Matrigel® includes the standardisation of tumour inoculation: many tumours do not grow in mice unless inoculated with Matrigel®.

Also, the inability to capture serum markers represent another key limitation of this study. The attempt made to capture data regarding a panel of cytokines and growth factors using a Luminex Bead-based Multiplex Assay was unsuccessful due to results falling below the detectable range. The results could have shed more light on both tolerance and resistance. As an example, the observation that DXR increased tumour growth might have resulted from DXR-tissue injury, stimulating the release of growth factors in order to expand the cell population during tissue regeneration. These cytokines or growth factors released could have accelerated tumour growth (explaining lower resistance in mice receiving DXR). Similarly, inflammatory markers as well as protein markers for liver damage (e.g. alanine amino transferase or alkaline phosphatase) could have provided additional information on liver-specific tolerance.

Arguably the biggest shortfall in the current study relates to the timing of tissue harvesting and the subsequent pooling of liver samples. Mice were administered DXR once tumours became

palpable, and subsequently sacrificed when tumours reached a size of approximately 400 mm^3. However, tumour growth rates varied greatly between mice, even within a group. Consequently, for mice with rapidly growing tumours, liver tissue was harvested near the time the last round of DXR were administered. In contrast, in mice with more slowly growing tumours, liver samples were harvested at a time point more distant to when the last round of DXR was received. Consequently, it is very likely that some livers were in a state of tissue regeneration, whereas livers of mice harvested more recently might have exhibited a stress response to the DXR recently administered. This factor most likely 'diluted' certain proteins, since different liver samples would have been enriched for different proteins. This might, as an example, explain why it was not possible to identify the relevance of an increase in cholesterol synthesis: mice might have all synthesised cholesterol, but for different purposes (e.g. local synthesis of cholic acid for bile formation versus cholesterol synthesised for the incorporation into cell membranes or hormone synthesis in distal tissue).

7.4 To conclude

Tolerance & resistance framework

● Immunologist distinguishes between the host's ability to resist infectious agents, versus capacity to accommodate stress imposed by the infection tolerance.

● Consequently, disease trajectory is dependent not only on pathogen load, but also the 'noxious phenotype' of the infectious agent.

● This demarcation implicit to the tolerance/resistance (T/R) framework is also applicable within an oncological context.

Quantifying cancer tolerance & resistance

● Cancer tolerance represents the 'unit health cost per unit tumour volume'

● Cancer tolerance can be expressed as the slope of a regression line, with cancer burden as predictor variable and a metric of health as the response variable.

● Cancer resistance can similarly be expressed as the slope of tumour growth during a log-linear growth (LLG) phase.

Implications of the T/R framework

● Treatment efficacy is emphasized by this approach: The ratio between the tolerance slope and LLG-slope (resistance slope) provides an expression of the harm-to-benefit ratio of a treatment intervention (i.e., reduction in tumour growth vs cost in terms of health).

● This approach allows a finer resolution on the disease state and can distinguish between pathology manifesting from tumour growth versus intolerance toward tumour.

● Although T/R is 'host centric', the framework can be extended to include cancer versus host factors that interact in dictating disease trajectory (e.g., distinguish between host tolerance vs cancer pathogenic phenotype).

7.5   Reference List

Altucci, L., and Gronemeyer, H. (2001). The promise of retinoids to fight against cancer. Nat. Rev. Cancer *1,* 181-193.

Bandyopadhyay, A., Wang, L., Agyin, J., Tang, Y., Lin, S., Yeh, I., De, K., and Sun, L. (2010). Doxorubicin in combination with a small TGFbeta inhibitor: a potential novel therapy for metastatic breast cancer in mouse models. PloS One *5,* e10365.

Cho, I., and Blaser, M.J. (2012). The human microbiome: at the interface of health and disease. Nat. Rev. Genet. *13,* 260-270.

Di Masi, A., Leboffe, L., De Marinis, E., Pagano, F., Cicconi, L., Rochette-Egly, C., Lo-Coco, F., Ascenzi, P., and Nervi, C. (2015). Retinoic acid receptors: from molecular mechanisms to cancer therapy. Mol. Aspects Med. *41,* 1-115.

Holohan, C., Van Schaeybroeck, S., Longley, D.B., and Johnston, P.G. (2013). Cancer drug resistance: an evolving paradigm. Nat. Rev. Cancer *13,* 714-726.

Larkin, J., Chiarion-Sileni, V., Gonzalez, R., Grob, J.J., Cowey, C.L., Lao, C.D., Schadendorf, D., Dummer, R., Smylie, M., and Rutkowski, P. (2015). Combined nivolumab and ipilimumab or monotherapy in untreated melanoma. N. Engl. J. Med. *373,* 23-34.

Louie, A., Song, K.H., Hotson, A., Tate, A.T., and Schneider, D.S. (2016). How Many Parameters Does It Take to Describe Disease Tolerance? PLoS Biol *14,* e1002435.

Nahta, R., Yu, D., Hung, M., Hortobagyi, G.N., and Esteva, F.J. (2006). Mechanisms of disease: understanding resistance to HER2-targeted therapy in human breast cancer. Nat. Clin. Pract. Oncol. *3,* 269-280.

Papac, R.J. (2001). Origins of cancer therapy. Yale J. Biol. Med. *74,* 391-398.

Perri, M., Pingitore, A., Cione, E., Vilardi, E., Perrone, V., and Genchi, G. (2010). Proliferative and anti-proliferative effects of retinoic acid at doses similar to endogenous levels in Leydig MLTC-1/R2C/TM-3 cells. Biochim Biophys Acta. *9,* 993-1001.

Ribas, A. (2015). Releasing the brakes on cancer immunotherapy. N. Engl. J. Med. *373,* 1490-1492.

Sears, B.F., Snyder, P.W., and Rohr, J.R. (2015). Host life history and host–parasite syntopy predict behavioural resistance and tolerance of parasites. J. Anim. Ecol. *84,* 625-636.

Štěrba, M., Popelová, O., Vávrová, A., Jirkovský, E., Kovaříková, P., Geršl, V., and Šimůnek, T. (2013). Oxidative stress, redox signaling, and metal chelation in anthracycline cardiotoxicity and pharmacological cardioprotection. Antioxid. Redox Signal. *18,* 899-929.

Appendix I

Haematoxylin and eosin progressive staining

8.1 Reagents

- Ethanol: 100%, 95%, 70%
- Xylene
- Acetic alcohol (10 ml 1% HCl in 1ℓ 70 % ethanol)
- Eosin (Stock: 10 g Eosin dissolved into 1ℓ dH2O)

Working solution: Prepare fresh: 10 ml Eosin stock in 90 ml dH2O. Filter solution. Add 2~3 drops glacial acetic acid in to 100 ml work-solution

- Mayer's Haematoxylin: Add the following reagents to 1ℓ dH2O
  o aluminium potassium 50g
  o dissolve in dH2O
  o 5 g Haematoxylin powder dissolve in dH2O
  o 0.4g sodium iodate
  o 20ml glacial acetic acid

Heat solution up to boiling point. Remove from heat and rapidly cool down in fridge ¾ Add 4 ml glacial acetic acid to 100 ml Haematoxylin solution before staining. Filter before use

- Scott's tap water
  o Dissolve 3.5 g NaHCO3 in tap water
  o Add 20 mg MgSO4 129
  o Add 10 ml 37% formalin

8.2 Methods

Prepare 21 Coplin jars in series flied 2/3 with the above mentioned reagents, according to following schedule for each sample incubation step:

175

1) Xylene (10 min)

2) 100% ethanol (10 dips)

3) 100% ethanol (10 dips)

4) 95% ethanol (10 dips)

5) 95% ethanol (10 dips)

6) 70% ethanol (10 dips)

7) dH2O (10 dips)

8) Haematoxylin (10 min)

9) dH2O (10 dips)

10) Acetic alcohol (10 dips)

11) dH2O (10 dips)

12) Scott's tap water (10 dips)

13) dH2O (10 dips)

14) Eosin (2 min)

15) dH2O (10 dips)

16) 70% ethanol (10 dips)

17) 95% ethanol (10 dips)

18) 95% ethanol (10 dips)

19) 100% ethanol (10 dips)

20) 100% ethanol (10 dips)

21) Xylene (10 dips)

Gently tap of execs xylene and mount sample with mounting media and coverslip.

8.3 Automatic tissue processing

- Reagents
  - o Paraffin wax (Histosec, Merk)
  - o Xylene (Sigma-Aldric) ~2ℓ
  - o Ethanol: 100%, 95%, 90% 70% (2.5, 1.5, 0.8 and1.5 ℓ respectively)
- Method

Tissue sample previously soaked in formaldehyde was (a) dehydrated, (b) "cleared" and (c) impregnation with paraffin. After preparing reagents, pour ~700 ml of each reagent into glass flask on tissue processor in the order (as indicated below). Tissue processor should be pre-programmed according to following time-schedule per sample incubation step:

(A) Dehydration

(1)	70%	ethanol	90 min
(2)	70%	ethanol	90 min
(3)	90%	ethanol	90 min
(4)	95%	ethanol	90 min
(5)	95%	ethanol	90 min
(6)	100%	ethanol	90 min
(7)	100%	ethanol	90 min
(8)	100%	ethanol	120 min

(B) Clearing

(9)	Xylene	90 min
(10)	Xylene	120 min

(C) Impregnation

(11)	paraffin wax	120 min
(12)	paraffin wax	120 min

=20 hours

Appendix II

List of differentially regulated proteins: liver proteomics

Key to groups:

H: high dose DXR group

L: low dose DXR group

T: tumour control (EO771 cancer cell line)

M: melanoma (B16 cancer cell line)

Group	Accession number	Description	Confidence score	Anova (p)	Fold change	
H	>sp|A2AS89|SPEB	Agmatinase, mitochondrial	60,52	8,590E-04	-4,0	☐
H	>sp|B1AR13|CISD3	CDGSH iron-sulfur domain-containing protein 3, mitochondrial	8,01	4,696E-04	-4,4	☐
H	>sp|G3X982|AOXC	Aldehyde oxidase 3	120,25	7,543E-03	-2,1	☐
H	>sp|O08749|DLDH	Dihydrolipoyl dehydrogenase, mitochondrial	137,90	2,428E-03	-2,2	☐
H	>sp|O08807|PRDX4	Peroxiredoxin-4	47,98	3,480E-03	3,3	☐
H	>sp|O09061|PSB1	Proteasome subunit beta type-1	34,47	7,949E-04	-6,1	☐
H	>sp|O35286|DHX15	Pre-mRNA-splicing factor ATP-dependent RNA helicase DHX15	13,23	4,279E-03	-2,3	☐
H	>sp|O55234|PSB5	Proteasome subunit beta type-5	16,24	5,481E-04	-4,2	☐
H	>sp|O70435|PSA3	Proteasome subunit alpha type-3	8,53	1,531E-03	-9,2	☐
H	>sp|O88451|RDH7	Retinol dehydrogenase 7	130,14	2,167E-05	-3,3	☐
H	>sp|O89017|LGMN	Legumain	36,28	2,645E-02	2,2	☐
H	>sp|P06330|HVM51	Ig heavy chain V region AC38 205.12	13,64	1,235E-03	5,7	☐
H	>sp|P10518|HEM2	Delta-aminolevulinic acid dehydratase	142,33	3,203E-03	-2,5	☐
H	>sp|P11352|GPX1	Glutathione peroxidase 1	154,94	8,793E-04	-3,5	☐
H	>sp|P14246|GTR2	Solute carrier family 2, facilitated glucose transporter member 2	6,57	2,175E-02	-2,1	☐
H	>sp|P16546|SPTN1	Spectrin alpha chain, non-erythrocytic 1	42,85	1,688E-05	5,7	☐
H	>sp|P17879|HS71B	Heat shock 70 kDa protein 1B	113,76	1,402E-04	3,0	☐
H	>sp|P18572|BASI	Basigin	30,31	5,610E-05	-2,3	☐
H	>sp|P20065|TYB4	Thymosin beta-4	39,98	2,860E-02	4,3	☐
H	>sp|P21300|ALD1	Aldose reductase-related protein 1	8,12	2,271E-03	-5,1	☐
H	>sp|P21614|VTDB	Vitamin D-binding protein	148,26	4,746E-04	-2,5	☐
H	>sp|P24456|CP2DA	Cytochrome P450 2D10	194,38	4,877E-04	-2,1	☐
H	>sp|P26041|MOES	Moesin	71,14	5,566E-04	2,0	☐

H	>sp|P27046|MA2A1	Alpha-mannosidase 2	14,55	1,903E-05	-2,4	☐
H	>sp|P28063|PSB8	Proteasome subunit beta type-8	16,08	1,910E-02	-2,2	☐
H	>sp|P28651|CAH8	Carbonic anhydrase-related protein	35,72	3,485E-05	4,8	☐
H	>sp|P28798|GRN	Granulins	16,30	3,485E-05	-29,9	☐
H	>sp|P34884|MIF	Macrophage migration inhibitory factor	74,65	1,105E-02	-2,2	☐
H	>sp|P34927|ASGR1	Asialoglycoprotein receptor 1	32,22	9,440E-04	-2,1	☐
H	>sp|P35492|HUTH	Histidine ammonia-lyase	376,41	1,676E-04	-2,6	☐
H	>sp|P35505|FAAA	Fumarylacetoacetase	449,36	2,350E-03	-5,2	☐
H	>sp|P42925|PXMP2	Peroxisomal membrane protein 2	6,68	2,080E-02	-2,3	☐
H	>sp|P50295|ARY2	Arylamine N-acetyltransferase 2	23,34	1,941E-04	2,1	☐
H	>sp|P52760|UK114	Ribonuclease UK114	168,04	2,244E-02	-2,2	☐
H	>sp|P52792|HXK4	Glucokinase	19,75	1,853E-03	2,1	☐
H	>sp|P52843|ST2A1	Bile salt sulfotransferase 1	22,62	8,574E-04	-7,3	☐
H	>sp|P53996|CNBP	Cellular nucleic acid-binding protein	12,28	5,797E-03	-2,3	☐
H	>sp|P55302|AMRP	Alpha-2-macroglobulin receptor-associated protein	14,28	5,040E-03	2,3	☐
H	>sp|P56391|CX6B1	Cytochrome c oxidase subunit 6B1	14,61	9,768E-03	-2,6	☐
H	>sp|P59325|IF5	Eukaryotic translation initiation factor 5	17,03	1,622E-03	-2,6	☐
H	>sp|P60229|EIF3E	Eukaryotic translation initiation factor 3 subunit E	24,24	7,426E-04	12,0	☐
H	>sp|P61514|RL37A	60S ribosomal protein L37a	13,94	5,379E-04	5,2	☐
H	>sp|P62204|CALM	Calmodulin	15,87	7,850E-03	2,3	☐
H	>sp|P62827|RAN	GTP-binding nuclear protein Ran	24,89	7,816E-06	-4,6	☐
H	>sp|P62862|RS30	40S ribosomal protein S30	8,12	6,148E-04	-3,7	☐
H	>sp|P63073|IF4E	Eukaryotic translation initiation factor 4E	13,97	4,136E-03	4,2	☐
H	>sp|P63085|MK01	Mitogen-activated protein kinase 1	13,73	3,247E-03	-2,4	☐
H	>sp|P70398|USP9X	Probable ubiquitin carboxyl-terminal hydrolase FAF-X	14,40	3,994E-03	2,6	☐
H	>sp|P83882|RL36A	60S ribosomal protein L36a	6,64	8,349E-05	-4,2	☐
H	>sp|P84091|AP2M1	AP-2 complex subunit mu	21,34	9,765E-04	-3,6	☐
H	>sp|P84244|H33	Histone H3.3	4,86	4,396E-03	-2,4	☐
H	>sp|P99026|PSB4	Proteasome subunit beta type-4	23,09	2,587E-03	-6,1	☐
H	>sp|P99028|QCR6	Cytochrome b-c1 complex subunit 6, mitochondrial	26,22	1,040E-02	-2,1	☐
H	>sp|Q00519|XDH	Xanthine dehydrogenase/oxidase	120,97	2,592E-03	-3,6	☐
H	>sp|Q07813|BAX	Apoptosis regulator BAX	7,24	1,035E-02	-2,5	☐
H	>sp|Q3THK7|GUAA	GMP synthase [glutamine-hydrolyzing]	22,83	8,233E-04	-2,5	☐
H	>sp|Q3UNZ8|QORL2	Quinone oxidoreductase-like protein 2	33,01	1,030E-05	10,4	☐
H	>sp|Q5SUR0|PUR4	Phosphoribosylformylglycinamidine synthase	14,96	1,334E-03	-2,2	☐
H	>sp|Q60692|PSB6	Proteasome subunit beta type-6	24,38	9,348E-04	-4,4	☐
H	>sp|Q61699|HS105	Heat shock protein 105 kDa	65,84	4,202E-02	2,9	☐
H	>sp|Q62264|THRSP	Thyroid hormone-inducible hepatic protein	63,13	1,352E-03	-3,5	☐
H	>sp|Q62348|TSN	Translin	3,38	4,956E-03	-3,6	☐
H	>sp|Q62376|RU17	U1 small nuclear ribonucleoprotein 70 kDa	6,88	6,792E-04	-2,9	☐
H	>sp|Q62452|UD19	UDP-glucuronosyltransferase 1-9	134,47	2,394E-03	-2,0	☐
H	>sp|Q64374|RGN	Regucalcin	474,77	1,225E-04	-2,7	☐

179

H	>sp|Q6P8I4|PCNP	PEST proteolytic signal-containing nuclear protein	8,89	5,262E-05	-3,3	☐
H	>sp|Q76LS9|FA63A	Protein FAM63A	14,09	1,605E-02	2,1	☐
H	>sp|Q7TPV4|MBB1A	Myb-binding protein 1A	9,94	2,593E-03	2,1	☐
H	>sp|Q8BFZ3|ACTBL	Beta-actin-like protein 2	194,76	1,488E-02	-2,3	☐
H	>sp|Q8BH69|SPS1	Selenide, water dikinase 1	16,62	1,181E-05	-3,5	☐
H	>sp|Q8BWM0|PGES2	Prostaglandin E synthase 2	3,99	1,695E-02	-2,4	☐
H	>sp|Q8C1B7|SEP11	Septin-11	26,97	3,914E-04	2,3	☐
H	>sp|Q8CAQ8|MIC60	MICOS complex subunit Mic60	7,80	5,560E-03	2,5	☐
H	>sp|Q8CAS9|PARP9	Poly [ADP-ribose] polymerase 9	11,36	7,125E-04	2,1	☐
H	>sp|Q8K010|OPLA	5-oxoprolinase	206,63	3,220E-07	27,5	☐
H	>sp|Q8R050|ERF3A	Eukaryotic peptide chain release factor GTP-binding subunit ERF3A	20,28	6,261E-05	2,9	☐
H	>sp|Q8R317|UBQL1	Ubiquilin-1	38,38	3,764E-02	2,3	☐
H	>sp|Q8VCC1|PGDH	15-hydroxyprostaglandin dehydrogenase [NAD(+)]	41,97	1,041E-02	-2,7	☐
H	>sp|Q8VCH6|DHC24	Delta(24)-sterol reductase	10,41	6,011E-04	-2,8	☐
H	>sp|Q91VS7|MGST1	Microsomal glutathione S-transferase 1	110,95	5,391E-03	-3,8	☐
H	>sp|Q91W97|HKDC1	Putative hexokinase HKDC1	3,11	3,555E-03	2,2	☐
H	>sp|Q91XE8|TM205	Transmembrane protein 205	16,47	4,048E-06	3,6	☐
H	>sp|Q920A5|RISC	Retinoid-inducible serine carboxypeptidase	14,69	1,412E-04	2,3	☐
H	>sp|Q922Q1|MARC2	Mitochondrial amidoxime reducing component 2	34,67	1,271E-05	-3,2	☐
H	>sp|Q99KP6|PRP19	Pre-mRNA-processing factor 19	11,47	1,564E-06	12,5	☐
H	>sp|Q99KV1|DJB11	DnaJ homolog subfamily B member 11	38,78	1,606E-02	2,0	☐
H	>sp|Q99LY9|NDUS5	NADH dehydrogenase [ubiquinone] iron-sulfur protein 5	6,11	2,114E-04	-4,7	☐
H	>sp|Q99P30|NUDT7	Peroxisomal coenzyme A diphosphatase NUDT7	132,96	4,441E-04	-2,4	☐
H	>sp|Q9CPU0|LGUL	Lactoylglutathione lyase	157,33	7,819E-05	-2,5	☐
H	>sp|Q9CPX6|ATG3	Ubiquitin-like-conjugating enzyme ATG3	6,07	2,944E-03	-2,3	☐
H	>sp|Q9CQC6|BZW1	Basic leucine zipper and W2 domain-containing protein 1	15,15	1,898E-03	-3,2	☐
H	>sp|Q9CXS4|CENPV	Centromere protein V	14,44	3,399E-02	2,1	☐
H	>sp|Q9CYZ2|TPD54	Tumor protein D54	24,45	2,177E-04	2,9	☐
H	>sp|Q9D1G1|RAB1B	Ras-related protein Rab-1B	43,53	8,573E-03	2,1	☐
H	>sp|Q9D1R9|RL34	60S ribosomal protein L34	12,19	9,227E-03	-2,1	☐
H	>sp|Q9D2R0|AACS	Acetoacetyl-CoA synthetase	22,28	5,676E-04	3,9	☐
H	>sp|Q9D2V7|CORO7	Coronin-7	24,62	1,647E-02	-2,6	☐
H	>sp|Q9D7G0|PRPS1	Ribose-phosphate pyrophosphokinase 1	48,75	1,538E-07	-67,2	☐
H	>sp|Q9D820|PRXD1	Prolyl-tRNA synthetase associated domain-containing protein 1	4,86	8,386E-05	-5,5	☐
H	>sp|Q9DBE0|CSAD	Cysteine sulfinic acid decarboxylase	131,84	1,735E-02	-2,5	☐
H	>sp|Q9DCH4|EIF3F	Eukaryotic translation initiation factor 3 subunit F	20,34	2,785E-02	-2,0	☐
H	>sp|Q9EPQ7|STAR5	StAR-related lipid transfer protein 5	8,78	1,901E-03	-2,2	☐
H	>sp|Q9EQ06|DHB11	Estradiol 17-beta-dehydrogenase 11	21,95	4,838E-03	-2,7	☐
H	>sp|Q9ERG0|LIMA1	LIM domain and actin-binding protein 1	28,82	9,280E-05	2,1	☐
H	>sp|Q9JHE3|ASAH2	Neutral ceramidase	8,73	4,741E-03	2,1	☐
H	>sp|Q9JHS4|CLPX	ATP-dependent Clp protease ATP-binding subunit clpX-like	25,06	1,323E-05	13,5	☐

H	>sp|Q9JIL4|NHRF3	Na(+)/H(+) exchange regulatory cofactor NHE-RF3	28,83	3,295E-03	2,8
H	>sp|Q9JLY0|SOCS6	Suppressor of cytokine signaling 6	2,73	2,485E-04	2,5
H	>sp|Q9JMA1|UBP14	Ubiquitin carboxyl-terminal hydrolase 14	43,37	4,681E-03	4,9
H	>sp|Q9QZD8|DIC	Mitochondrial dicarboxylate carrier	25,27	4,606E-02	-2,2
H	>sp|Q9R0A0|PEX14	Peroxisomal membrane protein PEX14	13,61	1,458E-03	2,3
H	>sp|Q9R0M5|TPK1	Thiamin pyrophosphokinase 1	8,59	9,983E-03	-4,8
H	>sp|Q9R0Q9|MPU1	Mannose-P-dolichol utilization defect 1 protein	7,59	6,942E-04	-2,4
H	>sp|Q9R1J0|NSDHL	Sterol-4-alpha-carboxylate 3-dehydrogenase, decarboxylating	18,92	4,937E-05	-2,3
H	>sp|Q9R1P1|PSB3	Proteasome subunit beta type-3	32,66	3,703E-04	-6,0
H	>sp|Q9R1P3|PSB2	Proteasome subunit beta type-2	27,17	4,797E-04	-6,3
H	>sp|Q9WU19|HAOX1	Hydroxyacid oxidase 1	67,82	1,064E-02	2,2
H	>sp|Q9Z2U0|PSA7	Proteasome subunit alpha type-7	61,80	4,219E-04	-5,1
H	>sp|Q9Z2U1|PSA5	Proteasome subunit alpha type-5	59,85	1,696E-03	-4,7
H	>sp|Q9Z2W0|DNPEP	Aspartyl aminopeptidase	43,74	8,086E-03	-2,5
H	>sp|Q9Z2Z6|MCAT	Mitochondrial carnitine/acylcarnitine carrier protein	20,71	4,390E-02	-2,3
H	>tr|A0A0A0MQC3	5-hydroxyisourate hydrolase	50,54	9,407E-05	-3,3
H	>tr|A2AGR0|A2AGR0	MAP kinase-activating death domain protein	4,87	3,710E-05	5,4
H	>tr|A2AQZ2|A2AQZ2	Phytanoyl-CoA dioxygenase domain-containing protein 1 (Fragment)	54,28	4,692E-05	4,4
H	>tr|D3Z0R5|D3Z0R5	Glucosamine-6-phosphate isomerase 1 (Fragment)	6,97	9,352E-04	-2,4
H	>tr|D3Z5G7|D3Z5G7	Carboxylic ester hydrolase	37,61	5,939E-03	2,4
H	>tr|E9PV38|E9PV38	Carboxylic ester hydrolase	53,04	1,976E-03	2,3
H	>tr|E9PW69|E9PW69	Proteasome subunit alpha type (Fragment)	31,99	2,768E-04	-6,3
H	>tr|E9PZ00|E9PZ00	Prosaposin	54,04	2,561E-02	-2,5
H	>tr|E9Q455|E9Q455	Tropomyosin alpha-1 chain	42,17	9,618E-05	4,6
H	>tr|E9Q9F5|E9Q9F5	Septin-7	57,02	3,489E-06	28,0
H	>tr|E9QNW6|E9QNW6	Platelet-activating factor acetylhydrolase 2, cytoplasmic	8,02	5,794E-04	4,1
H	>tr|F7CBP1|F7CBP1	Eukaryotic translation initiation factor 4 gamma 2	8,19	8,781E-05	-4,1
H	>tr|G3UWG1|G3UWG1	MCG115977	142,03	4,987E-04	-2,3
H	>tr|G5E902|G5E902	MCG10343, isoform CRA_b	35,02	2,884E-05	3,1
H	>tr|H3BJ51|H3BJ51	All-trans-retinol 13,14-reductase	31,98	4,332E-02	-2,2
H	>tr|H7BX99|H7BX99	Prothrombin	19,69	9,163E-06	14,0
H	>tr|Q3TUE1|Q3TUE1	Far upstream element-binding protein 1	18,66	3,536E-04	-2,6
H	>tr|Q6GT24|Q6GT24	Peroxiredoxin 6	341,89	1,388E-02	3,0
H	>tr|Q6ZWZ6|Q6ZWZ6	40S ribosomal protein S12	15,79	2,930E-04	-2,2
H	>tr|Q8BJL9|Q8BJL9	MCG131372	23,16	1,465E-03	-6,6
H	>tr|Q8BVD2|Q8BVD2	Cytochrome P450, family 2, subfamily d, polypeptide 12	46,90	1,882E-03	-2,4
H	>tr|Q91Z40|Q91Z40	Gbp6 protein	5,97	1,379E-03	-2,5
H	>tr|Q9CQM8|Q9CQM8	60S ribosomal protein L21	48,39	6,073E-04	4,7
H	>tr|Q9WUD0|Q9WUD0	Cytochrome P450 2B10	16,12	1,197E-03	-2,4
L	>sp|A2AS89|SPEB	Agmatinase, mitochondrial	60,52	5,357E-06	-4,0
L	>sp|B1AR13|CISD3	CDGSH iron-sulfur domain-containing protein 3, mitochondrial	8,01	1,656E-04	-5,4

L	>sp|E9Q4Z2|ACACB	Acetyl-CoA carboxylase 2	72,01	1,047E-04	2,4	☐
L	>sp|O08807|PRDX4	Peroxiredoxin-4	47,98	1,291E-03	3,1	☐
L	>sp|O09061|PSB1	Proteasome subunit beta type-1	34,47	2,916E-03	-4,3	☐
L	>sp|O35286|DHX15	Pre-mRNA-splicing factor ATP-dependent RNA helicase DHX15	13,23	1,830E-02	-2,1	☐
L	>sp|O55135|IF6	Eukaryotic translation initiation factor 6	47,88	8,102E-04	2,1	☐
L	>sp|O55137|ACOT1	Acyl-coenzyme A thioesterase 1	121,46	5,512E-05	-2,5	☐
L	>sp|O55142|RL35A	60S ribosomal protein L35a	14,18	7,236E-04	-2,1	☐
L	>sp|O55234|PSB5	Proteasome subunit beta type-5	16,24	2,810E-03	-3,6	☐
L	>sp|O70435|PSA3	Proteasome subunit alpha type-3	8,53	7,447E-04	-6,8	☐
L	>sp|O88451|RDH7	Retinol dehydrogenase 7	130,14	5,437E-06	-4,2	☐
L	>sp|O88456|CPNS1	Calpain small subunit 1	15,07	7,863E-05	2,3	☐
L	>sp|P02089|HBB2	Hemoglobin subunit beta-2	269,71	4,767E-05	-3,3	☐
L	>sp|P06330|HVM51	Ig heavy chain V region AC38 205.12	13,64	1,794E-05	5,9	☐
L	>sp|P06801|MAOX	NADP-dependent malic enzyme	364,83	5,985E-04	-2,0	☐
L	>sp|P07724|ALBU	Serum albumin	884,36	1,169E-05	-2,1	☐
L	>sp|P07759|SPA3K	Serine protease inhibitor A3K	132,97	9,592E-04	-2,0	☐
L	>sp|P08752|GNAI2	Guanine nucleotide-binding protein G(i) subunit alpha-2	16,63	6,090E-03	3,5	☐
L	>sp|P11352|GPX1	Glutathione peroxidase 1	154,94	2,192E-03	-3,0	☐
L	>sp|P12790|CP2B9	Cytochrome P450 2B9	26,56	1,136E-02	-2,2	☐
L	>sp|P14246|GTR2	Solute carrier family 2, facilitated glucose transporter member 2	6,57	8,786E-04	-3,1	☐
L	>sp|P14602|HSPB1	Heat shock protein beta-1	4,97	1,143E-03	2,9	☐
L	>sp|P16546|SPTN1	Spectrin alpha chain, non-erythrocytic 1	42,85	1,367E-05	7,9	☐
L	>sp|P16627|HS71L	Heat shock 70 kDa protein 1-like	78,03	3,586E-03	-2,3	☐
L	>sp|P17563|SBP1	Selenium-binding protein 1	448,05	7,429E-04	-2,1	☐
L	>sp|P17879|HS71B	Heat shock 70 kDa protein 1B	113,76	2,298E-04	3,0	☐
L	>sp|P18572|BASI	Basigin	30,31	5,715E-05	-2,2	☐
L	>sp|P21614|VTDB	Vitamin D-binding protein	148,26	6,398E-05	-2,5	☐
L	>sp|P24456|CP2DA	Cytochrome P450 2D10	194,38	8,622E-04	-2,3	☐
L	>sp|P27046|MA2A1	Alpha-mannosidase 2	14,55	4,805E-04	-2,2	☐
L	>sp|P28651|CAH8	Carbonic anhydrase-related protein	35,72	1,027E-04	4,0	☐
L	>sp|P28798|GRN	Granulins	16,30	7,310E-05	-35,0	☐
L	>sp|P34927|ASGR1	Asialoglycoprotein receptor 1	32,22	1,830E-03	-2,0	☐
L	>sp|P35492|HUTH	Histidine ammonia-lyase	376,41	4,409E-04	-2,0	☐
L	>sp|P35505|FAAA	Fumarylacetoacetase	449,36	1,702E-04	-4,8	☐
L	>sp|P42925|PXMP2	Peroxisomal membrane protein 2	6,68	1,753E-03	-3,3	☐
L	>sp|P50295|ARY2	Arylamine N-acetyltransferase 2	23,34	1,452E-04	3,5	☐
L	>sp|P52792|HXK4	Glucokinase	19,75	2,568E-03	2,7	☐
L	>sp|P56391|CX6B1	Cytochrome c oxidase subunit 6B1	14,61	4,747E-02	-2,0	☐
L	>sp|P59325|IF5	Eukaryotic translation initiation factor 5	17,03	1,208E-04	-2,7	☐
L	>sp|P59999|ARPC4	Actin-related protein 2/3 complex subunit 4	23,53	1,045E-03	2,0	☐
L	>sp|P60229|EIF3E	Eukaryotic translation initiation factor 3 subunit E	24,24	5,137E-05	6,2	☐
L	>sp|P61514|RL37A	60S ribosomal protein L37a	13,94	2,530E-05	5,6	☐
L	>sp|P62204|CALM	Calmodulin	15,87	3,004E-02	2,0	☐

L	>sp|P62827|RAN	GTP-binding nuclear protein Ran	24,89	2,542E-04	-6,2	☐
L	>sp|P62862|RS30	40S ribosomal protein S30	8,12	5,254E-04	-8,0	☐
L	>sp|P63085|MK01	Mitogen-activated protein kinase 1	13,73	1,170E-03	-2,3	☐
L	>sp|P70398|USP9X	Probable ubiquitin carboxyl-terminal hydrolase FAF-X	14,40	9,517E-03	2,4	☐
L	>sp|P83882|RL36A	60S ribosomal protein L36a	6,64	4,079E-05	-5,8	☐
L	>sp|P84091|AP2M1	AP-2 complex subunit mu	21,34	3,118E-04	-4,5	☐
L	>sp|P84244|H33	Histone H3.3	4,86	5,960E-04	-4,8	☐
L	>sp|P97351|RS3A	40S ribosomal protein S3a	97,26	3,078E-04	-2,5	☐
L	>sp|P99026|PSB4	Proteasome subunit beta type-4	23,09	8,997E-03	-4,1	☐
L	>sp|Q00519|XDH	Xanthine dehydrogenase/oxidase	120,97	1,112E-03	-2,8	☐
L	>sp|Q01339|APOH	Beta-2-glycoprotein 1	13,44	1,240E-02	-2,3	☐
L	>sp|Q01730|RSU1	Ras suppressor protein 1	29,83	1,186E-03	2,8	☐
L	>sp|Q05915|GCH1	GTP cyclohydrolase 1	5,10	5,749E-05	3,2	☐
L	>sp|Q07813|BAX	Apoptosis regulator BAX	7,24	3,614E-03	-2,1	☐
L	>sp|Q3THK7|GUAA	GMP synthase [glutamine-hydrolyzing]	22,83	8,106E-04	-2,3	☐
L	>sp|Q3UNZ8|QORL2	Quinone oxidoreductase-like protein 2	33,01	2,044E-05	8,6	☐
L	>sp|Q4VAA2|CDV3	Protein CDV3	49,10	1,194E-02	2,3	☐
L	>sp|Q60692|PSB6	Proteasome subunit beta type-6	24,38	1,646E-03	-3,7	☐
L	>sp|Q61704|ITIH3	Inter-alpha-trypsin inhibitor heavy chain H3	7,97	8,595E-05	2,5	☐
L	>sp|Q62186|SSRD	Translocon-associated protein subunit delta	11,23	9,160E-03	2,7	☐
L	>sp|Q62264|THRSP	Thyroid hormone-inducible hepatic protein	63,13	1,618E-03	-3,5	☐
L	>sp|Q62348|TSN	Translin	3,38	8,647E-03	-3,0	☐
L	>sp|Q62376|RU17	U1 small nuclear ribonucleoprotein 70 kDa	6,88	3,308E-04	-3,2	☐
L	>sp|Q62452|UD19	UDP-glucuronosyltransferase 1-9	134,47	1,798E-04	-2,6	☐
L	>sp|Q64374|RGN	Regucalcin	474,77	1,666E-04	-2,1	☐
L	>sp|Q6P542|ABCF1	ATP-binding cassette sub-family F member 1	25,71	3,750E-03	2,8	☐
L	>sp|Q6P8I4|PCNP	PEST proteolytic signal-containing nuclear protein	8,89	2,347E-05	-3,6	☐
L	>sp|Q76LS9|FA63A	Protein FAM63A	14,09	9,562E-03	2,4	☐
L	>sp|Q76MZ3|2AAA	Serine/threonine-protein phosphatase 2A 65 kDa regulatory subunit	70,84	2,240E-03	2,2	☐
L	>sp|Q7TPV4|MBB1A	Myb-binding protein 1A	9,94	1,599E-03	2,5	☐
L	>sp|Q80VP1|EPN1	Epsin-1	18,13	5,771E-04	2,5	☐
L	>sp|Q8BFP9|PDK1	[Pyruvate dehydrogenase (acetyl-transferring)] kinase isozyme 1	6,93	6,219E-03	2,9	☐
L	>sp|Q8BFZ3|ACTBL	Beta-actin-like protein 2	194,76	3,010E-04	-2,9	☐
L	>sp|Q8BH69|SPS1	Selenide, water dikinase 1	16,62	8,027E-06	-4,9	☐
L	>sp|Q8BKZ9|ODPX	Pyruvate dehydrogenase protein X component, mitochondrial	10,55	1,090E-04	2,0	☐
L	>sp|Q8BL66|EEA1	Early endosome antigen 1	3,80	1,222E-03	2,0	☐
L	>sp|Q8BP56|ATHL1	Acid trehalase-like protein 1	5,60	2,255E-02	3,4	☐
L	>sp|Q8BWM0|PGES2	Prostaglandin E synthase 2	3,99	5,082E-03	-2,0	☐
L	>sp|Q8C1B7|SEP11	Septin-11	26,97	3,592E-05	2,7	☐
L	>sp|Q8CAQ8|MIC60	MICOS complex subunit Mic60	7,80	1,338E-04	2,6	☐
L	>sp|Q8CAS9|PARP9	Poly [ADP-ribose] polymerase 9	11,36	1,390E-03	2,1	☐

L	>sp|Q8K010|OPLA	5-oxoprolinase	206,63	1,399E-07	20,1	☐
L	>sp|Q8K0C4|CP51A	Lanosterol 14-alpha demethylase	31,93	3,170E-05	2,4	☐
L	>sp|Q8K297|GT251	Procollagen galactosyltransferase 1	7,80	1,756E-03	2,5	☐
L	>sp|Q8K3K7|PLCB	1-acyl-sn-glycerol-3-phosphate acyltransferase beta	16,90	1,444E-02	2,2	☐
L	>sp|Q8K411|PREP	Presequence protease, mitochondrial	38,78	6,749E-03	2,6	☐
L	>sp|Q8K441|ABCA6	ATP-binding cassette sub-family A member 6	26,53	6,478E-03	2,6	☐
L	>sp|Q8R016|BLMH	Bleomycin hydrolase	21,17	4,793E-03	-2,1	☐
L	>sp|Q8R050|ERF3A	Eukaryotic peptide chain release factor GTP-binding subunit ERF3A	20,28	1,690E-06	5,2	☐
L	>sp|Q8R317|UBQL1	Ubiquilin-1	38,38	1,739E-02	2,2	☐
L	>sp|Q8VCC1|PGDH	15-hydroxyprostaglandin dehydrogenase [NAD(+)]	41,97	1,346E-04	-2,5	☐
L	>sp|Q8VCH6|DHC24	Delta(24)-sterol reductase	10,41	3,133E-05	-3,1	☐
L	>sp|Q8VCH8|UBXN4	UBX domain-containing protein 4	14,67	6,364E-03	-2,2	☐
L	>sp|Q8VCT3|AMPB	Aminopeptidase B	63,09	1,369E-03	2,6	☐
L	>sp|Q8VCU1|EST3B	Carboxylesterase 3B	125,07	6,130E-03	-2,6	☐
L	>sp|Q91VS7|MGST1	Microsomal glutathione S-transferase 1	110,95	1,517E-04	-6,4	☐
L	>sp|Q91VT4|CBR4	Carbonyl reductase family member 4	63,93	8,152E-04	2,0	☐
L	>sp|Q91W97|HKDC1	Putative hexokinase HKDC1	3,11	1,580E-03	2,4	☐
L	>sp|Q91XE8|TM205	Transmembrane protein 205	16,47	8,595E-06	3,8	☐
L	>sp|Q921M3|SF3B3	Splicing factor 3B subunit 3	14,37	8,615E-03	2,2	☐
L	>sp|Q99KP3|CRYL1	Lambda-crystallin homolog	37,47	3,997E-03	3,0	☐
L	>sp|Q99KP6|PRP19	Pre-mRNA-processing factor 19	11,47	7,550E-06	13,2	☐
L	>sp|Q99LY9|NDUS5	NADH dehydrogenase [ubiquinone] iron-sulfur protein 5	6,11	2,175E-02	-2,8	☐
L	>sp|Q99P30|NUDT7	Peroxisomal coenzyme A diphosphatase NUDT7	132,96	3,369E-04	-2,2	☐
L	>sp|Q9CPX6|ATG3	Ubiquitin-like-conjugating enzyme ATG3	6,07	9,676E-04	-3,2	☐
L	>sp|Q9CQC6|BZW1	Basic leucine zipper and W2 domain-containing protein 1	15,15	7,564E-03	-2,5	☐
L	>sp|Q9CYZ2|TPD54	Tumor protein D54	24,45	6,048E-06	3,5	☐
L	>sp|Q9D154|ILEUA	Leukocyte elastase inhibitor A	3,96	2,427E-02	-2,0	☐
L	>sp|Q9D1M0|SEC13	Protein SEC13 homolog	41,90	8,547E-04	2,2	☐
L	>sp|Q9D1R9|RL34	60S ribosomal protein L34	12,19	1,829E-04	-3,0	☐
L	>sp|Q9D273|MMAB	Cob(I)yrinic acid a,c-diamide adenosyltransferase, mitochondrial	20,12	1,827E-03	2,2	☐
L	>sp|Q9D2R0|AACS	Acetoacetyl-CoA synthetase	22,28	3,568E-04	3,8	☐
L	>sp|Q9D7G0|PRPS1	Ribose-phosphate pyrophosphokinase 1	48,75	1,259E-05	-112,1	☐
L	>sp|Q9D820|PRXD1	Prolyl-tRNA synthetase associated domain-containing protein 1	4,86	1,327E-04	-10,6	☐
L	>sp|Q9DBC7|KAP0	cAMP-dependent protein kinase type I-alpha regulatory subunit	3,95	2,634E-03	2,7	☐
L	>sp|Q9DBE0|CSAD	Cysteine sulfinic acid decarboxylase	131,84	4,147E-04	-6,5	☐
L	>sp|Q9DBH5|LMAN2	Vesicular integral-membrane protein VIP36	24,00	5,650E-03	2,2	☐
L	>sp|Q9DBS5|KLC4	Kinesin light chain 4	8,68	2,550E-03	3,8	☐
L	>sp|Q9DCH4|EIF3F	Eukaryotic translation initiation factor 3 subunit F	20,34	1,803E-02	-3,7	☐
L	>sp|Q9DCT2|NDUS3	NADH dehydrogenase [ubiquinone] iron-sulfur protein 3	13,34	9,044E-03	2,0	☐
L	>sp|Q9DD20|MET7B	Methyltransferase-like protein 7B	53,21	6,404E-04	-2,0	☐

L	>sp|Q9EPQ7|STAR5	StAR-related lipid transfer protein 5	8,78	2,425E-04	-4,9	☐
L	>sp|Q9EQ06|DHB11	Estradiol 17-beta-dehydrogenase 11	21,95	1,067E-04	-3,7	☐
L	>sp|Q9ET22|DPP2	Dipeptidyl peptidase 2	5,13	7,200E-03	-2,0	☐
L	>sp|Q9JHE3|ASAH2	Neutral ceramidase	8,73	2,495E-04	3,9	☐
L	>sp|Q9JHS4|CLPX	ATP-dependent Clp protease ATP-binding subunit clpX-like	25,06	4,975E-05	10,8	☐
L	>sp|Q9JIL4|NHRF3	Na(+)/H(+) exchange regulatory cofactor NHE-RF3	28,83	1,751E-04	4,6	☐
L	>sp|Q9JLY0|SOCS6	Suppressor of cytokine signaling 6	2,73	8,931E-04	2,4	☐
L	>sp|Q9JMA1|UBP14	Ubiquitin carboxyl-terminal hydrolase 14	43,37	9,072E-03	3,9	☐
L	>sp|Q9JMA7|CP341	Cytochrome P450 3A41	142,20	3,709E-02	2,1	☐
L	>sp|Q9R092|H17B6	17-beta-hydroxysteroid dehydrogenase type 6	98,04	5,570E-04	-2,5	☐
L	>sp|Q9R0M5|TPK1	Thiamin pyrophosphokinase 1	8,59	1,128E-02	-2,8	☐
L	>sp|Q9R0Q9|MPU1	Mannose-P-dolichol utilization defect 1 protein	7,59	1,780E-04	-2,5	☐
L	>sp|Q9R1J0|NSDHL	Sterol-4-alpha-carboxylate 3-dehydrogenase, decarboxylating	18,92	7,055E-04	-2,3	☐
L	>sp|Q9R1P1|PSB3	Proteasome subunit beta type-3	32,66	3,443E-04	-5,4	☐
L	>sp|Q9R1P3|PSB2	Proteasome subunit beta type-2	27,17	4,611E-04	-4,7	☐
L	>sp|Q9WV02|RBMX	RNA-binding motif protein, X chromosome	6,24	8,392E-03	3,2	☐
L	>sp|Q9Z1J3|NFS1	Cysteine desulfurase, mitochondrial	15,05	2,370E-04	2,7	☐
L	>sp|Q9Z2U0|PSA7	Proteasome subunit alpha type-7	61,80	3,203E-04	-4,3	☐
L	>sp|Q9Z2U1|PSA5	Proteasome subunit alpha type-5	59,85	1,348E-03	-5,0	☐
L	>sp|Q9Z2W0|DNPEP	Aspartyl aminopeptidase	43,74	3,760E-03	-2,5	☐
L	>sp|Q9Z2Z6|MCAT	Mitochondrial carnitine/acylcarnitine carrier protein	20,71	6,473E-03	-2,5	☐
L	>tr|A0A0A0MQC3	5-hydroxyisourate hydrolase	50,54	5,446E-04	-3,6	☐
L	>tr|A2AGR0|A2AGR0	MAP kinase-activating death domain protein	4,87	8,213E-05	4,9	☐
L	>tr|A2AQZ2|A2AQZ2	Phytanoyl-CoA dioxygenase domain-containing protein 1 (Fragment)	54,28	3,414E-07	4,8	☐
L	>tr|D3YUK4|D3YUK4	NADH dehydrogenase [ubiquinone] 1 beta subcomplex subunit 10 (Fragment)	7,57	1,386E-02	2,1	☐
L	>tr|D3YUP6|D3YUP6	Protein Ugt2b36 (Fragment)	48,07	3,814E-05	-2,1	☐
L	>tr|D3Z0R5|D3Z0R5	Glucosamine-6-phosphate isomerase 1 (Fragment)	6,97	1,559E-03	-2,1	☐
L	>tr|D3Z5G7|D3Z5G7	Carboxylic ester hydrolase	37,61	2,179E-03	2,3	☐
L	>tr|E9PV38|E9PV38	Carboxylic ester hydrolase	53,04	3,002E-04	2,2	☐
L	>tr|E9PVM7|E9PVM7	Glutathione S-transferase Mu 5 (Fragment)	16,27	3,864E-02	2,0	☐
L	>tr|E9PW69|E9PW69	Proteasome subunit alpha type (Fragment)	31,99	5,818E-04	-4,8	☐
L	>tr|E9PXC3|E9PXC3	Protein Cyp2c69	134,37	1,542E-03	-2,8	☐
L	>tr|E9PZ00|E9PZ00	Prosaposin	54,04	1,230E-02	-2,4	☐
L	>tr|E9Q455|E9Q455	Tropomyosin alpha-1 chain	42,17	7,525E-07	7,7	☐
L	>tr|E9Q9F5|E9Q9F5	Septin-7	57,02	4,623E-07	23,7	☐
L	>tr|E9QNW6|E9QNW6	Platelet-activating factor acetylhydrolase 2, cytoplasmic	8,02	6,299E-03	5,8	☐
L	>tr|F7CBP1|F7CBP1	Eukaryotic translation initiation factor 4 gamma 2	8,19	9,533E-05	-3,6	☐
L	>tr|G5E902|G5E902	MCG10343, isoform CRA_b	35,02	3,334E-05	3,0	☐
L	>tr|H3BJ51|H3BJ51	All-trans-retinol 13,14-reductase	31,98	5,624E-03	-4,0	☐
L	>tr|H7BX99|H7BX99	Prothrombin	19,69	2,154E-05	11,5	☐

L	>tr|Q3TKD0|Q3TKD0	Transportin-1 (Fragment)	7,72	9,237E-03	2,4	☐
L	>tr|Q5EBP8|Q5EBP8	Heterogeneous nuclear ribonucleoprotein A1	42,56	1,360E-03	2,2	☐
L	>tr|Q6ZWZ6|Q6ZWZ6	40S ribosomal protein S12	15,79	6,019E-04	-2,2	☐
L	>tr|Q8BH80|Q8BH80	Vesicle-associated membrane protein, associated protein B and C	5,82	1,157E-02	-2,4	☐
L	>tr|Q8CBB6|Q8CBB6	Histone H2B	17,91	2,921E-03	-3,6	☐
L	>tr|Q8K169|Q8K169	MCG1789	99,83	1,187E-03	-2,2	☐
L	>tr|Q91X75|Q91X75	Cyp2a4 protein	92,05	3,009E-03	-2,0	☐
L	>tr|Q91Z40|Q91Z40	Gbp6 protein	5,97	1,288E-04	-3,1	☐
L	>tr|Q9CQM8|Q9CQM8	60S ribosomal protein L21	48,39	2,179E-04	3,0	☐
L	>tr|Q9WUD0|Q9WUD0	Cytochrome P450 2B10	16,12	3,394E-04	-2,1	☐
M	>sp|A2AS89|SPEB	Agmatinase, mitochondrial	60,52	4,295E-05	-8,1	☐
M	>sp|B1AR13|CISD3	CDGSH iron-sulfur domain-containing protein 3, mitochondrial	8,01	1,327E-02	-3,4	☐
M	>sp|E9Q4Z2|ACACB	Acetyl-CoA carboxylase 2	72,01	4,871E-05	2,1	☐
M	>sp|O08583|THOC4	THO complex subunit 4	14,57	6,252E-05	3,9	☐
M	>sp|O08709|PRDX6	Peroxiredoxin-6	360,97	3,286E-03	12,3	☐
M	>sp|O08749|DLDH	Dihydrolipoyl dehydrogenase, mitochondrial	137,90	1,330E-03	-2,0	☐
M	>sp|O09061|PSB1	Proteasome subunit beta type-1	34,47	5,185E-03	-7,1	☐
M	>sp|O35215|DOPD	D-dopachrome decarboxylase	23,57	1,835E-02	-9,2	☐
M	>sp|O35841|API5	Apoptosis inhibitor 5	15,45	5,115E-03	-3,5	☐
M	>sp|O35945|AL1A7	Aldehyde dehydrogenase, cytosolic 1	341,03	1,749E-03	-2,9	☐
M	>sp|O55234|PSB5	Proteasome subunit beta type-5	16,24	1,051E-02	-3,0	☐
M	>sp|O70435|PSA3	Proteasome subunit alpha type-3	8,53	3,589E-03	-6,3	☐
M	>sp|O88451|RDH7	Retinol dehydrogenase 7	130,14	5,368E-04	-2,5	☐
M	>sp|P00329|ADH1	Alcohol dehydrogenase 1	490,89	1,900E-05	-2,6	☐
M	>sp|P00920|CAH2	Carbonic anhydrase 2	139,00	2,904E-03	-2,1	☐
M	>sp|P01864|GCAB	Ig gamma-2A chain C region secreted form	9,98	5,539E-03	-2,5	☐
M	>sp|P02089|HBB2	Hemoglobin subunit beta-2	269,71	1,260E-05	7,2	☐
M	>sp|P06330|HVM51	Ig heavy chain V region AC38 205.12	13,64	7,381E-06	11,7	☐
M	>sp|P07724|ALBU	Serum albumin	884,36	1,476E-04	-2,1	☐
M	>sp|P08752|GNAI2	Guanine nucleotide-binding protein G(i) subunit alpha-2	16,63	1,169E-02	4,2	☐
M	>sp|P12790|CP2B9	Cytochrome P450 2B9	26,56	3,613E-02	-2,0	☐
M	>sp|P13634|CAH1	Carbonic anhydrase 1	24,59	3,060E-04	2,9	☐
M	>sp|P14602|HSPB1	Heat shock protein beta-1	4,97	3,320E-02	2,1	☐
M	>sp|P15105|GLNA	Glutamine synthetase	404,84	9,960E-06	-2,1	☐
M	>sp|P16045|LEG1	Galectin-1	21,49	5,079E-03	-3,2	☐
M	>sp|P16546|SPTN1	Spectrin alpha chain, non-erythrocytic 1	42,85	1,154E-04	6,8	☐
M	>sp|P17879|HS71B	Heat shock 70 kDa protein 1B	113,76	2,296E-03	3,1	☐
M	>sp|P20152|VIME	Vimentin	70,04	1,641E-02	-2,9	☐
M	>sp|P21614|VTDB	Vitamin D-binding protein	148,26	9,237E-06	-2,8	☐
M	>sp|P23953|EST1C	Carboxylesterase 1C	68,02	2,005E-03	3,3	☐
M	>sp|P28651|CAH8	Carbonic anhydrase-related protein	35,72	6,405E-04	4,8	☐
M	>sp|P28798|GRN	Granulins	16,30	5,444E-04	-29,8	☐
M	>sp|P29758|OAT	Ornithine aminotransferase, mitochondrial	309,01	1,074E-02	-2,5	☐

M	>sp|P34884|MIF	Macrophage migration inhibitory factor	74,65	2,422E-03	-2,4	☐
M	>sp|P35492|HUTH	Histidine ammonia-lyase	376,41	1,558E-04	-3,3	☐
M	>sp|P35505|FAAA	Fumarylacetoacetase	449,36	2,068E-05	-15,0	☐
M	>sp|P40936|INMT	Indolethylamine N-methyltransferase	232,81	5,185E-04	-2,3	☐
M	>sp|P47738|ALDH2	Aldehyde dehydrogenase, mitochondrial	479,74	2,325E-04	-2,0	☐
M	>sp|P50295|ARY2	Arylamine N-acetyltransferase 2	23,34	4,434E-04	-3,9	☐
M	>sp|P52760|UK114	Ribonuclease UK114	168,04	5,839E-03	-2,3	☐
M	>sp|P52792|HXK4	Glucokinase	19,75	4,395E-03	2,5	☐
M	>sp|P55050|FABPI	Fatty acid-binding protein, intestinal	22,35	3,018E-02	2,4	☐
M	>sp|P55258|RAB8A	Ras-related protein Rab-8A	15,71	6,228E-03	-2,3	☐
M	>sp|P56389|CDD	Cytidine deaminase	20,42	1,627E-03	-2,2	☐
M	>sp|P56654|CP237	Cytochrome P450 2C37	235,53	8,530E-06	-4,9	☐
M	>sp|P56656|CP239	Cytochrome P450 2C39	77,68	3,695E-04	19,7	☐
M	>sp|P59325|IF5	Eukaryotic translation initiation factor 5	17,03	1,313E-03	-2,5	☐
M	>sp|P60229|EIF3E	Eukaryotic translation initiation factor 3 subunit E	24,24	8,432E-04	18,7	☐
M	>sp|P61514|RL37A	60S ribosomal protein L37a	13,94	8,781E-03	4,8	☐
M	>sp|P62827|RAN	GTP-binding nuclear protein Ran	24,89	4,075E-04	-3,8	☐
M	>sp|P62862|RS30	40S ribosomal protein S30	8,12	1,366E-03	-4,0	☐
M	>sp|P63073|IF4E	Eukaryotic translation initiation factor 4E	13,97	2,772E-02	3,4	☐
M	>sp|P63085|MK01	Mitogen-activated protein kinase 1	13,73	9,588E-03	-2,5	☐
M	>sp|P70699|LYAG	Lysosomal alpha-glucosidase	34,98	1,355E-02	2,7	☐
M	>sp|P83882|RL36A	60S ribosomal protein L36a	6,64	1,310E-03	-3,2	☐
M	>sp|P84091|AP2M1	AP-2 complex subunit mu	21,34	6,561E-03	-2,9	☐
M	>sp|P84244|H33	Histone H3.3	4,86	8,209E-03	-2,7	☐
M	>sp|P99026|PSB4	Proteasome subunit beta type-4	23,09	5,296E-03	-7,6	☐
M	>sp|Q00519|XDH	Xanthine dehydrogenase/oxidase	120,97	1,007E-03	-3,9	☐
M	>sp|Q00897|A1AT4	Alpha-1-antitrypsin 1-4	107,74	1,200E-02	-3,0	☐
M	>sp|Q01339|APOH	Beta-2-glycoprotein 1	13,44	2,845E-02	-3,3	☐
M	>sp|Q03249|GALT	Galactose-1-phosphate uridylyltransferase	44,59	2,856E-02	-2,9	☐
M	>sp|Q05816|FABP5	Fatty acid-binding protein, epidermal	129,51	3,401E-02	2,1	☐
M	>sp|Q05915|GCH1	GTP cyclohydrolase 1	5,10	2,583E-03	2,1	☐
M	>sp|Q07813|BAX	Apoptosis regulator BAX	7,24	2,189E-02	-2,1	☐
M	>sp|Q3THK7|GUAA	GMP synthase [glutamine-hydrolyzing]	22,83	7,200E-04	-2,0	☐
M	>sp|Q3TW96|UAP1L	UDP-N-acetylhexosamine pyrophosphorylase-like protein 1	10,69	3,620E-02	2,4	☐
M	>sp|Q3UNZ8|QORL2	Quinone oxidoreductase-like protein 2	33,01	1,049E-05	10,3	☐
M	>sp|Q4VAA2|CDV3	Protein CDV3	49,10	3,403E-02	2,1	☐
M	>sp|Q5RKZ7|MOCS1	Molybdenum cofactor biosynthesis protein 1	29,26	3,212E-02	2,3	☐
M	>sp|Q5SUR0|PUR4	Phosphoribosylformylglycinamidine synthase	14,96	4,154E-03	-2,4	☐
M	>sp|Q5U4C1|GASP1	G-protein coupled receptor-associated sorting protein 1	3,61	7,753E-03	2,4	☐
M	>sp|Q60692|PSB6	Proteasome subunit beta type-6	24,38	2,465E-03	-3,7	☐
M	>sp|Q60866|PTER	Phosphotriesterase-related protein	81,65	8,475E-04	-2,4	☐
M	>sp|Q61704|ITIH3	Inter-alpha-trypsin inhibitor heavy chain H3	7,97	1,345E-04	3,4	☐

M	>sp|Q62348|TSN	Translin	3,38	4,009E-02	-2,9	☐
M	>sp|Q62376|RU17	U1 small nuclear ribonucleoprotein 70 kDa	6,88	2,460E-02	-2,6	☐
M	>sp|Q63836|SBP2	Selenium-binding protein 2	488,39	1,804E-02	2,5	☐
M	>sp|Q63886|UD11	UDP-glucuronosyltransferase 1-1	187,68	1,540E-03	-2,4	☐
M	>sp|Q64374|RGN	Regucalcin	474,77	1,370E-03	-2,2	☐
M	>sp|Q6P1B1|XPP1	Xaa-Pro aminopeptidase 1	13,35	1,094E-02	3,3	☐
M	>sp|Q6P542|ABCF1	ATP-binding cassette sub-family F member 1	25,71	3,504E-02	2,0	☐
M	>sp|Q6P8I4|PCNP	PEST proteolytic signal-containing nuclear protein	8,89	6,437E-04	-3,4	☐
M	>sp|Q76LS9|FA63A	Protein FAM63A	14,09	4,205E-02	2,2	☐
M	>sp|Q7TMK9|HNRPQ	Heterogeneous nuclear ribonucleoprotein Q	42,82	1,907E-03	2,2	☐
M	>sp|Q80VP1|EPN1	Epsin-1	18,13	3,321E-02	3,1	☐
M	>sp|Q80W22|THNS2	Threonine synthase-like 2	51,71	1,098E-03	-3,9	☐
M	>sp|Q8BFP9|PDK1	[Pyruvate dehydrogenase (acetyl-transferring)] kinase isozyme 1	6,93	2,337E-03	6,5	☐
M	>sp|Q8BFZ3|ACTBL	Beta-actin-like protein 2	194,76	2,087E-02	-2,6	☐
M	>sp|Q8BH69|SPS1	Selenide, water dikinase 1	16,62	4,584E-03	-3,8	☐
M	>sp|Q8BKZ9|ODPX	Pyruvate dehydrogenase protein X component, mitochondrial	10,55	3,590E-04	-4,8	☐
M	>sp|Q8BLF1|NCEH1	Neutral cholesterol ester hydrolase 1	3,69	3,316E-02	2,1	☐
M	>sp|Q8BMA6|SRP68	Signal recognition particle subunit SRP68	27,06	8,770E-04	2,5	☐
M	>sp|Q8BRK8|AAPK2	5'-AMP-activated protein kinase catalytic subunit alpha-2	16,94	3,148E-03	2,5	☐
M	>sp|Q8BTY1|KAT1	Kynurenine--oxoglutarate transaminase 1	73,86	1,724E-02	-2,4	☐
M	>sp|Q8C5W3|TBCEL	Tubulin-specific chaperone cofactor E-like protein	21,28	4,150E-03	-2,3	☐
M	>sp|Q8CAS9|PARP9	Poly [ADP-ribose] polymerase 9	11,36	2,121E-04	2,1	☐
M	>sp|Q8K010|OPLA	5-oxoprolinase	206,63	5,570E-06	22,2	☐
M	>sp|Q8K3J1|NDUS8	NADH dehydrogenase [ubiquinone] iron-sulfur protein 8	16,46	7,938E-04	-3,5	☐
M	>sp|Q8K3W0|BRE	BRCA1-A complex subunit BRE	4,24	2,680E-02	-2,6	☐
M	>sp|Q8K411|PREP	Presequence protease, mitochondrial	38,78	1,387E-02	2,2	☐
M	>sp|Q8R050|ERF3A	Eukaryotic peptide chain release factor GTP-binding subunit ERF3A	20,28	2,326E-04	4,0	☐
M	>sp|Q8R123|FAD1	FAD synthase	18,17	8,777E-03	-2,0	☐
M	>sp|Q8VCB3|GYS2	Glycogen [starch] synthase, liver	36,35	3,517E-04	8,2	☐
M	>sp|Q8VCH6|DHC24	Delta(24)-sterol reductase	10,41	6,807E-03	-2,7	☐
M	>sp|Q8VCH8|UBXN4	UBX domain-containing protein 4	14,67	3,233E-02	-2,2	☐
M	>sp|Q8VCR2|DHB13	17-beta-hydroxysteroid dehydrogenase 13	51,73	1,498E-02	-4,2	☐
M	>sp|Q91VF2|HNMT	Histamine N-methyltransferase	10,60	1,160E-02	-4,0	☐
M	>sp|Q91VS7|MGST1	Microsomal glutathione S-transferase 1	110,95	3,732E-03	-3,2	☐
M	>sp|Q91VT4|CBR4	Carbonyl reductase family member 4	63,93	4,840E-03	2,2	☐
M	>sp|Q91W97|HKDC1	Putative hexokinase HKDC1	3,11	2,551E-03	-4,0	☐
M	>sp|Q91WS4|BHMT2	S-methylmethionine--homocysteine S-methyltransferase BHMT2	100,28	6,396E-05	13,5	☐
M	>sp|Q91WU5|AS3MT	Arsenite methyltransferase	32,67	4,108E-03	-2,5	☐
M	>sp|Q91XE8|TM205	Transmembrane protein 205	16,47	2,132E-05	3,0	☐
M	>sp|Q91YP0|L2HDH	L-2-hydroxyglutarate dehydrogenase, mitochondrial	32,92	2,574E-03	-2,2	☐

M	>sp|Q91Z98|CHIL4	Chitinase-like protein 4	9,09	9,410E-03	-2,6	☐
M	>sp|Q921H8|THIKA	3-ketoacyl-CoA thiolase A, peroxisomal	497,03	1,385E-05	2,1	☐
M	>sp|Q921M3|SF3B3	Splicing factor 3B subunit 3	14,37	1,513E-02	2,5	☐
M	>sp|Q922Q1|MARC2	Mitochondrial amidoxime reducing component 2	34,67	2,267E-02	-2,3	☐
M	>sp|Q99KP3|CRYL1	Lambda-crystallin homolog	37,47	1,221E-03	2,7	☐
M	>sp|Q99KP6|PRP19	Pre-mRNA-processing factor 19	11,47	1,401E-05	11,6	☐
M	>sp|Q99MN1|SYK	Lysine--tRNA ligase	53,77	1,133E-02	-2,1	☐
M	>sp|Q99PG0|AAAD	Arylacetamide deacetylase	121,17	2,289E-04	-2,1	☐
M	>sp|Q9CPU0|LGUL	Lactoylglutathione lyase	157,33	3,293E-05	-2,4	☐
M	>sp|Q9CPX6|ATG3	Ubiquitin-like-conjugating enzyme ATG3	6,07	4,432E-02	-2,3	☐
M	>sp|Q9CQC6|BZW1	Basic leucine zipper and W2 domain-containing protein 1	15,15	7,398E-03	-2,7	☐
M	>sp|Q9D0M1|KPRA	Phosphoribosyl pyrophosphate synthase-associated protein 1	35,38	8,411E-07	18,2	☐
M	>sp|Q9D1R9|RL34	60S ribosomal protein L34	12,19	2,888E-03	-2,1	☐
M	>sp|Q9D2R0|AACS	Acetoacetyl-CoA synthetase	22,28	7,333E-04	3,4	☐
M	>sp|Q9D2V7|CORO7	Coronin-7	24,62	2,131E-03	-3,2	☐
M	>sp|Q9D7G0|PRPS1	Ribose-phosphate pyrophosphokinase 1	48,75	1,845E-04	-29,9	☐
M	>sp|Q9D820|PRXD1	Prolyl-tRNA synthetase associated domain-containing protein 1	4,86	1,819E-04	-6,0	☐
M	>sp|Q9D8T2|GSDMD	Gasdermin-D	7,69	6,625E-03	2,6	☐
M	>sp|Q9DAR7|DCPS	m7GpppX diphosphatase	33,32	2,266E-03	-2,5	☐
M	>sp|Q9DB29|IAH1	Isoamyl acetate-hydrolyzing esterase 1 homolog	50,22	6,319E-04	-3,8	☐
M	>sp|Q9DBE0|CSAD	Cysteine sulfinic acid decarboxylase	131,84	8,841E-03	-3,5	☐
M	>sp|Q9DBS5|KLC4	Kinesin light chain 4	8,68	3,762E-02	2,0	☐
M	>sp|Q9DCD0|6PGD	6-phosphogluconate dehydrogenase, decarboxylating	80,30	3,403E-03	-2,1	☐
M	>sp|Q9EPQ7|STAR5	StAR-related lipid transfer protein 5	8,78	4,186E-02	-2,0	☐
M	>sp|Q9EQ06|DHB11	Estradiol 17-beta-dehydrogenase 11	21,95	2,815E-03	-2,2	☐
M	>sp|Q9JHE3|ASAH2	Neutral ceramidase	8,73	8,710E-04	3,1	☐
M	>sp|Q9JHS4|CLPX	ATP-dependent Clp protease ATP-binding subunit clpX-like	25,06	5,596E-04	11,0	☐
M	>sp|Q9JIL4|NHRF3	Na(+)/H(+) exchange regulatory cofactor NHE-RF3	28,83	1,048E-02	3,8	☐
M	>sp|Q9JLF6|TGM1	Protein-glutamine gamma-glutamyltransferase K	8,63	4,134E-02	-2,4	☐
M	>sp|Q9JLY0|SOCS6	Suppressor of cytokine signaling 6	2,73	7,824E-04	2,7	☐
M	>sp|Q9JMA1|UBP14	Ubiquitin carboxyl-terminal hydrolase 14	43,37	1,689E-02	3,0	☐
M	>sp|Q9JMA7|CP341	Cytochrome P450 3A41	142,20	2,876E-03	9,8	☐
M	>sp|Q9NYQ2|HAOX2	Hydroxyacid oxidase 2	46,32	2,122E-04	8,2	☐
M	>sp|Q9QWR8|NAGAB	Alpha-N-acetylgalactosaminidase	6,07	1,521E-02	-2,2	☐
M	>sp|Q9QXD6|F16P1	Fructose-1,6-bisphosphatase 1	562,37	9,500E-04	-2,3	☐
M	>sp|Q9QYB1|CLIC4	Chloride intracellular channel protein 4	85,49	8,122E-04	3,1	☐
M	>sp|Q9QYY9|ADH4	Alcohol dehydrogenase 4	39,13	1,165E-03	4,7	☐
M	>sp|Q9R0M5|TPK1	Thiamin pyrophosphokinase 1	8,59	5,719E-04	-3,6	☐
M	>sp|Q9R1P1|PSB3	Proteasome subunit beta type-3	32,66	9,657E-04	-6,0	☐
M	>sp|Q9R1P3|PSB2	Proteasome subunit beta type-2	27,17	1,070E-03	-6,4	☐
M	>sp|Q9WUR9|KAD4	Adenylate kinase 4, mitochondrial	46,10	1,938E-02	2,1	☐
M	>sp|Q9WV54|ASAH1	Acid ceramidase	22,25	6,901E-03	-3,2	☐

M	>sp|Q9WVE8|PACN2	Protein kinase C and casein kinase substrate in neurons protein 2	8,88	1,136E-03	-2,1	☐
M	>sp|Q9Z1J3|NFS1	Cysteine desulfurase, mitochondrial	15,05	2,627E-03	2,1	☐
M	>sp|Q9Z2U0|PSA7	Proteasome subunit alpha type-7	61,80	1,671E-03	-4,6	☐
M	>sp|Q9Z2U1|PSA5	Proteasome subunit alpha type-5	59,85	9,868E-03	-4,2	☐
M	>tr|A0A0A0MQC3	5-hydroxyisourate hydrolase	50,54	2,784E-04	-2,2	☐
M	>tr|A2AGR0|A2AGR0	MAP kinase-activating death domain protein	4,87	1,235E-03	4,2	☐
M	>tr|A2AQZ2|A2AQZ2	Phytanoyl-CoA dioxygenase domain-containing protein 1 (Fragment)	54,28	5,865E-05	4,1	☐
M	>tr|A8DUK4|A8DUK4	Beta-globin	426,02	1,084E-05	-91,4	☐
M	>tr|A8Y5N4|A8Y5N4	17-beta-hydroxysteroid dehydrogenase 13	54,29	6,720E-03	-17,7	☐
M	>tr|D3YUP6|D3YUP6	Protein Ugt2b36 (Fragment)	48,07	2,380E-03	-2,1	☐
M	>tr|D3Z5G7|D3Z5G7	Carboxylic ester hydrolase	37,61	1,281E-03	5,0	☐
M	>tr|E9PW69|E9PW69	Proteasome subunit alpha type (Fragment)	31,99	2,830E-03	-4,9	☐
M	>tr|E9PXC3|E9PXC3	Protein Cyp2c69	134,37	6,226E-03	-2,1	☐
M	>tr|E9Q455|E9Q455	Tropomyosin alpha-1 chain	42,17	2,770E-04	6,1	☐
M	>tr|E9Q9F5|E9Q9F5	Septin-7	57,02	5,362E-05	22,2	☐
M	>tr|E9QNW6|E9QNW6	Platelet-activating factor acetylhydrolase 2, cytoplasmic	8,02	3,568E-02	3,0	☐
M	>tr|E9QPE7|E9QPE7	Myosin-11	74,90	4,057E-03	-2,0	☐
M	>tr|G5E902|G5E902	MCG10343, isoform CRA_b	35,02	9,685E-04	3,3	☐
M	>tr|H3BJ51|H3BJ51	All-trans-retinol 13,14-reductase	31,98	2,324E-03	-19,1	☐
M	>tr|H7BX99|H7BX99	Prothrombin	19,69	1,877E-03	14,4	☐
M	>tr|I7HPX6|I7HPX6	Cytochrome b-c1 complex subunit 8	10,16	3,114E-04	13,0	☐
M	>tr|L7N466|L7N466	5-formyltetrahydrofolate cyclo-ligase	22,29	6,265E-05	2,2	☐
M	>tr|Q059N0|Q059N0	Sulfotransferase	81,14	6,033E-04	6,7	☐
M	>tr|Q3TUE1|Q3TUE1	Far upstream element-binding protein 1	18,66	4,925E-03	-2,3	☐
M	>tr|Q3U3J1|Q3U3J1	2-oxoisovalerate dehydrogenase subunit alpha, mitochondrial	239,03	1,966E-04	3,1	☐
M	>tr|Q3UW66|Q3UW66	Sulfurtransferase	118,51	1,251E-05	2,4	☐
M	>tr|Q91VB8|Q91VB8	Alpha globin 1	413,96	3,541E-04	-2,9	☐
M	>tr|Q91Z40|Q91Z40	Gbp6 protein	5,97	2,637E-02	-2,4	☐
M	>tr|Q9CQM8|Q9CQM8	60S ribosomal protein L21	48,39	3,912E-04	5,1	☐
T	>sp|A2AS89|SPEB	Agmatinase, mitochondrial	60,52	2,171E-03	-3,5	☐
T	>sp|B1AR13|CISD3	CDGSH iron-sulfur domain-containing protein 3, mitochondrial	8,01	3,703E-02	-3,2	☐
T	>sp|G3X982|AOXC	Aldehyde oxidase 3	120,25	2,567E-02	-2,0	☐
T	>sp|O08807|PRDX4	Peroxiredoxin-4	47,98	3,758E-04	3,4	☐
T	>sp|O09061|PSB1	Proteasome subunit beta type-1	34,47	1,076E-02	-3,5	☐
T	>sp|O35215|DOPD	D-dopachrome decarboxylase	23,57	3,090E-02	-4,9	☐
T	>sp|O35286|DHX15	Pre-mRNA-splicing factor ATP-dependent RNA helicase DHX15	13,23	1,015E-02	-2,3	☐
T	>sp|O35841|API5	Apoptosis inhibitor 5	15,45	9,009E-03	-2,1	☐
T	>sp|O55234|PSB5	Proteasome subunit beta type-5	16,24	5,636E-04	-3,9	☐
T	>sp|O70435|PSA3	Proteasome subunit alpha type-3	8,53	1,621E-03	-6,0	☐
T	>sp|O88451|RDH7	Retinol dehydrogenase 7	130,14	1,416E-04	-3,7	☐
T	>sp|O88456|CPNS1	Calpain small subunit 1	15,07	1,108E-04	2,1	☐
T	>sp|O89017|LGMN	Legumain	36,28	2,168E-02	2,4	☐

190

T	>sp|P02089|HBB2	Hemoglobin subunit beta-2	269,71	4,909E-04	-2,7	☐
T	>sp|P06330|HVM51	Ig heavy chain V region AC38 205.12	13,64	2,489E-05	5,4	☐
T	>sp|P07724|ALBU	Serum albumin	884,36	2,028E-04	-2,3	☐
T	>sp|P10518|HEM2	Delta-aminolevulinic acid dehydratase	142,33	4,713E-03	-2,5	☐
T	>sp|P11352|GPX1	Glutathione peroxidase 1	154,94	1,267E-02	-2,8	☐
T	>sp|P16546|SPTN1	Spectrin alpha chain, non-erythrocytic 1	42,85	3,474E-05	5,5	☐
T	>sp|P17563|SBP1	Selenium-binding protein 1	448,05	7,712E-03	-2,0	☐
T	>sp|P17879|HS71B	Heat shock 70 kDa protein 1B	113,76	2,589E-02	2,2	☐
T	>sp|P20065|TYB4	Thymosin beta-4	39,98	4,230E-02	3,5	☐
T	>sp|P21300|ALD1	Aldose reductase-related protein 1	8,12	1,419E-04	-4,5	☐
T	>sp|P21614|VTDB	Vitamin D-binding protein	148,26	5,050E-06	-2,8	☐
T	>sp|P24456|CP2DA	Cytochrome P450 2D10	194,38	1,891E-03	-2,2	☐
T	>sp|P27046|MA2A1	Alpha-mannosidase 2	14,55	1,302E-03	-2,1	☐
T	>sp|P27612|PLAP	Phospholipase A-2-activating protein	24,01	2,839E-03	-2,1	☐
T	>sp|P28063|PSB8	Proteasome subunit beta type-8	16,08	4,500E-02	-2,2	☐
T	>sp|P28651|CAH8	Carbonic anhydrase-related protein	35,72	1,295E-06	5,5	☐
T	>sp|P28798|GRN	Granulins	16,30	7,131E-08	-36,2	☐
T	>sp|P34884|MIF	Macrophage migration inhibitory factor	74,65	1,182E-03	-2,5	☐
T	>sp|P34927|ASGR1	Asialoglycoprotein receptor 1	32,22	9,805E-04	-2,1	☐
T	>sp|P35492|HUTH	Histidine ammonia-lyase	376,41	1,953E-04	-2,5	☐
T	>sp|P35505|FAAA	Fumarylacetoacetase	449,36	1,390E-03	-5,6	☐
T	>sp|P50295|ARY2	Arylamine N-acetyltransferase 2	23,34	1,178E-03	2,1	☐
T	>sp|P51880|FABP7	Fatty acid-binding protein, brain	15,14	3,933E-02	3,3	☐
T	>sp|P52760|UK114	Ribonuclease UK114	168,04	2,018E-02	-2,3	☐
T	>sp|P52792|HXK4	Glucokinase	19,75	8,124E-03	2,1	☐
T	>sp|P52843|ST2A1	Bile salt sulfotransferase 1	22,62	6,065E-05	-3,1	☐
T	>sp|P55302|AMRP	Alpha-2-macroglobulin receptor-associated protein	14,28	2,931E-03	2,2	☐
T	>sp|P56389|CDD	Cytidine deaminase	20,42	3,585E-03	-2,3	☐
T	>sp|P56391|CX6B1	Cytochrome c oxidase subunit 6B1	14,61	3,029E-02	-3,0	☐
T	>sp|P58389|PTPA	Serine/threonine-protein phosphatase 2A activator	16,25	4,027E-03	-2,1	☐
T	>sp|P59325|IF5	Eukaryotic translation initiation factor 5	17,03	5,914E-03	-2,5	☐
T	>sp|P60229|EIF3E	Eukaryotic translation initiation factor 3 subunit E	24,24	4,645E-05	6,7	☐
T	>sp|P61514|RL37A	60S ribosomal protein L37a	13,94	5,730E-05	3,8	☐
T	>sp|P62827|RAN	GTP-binding nuclear protein Ran	24,89	1,481E-04	-4,4	☐
T	>sp|P62862|RS30	40S ribosomal protein S30	8,12	4,048E-03	-3,5	☐
T	>sp|P63073|IF4E	Eukaryotic translation initiation factor 4E	13,97	6,956E-03	3,7	☐
T	>sp|P63085|MK01	Mitogen-activated protein kinase 1	13,73	3,804E-03	-2,3	☐
T	>sp|P68373|TBA1C	Tubulin alpha-1C chain	288,68	3,683E-02	-2,0	☐
T	>sp|P83882|RL36A	60S ribosomal protein L36a	6,64	7,129E-05	-4,6	☐
T	>sp|P84091|AP2M1	AP-2 complex subunit mu	21,34	1,384E-03	-3,9	☐
T	>sp|P84244|H33	Histone H3.3	4,86	3,822E-03	-3,1	☐
T	>sp|P97328|KHK	Ketohexokinase	169,67	3,835E-03	-12,4	☐
T	>sp|P99026|PSB4	Proteasome subunit beta type-4	23,09	6,686E-03	-6,3	☐

T	>sp|Q00519|XDH	Xanthine dehydrogenase/oxidase	120,97	1,097E-03	-3,2	☐
T	>sp|Q07813|BAX	Apoptosis regulator BAX	7,24	5,203E-03	-2,8	☐
T	>sp|Q3THK7|GUAA	GMP synthase [glutamine-hydrolyzing]	22,83	1,579E-04	-2,7	☐
T	>sp|Q3UNZ8|QORL2	Quinone oxidoreductase-like protein 2	33,01	1,785E-06	12,0	☐
T	>sp|Q4VAA2|CDV3	Protein CDV3	49,10	2,387E-02	2,0	☐
T	>sp|Q60692|PSB6	Proteasome subunit beta type-6	24,38	1,384E-03	-3,6	☐
T	>sp|Q62264|THRSP	Thyroid hormone-inducible hepatic protein	63,13	1,342E-03	-5,7	☐
T	>sp|Q62376|RU17	U1 small nuclear ribonucleoprotein 70 kDa	6,88	6,483E-04	-2,5	☐
T	>sp|Q62452|UD19	UDP-glucuronosyltransferase 1-9	134,47	1,305E-03	-2,1	☐
T	>sp|Q64374|RGN	Regucalcin	474,77	4,121E-04	-2,3	☐
T	>sp|Q6P8I4|PCNP	PEST proteolytic signal-containing nuclear protein	8,89	8,632E-04	-3,2	☐
T	>sp|Q76LS9|FA63A	Protein FAM63A	14,09	2,016E-02	2,1	☐
T	>sp|Q7TPV4|MBB1A	Myb-binding protein 1A	9,94	8,120E-04	2,4	☐
T	>sp|Q80VP1|EPN1	Epsin-1	18,13	1,210E-04	2,1	☐
T	>sp|Q8BFP9|PDK1	[Pyruvate dehydrogenase (acetyl-transferring)] kinase isozyme 1	6,93	1,022E-02	2,4	☐
T	>sp|Q8BFZ3|ACTBL	Beta-actin-like protein 2	194,76	1,242E-02	-2,1	☐
T	>sp|Q8BH69|SPS1	Selenide, water dikinase 1	16,62	3,679E-03	-3,4	☐
T	>sp|Q8C0Y0|PP4R4	Serine/threonine-protein phosphatase 4 regulatory subunit 4	4,86	1,966E-03	2,0	☐
T	>sp|Q8C1B7|SEP11	Septin-11	26,97	1,601E-04	2,2	☐
T	>sp|Q8C5W3|TBCEL	Tubulin-specific chaperone cofactor E-like protein	21,28	3,389E-02	-2,2	☐
T	>sp|Q8CAQ8|MIC60	MICOS complex subunit Mic60	7,80	2,123E-02	2,2	☐
T	>sp|Q8K010|OPLA	5-oxoprolinase	206,63	1,907E-06	22,6	☐
T	>sp|Q8R050|ERF3A	Eukaryotic peptide chain release factor GTP-binding subunit ERF3A	20,28	1,127E-06	3,2	☐
T	>sp|Q8VCC1|PGDH	15-hydroxyprostaglandin dehydrogenase [NAD(+)]	41,97	4,754E-04	-2,4	☐
T	>sp|Q8VCH6|DHC24	Delta(24)-sterol reductase	10,41	4,007E-03	-2,6	☐
T	>sp|Q8VCH8|UBXN4	UBX domain-containing protein 4	14,67	5,336E-03	-2,1	☐
T	>sp|Q91VS7|MGST1	Microsomal glutathione S-transferase 1	110,95	4,745E-03	-3,7	☐
T	>sp|Q91W97|HKDC1	Putative hexokinase HKDC1	3,11	5,125E-03	2,4	☐
T	>sp|Q91XE8|TM205	Transmembrane protein 205	16,47	7,710E-06	3,5	☐
T	>sp|Q921M3|SF3B3	Splicing factor 3B subunit 3	14,37	1,303E-02	2,1	☐
T	>sp|Q922Q1|MARC2	Mitochondrial amidoxime reducing component 2	34,67	3,745E-03	-3,6	☐
T	>sp|Q99KP6|PRP19	Pre-mRNA-processing factor 19	11,47	1,733E-06	10,5	☐
T	>sp|Q99LC3|NDUAA	NADH dehydrogenase [ubiquinone] 1 alpha subcomplex subunit 10	39,77	6,221E-05	-2,1	☐
T	>sp|Q99LY9|NDUS5	NADH dehydrogenase [ubiquinone] iron-sulfur protein 5	6,11	3,469E-03	-7,4	☐
T	>sp|Q99P30|NUDT7	Peroxisomal coenzyme A diphosphatase NUDT7	132,96	3,381E-04	-2,4	☐
T	>sp|Q9CPU0|LGUL	Lactoylglutathione lyase	157,33	5,006E-05	-2,5	☐
T	>sp|Q9CQC6|BZW1	Basic leucine zipper and W2 domain-containing protein 1	15,15	1,282E-04	-3,3	☐
T	>sp|Q9CYZ2|TPD54	Tumor protein D54	24,45	6,887E-03	2,6	☐
T	>sp|Q9D1G1|RAB1B	Ras-related protein Rab-1B	43,53	1,165E-02	2,1	☐
T	>sp|Q9D1R9|RL34	60S ribosomal protein L34	12,19	4,462E-03	-2,4	☐

T	>sp|Q9D2V7|CORO7	Coronin-7	24,62	2,381E-03	-2,8	☐
T	>sp|Q9D7G0|PRPS1	Ribose-phosphate pyrophosphokinase 1	48,75	8,027E-05	-106,1	☐
T	>sp|Q9D820|PRXD1	Prolyl-tRNA synthetase associated domain-containing protein 1	4,86	4,981E-04	-5,1	☐
T	>sp|Q9DBE0|CSAD	Cysteine sulfinic acid decarboxylase	131,84	3,709E-03	-3,3	☐
T	>sp|Q9DD20|MET7B	Methyltransferase-like protein 7B	53,21	2,502E-02	-2,0	☐
T	>sp|Q9EPQ7|STAR5	StAR-related lipid transfer protein 5	8,78	3,777E-04	-2,4	☐
T	>sp|Q9EQ06|DHB11	Estradiol 17-beta-dehydrogenase 11	21,95	4,243E-03	-2,7	☐
T	>sp|Q9JHE3|ASAH2	Neutral ceramidase	8,73	1,402E-03	2,3	☐
T	>sp|Q9JHS4|CLPX	ATP-dependent Clp protease ATP-binding subunit clpX-like	25,06	3,321E-05	11,0	☐
T	>sp|Q9JIL4|NHRF3	Na(+)/H(+) exchange regulatory cofactor NHE-RF3	28,83	2,805E-02	2,6	☐
T	>sp|Q9JKV1|ADRM1	Proteasomal ubiquitin receptor ADRM1	27,79	8,805E-04	-2,0	☐
T	>sp|Q9JMA1|UBP14	Ubiquitin carboxyl-terminal hydrolase 14	43,37	4,662E-03	4,6	☐
T	>sp|Q9QYJ0|DNJA2	DnaJ homolog subfamily A member 2	34,68	1,824E-02	-2,1	☐
T	>sp|Q9R0M5|TPK1	Thiamin pyrophosphokinase 1	8,59	1,072E-03	-7,4	☐
T	>sp|Q9R0Q7|TEBP	Prostaglandin E synthase 3	26,48	7,458E-03	-2,1	☐
T	>sp|Q9R0Q9|MPU1	Mannose-P-dolichol utilization defect 1 protein	7,59	8,970E-03	-2,3	☐
T	>sp|Q9R1J0|NSDHL	Sterol-4-alpha-carboxylate 3-dehydrogenase, decarboxylating	18,92	1,303E-02	-2,2	☐
T	>sp|Q9R1P1|PSB3	Proteasome subunit beta type-3	32,66	2,233E-04	-5,3	☐
T	>sp|Q9R1P3|PSB2	Proteasome subunit beta type-2	27,17	9,446E-04	-4,9	☐
T	>sp|Q9WVE8|PACN2	Protein kinase C and casein kinase substrate in neurons protein 2	8,88	1,946E-03	-2,0	☐
T	>sp|Q9Z2U0|PSA7	Proteasome subunit alpha type-7	61,80	9,058E-04	-4,0	☐
T	>sp|Q9Z2U1|PSA5	Proteasome subunit alpha type-5	59,85	1,426E-03	-5,0	☐
T	>sp|Q9Z2Z6|MCAT	Mitochondrial carnitine/acylcarnitine carrier protein	20,71	3,653E-02	-2,4	☐
T	>tr|A0A0A0MQC3	5-hydroxyisourate hydrolase	50,54	4,155E-03	-3,6	☐
T	>tr|A2AGR0|A2AGR0	MAP kinase-activating death domain protein	4,87	5,471E-04	5,1	☐
T	>tr|A2AQZ2|A2AQZ2	Phytanoyl-CoA dioxygenase domain-containing protein 1 (Fragment)	54,28	4,431E-06	4,5	☐
T	>tr|D3YUP6|D3YUP6	Protein Ugt2b36 (Fragment)	48,07	6,004E-03	-2,1	☐
T	>tr|D3Z0R5|D3Z0R5	Glucosamine-6-phosphate isomerase 1 (Fragment)	6,97	1,096E-03	-2,4	☐
T	>tr|D3Z5G7|D3Z5G7	Carboxylic ester hydrolase	37,61	1,088E-03	2,6	☐
T	>tr|E9PV38|E9PV38	Carboxylic ester hydrolase	53,04	9,379E-04	2,2	☐
T	>tr|E9PW69|E9PW69	Proteasome subunit alpha type (Fragment)	31,99	4,343E-04	-5,4	☐
T	>tr|E9PXC3|E9PXC3	Protein Cyp2c69	134,37	1,596E-02	-2,4	☐
T	>tr|E9PZ00|E9PZ00	Prosaposin	54,04	6,531E-03	-3,1	☐
T	>tr|E9Q1Q9|E9Q1Q9	Ketohexokinase	166,27	7,333E-04	-5,1	☐
T	>tr|E9Q455|E9Q455	Tropomyosin alpha-1 chain	42,17	8,595E-05	4,3	☐
T	>tr|E9Q9F5|E9Q9F5	Septin-7	57,02	5,275E-07	19,6	☐
T	>tr|E9QNW6|E9QNW6	Platelet-activating factor acetylhydrolase 2, cytoplasmic	8,02	4,329E-03	2,4	☐
T	>tr|F7CBP1|F7CBP1	Eukaryotic translation initiation factor 4 gamma 2	8,19	4,915E-03	-3,1	☐
T	>tr|G5E902|G5E902	MCG10343, isoform CRA_b	35,02	1,235E-05	3,5	☐
T	>tr|H7BX99|H7BX99	Prothrombin	19,69	7,435E-05	15,6	☐

T	>tr|Q5JC28|Q5JC28	Epidermal growth factor receptor pathway substrate 15 isoform B	17,82	2,164E-02	2,1	☐
T	>tr|Q5SW88|Q5SW88	Ras-related protein Rab-1A	46,59	1,209E-03	2,1	☐
T	>tr|Q6ZWZ4|Q6ZWZ4	60S ribosomal protein L36	14,98	3,452E-02	2,3	☐
T	>tr|Q6ZWZ6|Q6ZWZ6	40S ribosomal protein S12	15,79	1,497E-02	-2,1	☐
T	>tr|Q91Z40|Q91Z40	Gbp6 protein	5,97	1,239E-02	-2,2	☐
T	>tr|Q9CQM8|Q9CQM8	60S ribosomal protein L21	48,39	1,610E-03	3,2	☐
T	>tr|Q9WUD0	Cytochrome P450 2B10	16,12	6,634E-03	-2,1	☐